

# **Pool Boiling of Dielectric Liquids on Porous Graphite and Extended Copper Surfaces**

**Jack L. Parker and Mohamed S. El-Genk**

**Institute for Space and Nuclear Power Studies and  
The department of Chemical and Nuclear  
Engineering**

**Technical Report No. UNM-ISNPS-1-2008  
Institute for Space and Nuclear Power Studies  
University of New Mexico**

**August 2008**

## **ACKNOWLEDGMENTS**

The University of New Mexico's Institute for Space and Nuclear Power Studies funded this research. The authors acknowledge the assistance provided by former graduate students Dr. Hamed Saber, Dr. Yoichi Momozaki, and Dr. Larry James, and the current graduate students working on related topics, Yang In-Hwan and Amir Ali.

## ABSTRACT

This work investigated pool boiling of the dielectric liquids HFE-7100 and FC-72 on plane copper and porous graphite and on copper surfaces with corner pins. The work investigated the effects of surface orientation and liquid subcooling and, for the copper surfaces with corner pins, the effect of surface roughness. In addition, investigations were made studying the heat transfer by natural convection and nucleate boiling, as well as the effects of liquid subcooling (up to 30 K) and surface inclination ( $0^\circ$ –upward facing, to  $180^\circ$ –downward facing) on nucleate boiling heat transfer and Critical Heat Flux (CHF). The results are applicable to direct immersion cooling by nucleate boiling of high power computer chips dissipating 50 - 100 W/cm<sup>2</sup> while maintaining the junction temperature for the chips below the recommended values ( $\sim 85^\circ\text{C}$ ).

Pool boiling experiments are performed with degassed HFE-7100 and FC-72 liquids using uniformly heated 10 x 10 mm porous graphite and copper surfaces with corner pins. The measured footprint temperatures and thermal power removed from the surfaces are used to construct the pool boiling curves and determine the critical heat flux and corresponding surface superheat. Results are compared with those obtained on plane copper of same heated footprint area. The obtained CHF values are also compared with those reported in the open literature for plane, micro-porous, and macro-structured surfaces. Digital photographs and video are obtained to help explain and interpret the results.

For the first time, natural convection correlations for dielectric liquids on plane, porous, and copper with corner pins developed. These correlations are important to electronic cooling in the stand-by mode when the heat dissipation by the chips is only a few watts. Results show that the power removed by natural convection from surfaces with corner pins is 67% more than from plane Si and Cu surfaces at the same surface superheat. Increasing the ratio of the wetted surface area increases the rate of heat removal in natural convection. The developed correlations indicate that the power removed by natural convection increases with the footprint superheat raised to the 1.2 power for plane, micro-porous, and macro-structured surfaces. For plane Si and Cu

surfaces, the correlation fit the data of nearly 1500 points to within  $\pm 7\%$ . The natural convection correlations for micro-porous surfaces and macro-structured surfaces (each with  $> 500$  points) are within  $\pm 10\%$  and  $\pm 12\%$  of the data, respectively.

Using porous graphite and copper with Cu pins increases the nucleate boiling heat transfer rate over that on plane copper. On all surfaces, as the inclination angle increases, the heat transfer rate at low superheats increases slightly, then decreases with increasing angle at high superheats. However, the porous graphite and the Cu with corner pins significantly reduce the decline in boiling heat transfer rate with increasing inclination. The peak heat transfer coefficient corresponds to the minimum thermal boiling resistance and occurs at a heat flux  $\sim 10\%$  lower than that at CHF. This also increases as pin height increases. For of electronics cooling, the most optimal operational point is at the minimum boiling resistance. Although the power dissipated at the minimum boiling resistance increases as the liquid subcooling increases, the minimum boiling resistance also increases as does the surface superheat. In saturation boiling of HFE-7100 on 5 mm tall corner pins, the minimum boiling resistance is 0.42 K/W and occurs at a surface superheat of 21.2 K. For 30 K subcooled boiling of HFE-7100 on the same surface, the minimum boiling resistance and corresponding surface superheat are 0.66 K/W and 29.4 K, respectively. The dissipated powers at these minimum resistances are 50.2 W for saturation boiling and 89.8 W for 30 K subcooled boiling of HFE-7100. In addition, increasing the surface roughness of the copper with corner pins increases the nucleate boiling heat transfer rate, the peak nucleate boiling heat transfer coefficient, and CHF.

Although the heat flux at the peak heat transfer coefficient is the most desirable operational point, CHF is the upper limit for cooling by nucleate boiling. Beyond CHF the electronics would overheat. Results also show that increasing the height of the corner pins increases the thermal power removed in nucleate boiling and at CHF. CHF increases linearly with increased liquid subcooling, but decreases with increased surface inclination. The decrease in CHF with increased inclination for the surfaces with corner pins is significantly smaller than on plane surfaces. A total of 93 W of thermal power is removed from the copper surface with 5 mm tall pins in the upward facing orientation at CHF for 30 K subcooled HFE-7100. This power is 2.2 times that removed from the

plane copper surface (41.5 W). The thermal power removed at CHF on the surface with 5 mm tall pins in the downward facing orientation is as much as 85% of that in the upward facing orientation, compared with only 20% for plane copper. The relative decrease in thermal power removed at CHF is independent of liquid subcooling. The correlations developed for CHF fit the data to within  $\pm 10\%$  for both macro-structured surfaces (104 points) and micro-porous surfaces (150 points).

For electronics cooling applications, the best mode of cooling by nucleate boiling is in saturation boiling of HFE-7100 on 5 mm tall corner pins operating at the heat flux corresponding to the minimum boiling resistance. At this condition and using the saturation temperature of HFE-7100 of 54 °C, the wall temperature is 75.2 °C, well below the limit of 85 °C. If more robust electronics are used and have a higher maximum temperature limit, boiling in 30 K subcooled liquid removed much more power. At the minimum boiling resistance, the wall temperature is 83.4 °C.

# Table of Contents

Table of Contents .....	x
List of Figures .....	xii
List of Tables .....	xvi
Nomenclature .....	xvii
1 Introduction.....	1
1.1 Boiling of Dielectric Liquids .....	6
1.2 Effect of Surface Conditions.....	9
1.2.1 Surface Structure.....	11
1.2.2 Extended Surfaces.....	12
1.2.2.1 Micro-Structured Surfaces (Length Scale < 0.5 mm).....	13
1.2.2.2 Macro-Structured Surfaces (Length Scale > 0.5 mm).....	16
1.3 Effect of Liquid Subcooling.....	17
1.4 Effect of Surface Inclination.....	17
1.5 Objectives .....	19
2 Background.....	22
2.1 Natural Convection .....	24
2.2 Pool Boiling and Nucleate Boiling Heat Transfer .....	25
2.2.1 Ebullition Cycle .....	28
2.2.2 Boiling Regimes.....	32
2.3 Critical Heat Flux.....	35
2.4 Enhancements in Nucleate Boiling.....	41
2.4.1 Effect of Surface Preparation.....	44
2.4.1.1 Re-Structured Surfaces .....	50
2.4.1.2 Micro-Structured Surfaces.....	53
2.4.1.3 Macro-Structured Surfaces .....	59
2.4.2 Effect of Liquid Thermophysical Properties.....	61
2.4.3 Effect of Surface Orientation.....	63
2.5 Summary.....	66
3 Pool Boiling Experiments.....	70
3.1 Test Section Design and Construction.....	70
3.1.1 Plane Cu Surfaces .....	72
3.1.2 Plane Porous Graphite Surface .....	77
3.1.3 Copper with Corner Pins.....	82
3.1.4 Thermal Analysis of Test Sections .....	85
3.2 Experimental setup.....	91
3.2.1 Test Section Holder and Rotation Assembly .....	91
3.2.2 Test Vessel.....	96
3.2.3 Water Bath Vessel.....	99
3.2.4 Power and Data Acquisition .....	100
3.3 Experimental Procedures .....	100

4	Pool Boiling on Plane Surfaces.....	108
4.1	Reproducibility and Hysteresis of Boiling Curves .....	108
4.2	Typical Pool Boiling Curve .....	110
4.3	Natural Convection .....	114
4.4	Nucleate Boiling .....	115
4.4.1	Effect of Liquid Properties.....	121
4.4.2	Effect of Liquid Subcooling.....	127
4.4.3	Liquid Aging Effect .....	130
4.4.4	Effect of Surface Orientation .....	132
4.4.5	Nucleate Boiling Heat Transfer Coefficient .....	139
4.4.6	Boiling Resistance .....	141
4.5	Critical Heat Flux Correlation .....	143
4.5.1	Effect of Surface Characteristics and Liquid Properties on CHF .....	145
4.5.2	Effect of Surface Orientation on CHF .....	147
4.5.3	Effect of Liquid Subcooling.....	155
4.5.4	Combined Effect of Subcooling and Surface Orientation on CHF.....	160
4.6	Discussion on Nucleate Boiling of Dielectric Liquids .....	164
4.7	Selected Photographs of Nucleate Boiling .....	167
4.8	Summary .....	178
5	Pool Boiling on Surface with Corner Pins.....	180
5.1	Results for Porous Graphite with Corner Pins.....	180
5.2	Natural Convection .....	184
5.3	Nucleate Boiling .....	187
5.3.1	Effect of Surface Orientation .....	191
5.3.2	Nucleate Boiling Heat Transfer Coefficient .....	191
5.3.3	Effect of Surface Roughness.....	198
5.3.4	Effect of Liquid Subcooling on Nucleate Boiling .....	203
5.3.5	Boiling Resistance .....	207
5.4	Critical Heat Flux.....	209
5.4.1	CHF correlation for extended surfaces .....	211
5.4.2	Subcooled Boiling Critical Heat Flux.....	215
5.5	Photographs of Boiling on Cu with Corner Pins .....	220
5.6	Summary .....	234
6	Summary and Conclusions .....	238
7	References.....	243
	Appendix A. Details of Thermal Analysis.....	256
	Appendix B: Experimental Uncertainty.....	259
	Appendix C: List of Publications Related to Work .....	264

## List of Figures

Figure 1.1 Increase in clock speed and dissipated power for high performance computer chips. ....	2
Figure 1.2. Block layout of computer chip showing map of power density and temperature profile (from Lin and Banerjee, 2008).....	4
Figure 2.1. Relative magnitude of heat transfer coefficients for various mode of heat transfer (from Simmons, 1996).....	23
Figure 2.2 Gas entrapment in a cavity for an advancing liquid front. ....	26
Figure 2.3 Growth of entrapped gas to bubble nucleation.....	27
Figure 2.4 Range of cavity mouth sizes for active nucleation sites.....	29
Figure 2.5 Ebullition cycle.....	31
Figure 2.6 Typical nucleate pool boiling curve. ....	33
Figure 2.7 Sketch of different nucleate boiling regions.....	34
Figure 2.8 Hydrodynamic model for CHF.....	37
Figure 2.9 Microlayer (mushroom-and-stem) model for CHF. ....	40
Figure 2.10. Selected Surface Microstructures. ....	46
Figure 2.11 Micro-Structured Extended Boiling Surfaces (Length Scale < 0.5 mm). ....	47
Figure 2.12 Macro-Structured Extended Boiling Surfaces (Length Scale > 0.5 mm).....	48
Figure 2.13 Different modes of heat transfer during nucleate boiling for surfaces inclined > 90°. ....	68
Figure 3.1 Test section parts and assembly. ....	72
Figure 3.2. Cross sectional views and photograph of fully assembled plane copper test section. ....	75
Figure 3.3 SEM images of prepared copper boiling surface prepared using #1500 emery paper. Groove sizes average ~ 1.6 μm. ....	76
Figure 3.4 Cross sectional views and photograph of fully assembled plane porous graphite test section.....	79
Figure 3.5 SEM images of the plane porous graphite surface. ....	81
Figure 3.6 Cross sectional views and photograph of fully assembled test section of copper with corner pins.....	84
Figure 3.7 Location of thermocouples used for thermal analysis verification for plane surfaces. ....	88
Figure 3.8 Numerical thermal analysis of plane copper and porous graphite test sections. ....	89
Figure 3.9. Cross sectional temperature profile of copper with 5 mm corner pins near CHF.....	90
Figure 3.10 Line diagram of the pool boiling test facility. ....	93
Figure 3.11 Photograph of the pool boiling facility.....	94
Figure 3.12 Fully assembled test section support. ....	95
Figure 3.13 Photographs of rotation assembly and fully assembled rotation mechanism.....	97
Figure 3.14 Photographs of pool boiling test vessel and assembly ....	98
Figure 3.15 Voltage and power adjustment during the pool boiling experiments.....	102
Figure 3.16. Temperature measurements of the thermocouples embedded in the heated surfaces. ....	103

Figure 3.17. Saturation boiling curves on 5 mm corner pins using thermocouples under the pin and the middle or flat part of the heated surface.....	104
Figure 3.18. Temporal boiling curve of saturated FC-72 on copper. ....	106
Figure 4.1 Reproducibility of boiling curves.....	109
Figure 4.2 Boiling curve hysteresis. ....	111
Figure 4.3 Boiling regimes of FC-72 on porous graphite and copper .....	112
Figure 4.4 Photographs of different boiling regimes of FC-72 on porous graphite. ....	113
Figure 4.5 Natural convection data of dielectric liquids on smooth, porous, micro-structured, and micro-porous surfaces .....	117
Figure 4.6 Saturation and subcooled pool boiling curves of FC-72 on porous graphite and plane copper. ....	119
Figure 4.7 Saturation and subcooled pool boiling curves of HFE-7100 on porous graphite and plane copper .....	120
Figure 4.8 Comparison of boiling curves for HFE-7100 and FC-72 on porous graphite and copper. ....	123
Figure 4.9 Photographs of boiling of FC-72 and HFE-7100 on porous graphite and plane copper at similar surface superheats. ....	126
Figure 4.10 Effect of subcooling on pool boiling of HFE-7100 and FC-72 on copper and porous graphite.....	128
Figure 4.11 Ratio of nucleate boiling heat transfer coefficient on porous graphite to copper.....	129
Figure 4.12 Effect of aging on pool boiling of FC-72 on porous graphite. ....	131
Figure 4.13 Effect of inclination angle on saturation and subcooled pool boiling of FC-72 on porous graphite.....	133
Figure 4.14 Comparison of saturation pool boiling curves of FC-72 and HFE-7100 at different inclinations on smooth copper. ....	136
Figure 4.15 Saturation boiling curves of FC-71 and copper at different inclinations. ...	137
Figure 4.16 Saturation boiling curves of HFE-7100 on porous graphite and copper at different inclinations. ....	138
Figure 4.17 Saturation nucleate boiling heat transfer coefficient for FC-72 and HFE-7100 on porous graphite and plane copper. ....	140
Figure 4.18 Ratios of saturation FC-72 nucleate boiling heat transfer coefficient on porous graphite and plane copper. ....	142
Figure 4.19 Boiling resistance for saturated and subcooled FC-72 and HFE-7100 on porous graphite at different inclination angles.....	144
Figure 4.20 Saturation CHF coefficients for FC-72 and HFE-7100 of different surfaces. ....	146
Figure 4.21 Effect of surface inclination on saturation CHF of FC-72 and HFE-7100 on different surfaces.....	148
Figure 4.22 Effect of inclination on and liquid subcooling on CHF of FC-72 and HFE-7100 boiling on porous graphite. ....	151
Figure 4.23 Relative decrease in saturation CHF of dielectric liquids on plane copper, micro-porous coatings, and porous graphite.....	152
Figure 4.24 Ratios of saturation CHF of FC-72 on porous graphite and micro-porous coatings to that measured on copper. ....	154
Figure 4.25 Effect of liquid subcooling on CHF of FC-72 on different surfaces. ....	156

Figure 4.26 Effect of liquid subcooling on CHF of HFE-7100 on different surfaces. ...	158
Figure 4.27 Summary of the effect of liquid subcooling and surface characteristics on CHF of FC-72. ....	159
Figure 4.28 Effect of surface inclination on subcooled CHF coefficient for porous graphite. ....	161
Figure 4.29 Effect of surface inclination on subcooled HFE-7100 CHF coefficient for copper. ....	162
Figure 4.30 CHF subcooling coefficient on plane porous graphite and copper as a function of inclination angle. ....	163
Figure 4.31 Predicted and measured CHF values for saturation and subcooled boiling on porous graphite and plane copper. ....	165
Figure 4.32 Photograph and sketch of low heat flux heat transfer in porous graphite. ..	166
Figure 4.33 Photograph and sketch of moderate heat flux heat transfer in porous graphite. ....	168
Figure 4.34 Photographs of saturation and subcooled nucleate boiling on porous graphite and smooth copper at similar heat fluxes. ....	169
Figure 4.35 Photographs of FC-72 saturation boiling on porous graphite and copper ( $\theta = 60^\circ$ ). ....	171
Figure 4.36 Photographs of FC-72 saturation boiling on porous graphite and copper ( $\theta = 90^\circ$ ). ....	172
Figure 4.37 Photographs of FC-72 saturation boiling on porous graphite and copper ( $\theta = 120^\circ$ ). ....	173
Figure 4.38 Photographs of FC-72 saturation boiling on porous graphite and copper ( $\theta = 150^\circ$ ). ....	174
Figure 4.39 Photographs of FC-72 saturation boiling on porous graphite and copper ( $\theta = 180^\circ$ ). ....	175
Figure 4.40 Pumping action during saturation boiling of FC-72 on porous graphite at $\theta = 180^\circ$ ( $q'' = 11.9 \text{ W/cm}^2$ , $\Delta T_{sat} = 11.7 \text{ K}$ ). ....	177
Figure 5.1 Saturation boiling curve for HFE-7100 on porous graphite with 5 mm tall corner pins. ....	181
Figure 5.2 Thermal analysis of porous graphite with 5 mm corner pins at 65 W. ....	183
Figure 5.3 Photograph of test porous graphite with corner pins after tests. ....	185
Figure 5.4 Natural convection data of plane Cu and Cu surface with corner pins ....	186
Figure 5.5 Saturation boiling curve for a Cu surface with 3 mm corner pins at $\theta = 90^\circ$	188
Figure 5.6 Effect of pin height on saturation boiling of HFE-7100 on plane Cu and Cu surfaces with corner pins. ....	190
Figure 5.7 Saturation boiling curves for HFE-7100 at different surface inclinations. ...	192
Figure 5.8 Effect of surface orientation on nucleate boiling heat transfer coefficient for saturation boiling of HFE-7100 on copper corner pins. ....	193
Figure 5.9 Effect of pin height and orientation on the nucleate boiling heat transfer coefficient. ....	195
Figure 5.10 Effect of the corner pin height on saturation nucleate boiling heat transfer coefficients based on footprint and total area. ....	197
Figure 5.11 Effect of surface orientation on $h^*$ based on footprint and total area. ....	199
Figure 5.12 SEM images of copper surfaces. ....	200

Figure 5.13 Effect of surface roughness on nucleate boiling on Cu surfaces with corner pins.....	201
Figure 5.14 Effect of surface orientation and surface roughness on $h^*$ .....	202
Figure 5.15 Saturation boiling curves for HFE-7100 on copper with different lengths of corner pins and at different inclinations.....	204
Figure 5.16 Effect of liquid subcooling on boiling of HFE-7100 on inclined extended copper surfaces.....	206
Figure 5.17 Effect of surface orientation and subcooling on boiling resistance.....	208
Figure 5.18 Power removal at CHF of saturation boiling of dielectric liquids on extended surfaces in the upward facing orientation. ....	210
Figure 5.19 Saturation CHF coefficient in the upward facing orientation $C_{CHF,sat}(0^\circ)$ ...	213
Figure 5.20 Effect of area ratio on saturation CHF in the upward facing orientation. ...	214
Figure 5.21 Relative decrease in CHF on Cu with different pin heights. ....	217
Figure 5.22 Effect of subcooling of CHF on plane surface and Cu surfaces with corner pins.....	218
Figure 5.23 Subcooling coefficients for all surfaces and orientations.....	222
Figure 5.24 Effect of area ratio on the subcooling coefficient at different orientations. ....	223
Figure 5.25 Measured and predicted CHF for plane and extended surfaces. ....	224
Figure 5.26 Boiling incipience from base of a corner pin .....	225
Figure 5.27 HFE-7100 saturation boiling curve for Cu with 3 mm corner pins at $\theta = 90^\circ$ . .....	227
Figure 5.28 Photographs of saturation boiling of HFE-7100 on 5 mm Cu corner pins at different inclination angles. ....	228
Figure 5.29 Photographs of subcooled boiling in the upward facing orientation. ....	230
Figure 5.30 Photographs of saturation and subcooled boiling in the vertical orientation. .....	231
Figure 5.31 Photographs of saturation and subcooled boiling in the downward facing orientation. ....	233
Figure 5.32 Rise frequency of vapor clusters near CHF.....	235
Figure 5.33 Formation and departure of vapor clusters near boiling surface. ....	236
Figure A.0.1 Layout of test section for thermal analysis.....	258
Figure B.0.1 Saturation boiling of HFE-7100 on plane copper with associated uncertainties. ....	263

## List of Tables

Table 1.1 Selected thermal and physical properties of HFE-7100, FC-72, and Water (3M, 2001; 2003) .....	7
Table 1.2 Environmental and electrical properties of HFE-7100 and FC-72 (3M, 2001)..	7
<b>Table 2.1 Summary of selected investigations on enhanced boiling in dielectric liquids.</b> .....	43
Table 3.1 Estimated heat losses near CHF from test sections in saturation and subcooled boiling of FC-72.....	86
<b>Table 4.1. Comparison of boiling data for FC-72 and HFE-7100</b> .....	121
Table 4.2. Frequency of formation and rise of vapor slugs in saturation boiling of HFE-7100.....	176
Table B.1 Selected values and associated uncertainties for test measurements. ....	261

## Nomenclature

$A$	Area ( $\text{cm}^2$ )
$AR$	Area Ratio
$C$	Correlation coefficient
$CHF$	Critical Heat Flux ( $\text{W}/\text{cm}^2$ )
$CNT$	Carbon Nanotubes
$c_p$	Heat capacity at constant pressure ( $\text{J}/\text{kg K}$ )
$d_d$	Bubble departure diameter (m)
$f$	Ebullition cycle frequency ( $\text{s}^{-1}$ )
$F$	CHF correlation coefficient
$G$	General function
$g$	Gravitational acceleration ( $\text{m}/\text{s}^2$ )
$h$	Heat transfer coefficient ( $\text{W}/\text{m}^2 \text{K}$ )
$h^*$	Maximum or peak heat transfer coefficient ( $\text{W}/\text{cm}^2 \text{K}$ or $\text{W}/\text{m}^2 \text{K}$ )
$\bar{h}$	Surface averaged heat transfer coefficient ( $\text{W}/\text{cm}^2 \text{K}$ or $\text{W}/\text{m}^2 \text{K}$ )
$h_{fg}$	Latent heat of vaporization ( $\text{J}/\text{kg}$ )
$H$	Height of liquid above heated surface (m)
$I$	Current (A)
$Ja$	Jakob number
$k$	Thermal conductivity ( $\text{W}/\text{m K}$ )
$L$	Length (m)
$M$	General measurement of independent variable
$P$	Power (W)
$P_l$	Ambient liquid pressure (Pa)
$a$	Total heat or power (W)
$q''$	Heat flux ( $\text{W}/\text{cm}^2$ )
$q'''$	Volumetric heat generation ( $\text{W}/\text{m}^3$ )
$r$	Radius of a cavity opening (m)
$r_B$	Boiling thermal resistance ( $\text{K}/\text{W}$ )
$r_c$	Critical radius (m)

$R$	Angular dependent CHF coefficient
$t$	Time
$T$	Temperature (K)
$Th$	Thickness (m)
$V$	Voltage measurement (V)
$w$	General variable for function F
$x, y, z$	Cartesian coordinates

#### Greek Symbols

$\Delta$	Uncertainty estimate
$\delta_t$	Thermal boundary layer thickness (m)
$\Delta T$	Temperature difference (K)
$\mu$	Viscosity (kg/m s)
$\rho$	Density (kg/m <sup>3</sup> )
$\sigma$	Surface tension (N/m)
$\theta$	Inclination angle (°)

#### Subscripts

$AR$	Relating to area ratio
$b$	Bulk or pool
$B$	Relating to base or footprint
$cav$	Cavity
$CHF$	At Critical Heat Flux
$E$	Enhanced surface
$epo$	Epoxy filler
$ex$	Excursion
$g$	Growth
$htr$	Heater
$i$	Index counter
$inc$	At incipient boiling
$l$	Liquid

<i>Lex</i>	Lexan
<i>loss</i>	Refers to estimated heat losses
<i>max</i>	Maximum
<i>min</i>	Minimum
<i>NC</i>	Natural convection
<i>NB</i>	Nucleate boiling
<i>OB</i>	Omegabond 200 epoxy
<i>S</i>	Smooth surface
<i>sat</i>	At saturation conditions
<i>sf</i>	Surface
<i>sub</i>	At subcooled conditions
<i>Tef</i>	Teflon
<i>v</i>	Vapor
<i>w</i>	Wall or surface
<i>wait</i>	Waiting

# 1 Introduction

As the speed of microprocessors and CPU chips continue to increase, the dissipated power and local heat flux at the hot spot also increase. The latter could be two to three times the surface average heat flux. Current dissipation heat fluxes from high performance computer chips exceed  $100 \text{ W/cm}^2$  and are projected to increase (Refai-Ahmed, 2007; Xu, Buenin, and Vogel, 2004; ITRS, 2007; Knickerbocker et al. 2002). Figure 1.1a shows that over the past few decades the clock speed of chips has been doubling about every two to three years. The surface average heat flux also has been increasing, and is currently between  $50$  and  $150 \text{ W/cm}^2$  (Figure 1.1b). If the current trends continue, the average heat fluxes will exceed  $300 \text{ W/cm}^2$  in a few years (Refai-Ahmed, 2007). In addition, there is a non-uniform heat flux from the chip surface. Figure 1.2a shows a power density map of a  $1 \times 1 \text{ cm}$  chip operating at  $90 \text{ W}$  (Lin and Banjeree, 2008). The bright spots in the figure show localized heat flux values above  $250 \text{ W/cm}^2$ , leading to temperature gradients along the chip. Figure 1.2b shows that for this chip, the temperature difference between the hot spots and the coldest portion of the chip is  $10 - 15 \text{ }^\circ\text{C}$ . The high and non-uniform dissipation heat flux from the surface of CPU chips induces mechanical stresses that could damage the chips and /or shorten their service lifetime. Therefore, it is important not only to efficiently remove the dissipated power, but also to minimize the temperature gradient across the chip. Because of the ever-increasing dissipation power by CPU chips, cooling methods are transitioning from air based to liquid-based. Using liquids as cooling media offers the advantage of greater convective heat transfer and much larger heat transfer rates with boiling at near isothermal conditions.

Liquid cooling methods that are being considered include forced convection in microchannels, spray and impinging jets, capillary pumped loops, and direct immersion cooling (Rainey and You, 2000; Arik and Bar-Cohen, 2001; Mathews, Lee, and Peters, 2003; El-Genk and Bostanci, 2003a,b; Maydanik et al, 2004; Chen et al, 2004). In direct immersion cooling, the CPU or the circuit board or heat sink structure is fully submerged in either a stagnant or a flowing dielectric liquid, such as FC-86, FC-72, PF-5060, and

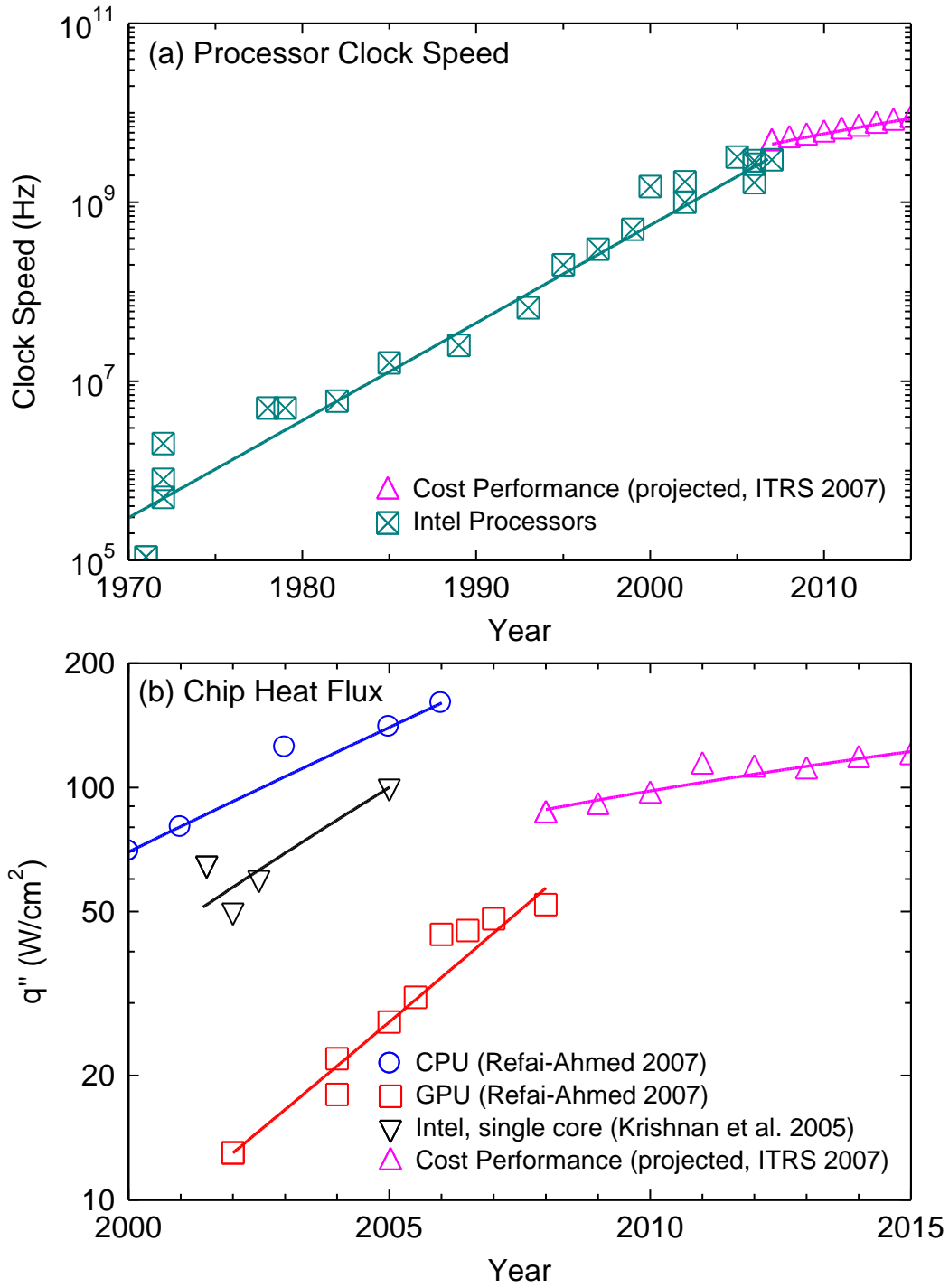
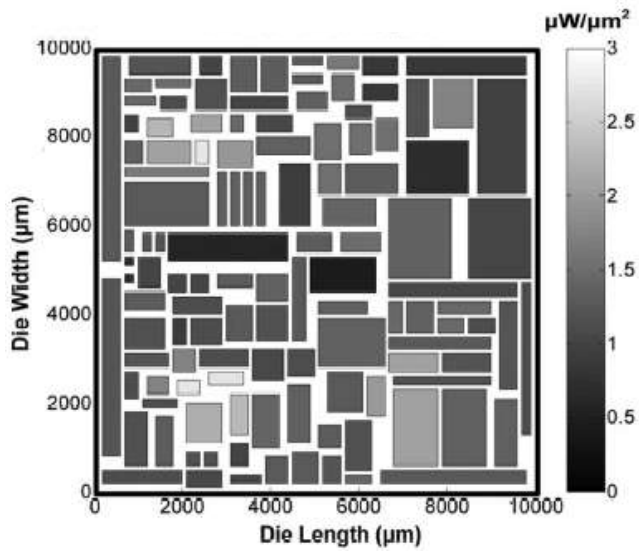
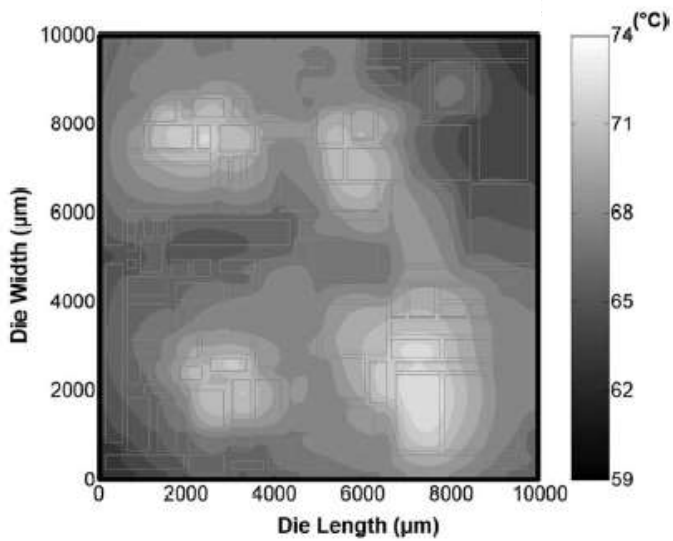


Figure 1.1 Increase in clock speed and dissipated power for high performance computer chips.



(a) Power density map of chip.



(b) Temperature profile.

**Figure 1.2. Block layout of computer chip showing map of power density and temperature profile  
(from Lin and Banerjee, 2008)**

HFE-7100. Because of the potential for direct contact between the liquid and the hot electronics, it is imperative that the selected liquid be chemically inert and dielectric and have a relatively low saturation temperature ( $< 80$  °C). However, these highly wetting liquids have poor thermo-physical properties compared with non-dielectric liquids such as water, and thus methods to improve the boiling heat transfer must be employed to achieve a nucleate boiling heat transfer rate sufficient to remove the dissipated power.

Some approaches for improving nucleate boiling heat transfer of dielectric liquids have focused on increasing the active nucleation site density using surfaces with fabricated pores, porous and roughened surfaces, micro-porous coatings, and surfaces covered fully or partially with carbon nanotubes (Parker and El-Genk 2005; Vemuri and Kim 2005; Nimkar, Bhavnani, and Jaeger 2006; Jung and Kwak 2006; Yu, Lu, and Cheng 2006; Launay et al., 2006; Ujereh, Fisher, and Mudawar, 2007; Arik, Bar-Cohen, and You 2007). In addition to increasing the nucleate boiling heat transfer coefficient,  $h_{NB}$ , and the Critical Heat Flux (CHF), these surfaces reduced, and in some cases eliminated, the temperature excursion prior to boiling incipience of dielectric liquids.

Other approaches have focused on increasing the rate of removal of dissipated heat from the underlying surface by increasing the total surface area in contact with the boiling dielectric liquid. Surfaces with micro-fins, micro- and macro-structures, and pins of various length, cross section and density have been investigated (Nakayama et al. 1980; Anderson and Mudawar 1989; Misale et al. 1999; Rainey and You 2000; Wei and Honda 2003; Ramaswamy et al. 2003; Ghiu and Joshi 2005; Geisler and Bar-Cohen 2005; Al-Hajri et al. 2005; Ferjančič, Rajšelj, and Golobič 2006; Launay et al. 2006; Yu and Lu 2007; Ujereh, Fisher, and Mudawar 2007). These extended surfaces can be divided into two general categories: (a) micro-structured surfaces with a length scale  $< \sim 0.5$  mm, and (b) macro-structures surfaces with a length scale  $> \sim 0.5$  mm. Other criteria have also been used in the literature to classify micro-structured and macro-structured surfaces.

Most of the reported work with these surfaces has been for saturation boiling in the upward-facing orientation; only a few experimental studies have also investigated

nucleate boiling in the vertical orientation. The reported work has investigated other parameters affecting nucleate boiling, such as the properties of the dielectric liquids, surface roughness and orientation, and liquid subcooling. These parameters are discussed in the next subsections.

## **1.1 Boiling of Dielectric Liquids**

Direct immersion cooling implies immediate contact between the liquid and the heated electronic component and for this reason, the liquid must be dielectric. For submersion cooling applications, the most promising dielectric liquids are those with saturation temperatures  $< 80$  °C, such as the Fluorinert FC-72 and Novec HFE-7100. Tables 1.1 and 1.2 list some of the thermophysical properties of these liquids as compared to water as well as some of the environmental and electrical properties. The dielectric properties and chemical inertness of HFE-7100 and FC-72 make them candidate liquids for direct immersion cooling of computer chips. Because of the high elevation of Albuquerque, New Mexico ( $\sim 1600$  m), where all experiments were completed, the properties are listed for sea level atmospheric pressure and the local atmospheric pressure ( $\sim 0.085$  MPa).

These dielectric liquids are environmentally friendly and chemically inert, however, they have very low surface tensions. These highly wetting liquids reduce the amount of air entrapped in surface cavities for promoting bubble nucleation. As a result, boiling incipience of dielectric liquids on commercial surfaces is delayed until reaching high superheats that could exceed 35 K (Rainey and You, 2000; El-Genk and Parker, 2004a,b; Chang, You, and Haji-Sheikh, 1998; El-Genk and Bostanci, 2003a,b), also referred to as temperature excursion. Such high temperature excursions occur at low surface heat fluxes, which are at or below those of the CPUs chips in actual devices operating for extended periods of time in stand-by mode. Consequently, the lifetime of these devices could be reduced and their failure frequency increased (Peterson, 1994).

**Table 1.1 Selected thermal and physical properties of HFE-7100, FC-72, and Water (3M, 2001; 2003)**

Physical Properties at Saturation	HFE-7100 (0.1 MPa)	HFE-7100 (0.085 MPa)	FC-72 (0.1 MPa)	FC-72 (0.085 MPa)	Water (0.1 MPa)
Boiling Point (°C)	60	54	56	52	100
Freeze Point (°C)	-135	-135	-90	-90	0
Average Molecular Weight (g/mole)	250	250	338	338	18
Liquid Density (kg/m <sup>3</sup> )	1372	1387	1599	1619	958
Vapor Density (kg/m <sup>3</sup> )	9.7	8.1	13.4	11.4	0.6
Viscosity (kg/m s)	3.7x10 <sup>-4</sup>	3.9x10 <sup>-4</sup>	4.8x10 <sup>-4</sup>	4.4 x10 <sup>-4</sup>	2.8 x10 <sup>-4</sup>
Specific Heat (J/kg K)	1253	1241	1102	1094	4220
Latent Heat of Vaporization (kJ/kg)	111.5	113.4	94.8	96.4	2256.7
Thermal Conductivity (W/m K)	0.062	0.063	0.054	0.054	0.68
Surface Tension (N/m)	0.010	0.011	0.0083	0.00864	0.059

**Table 1.2 Environmental and electrical properties of HFE-7100 and FC-72 (3M, 2001)**

	HFE-7100	FC-72
Environmental Properties		
Ozone Depletion Potential (CFC-11 = 1.0)	0	0
Global Warming Potential (100 y integrated time horizon)	320	7400
Atmospheric Lifetime (y)	4.1	3200
Electrical Properties		
Dielectric Strength (kV in 0.1" gap @ 25 °C)	28	38
Dielectric Constant (@ 25 °C)	7.39 (100 – 10 <sup>7</sup> Hz)	1.75 (1 kHz)
Volume Resistivity (Ω cm @ 25 °C)	3.3 x10 <sup>9</sup>	1 x10 <sup>15</sup>

FC-72 (C<sub>6</sub>F<sub>14</sub>, perfluorohexane) and HFE-7100 (C<sub>4</sub>F<sub>9</sub>OCH<sub>3</sub>, methoxy-nonafluorobutane) have been the subject of extensive research on electronics cooling by nucleate boiling. Their chemical and physical properties are compatible with common materials used in computers. The saturation temperature for FC-72 are low enough to keep the junction temperature of commercial chips below 85 °C. At these temperatures, standard packaging materials and handling procedures may be used.

The poor thermophysical properties of dielectric liquids result in lower nucleate boiling heat transfer rates than non-dielectric liquids, such as water. Enhancements in nucleate boiling are realized through increasing the number density of the active

nucleation sites on the surface, increasing the total surface area over which boiling occurs, and/or the increasing the frequency of the departing vapor bubbles. It is well established that the low surface tension of dielectric liquids decreases the bubble departure diameter and increases the bubble departure frequency and thus increases the nucleate boiling heat removal rate. In addition, increasing the nucleation site density decreases the wall superheat and increases the nucleate boiling heat flux (Ivey, 1967; Mikic and Rohsenow, 1969). The small surface tension of dielectric liquids such as FC-72 and HFE-7100 decreases the diameter of detaching bubbles to  $\sim 0.50 - 0.55$  mm, compared to  $2 - 3$  mm for water at atmospheric pressure.

Ramaswamy et al. (2002) have measured the average detachment diameter of FC-72 bubbles from a structured porous surface to be  $\sim 0.5 - 0.7$  mm and the average departure frequency  $\sim 150 - 200 \text{ s}^{-1}$ , depending on the wall superheat. Rini, Chen, and Chow (2001) measured the departure diameter of a bubble to be between  $0.4$  and  $0.5$  mm for the same liquid boiling on a synthetic diamond surface, and the departure frequency increased from  $\sim 100 \text{ s}^{-1}$  to  $\sim 170 \text{ s}^{-1}$  as the heat flux increased. The reported values of the average diameter of detaching bubbles in pool boiling experiments of HFE-7100 on copper is  $\sim 0.55$  mm with a frequency of  $100 \text{ s}^{-1}$  (El-Genk and Bostanci, 2003a,b).

To quantify the difference in nucleate boiling of different liquids, Marto and Lepere (1982) experimented with R-113 and FC-72 on commercially available enhanced surfaces. They reported that the temperature excursion at boiling incipience ( $10 - 11$  K) and the boiling incipience superheat ( $1 - 4$  K) were larger for R-113 than for FC-72 ( $5-8$  K and  $1-3$  K, respectively). Arik and Bar-Cohen (2001), El-Genk and Bostanci (2003 a,b), Priarone (2005), Parker and El-Genk (2006a,b), and El-Genk and Parker (2008) all reported higher critical heat flux for saturation and subcooled boiling of HFE-7100 than for FC-72. Danielson, Tousignant, and Bar-Cohen (1987) conducted a study that investigated saturation boiling on a platinum wire with several different inert liquids (FC-43, FC-72, FC-75, FC-77, FC-84, FC-87, L-1402, and R-113). One of their findings is that a temperature overshoot nearly always occurs at boiling incipience, however the magnitude varied. They reported little differences in the boiling heat transfer rate of the different liquids on the same heater wire. However, the boiling curves differed from wire

to wire, even among tests with the same liquid, showing that boiling heat transfer is highly dependent on the surface characteristics. Previous research investigating the effect of the surface is discussed in the next section.

## **1.2 Effect of Surface Conditions**

Past research has shown that changing the roughness or modifying morphology or structure of the surface affects the heat removal rate during nucleate boiling. Kurihara and Myers (1960) have investigated boiling of different liquids on different surfaces and concluded that the nucleate boiling heat transfer coefficient is proportional to the active nucleation site density, which is directly related to the roughness of the surface. Similarly, Ramilison, Sadasivan, and Lienhard (1992), based on data obtained from the open literature, determined that CHF increases with increasing surface roughness, which was confirmed by Ferjančič and Golobič (2002) for both FC-72 and water. Likewise, increasing the total wetted surface area increased the thermal power removed by nucleate boiling. The following paragraphs briefly summarize some of the reported work on pool boiling on roughened, porous, and extended surfaces.

Honda, Takamatsu, and Wei (2002) reported results on saturation and subcooled ( $\Delta T_{\text{sub}} = 3, 25, \text{ and } 45 \text{ K}$ ) boiling of FC-72 on smooth silicon and silicon sputtered with  $\text{SiO}_2$  and chemically etched to a RMS roughness of 25 - 32 nm. The measured temperature excursions at boiling incipience on smooth silicon were as much as 18 K, but only  $\sim 10 \text{ K}$  on the roughened surface. The lower temperature excursions on the latter may be attributed to the larger amount of trapped air in the surface features. In addition to the reported enhancement in nucleate boiling, CHF was  $\sim 40\%$  higher than on smooth Si. Rainey and You (2000) have reported similar enhancements in nucleate boiling of FC-72 on a machine roughened copper surface. The reported temperature excursion at boiling incipience was lower than on a polished copper surface. The value of CHF for FC-72 on roughened Cu of  $18.8 \text{ W/cm}^2$  was  $\sim 40\%$  higher than on polished Cu ( $13.2 \text{ W/cm}^2$ ).

Many saturation and subcooled boiling experiments of FC-72 liquid on micro-porous coatings have been reported with very promising results. The tiny pores in micro-porous coatings are believed to range in size from 0.1 – 1  $\mu\text{m}$  (Rainey and You, 2000; Rainey, You, and Lee, 2003; Kim et al., 2007). However, those coatings made with 1-20  $\mu\text{m}$  particles bonded with epoxy, have low effective thermal conductivity of  $\sim 0.95 \text{ W/m K}$  (O'Connor and You, 1995). With thin layers of the coatings ( $\sim 50 \mu\text{m}$ ) applied to flat surfaces and wires, a significant enhancement in nucleate boiling heat flux of FC-72 liquid at lower surface superheat and a decrease in the temperature excursions at incipient boiling have been reported (Rainey and You, 2000; Chang and You, 1996; Chang and You, 1997a,b; Rainey, You, and Lee, 2003; O'Connor, You, and Chang, 1996; Kim et al, 2007). The results have been attributed to the increase in the number of nucleation sites as well as the ability to entrap air in the micro-pores of the coatings. In saturation boiling of FC-72 on surfaces with micro-porous paint, O'Connor, You, and Chang (1996) reported  $\sim 330\%$  increase in the nucleate boiling heat flux and  $\sim 100\%$  increase in CHF, compared to untreated copper surfaces. For FC-72 on micro-porous coatings, increases of  $\sim 33\%$  in nucleate boiling heat flux and  $\sim 100\%$  in CHF, compared to untreated copper, have been reported (Chang and You, 1997b). The results of Kim et al. (2007) for saturation boiling of FC-72 showed an increase in the nucleate boiling heat transfer coefficient up to 250% and an increase in CHF of up to 40%, depending on the size of the particles used. These paints are not commercially available and must be made on site if they are to be used.

Both Ujereh, Fisher, and Mudawar (2007) and Launay et al. (2006) grew carbon nanotubes on silicon and copper surfaces, both flat and structured, to study the effect of carbon nanotubes on saturation boiling of FC-72 and PF-5060 (identical to FC-72). The carbon nanotubes generally increased the nucleate boiling heat transfer rate and reduced or eliminated the temperature overshoot at boiling incipience. However, the values of CHF did not increase as much as with other surfaces. Ujereh, Fisher, and Mudawar (2007) reported that CHF for FC-72 on a silicon surface fully coated with carbon nanotubes increased by 6-44% over that on an uncoated silicon surface. Launay et al

(2006) reported essentially the same CHF on both uncoated and carbon nanotubes coated surfaces.

Kim (2006) reported results for saturation boiling of FC-72 on high thermal conductivity coatings. One is a copper coating electrodeposited onto a copper substrate, forming a porous structure. For the other coating, nickel micro-spheres (8 – 12  $\mu\text{m}$ , 30 – 50  $\mu\text{m}$ , and 150 – 200  $\mu\text{m}$  diameter) were soldered onto a copper substrate. The peak heat transfer coefficient reported (electrodeposited surface) increased nearly 600% over that on the plain surfaces and the CHF increased by nearly 65% (on the surface with Ni spheres).

### **1.2.1 Surface Structure**

In saturation pool boiling of FC-72 on commercially available, structured surfaces (Union Carbide's High Flux, Hitachi's Thermoexel-E, and Wieland's Gewa-T) Marto and Lepere (1982) have reported 2-5 times increase in the nucleate boiling heat flux and lower incipient boiling temperatures compared to commercial grade copper tubes. In addition, on the three structured surfaces, the temperature excursion prior to boiling incipience was lower. They reported little or no enhancement in the CHF. In the same investigation, but with a Turbo-B surface, they reported a 91% increase in CHF.

Baldwin, Bhavnani, and Jaeger (1998) have investigated saturation boiling of FC-72 liquid on surfaces with bulb- and pyramidal-shaped re-entrant cavities having center-to-center spacing of 0.5, 1.0, and 1.5 mm. The cavity mouths were 45  $\mu\text{m}$  rounded squares. The surface with pyramidal shaped cavities resulted in higher nucleate boiling heat transfer rate and CHF than smooth surfaces and surfaces with bulb shaped cavities. The reported CHF of  $\sim 40 \text{ W/cm}^2$  for FC-72 liquid on the surface with pyramidal-shaped re-entrant cavities is 15% higher and the corresponding surface superheat of  $\sim 35 \text{ K}$  is 40% lower than those measured on the surface with bulb shaped cavities. This CHF value is also much higher than those reported for FC-72 on smooth surfaces of  $\sim 13 - 16 \text{ W/cm}^2$  (Chang and You, 1996; Chang and You, 1997a,b; J. W. Liu et al., 2001; Watwe, Bar-Cohen, and McNiel, 1997).

Kubo, Takamatsu, and Honda (1999) studied nucleate boiling of subcooled ( $\Delta T_{\text{sub}} = 3$  K and 25 K) FC-72 liquid on smooth silicon and of silicon with re-entrant cavities. The cavities with average mouth diameters of 1.6 and 3.1  $\mu\text{m}$  were spaced 1.0 mm and 0.1 mm and had a number density of 81/cm<sup>2</sup> and  $9.3 \times 10^3/\text{cm}^2$ , respectively. The surfaces with the re-entrant cavities showed increases in the nucleate boiling heat flux and CHF; the best results are for the surface with the large number density of cavities with larger mouth sizes. For degassed and 25 K subcooled FC-72, nucleate boiling ensued on the surface with re-entrant cavities at a superheat of  $\sim 4.8$  K, compared to  $\sim 15$  K on smooth silicon.

Arbelaez, Sett, and Mahajan (2000) investigated saturation boiling of FC-72 on aluminum foam measuring 2.54 x 6.35 x 6.35 cm with porosities of 90 – 98% and 5 - 40 pores per linear inch. Measured surface superheats at boiling incipience were 8-10 K with no temperature excursion, except in two cases where it was 12 K. The nucleate boiling heat flux was  $\sim 5$  times higher and CHF (28.8 W/cm<sup>2</sup>) was  $\sim 50\%$  higher than those on measured on a machined aluminum block measuring 1.0 x 2.5 x 2.5 cm, however, the surface superheat at CHF on the foam was  $\sim 40$  K higher than the CHF superheat on the reference aluminum block.

### **1.2.2 Extended Surfaces**

One method to increase the total heat removal rate by nucleate boiling is to increase the surface area wetted with the boiling liquid for the same footprint. Several extended surfaces with pins, pores, and fins of varying length, density and thickness, have been tested in boiling experiments of dielectric liquids. These surfaces may be divided into two categories based on the bubble departure diameter: (a) micro-structured surfaces (length scale  $< 0.5$  mm), and (b) macro-structured surfaces (length scale  $> 0.5$  mm). Other criteria for defining macro-structured and micro-structured surfaces have also been reported and used in the literature. Although micro-structured surfaces greatly increase the wetted surface area, tight structure spacing tends to restrict the upward flow of vapor and the downward flow of liquid, which may reduce the nucleate boiling heat transfer.

The following sections discuss some of the reported research on pool boiling of dielectric liquids on both micro- and macro-structured surfaces.

### **1.2.2.1 Micro-Structured Surfaces (Length Scale < 0.5 mm)**

Nakayama et al. (1980) have investigated pool boiling of R-11 on a copper with parallel channels running underneath a lid in which openings of various sizes were punched, making a network of small, interconnected pores. They reported large enhancement in the nucleate boiling heat transfer and as much as a 90% reduction in the wall superheat compared to a plane Cu surface at the same heat flux. The captured images of the surface in the pool boiling experiments suggested significant boiling inside the interconnected tunnels.

On surfaces with micro-fins, micro-studs, and inclined microgrooves, Anderson and Mudawar (1989) have reported higher values of the FC-72 nucleate boiling heat flux and CHF based on the footprint area, compared to a plane, mirror-polished surface of the same footprint. Saturation boiling CHF for FC-72 on the plane surface was  $19.8 \text{ W/cm}^2$ , compared to  $30.0$ ,  $34.6$ , and  $51.2 \text{ W/cm}^2$  on the surfaces with micro-grooves, micro-fins, and micro-studs, respectively. However, the surface superheats at CHF on these surfaces exceeded  $40 \text{ K}$ . The corresponding surface temperature of  $> 96 \text{ }^\circ\text{C}$  is higher than recommended by industry for the chip junctions ( $85 \text{ }^\circ\text{C}$ ).

Experiments by Misale et al (1999) investigated the effect of pin width and pin spacing on saturation pool boiling of FC-72. The copper surface had  $3 \text{ mm}$  high pins,  $0.4 \text{ mm}$  wide or  $0.8 \text{ mm}$  wide. The pin spacing was the same as the pin width. The experiments were conducted in both the upward facing and the vertical orientations. They reported that for both surface configurations CHF in the upward facing orientation was slightly higher than in the vertical orientation, and that the surface with the smaller pin widths and spacing (more surface area) performed slightly better than the surface with the  $0.8 \text{ mm}$  pins.

The effects of the height and thickness of the square micro-pins on saturation boiling of FC-72 on a  $10 \times 10 \text{ mm}$  silicon surface with micro-pins have been investigated by

Honda, Takamatsu, and Wei (2002), Wei and Honda (2003), and Wei, Guo, and Honda (2005). The thickness and height of the pins varied from 30 to 50  $\mu\text{m}$ , and from 60 – 270  $\mu\text{m}$ , and the pitch was twice the pin thickness. The results showed a significant increase in the total thermal power removed in nucleate boiling, compared to previous data on a plane silicon surface of the same dimensions (10 x 10 mm). Surface roughness etched into the pin flanks during the fabrication process improved nucleate boiling by increasing the number of active nucleation sites. The reported CHF values based on the same footprint area (10 x 10 mm) (26.1 – 32.4  $\text{W}/\text{cm}^2$ ) are 60% to 100% higher than on a plane silicon surface (16.2  $\text{W}/\text{cm}^2$ ). The higher CHF values were a direct result of both the increase in the total wetted surface area with the FC-72 liquid and the nucleation site density on the roughened surface.

Ramaswamy et al. (2003) have investigated the effect of pore size, and the pitch and height of the structure of a micro-fabricated copper and silicon surfaces on saturation boiling of FC-72 . The rate of heat removal generally increased as the pore size increased and/or the pitch of the microstructure decreased. The heat removal rate at low ( $< 6 \text{ K}$ ) and high surface superheats ( $> 25\text{K}$ ) increased as the height of the structure increased, but at the intermediate surface superheats, the reported improvement in heat removal rate was negligible.

Ghiu and Joshi (2005) have used a single layer of copper microstructure, similar to that of Ramaswamy et al. (2003), to investigate the effect of varying the channel width and pitch in the microstructure on saturation boiling of PF-5060. Results showed measurable enhancement in the total power removed as the width of the micro-channels increased (65 – 105  $\mu\text{m}$ ) and the pitch decreased (0.2 – 0.7 mm). They reported no CHF, as they terminated the experiments when the base temperature of the copper microstructures reached or exceeded 85  $^{\circ}\text{C}$  ( $\Delta T_{sat} = 29 \text{ }^{\circ}\text{C}$ ), which occurred prior to CHF.

Al-Hajri et al. (2005) have investigated saturation boiling of HFE-7100 on micro-finned, copper surfaces. They varied the fin density from 100 to 200 per linear inch, thickness from 85 to 170  $\mu\text{m}$ , and height from 229 – 899  $\mu\text{m}$ . On these micro-finned structures with footprints of 10 x 10 mm and 10 x 17 mm, the average nucleate boiling

heat transfer coefficients based on the footprint were 1.5 - 2.8 W/cm<sup>2</sup> K, and in one test the heat transfer coefficient at CHF was 5.0 W/cm<sup>2</sup> K. The reported CHF values based on the footprint area varied from 35 - 45 W/cm<sup>2</sup>. Increasing the fins spacing and/or height increased CHF and the corresponding surface superheat.

The experiments performed by Launay et al. (2006) investigated saturation boiling of PF-5060 dielectric liquid on many extended surfaces. One of the surfaces had a silicon microstructure (area ratio of 6.4), similar to those used by Ramaswamy et al. (1999, 2000, 2003) and by Ghiu and Joshi (2005), and other surfaces had cylindrical silicon micro-pins, 70 μm in diameter and 250 μm high, with a pitch of 200 μm, for an area ratio of 1.5. The experiments were terminated at CHF or when the wall temperature exceeded 85 °C, whichever came first. For the surfaces with micro-pins, they reported measurable improvement in the nucleate boiling heat transfer. The highest nucleate boiling heat flux based on the footprint area of 1.0 cm<sup>2</sup> (21 W/cm<sup>2</sup>) occurred at a surface temperature of 85 °C. The reported heat flux for a plane surface at the same surface temperature was only 12 W/cm<sup>2</sup>. On the surface with the silicon micro-structure, CHF (27 W/cm<sup>2</sup>) is 2.25 times the highest nucleate boiling heat flux obtained on plane silicon at a footprint surface temperature of 85 °C.

Ujereh, Fisher, and Mudawar (2007) recently investigated saturation boiling of FC-72 on copper surfaces with microstuds and microstuds with carbon nanotubes. The cubic microstuds were 250 μm on the side and had a pitch of 500 μm. The surface footprint was 12.7 x 12.7 mm. The reported CHF based on the footprint area for the surface with the uncoated microstuds was 32 W/cm<sup>2</sup>, however, the highest heat transfer coefficient was only 1.19 W/cm<sup>2</sup> K; ~ 10% lower than the highest value on plane copper. The micro-studded surface configuration reduced the surface temperature at boiling incipience.

Kahn, Toh, and Pinjala (2008) employed a silver based epoxy to attach a structure of micro-channels with micro-pores to a heated die which was cooled by saturation boiling of FC-72. The silver based epoxy, when cured, left a micro-porous structure on the die surface which effectively trapped air and promoted bubble nucleation without

temperature excursion. The overlying micro-channels with micro-pores increased the total boiling surface area. Their results, compared to those on a plane silicon surface, showed that the micro-channels with micro-pores reduced the surface temperature by about 50% for nucleate boiling heat fluxes less than  $10 \text{ W/cm}^2$ . The reported CHF for the surfaces with the different pore sizes and pitches ranged from  $26.6 \text{ W/cm}^2$  to  $38.3 \text{ W/cm}^2$ , compared to  $14.8 \text{ W/cm}^2$  for the plane silicon. The footprint temperature CHF, however, exceeded  $106 \text{ }^\circ\text{C}$  on the surfaces with enhanced structures.

### **1.2.2.2 Macro-Structured Surfaces (Length Scale > 0.5 mm)**

Rainey and You (2000) have investigated saturation boiling of FC-72 liquid on a copper surface with a  $5 \times 5$  array of square pins (1 mm wide and 1 - 8 mm high with a 2 mm pitch). The total rate of heat removal increased as the fin height increased, but the total surface averaged nucleate boiling heat transfer coefficient and CHF decreased. Such decreases were attributed to lower fin efficiency and higher resistance to departing vapor bubbles from the surface as the pin height increased.

Recently, Ferjančič, Rajšelj, and Golobič, (2006) investigated saturation boiling of FC-72 on structured porous surfaces composed of sintered cones of 200 and 50  $\mu\text{m}$  copper particles. The cones were 0.5 and 1 mm high and spaced 0.5 and 1 mm apart. The CHF values based on the footprint area of the surfaces with the smaller cones and larger cones were 1.34 and 2.23 times that on plane copper. They noted the absence of temperature overshoots prior to boiling incipience.

The most recent work of Yu and Lu (2007) used surfaces with an array of 1 mm wide and 0.5 – 4.0 mm high square pins spaced 0.5 - 2.0 mm apart. The pins increased the wetted area to 1.98 and 8.84 times that of the  $10 \times 10 \text{ mm}$  footprint. The wall superheat at boiling incipience decreased with increasing pin height and density. The total removed power increased with increasing pin height and decreasing pin spacing; however, the surface averaged CHF and the heat transfer coefficient decreased due to the increased resistance encountered by the departing bubbles in the small pin spacing.

### **1.3 Effect of Liquid Subcooling**

Most all of the reported results on nucleate boiling of dielectric liquids on enhanced surfaces have been for saturation, and some for subcooled liquid. Subcooled liquid improves the nucleate boiling heat transfer rate and increases CHF, but also increases the footprint temperature at CHF. The vapor in the detached bubbles from the heated surface condenses as the bubbles rise through the subcooled liquid pool. Liquid subcooling thus reduces the bubble crowding on the surface and increases the boiling heat transfer. It has been shown that CHF increases linearly with liquid subcooling in both non-dielectric liquids (Kutateladze, 1952; Zuber, Tribus, and Westwater, 1962; Ivey and Morris, 1966) and dielectric liquids (El-Genk and Bostanci, 2003b; Rainey, You, and Lee, 2003; O'Connor, You, and Chang, 1996; Wei and Honda, 2003; Watwe, Bar-Cohen, and McNiel, 1997). However, the rate of increase depends on the surface characteristics, the properties of boiling liquid, and the inclination angle of the surface. Generally, surfaces with micro-porous coatings and micro-fins have shown much higher rate of increase in CHF with liquid subcooling than smooth and roughened copper, silicon, and roughened SiO<sub>2</sub> surfaces. On smooth surfaces, CHF increases more rapidly with increased liquid subcooling for HFE-7100 than for FC-72 (El-Genk and Bostanci, 2003b; Z. W, Liu et al., 2001; Arik and Bar-Cohen, 2001; Rainey, You, and Lee, 2003; O'Connor, You, and Chang, 1996; Wei and Honda, 2003; Watwe, Bar-Cohen, and McNiel, 1997).

### **1.4 Effect of Surface Inclination**

Since electronics packaging may necessitate an orientation of the CPU or computer chips other than horizontal, several investigations have been reported on the effect of the surface inclination on nucleate boiling and CHF of dielectric liquids on smooth copper and surfaces with micro-porous coatings (Chang and You, 1996; El-Genk and Bostanci 2003a,b; Honda and Wei, 2003; Howard and Mudawar, 1999; Mudawar, Howard, and Gersey, 1997; Rainey and You, 2001; Reed and Mudawar, 1997, Priarone, 2005). Earlier work has also been reported for water, liquid nitrogen, and liquid helium boiling on inclined surfaces (Beduz, Scurlock, and Sousa, 1998; El-Genk and Guo, 1993; Nishikawa

et al. 1984; Vishnev et al., 1976). The reported results for dielectric and non-dielectric liquids have been consistent, confirming that:

(a) At low surface superheats, the nucleate boiling heat transfer coefficient increases as the inclination angle of the surface increases from  $0^\circ$  (upward facing) to  $180^\circ$  (downward-facing). Conversely, at high surface superheats, the nucleate boiling heat transfer coefficient decreases with increased inclination angle.

(b) CHF decreases slightly as the angle increases from  $0^\circ$  to  $90^\circ$  then decreases rapidly to its lowest value as the inclination angle increases to  $180^\circ$ . The saturation CHF values for dielectric liquids of FC-72 and HFE-7100 in the downward-facing orientation ( $180^\circ$ ) on smooth copper and micro-porous coatings are ~7% to 28% of those in the upward facing position ( $0^\circ$ ) (Chang and You 1996; El-Genk and Bostanci 2003a,b; Howard and Mudawar 1999; Mudawar, Howard, and Gersey 1997; Rainey and You 2001; Reed and Mudawar 1997, Priarone, 2005).

The reported dependency of the normalized CHF to that for the upward-facing orientation on the inclination angle is consistent for both FC-72 and HFE-7100 liquids on smooth copper and micro-porous coatings. The actual values of CHF, however, for HFE-7100 were much higher than for FC-72 and those on micro-porous coatings and micro-finned surfaces were higher than on smooth copper and on silicon (Chang and You 1997a,b; El-Genk and Bostanci 2003a,b; Honda, Takamastu and Wei 2003; Rainey, You, and Lee 2003; Wei and Honda 2003). Saturation CHF correlations that incorporated the effect of surface orientation have been developed for dielectric and non-dielectric liquids (Vishnev 1974; Chang and You 1996; El-Genk and Bostanci 2003a,b; El-Genk and Guo 2003, Priarone, 2005).

In summary, the enhancement in nucleate boiling depends on several factors. These include the liquid thermo-physical properties and subcooling, surface roughness and the structure and orientation of the heated surface. Previously reported work investigating the effect of liquid subcooling on nucleate boiling and CHF of dielectric liquids generally involved only one inclination angle (usually  $0^\circ$  or  $90^\circ$ ), and those focusing on the effect

of inclination angle used liquid at saturation conditions. The data in the literature are limited in reporting the combined effects of both surface orientation and liquid subcooling on nucleate boiling heat transfer and CHF of dielectric liquids, especially on porous, micro-porous, and extended surfaces. Electronic packaging may involve other orientations other than upward-facing such as vertical or downward facing, and will likely use subcooled liquid. Therefore further research in this area is needed. In addition, direct comparisons between boiling heat transfer and CHF of FC-72 and HFE-7100 on similar surfaces and liquid subcooling are limited.

### **1.5 Objectives**

The objectives of the present work are to experimentally investigate nucleate boiling of FC-72 and HFE-7100 dielectric liquids on plane porous graphite and copper and on copper surfaces with 3 x 3 mm square corner pins. These surfaces have the same footprint area of 10 x 10 mm. Of particular interest are improving the nucleate boiling heat transfer in these dielectric liquids, and reducing or eliminating the temperature excursion at boiling incipience, and removing 50 - 100 W of thermal power from a 1 cm<sup>2</sup> heated area. The liquids FC-72 and HFE-7100 are selected because their saturation temperatures (56 °C and 61 °C at atmospheric pressure) are favorable to maintain chip junction temperatures below 85 °C during nucleate boiling. Also, they are chemically compatible with common manufacturing materials used in computers and are environmentally friendly and have zero ozone depletion potential.

The variables in the experiments are liquid subcooling (up to 30 K), surface orientation (0° - 180°), surface roughness (copper prepared with #400 emery paper and #1500 emery paper) and the height of the corner pins (2 – 5 mm). The dimensions and spacing of the corner pins are chosen to reduce bubble crowding between the pins and reduce the fin effect, thus, increasing the wetted surface area while reducing the temperature gradient along the pins. The highly porous graphite (61% volume porosity) makes this an excellent choice to increase the nucleation site density of the heated surface. The high volume porosity and varying pore sizes trap air efficiently to induce

bubble nucleation and reduce or eliminate the temperature excursion at boiling incipience.

To quantify the enhancements in nucleate boiling heat transfer and critical heat flux, the results obtained from porous and extended Cu surfaces are compared to those obtained on plane copper under identical conditions. In addition, the effect of the surface roughness of the copper with corner pins is made. The nucleate boiling heat transfer rate and CHF are compared under otherwise identical experimental conditions (liquid subcooling and surface orientation) for surfaces prepared using #400 emery paper and #1500 emery paper. Comparisons are made of the temperature excursion at boiling incipience, the nucleate boiling heat transfer coefficient, CHF, and the wall superheat at CHF. CHF results are compared to those previously reported in the literature for pool boiling of FC-72 and HFE-7100 dielectric liquids on copper, silicon, and enhanced surfaces, such as etched surfaces, micro- and macro-finned surfaces, and micro-porous coatings. Computer chips operating in stand-by mode dissipate only few watts, and therefore in immersion cooling will be cooled by natural convection. A correlation for natural convection for dielectric liquids on plane, micro-porous, and macro-structured surfaces is developed. A correlation for CHF is also developed which takes into account the contributions of liquid subcooling, microscopic surface features, macroscopic surface area enhancement, and surface orientation. Still photographs and video footage of the boiling process are recorded and used to help explain and interpret the obtained results.

The background section (Chapter 2) provides details on pool boiling, which can be used to remove large amounts of heat from CPUs and/or their heat sinks. Included in this chapter are a description of the boiling curve and a brief discussion of boiling theory. This chapter also reviews published work on the effectiveness of using porous, micro- and macro-structured surfaces to reduce the temperature excursion at boiling incipience, increase the heat removal rate during nucleate boiling, and increase CHF of dielectric liquids. In addition, the effect of liquid thermophysical properties and subcooling and surface orientation as reported in the literature on nucleate boiling heat transfer and CHF are discussed. The following chapter entitled Pool Boiling Experiments (Chapter 3) details the experimental pool boiling facility, the design and assembly of the test section,

and the experimental procedures. A thermal analysis is performed to estimate heat losses and understand the nucleate boiling heat transfer from copper surfaces with corner pins. Chapter 4 reports the results obtained for saturation and subcooled boiling of FC-72 and HFE-7100 on plane copper and porous graphite surfaces at different orientations, and Chapter 5 presents the results for copper surfaces with corner pins at different surface orientations and liquid subcooling. The obtained CHF results are compared with those reported by researchers on plane, porous, and micro- and macro-structured surfaces. Chapter 6 gives a summary and conclusions.

## 2 Background

Technological advances in microelectronics are increasing the power dissipation heat flux by both reducing the size of microchips and increasing their speed. IBM has developed a microprocessor chip that currently has local heat flux dissipation near  $100 \text{ W/cm}^2$  (Knickerbocker et al., 2002). In the 2007 International Technology Roadmap for Semiconductors assessment of the semiconductor technology requirements and challenges, power dissipation from cost performance integrated circuits is projected to exceed  $100 \text{ W/cm}^2$  in the next five years with localized heat fluxes exceeding  $200 \text{ W/cm}^2$  (ITRS, 2007). Some CPUs have already exceeded dissipation heat fluxes of  $100 \text{ W/cm}^2$  (Refai-Ahmed, 2007). Such high and localized heat fluxes can lead to severe temperature gradients across the chip, resulting in mechanical stresses that could damage the chip or shorten its lifetime. Additionally, increasing the heat flux from a surface will increase the temperature of the chip if this heat is not removed. Standard commercial chips should maintain a junction temperature below  $85 \text{ }^\circ\text{C}$ . Above this temperature, the failure frequency of the chips increases (Peterson, 1994). Although more robust integrated circuits and packaging modifications can help reduce thermal loads and stresses and allow for current technologies (e.g. heat pipes, heat sinks, fans, etc.) to remove the heat, the limits of conventional thermal management are being approached.

Figure 2.1 shows the dependency of the relative magnitude of the heat transfer coefficient on both the working fluid and the mode of heat transfer. Using the fluids in direct contact with heat-generating surfaces avoids additional thermal resistance from intervening material. Some liquid-based cooling schemes being researched for applications to electronics cooling involve forced convection in microchannels, spray and impinging jets, capillary pumped loops, and immersion cooling through both flow boiling and pool boiling (Rainey and You, 2000; 2003; Arik and Bar-Cohen, 2001; El-Genk and Bostanci, 2003a,b; Maydanik et al., 2004; Chen et al., 2004; Ravigururajan and Dorst, 1999; Mathews, Lee, and Peters, 2003; Arik, Bar-Cohen, and You, 2007). With pool boiling, in which the component is fully immersed in a stagnant volume of liquid, heat is removed from the surface isothermally by the vaporization of the liquid. Vapor

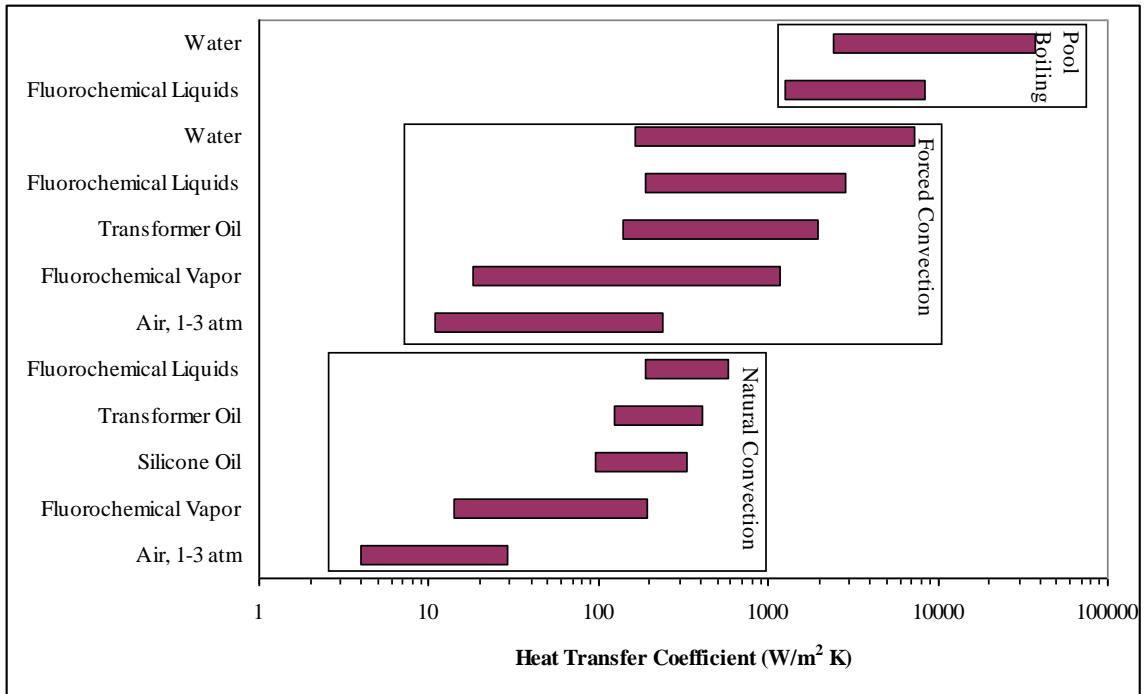


**Figure 2.1. Relative magnitude of heat transfer coefficients for various mode of heat transfer (from Simmons, 1996).**

condensation within a closed system maintains the liquid level in the pool while a heat sink connected with the condenser removes the heat from the system.

However, direct immersion cooling of electronics necessitates the use of dielectric liquids, ensuring that the electronics are not damaged. Additionally, the liquids must be chemically compatible with the components and be able to maintain the chip junction temperature below 85 °C. Certain Novec and Fluorinert liquids developed by 3M meet these requirements. Table 1.1 and 1.2 list some of the thermal and physical properties of Fluorinert FC-72 ( $C_6F_{14}$ , perfluorohexane) and Novec HFE-7100 ( $C_4F_9OCH_3$ , methoxy-nonafluorobutane) liquids as compared to water as well as some environmental and electrical properties of these dielectric liquids. The dielectric and chemical properties of HFE-7100 and FC-72 make them candidate liquids for direct immersion cooling of computer chips. These liquids are compatible chemically with standard electronic components and are environmentally friendly (Wallington et al., 1997; Tuma, 2001; 3M, 2001). But the poor thermophysical properties and the highly wetting nature of these liquids pose challenges in using them in for cooling of electronics. Through the use of enhanced surfaces, these obstacles can be overcome and some of the problems associated with boiling of dielectric liquids are mitigated. Pool boiling, therefore, is a viable option for thermal management of high powered electronics. The following sections will provide information about pool boiling in general and pool boiling in dielectric liquids with the specific application towards electronics cooling.

## **2.1 Natural Convection**

Prior to boiling incipience on a heated surface, heat transfer from that surface by natural convection is driven only by the difference between the wall temperature ( $T_w$ ) and the liquid's bulk temperature ( $T_b$ ). This temperature difference causes a density gradient in the layer of fluid near the heated surface. A buoyant force moves the warm fluid upward away from the heated surface and it is replenished with cooler fluid. For a wall uniformly heated, the heat flux in this heat transfer mode is proportional to the temperature difference ( $T_w - T_b$ ) raised to the power of 1.2:

$$q'' \propto (T_w - T_b)^{1.2}. \quad (2.1)$$

## 2.2 Pool Boiling and Nucleate Boiling Heat Transfer

While natural convection can occur anytime the wall temperature exceeds the liquid bulk temperature, the wall temperature must be larger than the liquid's saturation temperature to initiate and maintain nucleate boiling. When the system is filled with liquid, air is trapped in crevices and grooves in the surface (Figure 2.2). These air pockets serve as potential sites for initiating nucleate boiling. For poorly wetting liquids (Figure 2.2a), more air is trapped in the groves and crevices than for highly wetting liquids (Figure 2.2b). Because both FC-72 and HFE-7100 have low surface tensions, these liquids trap very little air in the crevices (Figure 2.2b). As the heat flux increases, the corresponding surface temperature increases, and the volume of trapped gas grows by thermal expansion and the evaporation of liquid into the cavity (Figure 2.3). For bubble nucleation to ensue, the radius of the cavity mouth must be greater than a critical value,  $r_c$ , which depends on the fluid's thermophysical properties and the wall superheat, given by (Carey, 1992)

$$r_c = \frac{2\sigma T_{sat}(P_l) \left( \frac{1}{\rho_v} - \frac{1}{\rho_l} \right)}{h_{fg} [T_w - T_{sat}(P_l)]}. \quad (2.2)$$

For poorly wetting liquids (Figure 2.2a), the expansion and thus the superheat necessary for nucleation is smaller than for highly wetting liquids (Figure 2.2b). In the case of liquids with a low surface tension such as dielectric liquids (Table 1.1), the wall temperature during natural convection exceeds the liquid saturation temperature and that for boiling incipience. When boiling initiates, there is a large increase in the heat transfer rate and therefore the wall temperature decreases precipitously. The elevated wall temperature before boiling incipience is referred to as temperature excursion. On smooth surfaces in dielectric liquids this temperature may exceed the industry recommended maximum junction temperature of 85 °C (Chang You, and Haji-Sheikh, 1998; El-Genk

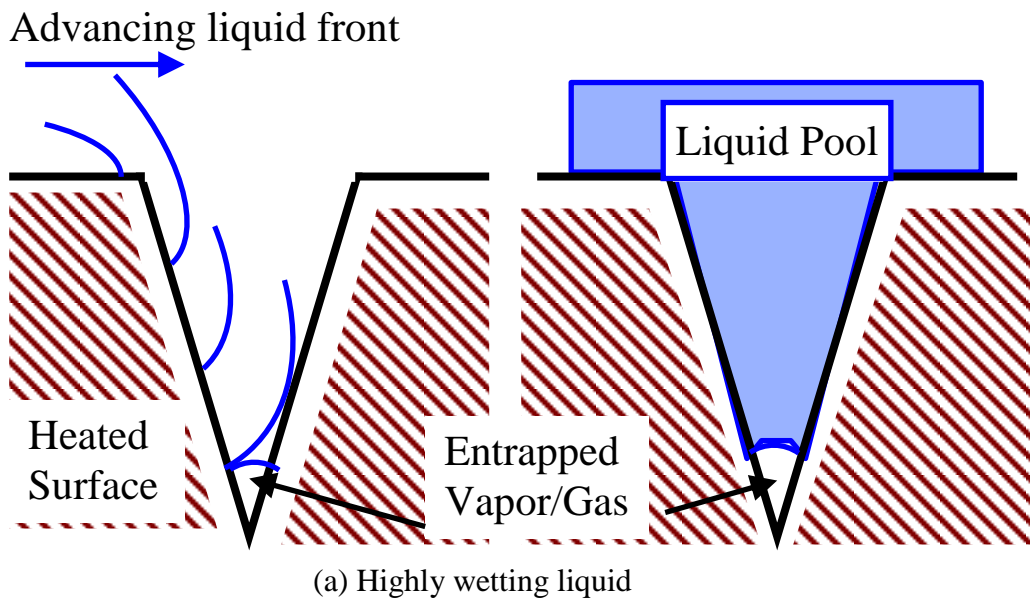
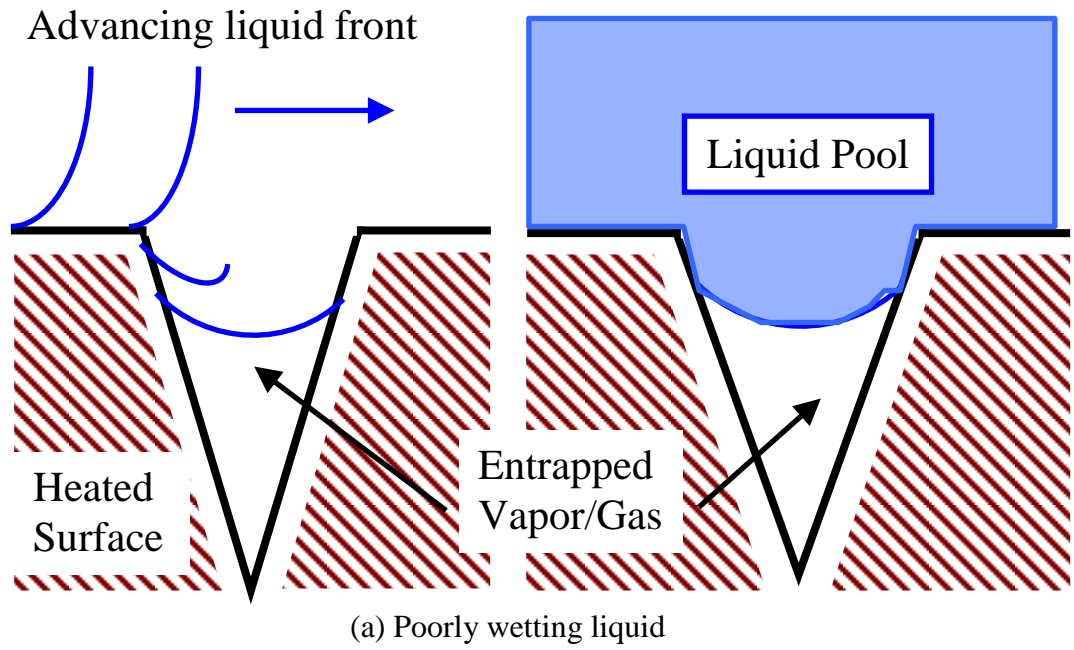
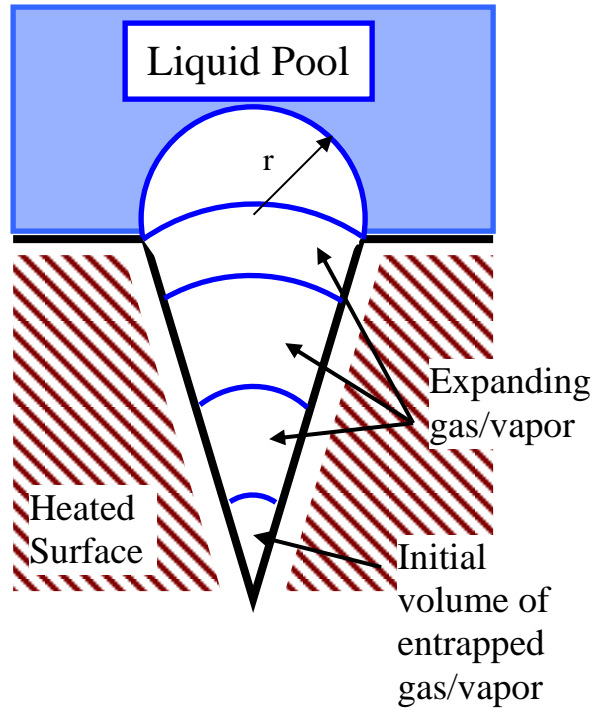


Figure 2.2 Gas entrapment in a cavity for an advancing liquid front.



**Figure 2.3 Growth of entrapped gas to bubble nucleation.**

and Bostanci, 2003a,b). In addition, a thermal shock may occur when there is a large temperature drop at boiling incipience.

Hsu (1962) proposed a semi-theoretical model outlining the size range of active nucleation sites during nucleate boiling. Assuming conical cavities, the model predicts; (a) that a certain wall superheat is necessary to activate potential nucleation sites, and (b) only a finite range of cavity sizes can become active boiling sites. The relationship describing the active range of cavity mouth radii is given by the following equation and is depicted in Figure 2.4:

$$\left\{ \begin{array}{l} r_{c,\max} \\ r_{c,\min} \end{array} \right\} = \frac{\delta_t}{4} \left[ 1 - \left( \frac{T_{sat} - T_b}{T_w - T_b} \right) \right] \left\{ \pm \right\} \sqrt{ 1 - \left( \frac{T_{sat} - T_b}{T_w - T_b} \right)^2 - \frac{12.8\sigma T_{sat}}{\rho_v h_{fg} \delta_t (T_w - T_b)} } \quad (2.3)$$

As can be seen in Figure 2.4, there is a range of cavity mouth sizes inside the envelope that will sustain bubble nucleation. As the wall temperature increases, the size range for active cavities also increases. However, there are some cavity sizes outside the envelope that will never become active regardless of the surface superheat. According to the Hsu (1962) model, there is also a minimum wall temperature above saturation at which cavities may become active. Figure 2.4 also shows that the range of active nucleation sites depends on the liquid. According to Hsu's (1962) equation, FC-72 has a wider range of cavities that may be activated during boiling than HFE-7100, and that for a given mouth radius, a site activates at lower surface superheat in FC-72 than in HFE-7100.

### 2.2.1 Ebullition Cycle

Once boiling starts, bubbles forming on the surface grow, and then detach when the buoyant force overcomes the surface tension force. The cyclic formation and release of vapor bubbles at an active nucleation site is called the ebullition cycle. It consists of four stages or periods: the waiting period, nucleation, bubble growth, and bubble departure. The waiting period starts immediately after the bubble detaches. Cool liquid from the

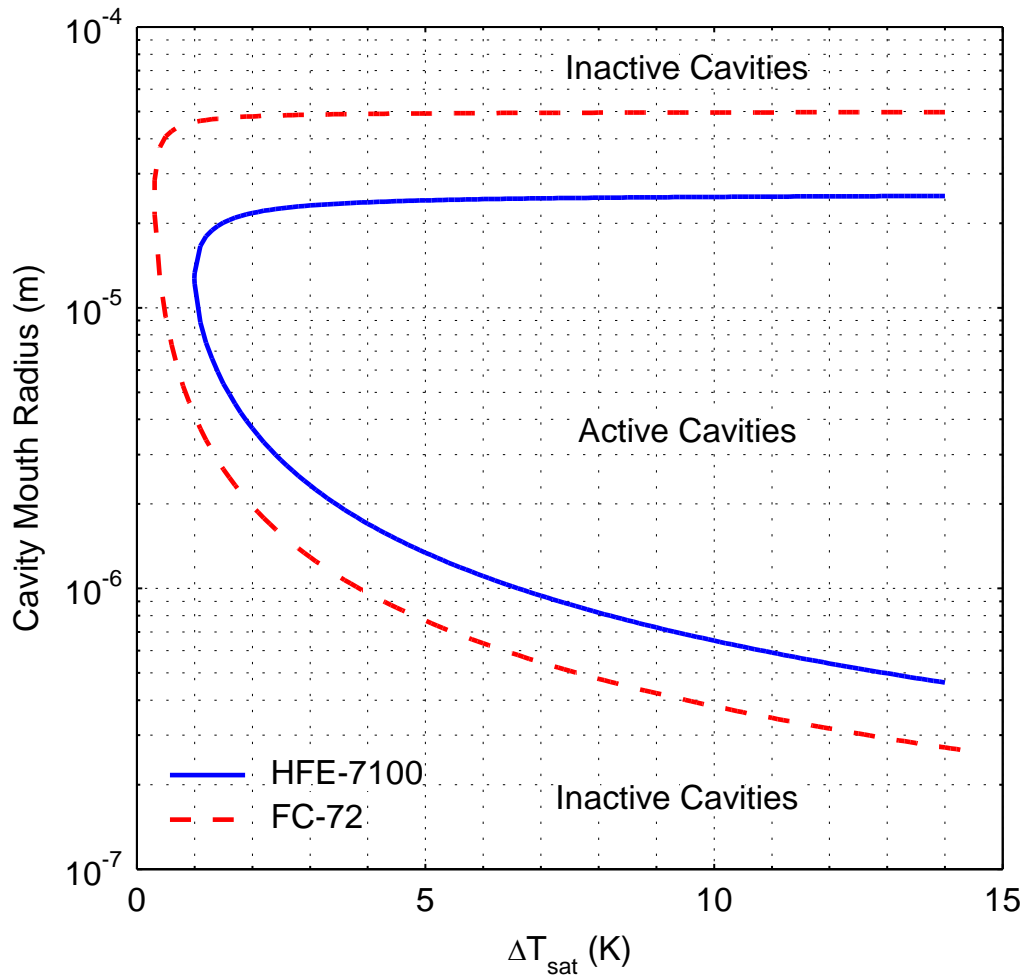


Figure 2.4 Range of cavity mouth sizes for active nucleation sites.

pool bulk fills the void left by the detached vapor bubble and destroys the previously established thermal boundary layer (Figure 2.5a). The waiting period is the time necessary for the thermal boundary layer to re-establish and for the nucleation site to become active again (Figure 2.5b).

At the end of the waiting period, the embryonic bubble reaches its critical size and begins to grow (Figure 2.5b). Energy supplied by the heated surface of the wall at the vapor-liquid-solid triple point evaporates the liquid which fills the bubble with vapor. Initially, bubble growth is rapid and is inertially driven (Figure 2.5c). Heat transfer from the heated wall is very fast and bubble growth is driven by the vapor pushing back the surrounding liquid. Bubble growth is radial and a thin micro-layer of liquid is left between the heated wall and bubble. Heat transfer across this liquid micro-layer directly vaporizes the liquid (Guo and El-Genk, 1994; Diao, Zhao, and Wang, 2007). As the bubble grows larger, heat transfer becomes the limiting factor for the bubble to grow (Figure 2.5d). The bubble continues to grow until the buoyant force pulling the bubble upward overcomes the surface tension holding the bubble down to the surface. As the bubble starts to pull away from the surface, liquid pinches and cuts the bubble from the nucleation site (Figure 2.5e) and the bubble detaches (Figure 2.5f).

When the bubble departs, liquid from the pool fills the space previously occupied by the bubble and destroys the thermal boundary layer and the ebullition cycle starts over. The frequency of this cycle is the inverse of the sum of the waiting time (time necessary for bubble nucleation and re-establishment of thermal boundary layer) and the growth period (time between bubble nucleating and detaching):

$$f = \frac{1}{t_{wait} + t_g}. \quad (2.4)$$

The ebullition frequency and the detached bubble diameter are inversely proportional. Zuber (1963) proposed the relationship between the two as:

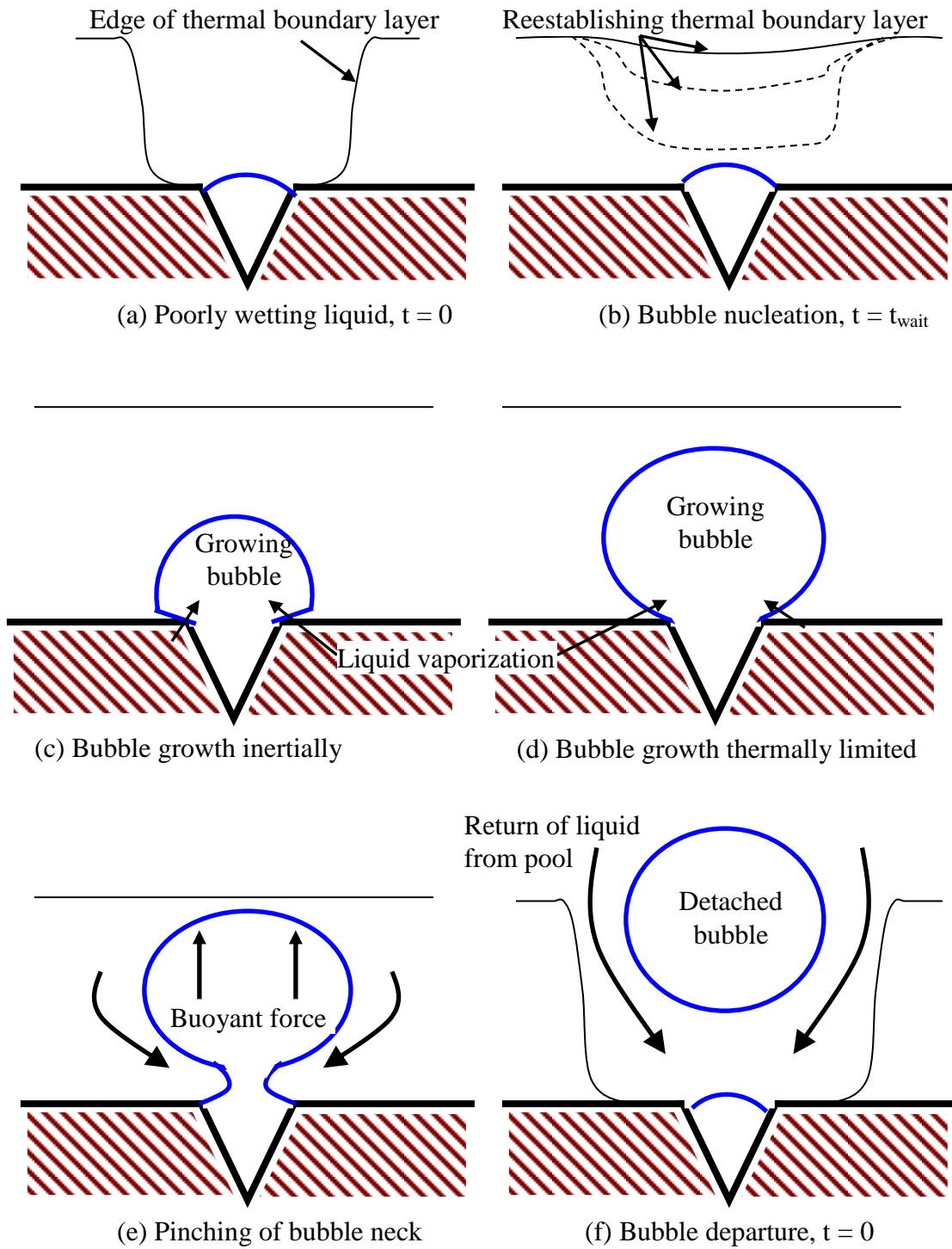


**Figure 2.5 Ebullition cycle.**

$$fd_d = 0.59 \left[ \frac{\sigma g (\rho_l - \rho_v)}{\rho_l^2} \right]^{1/4}. \quad (2.5)$$

### 2.2.2 Boiling Regimes

Figure 2.6 is a simple sketch of a typical nucleate boiling curve, which plots heat flux,  $q''$  (power dissipated per unit surface area), versus the wall superheat,  $\Delta T_{sat}$  ( $T_w - T_{sat}$ ), where  $T_w$  is the temperature of the surface or wall and  $T_{sat}$  is the liquid's saturation temperature. As discussed earlier, heat transfer will be by natural convection before bubble nucleation starts. With highly wetting liquids, there is often a temperature excursion at boiling incipience. In the case of a temperature excursion, there is a rapid decrease in the surface superheat because of the much greater heat transfer rate in nucleate boiling than in natural convection. In the case of no temperature excursion, there is a smooth transition between natural convection and nucleate boiling on the boiling curve (Figure 2.6).

The nucleate boiling portion of the curve can be divided into three different regions. In region I, that of discrete bubbles, not all of the potential active nucleation sites are active (Figure 2.7a). As the superheat increases, the number, density, and frequency of the discrete bubbles detaching from the surface increases, increasing the slope of the boiling curve and the boiling heat transfer coefficient.

Region II, that of intermediate surface superheats, is that of fully developed nucleate boiling (Figure 2.6). It experiences higher heat fluxes than in the discrete bubble region and is characterized by a steep slope of the boiling curve, which indicates the high density of active nucleation sites on the surface (Figure 2.7b). Departing bubbles cause mixing in the boundary layer, further enhancing the heat transfer. In addition to the high density of active nucleation sites on the surface, lateral coalescence among growing and departing vapor bubbles near the surface is negligible. Coalescence does, however, increase with increasing heat flux.

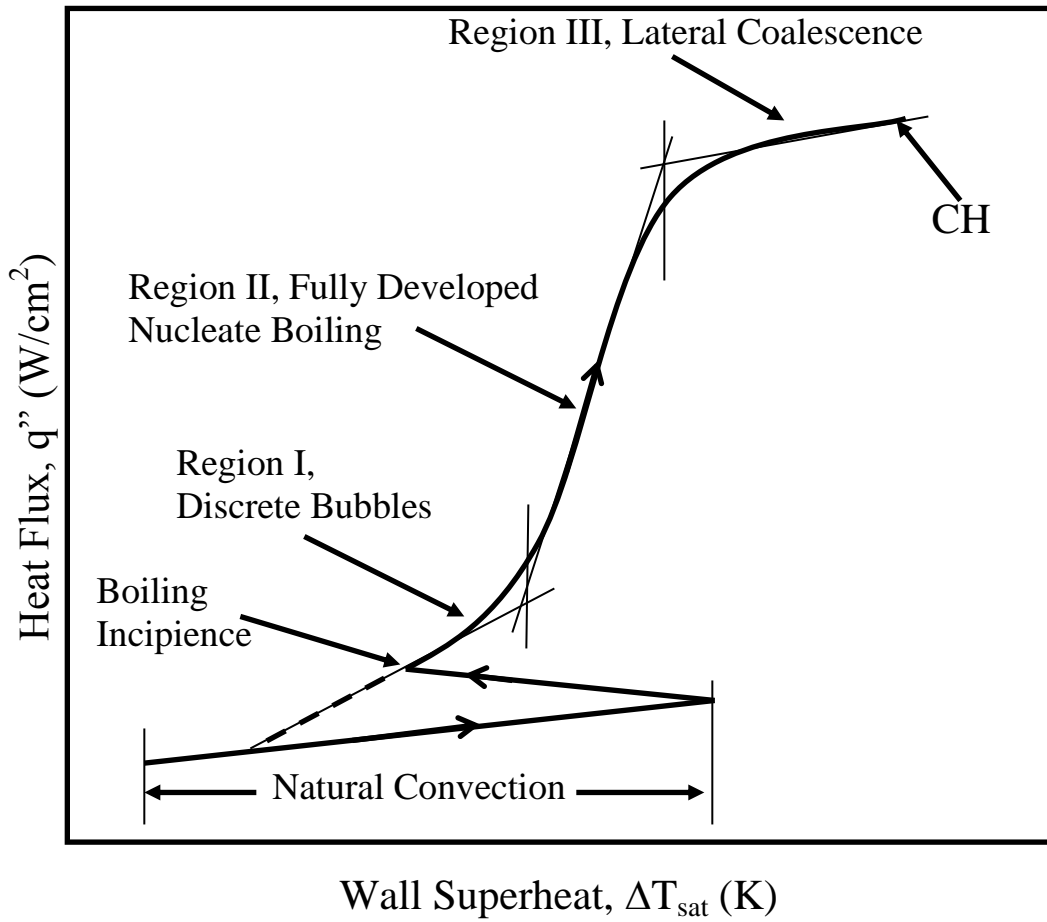
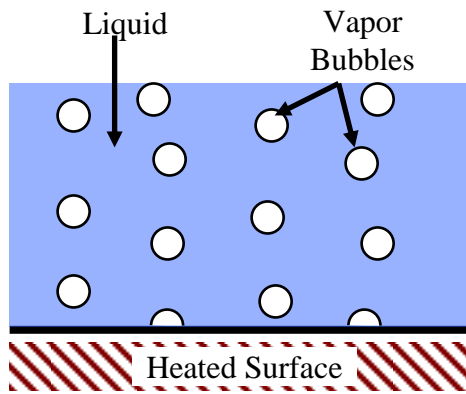
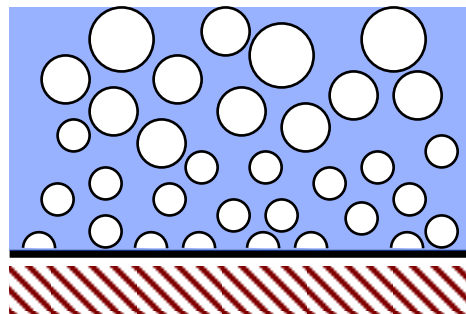


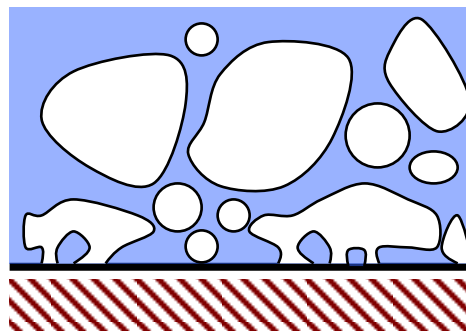
Figure 2.6 Typical nucleate pool boiling curve.



(a) Region I, discrete bubbles.



(b) Region II, fully developed nucleate boiling.



(c) Region III, lateral bubble coalescence.

**Figure 2.7 Sketch of different nucleate boiling regions.**

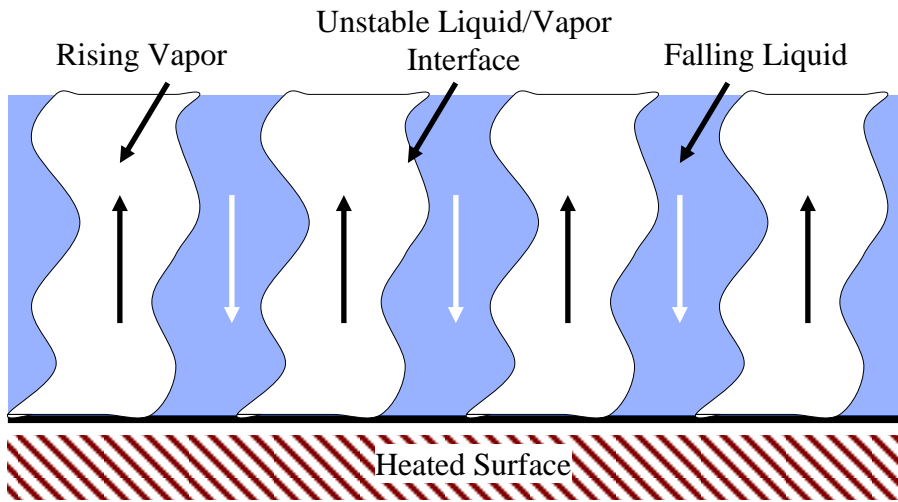
Region III, the region of lateral bubble coalescence, is topmost of the nucleate boiling curve. A gradually decreasing slope of the boiling curve characterized region III (Figure 2.6). The lateral coalescence of the growing and departing bubbles near the boiling surface into vapor globules (Figure 2.7c) results in a larger increase in the surface temperature with increased heat flux. Consequently, the rate of increase in the nucleate boiling heat flux in region III with increasing surface superheat is lower than those in regions I and II. Region III extends to CHF, marked as the last point on the boiling curve in Figure 2.6, before the surface temperature overshoots into the film boiling region.

### **2.3 Critical Heat Flux**

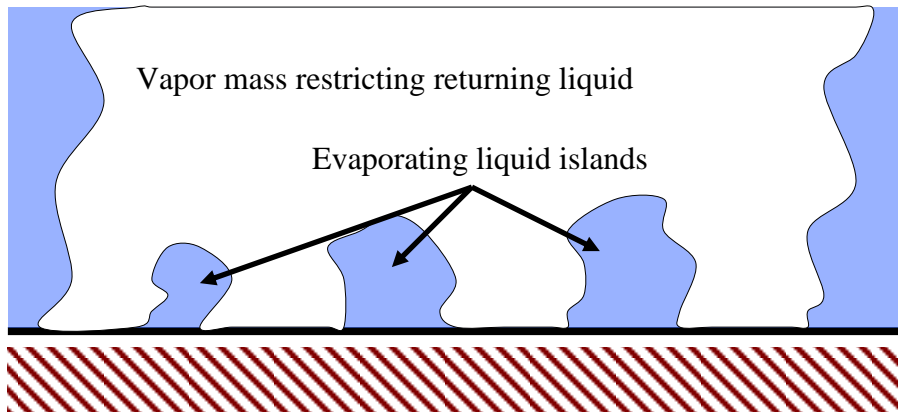
The end of the bubble coalescence region is marked by the Critical Heat Flux (CHF) (Figure 2.6). CHF is the maximum heat flux possible in the nucleate boiling mode. The occurrence of CHF is accompanied by an increase in the surface temperature for a surface-heat-flux-controlled system. The sudden and large increase in temperature can lead to a physical burnout of electronics.

Different models describing the mechanism responsible for CHF have been proposed (Kutateladze, 1952; Griffith, 1957; Zuber, 1959; Haramura and Katto, 1983). Details of these models differ, but each is based on the condition that vapor blankets part of the boiling surface, reducing the heat transfer rate. An early model for CHF was based on hydrodynamic instability of the interface of downward moving liquid and upward moving vapor (Figure 2.8a). In Zuber's (1959) hypothesis, he proposed that bubbles generated on the surface form columns or jets of vapor. CHF occurs when the instability of the vertical vapor-liquid interface distorts the jets and blocks the returning liquid to portions of the surface (Figure 2.8b). The liquid will continue to vaporize and, being starved of replenishing liquid, the surface will become partially or totally blanketed with vapor. Although there was widespread support for this model of CHF, there was a lack of concrete evidence to validate it. In addition, there are cases where the model cannot properly explain data (Chang and Baek, 2003). Therefore, another model for CHF was proposed.





(a) Vapor and liquid columns



(b) CHF—vapor columns collapse and choke liquid supply

Figure 2.8 Hydrodynamic model for CHF.

The CHF model proposed by Haramura and Katto (1983) focuses on a liquid microlayer of definite thickness beneath large vapor slugs. The slugs are formed by coalescing bubbles from a number of nucleation sites (Figure 2.9a). Vapor jets feed the large vapor slug through the thin film of liquid separating the vapor mass and the heated surface. The large slugs “hover” over the surface until accumulating sufficient vapor to escape. If the liquid film microlayer evaporates during the “hovering” time, CHF ensues (Figure 2.9b).

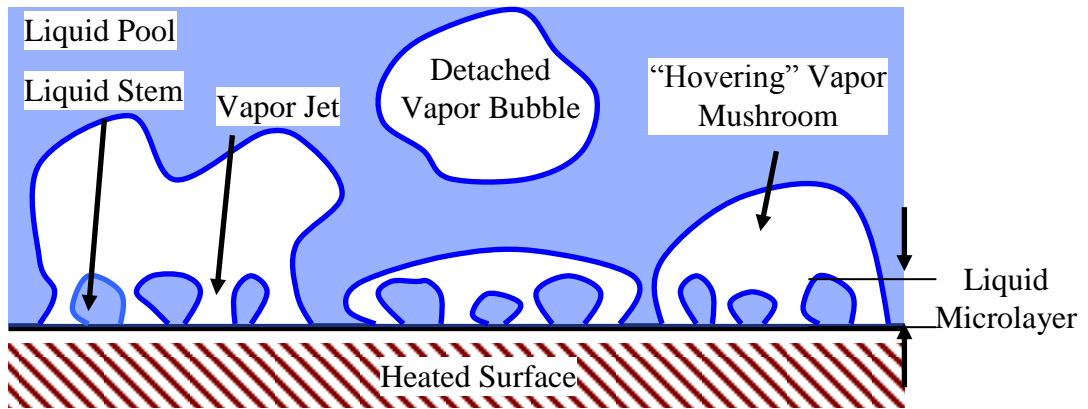
Accurate predictions of CHF for pool boiling are desirable to ensure that a boiling crisis does not occur. Kutateladze (1952) and Zuber (1959) independently arrived at a relationship based on liquid properties to predict CHF for saturation pool boiling on horizontal surfaces:

$$CHF_{sat} = C_{CHF,sat} h_{fg} \sqrt{\rho_v} [\sigma g (\rho_l - \rho_v)]^{1/4}. \quad (2.6)$$

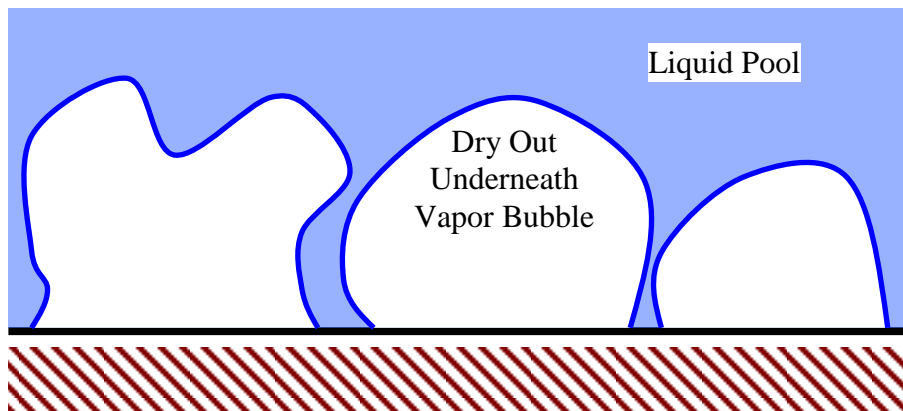
Their correlation differed in the value of the constant,  $C_{CHF,sat}$ . Zuber (1959) fixed the constant at  $\pi/24$  (~0.131). Average values of  $C_{CHF,sat}$  given by Kutateladze (1952) for water, and organic liquids boiling on graphite disks, chrome plated disks, and wires of different composition range from 0.13 – 0.19. The value of the coefficient,  $C_{CHF,sat}$ , depends on the boiling surface characteristics (morphology, geometry, orientation, etc.) (Parker and El-Genk, 2006a,b; Parker and El-Genk, 2008; El-Genk and Parker, 2008). Most other CHF correlations are based on Equation 2.6 (e.g., Carey, 1992; El-Genk and Guo, 1993; Mudawar, Howard, and Gersey, 1997; Arik, Bar-Cohen, and You, 2007; Parker and El-Genk, 2006a,b; Parker and El-Genk, 2008; El-Genk and Parker, 2008).

Liquid subcooling also affects the value of CHF. Holding other variable constant (system pressure, liquid properties, etc.), all data and models for subcooled CHF show a linear relationship between CHF and liquid subcooling (Kutateladze, 1952; Griffith; 1957, Zuber, 1959; Ivey and Morris, 1966):





(a) Mushrooms and stems—microlayer evaporation



(b) CHF—dry out of liquid microlayer before vapor mass lift off

**Figure 2.9 Microlayer (mushroom-and-stem) model for CHF.**

$$\frac{CHF_{sub}}{CHF_{sat}} = 1 + C_{CHF,sub} \Delta T_{sub}, \quad (2.7)$$

where the subcooling CHF constant,  $C_{CHF,sub}$ , depends on the surface characteristics, liquid properties and surface orientation. Though the correlation is based on boiling data of non-dielectric liquids (such as water, ethyl alcohol, and isooctane), this linear relationship between CHF and liquid subcooling has been confirmed by many investigators in dielectric liquid such as HFE-7100 (Arik and Bar-Cohen, 2001; Liu, Lee, and Su, 2001; El-Genk and Bostanci, 2003; El-Genk and Parker, 2005) and FC-72 (Rainey, You, and Lee, 2003; O'Connor, You, and Chang, 1996; Honda, Takamatsu, and Wei, 2002; Wei and Honda, 2003; Z. W. Liu et al., 2001; Watwe, Bar-Cohen, and McNiel, 1997, Parker and El-Genk, 2005).

## **2.4 Enhancements in Nucleate Boiling**

Pirotto, Rohsenow, and Doerffer (2004) reviewed the parametric effects of nucleate boiling, some of which influence boiling performance more than others. Included in these effects are the surface microstructure, liquid subcooling, dissolved non-condensable gasses in the liquid, thermophysical properties of the liquid, and the orientation of the boiling surface with respect to gravity. Improved boiling heat transfer can be quantified by measured reductions in the temperature excursion at boiling incipience, increases in the nucleate boiling heat transfer coefficient, and increases in the critical heat flux. Several researchers have studied boiling in dielectric liquids and the effect that these parameters have on boiling heat transfer.

Table 2.1 is a brief summary of selected studies investigating boiling in dielectric liquids. The review given in the table is not exhaustive, but is representative of some previous research.

The investigations listed in Table 2.1 considered the effect of the various parameters (e.g. surface, liquid subcooling, pressure, inclination) on nucleate boiling heat transfer and CHF. Most of the effects were studied individually, while a few studied the effect of

**Table 2.1 Summary of selected investigations on enhanced boiling in dielectric liquids.**

Reference	Liquid	Surface	$\Delta T_{sub}$ (K)	Inclination (degrees)	Study Parameters
Howard and Mudawar, 1999.	FC-72, PF-5052	Cu, 12.7 x 12.7 mm (FC), 3.2 x 35 mm (PF)	"near saturated"	0, 30, 45, 60, 75, 90, 120, 135, 150, 165, 170, 175, 180	Inclination
El-Genk and. Bostanci, 2003b	HFE-7100	10 x 10 mm Cu	0, 10, 20, 30	0, 30, 60, 90, 120, 150, 180,	Inclination, Subcooling
Priarone, 2005	HFE-7100, FC-72	30 mm dia. Cu	0	0, 45, 90, 135, 175	Inclination, Liquid
O'Connor, You and Chang, 1996	FC-72	Smooth Cu and microporous coatings	0, 20, 40, 60, 90	0	Dissolved gas content, Pressure, Subcooling, Surface
Ujereh, Fisher, and Mudawar, 2007	FC-72	Cu studs, carbon nanotubes	0	0	Surface
Yu and Lu, 2007	FC-72	Cu square fins	0	0	Fin height and pitch
Kubo, Takamatsu and Honda, 1999	FC-72	smooth, and re-entrant cavities in Si , 1.6 and 3.1 micron diameter, 0.1 and 1 mm apart	3, 25	0	Mouth diameter, Pitch, Subcooling, Gas content
Rainey and You, 2001	FC-72	1cm x 1cm, 2cm x 2cm, 5cm x 5cm, "DOM" 50 mm	0	0, 45, 90, 135, 160, 180	Surface, Heater size, Inclination angle
Ferjančič and Golobič, 2002	FC-72, Water	ribbon SS302, steel 1010, smooth, sanded, etched	0	0, 90	Surface roughness on CHF
Ramaswamy, Joshi, Nakayama, and Johnson, 2003	FC-72	Grooved / machined plates w/ small features (0.1-0.8 mm)-- Array of channels	"Room Temperature", degassed	0	Channel width, pitch, height, Layer thickness
Rainey, You, and Lee, 2003	FC-72	Pins with microporous coatings	0, 10, 30, 50	0, 90	Pressure, Subcooling, Gas content, Pin height, Inclination
Wei and Honda, 2003	FC-72	10x10 mm, S, PF 30-60, 30-120, 30-200, 50-60, 50-200, 50-270	0, 3, 25, 45	0, 90	Microfin geometry, Subcooling, Gas content
Liu, Lin, Lee and Peng, 2001	FC-72, HFE-7100	80x15 mm Cu	0, 10, 20	0	Fluid, Subcooling
Vemuri and Kim, 2005	FC-72	Al, Al <sub>2</sub> O <sub>3</sub> nano-porous	0	0	Surface
Anderson and Mudawar, 1989	FC-72	Cu-- polished, sanded (600), vapor blasted, microfin, microstud, inclined microgroove, drilled cavities	0	90	Surface
Miller, Gebhart and Wright, 1990	FC-72	12.7x12.7 mm Si with hexagonal dimples 9.4 micron dia, 3.3 micron deep	0	90	Boiling history
Marto and Lepere, 1982	FC-72, R-113	High Flux, Thermoexel-E, Gewa-T, Copper 15.8 mm o.d. horizontal tube	0	N/A	Fluid, Surface
Danielson, Tousignant, and Bar-Cohen, 1987	FC-43, FC-72, FC-75, FC-77, FC-84, FC-87, L-1402, R-113	0.25 mm Pt wire	0	N/A	Fluid

the different parameters. For example, some looked at the effect of liquid subcooling and dissolved gas in the liquid for different surfaces (O'Connor, You, and Chang, 1996;

Kubo, Tatamatsu, and Honda, 1999; Rainey, You, and Lee, 2003; Wei and Honda, 2003). El-Genk and Bostanci (2003b) are the only ones to have reported on the combined effects of liquid subcooling and surface inclination on boiling heat transfer. No research has been reported including the combined effects of liquid subcooling, inclination, and surface structure over the range of angles from 0° to 180°.

The following sections describe some of the investigations in pool boiling heat transfer using dielectric liquids while varying certain parameters that affect the boiling performance. In general, modifying the surface with microstructures or extensions improves the boiling heat transfer by reducing or eliminating the temperature excursion at boiling incipience, improving the nucleate boiling heat transfer coefficient, and increasing the critical heat flux (e.g., O'Connor, You, and Chang, 1996; Ujereh, Fisher, and Mudawar, 2007; Vemuri and Kim, 2005; Yu and Lu, 2007). Increasing the liquid subcooling of the fluid increases the CHF in a linear fashion (e.g., El-Genk and Bostanci, 2003b; Rainey, You, and Lee, 2003; J. W. Liu et al., 2001; Z. W. Liu et al., 2001). Changing the orientation of the boiling surface also changes the boiling performance (e.g., El-Genk and Bostanci, 2003a; Priarone, 2005; Howard and Mudawar, 1999). In the horizontal, upward facing position, a flat surface has the highest value of CHF but the lowest nucleate boiling heat transfer coefficient at low superheats. The CHF decreases and the low superheat heat transfer coefficient increases as the surface inclination moves from upward facing to downward facing. The next sections detail studies in nucleate pool boiling which investigated the use of enhanced and extended surfaces, subcooled liquid, different surface orientations, and liquids with different thermophysical properties.

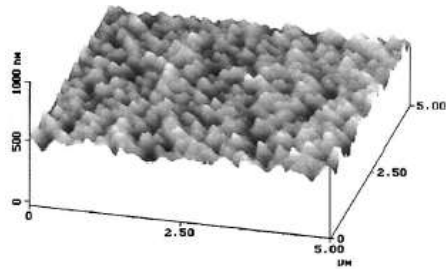
#### **2.4.1 Effect of Surface Preparation**

It has been established that modifying the heated surface has an effect on the nucleate boiling heat transfer. Kurihara and Myers (1960) performed a series of experiments using different liquids (water, acetone, n-hexane, carbon tetrachloride, and carbon disulfide) on a flat plate to study the number of active nucleation sites on boiling heat transfer rates. They concluded that the boiling heat transfer coefficient is proportional to the density of active nucleation sites raised to the 1/3 power. Ramilison, Sadasivan, and

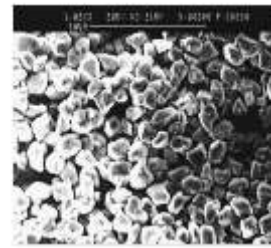
Lienhard (1992) used data obtained from the open literature for several boiling fluids on different surfaces to relate CHF to the RMS roughness of a surface. They determined that CHF is influenced by the RMS roughness to the power 0.125. By taking into account the surface roughness, the scatter of the data was reduced from  $\pm 40\%$  to  $\pm 15\%$ . Ferjančič and Golobič (2002) confirmed that in FC-72 and water, increasing the surface roughness increases CHF. However, the average roughness alone was not sufficient to fully correlate the increase in CHF. Experiments with dielectric liquids confirm that the surface micro-features will affect the boiling performance (e.g., Oktay, 1982; Chang and You, 1997b; Kahn, Toh, and Pinjala, 2008). Figure 2.10 shows examples of surface microstructures that have been tested with dielectric fluids. Figure 2.11 shows some micro-structured extended boiling surfaces (length scale  $\leq 0.5$  mm) and Figure 2.12 shows examples of macro-structured extended boiling surfaces (length scale  $\geq 0.5$  mm).

Honda, Takamatsu, and Wei (2002) investigated saturation and subcooled boiling ( $\Delta T_{\text{sub}} = 3, 25, \text{ and } 45$  K) of FC-72 on smooth silicon and  $\text{SiO}_2$  chemically etched to an RMS roughness of 25 – 32 nm (Figure 2.10a) in both gas dissolved and degassed liquid. The reported boiling performance on the roughened chip was significantly improved over the boiling performance of the smooth chip. In saturated FC-72, temperature excursions at boiling incipience were about 18 K on the smooth chip, but reduced to only about 12 K on the etched surface. The nucleate boiling heat transfer rate and critical heat flux for the rough chip also increased over these same values for the smooth chip at all levels of subcooling and in both gas dissolved and degassed liquid.

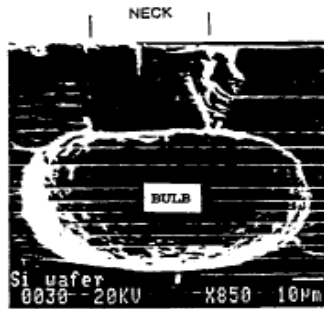
Similarly, Rainey and You (2000) reported differences between a machine roughened copper and a polished copper surface (Chang and You, 1996) in saturation boiling of FC-72. The temperature excursion at incipient boiling on the polished copper was 40 K and subsequent boiling ensued at 19 K. For the machine-roughened surface, the values were 27 K and 10 K, respectively. The heat transfer coefficient was about 5 times higher on the roughened surface, and the critical heat flux increased by about 40%. These



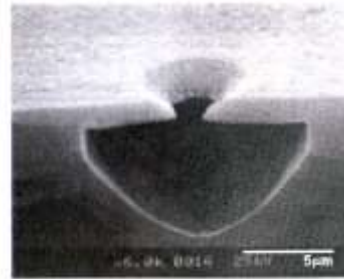
(a) Honda, Takamatsu, and Wei



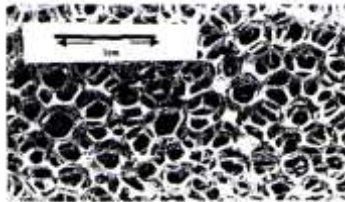
(b) Kim, Rainev, You, and Pak



(c) Baldwin, Bhavnani, and Jaeger



(d) Kubo, Takamatsu, and Honda



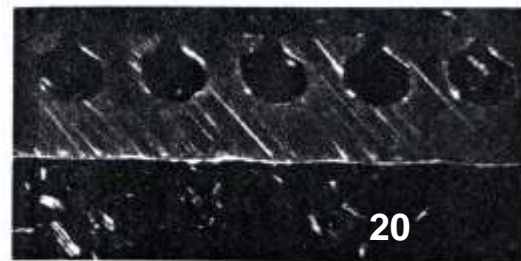
(e) Arbelaez, Sett, and Mahaian



(f) Union Carbide High Flux,



(g) Hitachi Thermoexel-E, Marto and Lepere (1982)



(h) Wieland Gewa-T, Marto and Lepere

**Figure 2.10. Selected Surface Microstructures.**

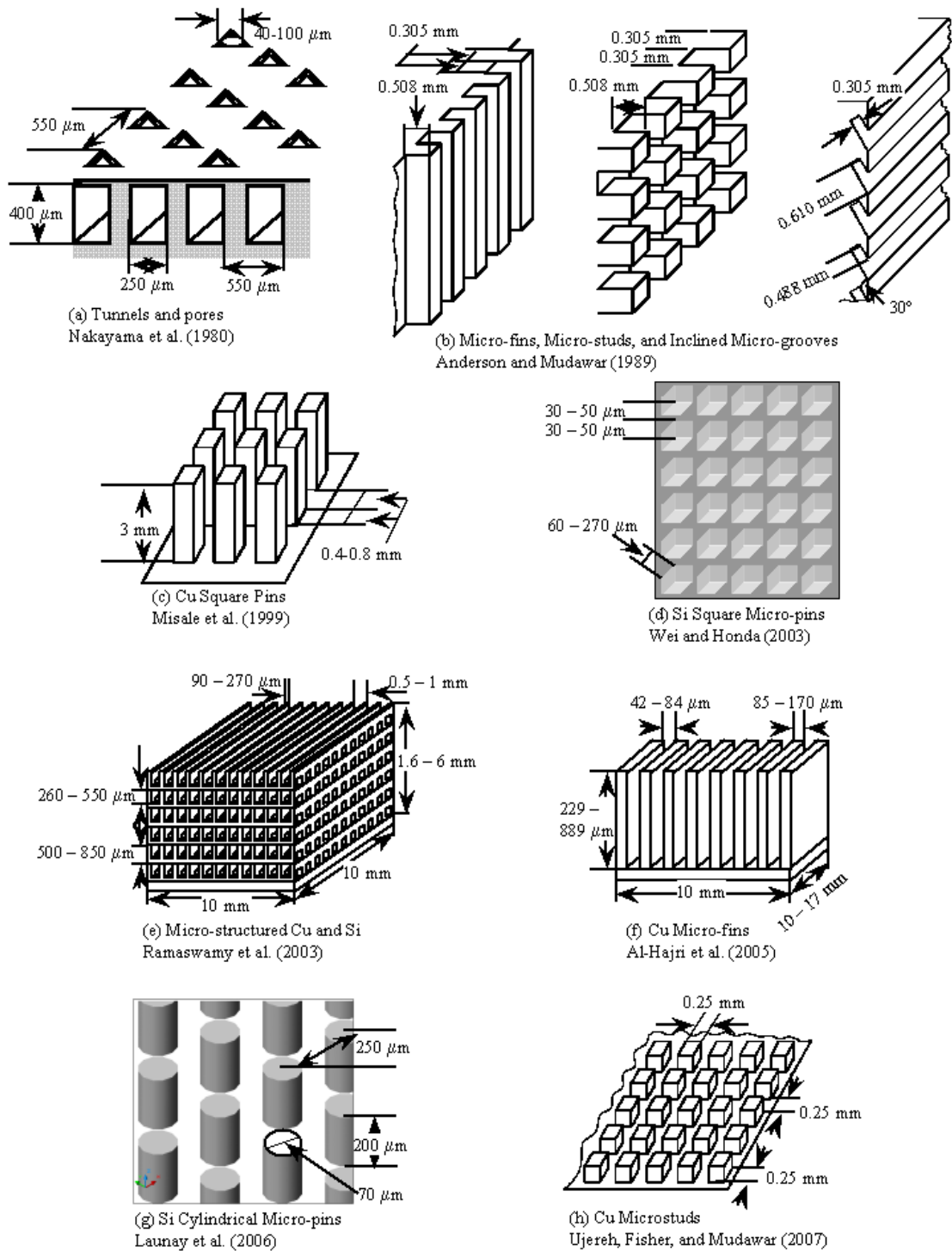
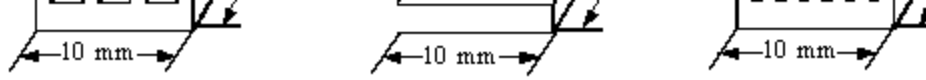


Figure 2.11 Micro-Structured Extended Boiling Surfaces (Length Scale < 0.5 mm).



(c) Cu Fin Array  
Yu and Lu (2007)

**Figure 2.12 Macro-Structured Extended Boiling Surfaces (Length Scale  $\geq 0.5$  mm).**

enhancements may be attributed to the trapped air in the small surface features and the increased number of active nucleation sites.

A micro-porous coating was developed by O'Connor and You (1995), improved by Chang and You (1997a,b) and Kim et al. (2007), and used by others (Rainey and You, 2000, Kim et al., 2002; Rainey, You, and Lee, 2003) to enhance boiling performance in dielectric liquids (Figure 2.10b). The coatings, made with particles 1 – 20  $\mu\text{m}$  in size that have been mixed with a volatile carrier and epoxy, are applied to a surface. The carrier evaporates and the particles remain behind, being bound together with the epoxy, leaving a microporous coating about 50  $\mu\text{m}$  thick. Chang and You (1997b) varied the coating composition and method and found that all forms of the microporous paint performed similarly. These coatings provide negligible increase to the surface area. The effective thermal conductivity of these coatings is relatively low at about 0.95 W/m K (O'Connor and You, 1995), due to the low thermal conductivity of the epoxy binder.

The pores of these coatings, believed to be on the order of 0.1 – 1.0  $\mu\text{m}$ , effectively trap air and serve to increase the total number of nucleation sites. Using these coatings, the temperature excursion at boiling incipience was < 10 K and boiling ensued at a surface superheat of about 3 K. Boiling heat transfer rates significantly increased over those on smooth surfaces, and the critical heat flux was greatly enhanced in both saturation and subcooled boiling of FC-72 (O'Connor and You, 1995; Chang and You, 1997a,b; Kim et al., 2002; Rainey and You, 2002; Rainey, You, and Lee, 2003; Kim et al. 2007).

Kim (2006) improved the boiling heat transfer of microporous coatings by using coating with high thermal conductivity. By immersing a copper substrate in a solution of sulfuric acid and cupric sulfate, a microporous copper coating was deposited when subject to a potential difference between the anode and the cathode (heated surface). Different porous structures were grown using different current densities. Compared to copper, the peak heat transfer coefficient improved by ~50 – 600% and CHF increased by 20 – 50%. Another surface tested by Kim (2006) was made of nickel spheres soldered onto the surface using a procedure that resulted in a porous coating. He reported an

increase in the peak heat transfer coefficient of up to 600% when compared to the plain surface and increases in the CHF of 30 – 80%.

#### **2.4.1.1 Re-Structured Surfaces**

Baldwin, Bhavnani, and Jaeger (1998) used silicon surfaces with bulb and pyramidal shaped re-entrant cavities (Figure 2.10c) in saturated FC-72. The cavities were regularly spaced, identically shaped, and had consistent sizes. The cavities were etched into a silicon surface and arranged in a square array, with center-to-center spacings of approximately one, two, and three bubble departure diameters (0.5, 1.0, and 1.5 mm respectively). The mouths of the cavities were 45  $\mu\text{m}$  squares with rounded corners.

They first compared the effects of cavity spacing on the nucleate boiling and CHF. The critical heat flux for single spaced cavities (0.5 mm) ranged from 33-36  $\text{W}/\text{cm}^2$ , slightly higher than what was achieved with a plain surface, 30-34  $\text{W}/\text{cm}^2$ . The double (1.0 mm) and triple (1.5 mm) spaced cavities gave CHF values from 41.4 to 47.0  $\text{W}/\text{cm}^2$ . The authors concluded that CHF was reached sooner on the surface with single spaced cavities because of bubble crowding from all of the active sites. With the nucleation sites or cavities spaced further apart, the CHF was higher, showing that since more heat was removed from fewer boiling locations, the cavities served as effective heat removal sites.

They also examined at the nucleate boiling heat transfer coefficient as a function of cavity spacing. For heat fluxes less than 30  $\text{W}/\text{cm}^2$ , the single spaced cavity surface had nucleate boiling heat transfer rates larger than those of the other two surfaces, which was attributed to the larger density of nucleation sites. For example, at 20 K superheat, the heat flux was  $\sim 20 \text{ W}/\text{cm}^2$  for single spaced cavities,  $\sim 10 \text{ W}/\text{cm}^2$  for double spaced cavities, and  $\sim 8 \text{ W}/\text{cm}^2$  for triple spaced cavities. However, as the power level increased, the boiling curves converged, resulting in the same nucleate boiling heat transfer rate for each surface, as the curves approached CHF.

Investigations into the effect of cavity shape were also conducted. The mouth size of the cavities was identical; the difference was that one type of cavity had sharp internal corners (inverse pyramidal), and the other was round (bulb shaped, Figure 2.10c).

Results showed the pyramidal shaped cavities to be superior to the bulb shaped cavities, resulting in a higher CHF ( $40 \text{ W/cm}^2$  compared to  $32 \text{ W/cm}^2$ ), higher nucleate boiling heat fluxes ( $30 \text{ W/cm}^2$  compared to  $20 \text{ W/cm}^2$  at 20 K superheat), and lower incipient boiling temperature overshoot (28 K compared to 40 K). Baldwin, Bhavnani, and Jaeger (1998) proposed that the pyramidal shaped cavities trapped vapor and air much more effectively due to the sharp internal corners.

Kubo, Takamatsu, and Honda (1999) also studied nucleate boiling on smooth silicon and silicon etched with micro-re-entrant cavities (Figure 2.10d). Their cavities had round mouths of about  $1.6 \mu\text{m}$  and  $3.1 \mu\text{m}$  in diameter and were spaced 0.1 mm and 1 mm apart, giving them four different surface configurations. Their experiments were carried out in degassed and gas dissolved FC-72, subcooled by 3 K and 25 K.

The results showed that boiling incipience was greatly affected by the dissolved gas content, not by the size of the cavity mouth. Using subcooled liquid with dissolved gas, they observed no temperature excursion at boiling incipience. Using degassed liquid at 3 K or 25 K subcooling, temperature excursion at boiling incipience ranged from 8 to 20 K for the four surfaces with micro-re-entrant cavities and the smooth silicon surface. Nucleate boiling ensued at a surface superheat of about 6 K. The nucleate boiling heat transfer rates for the surfaces with micro-re-entrant cavities were significantly higher than on the smooth surface, and were highest for the surface with the larger sized mouths and larger number density of cavities (peak  $h_{NB}$  in saturation boiling  $\sim 1.1 \text{ W/cm}^2 \text{ K}$ ). Finally, Kubo, Takamatsu, and Honda (1999) reported that the heat transfer rate was higher with gas dissolved FC-72 than degassed FC-72. For example, in 25 K subcooled FC-72 with dissolved gasses, the wall superheat at  $10 \text{ W/cm}^2$  was 18 K, and in degassed FC-72 subcooled to 25 K, the wall superheat was 22 K.

Arbelaez, Sett, and Mahajan (2000) used porous aluminum foam as a boiling surface in saturated FC-72. The foam was  $2.54 \times 6.35 \times 6.35 \text{ cm}$  with porosities of 90-98% and 5-40 pores per linear inch (Figure 2.10e). The foam was uniformly heated using an underlying aluminum block,  $2.54 \times 6.35 \text{ cm}$  and 2.54 cm thick. The standard reference surface used in this study was a flat  $1.0 \times 2.5 \times 2.5 \text{ cm}$  block of machined aluminum.

They reported a 2-4 times improvement in the heat removal by natural convection with the aluminum foam. The foam acted like a finned extension of the heated area. They also stated that the flow through the complex foam matrix improved the mixing and thus improved the natural convective heat transfer.

Boiling ensued in the foam matrix at 8-10 K superheat based on the measured temperature by thermocouples located in the base plate. This superheat was slightly lower than that observed on the flat plate. A temperature excursion to 12 K occurred only in two cases, otherwise there was no incipient boiling temperature overshoot. The nucleate boiling heat transfer coefficient with the aluminum foam was about 5 times higher than on the flat block. They reported that in the high heat flux region, bubbles coalesced forming vapor envelopes over the metal foam fibers. However, while the film formation took place near the heated surface, the high thermal conductivity of the foam carried heat to other regions further away where nucleate boiling still took place. This tended to smooth the transition from nucleate boiling to stable film boiling. They reported that this transition was marked by a small surface temperature increase. The reported critical heat flux was  $28.8 \text{ W/cm}^2$ , 50% higher than on the flat plate; however, the corresponding surface superheat on the block with foam was about 40 K higher than on the flat aluminum block.

Porosity and pore pitch also had an effect on nucleate boiling heat transfer. For a given PPI (pores per inch), the lower porosity sample resulted in higher boiling heat transfer rate. The lower porosity implies more material in the matrix and thus more nucleation sites available. Arbelaez, Sett, and Mahajan (2000) stated that there was an increase in the range of 10 – 30% in the exposed surface area in the porosities considered. The improved boiling heat transfer rate as PPI increased was attributed to increased hydrodynamic disturbances and surface area. However, in the high PPI foams, the slope of the boiling curve decreased at lower heat fluxes than in the lower PPI foams. This was attributed to the vapor envelopes forming in small volumes over the thinner foam fibers.

Marto and Lepere (1982) studied saturation boiling of R-113 and FC-72 on commercially available structured surfaces; Union Carbide High Flux (Figure 2.10f),

Hitachi Thermoexel-E (Figure 2.10g), and Wieland Gewa-T (Figure 2.10h). These surfaces were used on a 15.8 mm outer diameter horizontal copper tube and the results were compared to those obtained on an untreated copper tube of the same diameter. They reported an increase of 2 to 5 times in the heat transfer coefficient on the enhanced surfaces in saturation boiling of FC-72. In general, their findings showed the High Flux surface results in the highest enhancement (lower superheat at a given heat flux) over a range of heat fluxes, but the Gewa-T surface at high heat fluxes. CHF on the High Flux and Thermoexel-E surfaces were only slightly higher than on the untreated copper tube ( $\sim 12 \text{ W/cm}^2$ ). Using the Gewa-T surface, the heat flux reached  $18.8 \text{ W/cm}^2$  without exceeding CHF. The surface superheat at the maximum heat flux achieved on the enhanced surfaces was lower than the superheat at the maximum heat flux on the untreated surface.

#### **2.4.1.2 Micro-Structured Surfaces**

Increasing the surface area wetted with the boiling liquid is one method to increase the total heat removal rate by nucleate boiling. Many different surfaces with pins, pores, and fins of varying length, density and thickness, have been tested in pool boiling experiments of dielectric liquids. These surfaces may be divided into two categories based on the bubble departure diameter: (a) micro-structured surfaces (length scale  $< 0.5 \text{ mm}$ ), and (b) macro-structured surfaces (length scale  $\geq 0.5 \text{ mm}$ ). Other criteria for defining macro-structured and micro-structured surfaces have also been reported and used in the literature.

In saturation pool boiling of R-11, Nakayama et al. (1980) used a copper surface with parallel channels cut into it (0.25 mm channel width, 0.55 mm pitch, 0.4 mm deep). A lid placed over the channels had triangular pores punched into it, making a network of small, interconnected pores (Figure 2.11a). The pore sizes were measured by the diameter of a circle that would fit inside the equilateral triangular pore. For R-11, the pore sizes were 0.04 mm, 0.06 mm, and 0.10 mm. All three surface configurations greatly improved the nucleate boiling heat transfer, reducing the superheat by up to 90% compared to a plane surface throughout the boiling curves. No CHF data were obtained in this work.

Anderson and Mudawar (1989) used several different boiling surfaces in saturation pool boiling experiments of FC-72. All surfaces were tested in the vertical orientation. Some of these were surfaces with micro-fins (0.305 mm width, 0.610 pitch, 0.508 height) oriented parallel to gravity, microstuds (0.305 mm width, 0.610 pitch, 0.508 height), and inclined micro-grooves (0.305 mm width, 0.610 pitch, 0.488 depth, 30° inclined from the vertical) cut perpendicular to gravity (Figure 2.11b). These results showed that these surfaces greatly enhanced the nucleate boiling heat transfer, but each also had a temperature overshoot prior to boiling incipience to a superheat between 10 K and 20 K. The boiling incipience superheat was ~ 6 K for each surface. On the smooth surface, boiling incipience ensued at a wall superheat of ~ 15 K. They reported a CHF of 19.8 W/cm<sup>2</sup> on the plane surface, compared with 30.0, 34.6, and 51.2 W/cm<sup>2</sup> for the surfaces with micro-grooves, micro-fins, and micro-studs, respectively. The surface superheat at CHF exceeded 40 K for each case, corresponding to a surface temperature > 96 °C. They concluded that the higher CHF was because of the increase in the surface area wetted by the boiling liquid.

Misale et al. (1999) have investigated saturation pool boiling of FC-72 on a 30 mm diameter heated surface with square copper pins, 3 mm high and 0.4 mm and 0.8 mm wide, both in the upward facing and vertical orientations (Figure 2.11c). The spacing of the pins was the same as their width. At low heat fluxes, the nucleate boiling heat transfer rates on the surface with 0.4 mm wide pins were higher than on the surface with 0.8 mm-wide pins. CHF on the former in the upward facing orientation (60 W/cm<sup>2</sup>) was slightly higher than in the vertical orientation (55 W/cm<sup>2</sup>). The corresponding CHF on the surface with 0.8 mm wide pins were 52 W/cm<sup>2</sup> (upward facing) and 50 W/cm<sup>2</sup> (vertical); these CHF values are based on the footprint area of 7.07 cm<sup>2</sup>. The reported ratio of the geometrical to the footprint area of the surfaces with the 0.4 mm and 0.8 mm wide pins was 8.5 and 4.75. Thus, the total surface averaged CHF for the surface with 0.4 mm wide pins is only 7.1 W/cm<sup>2</sup> in the upward facing orientation and 6.5 W/cm<sup>2</sup> in the vertical orientation and for the surface with the 0.8 mm wide-pins, the corresponding CHF values are 10.9 and 10.5 W/cm<sup>2</sup>. These CHF values are much lower than ~12 – 18 W/cm<sup>2</sup> reported by numerous investigators for saturation boiling of FC-72 on plane

copper and silicon surfaces (Rainey and You 2000; Chang and You 1997a,b; Watwe, Bar-Cohen, McNiel 1997; Wei and Honda 2003; Z. W. Liu et al. 2001; Mudawar, Howard, Gersey 1997; Priarone 2005; Parker and El-Genk 2005; Yu, Lu, and Cheng 2006; Jung and Kwak 2006; Ferjančič, Rajšelj, and Golobič 2006; Arik, Bar-Cohen, and You 2007; Yu and Lu 2007; Ujereh, Fisher, and Mudawar 2007).

Honda, Takamatsu and Wei (2002) investigated boiling in degassed and gas-dissolved FC-72 on micro-fins etched into silicon (Figure 2.11d). Their work was expanded by Wei and Honda (2003) and Wei, Guo, and Honda (2005). The sizes of the square micro-fins were 30 or 50  $\mu\text{m}$  thick and 60, 120, 200, or 270  $\mu\text{m}$  high. In each case, the fin pitch was twice the fin thickness. The fins were made by applying photoresist to a silicon surface, exposing the surface to UV light through a patterned mask, then etching the surface to the desired fin height and removing the photoresist. The process left the top of the pins smooth, with a fine roughness along the sides, and increased roughness near the fin base (Figure 2.11d). These enhanced boiling surfaces were tested in the pool boiling of FC-72 at saturation and 3, 25, 35, and 45 K subcooled for both gas dissolved and degassed liquid.

The results of their pool boiling tests showed that with gas dissolved in the FC-72 liquid, the surface temperature for boiling incipience decreased and the temperature excursion prior to boiling incipience was reduced or eliminated. As a result, the heat transfer rate in the low heat flux nucleate boiling region was higher than in the degassed liquid. In the high heat flux region, the dissolved gas content had little effect on the nucleate boiling heat transfer. The micro-finned surfaces showed a sharp increase in the heat flux with increasing wall superheat. The wall superheat was lower for the surfaces with increased roughness near the fin base. The slope of the boiling curve was much steeper for the enhanced surface than the smooth surface.

The measured CHF for all micro-finned surfaces increased over that for the smooth surface. For a fixed fin thickness, CHF increased monotonically with the fin height. For a fixed wetted surface area ratio (total area/projected area), CHF increased with increasing fin height, and increased linearly with increased liquid subcooling. The

highest CHF achieved was  $84.5 \text{ W/cm}^2$ , using gas saturated and 45 K subcooled FC-72 liquid and a chip with 50  $\mu\text{m}$  thick and 270  $\mu\text{m}$  high micro-fins

Ramaswamy, et al. (1999, 2000, 2003) investigated saturation boiling of FC-72 on micro-machined surfaces (Figure 2.11e). Similar structures (single layer) were used in boiling experiments performed by Ghiu and Joshi (2005) and Launay et al. (2006). The surfaces were made of layers of copper plates bonded together with gold, or of silicon or copper in the case of a single layer. Rectangular channels first were cut into the top side of the plate, then in the bottom side perpendicular to those channels on top. The channels intersected, creating pores in the structure. Several different configurations were tested with varying structure height, pore size, and pore pitch. Most of these tests were carried out in the nucleate boiling regime. The experiments were stopped when the temperature at the base of the structure reached  $85 \text{ }^\circ\text{C}$ , or the surface superheat was about 30 K, which was prior to CHF. Comparisons were made to a solid copper block of the same dimensions as the micro-machined structure.

The results showed enhancement in the natural convection region due to the increased surface area of the structure. In the only study involving the natural convection regime (Ramaswamy et al., 1999), they noted boiling incipience at a superheat of about 3 K with no associated temperature excursion. The power increments they used were 1 W in the natural convection region. They reported significant enhancement in the nucleate boiling heat transfer rate with the micro-machined surface. Their data showed increased heat dissipation with increased pore size in the range of 90 – 320  $\mu\text{m}$  and decreased pore pitch (larger pore density). The effects for each of these factors were most prominent in the low superheat region ( $\Delta T_{\text{sat}} = 4 - 12 \text{ K}$ ). In addition, as the stack height increased, heat dissipation increased at low and high wall superheats, but negligible improvement was noted in the intermediate superheat ranges (fully developed nucleate boiling).

Two possible reasons could have caused the observed effect. One is the difference between boiling from subsurface layers and the top layer. For a single-layered structure, the top of the channels are open to the liquid pool and liquid flows into the channels through all the pores. For a multi-layered structure, they hypothesized that the lower

layers are filled with vapor and bubbles will not nucleate from these pores. Liquid intake in the lower layers is only through the open end of the channels, resulting in less liquid supply compared to the single-layered structure and less evaporation inside the channels. Therefore, adding more layers to the structure will not result in a proportional increase in the heat transfer rate. In addition, the fin effect led to less efficient boiling on the top of the taller structures, contributing to negligible improvements in the boiling heat transfer rate at intermediate and high heat.

Al-Hajri et al. (2005) investigated saturation boiling of HFE-7100 on copper micro-fins of varying fin lengths, fin densities, and fin thickness (Figure 2.11f). Some of the parameters investigated were the effect of fin height and channel width on nucleate boiling heat transfer. For constant fin thickness (0.169 mm) and density (100 fins per inch), three different fin heights were tested, 0.456 mm, 0.660 mm, and 0.899 mm. They reported that all surfaces “extended the nucleate boiling range beyond that for a flat plate”, reporting values of CHF of 37 – 45 W/cm<sup>2</sup> and average nucleate boiling heat transfer coefficients of 1.5 – 2.8 W/cm<sup>2</sup> K. The nucleate boiling heat transfer coefficients increased with increasing fin height. However, no data for nucleate boiling on a flat plate were given. CHF for saturation boiling of HFE-7100 on plane copper surfaces has been reported by others to be between 22.0 and 25.2 W/cm<sup>2</sup>, and the peak heat transfer coefficient from ~0.8 – 1.4 W/cm<sup>2</sup> K (Z. W. Liu et al. 2001; J. W. Liu et al. 2001; El-Genk and Bostanci 2003a,b; Priarone 2005; El-Genk and Parker 2005; Parker and El-Genk 2008).

Additional experiments of saturation boiling of HFE-7100 were done by Al-Hajri et al. (2005) which investigated the effect of channel width and fin spacing. These experiments showed that as the fin spacing decreased from 0.089 mm to 0.042 mm, the superheat at a given nucleate boiling heat flux decreased. They stated that this might be due in part to the increased wetted surface area. However, CHF values on the surfaces with smaller fin spacings were lower. Experiments were also conducted with 10 x 10 mm and 10 x 17 mm surfaces; the 17 mm side was along the groove direction. They reported higher nucleate boiling heat transfer rates and CHF with the larger (10 x 17 mm) surface. At high heat fluxes in nucleate boiling, the authors stated that the ends of the

groves were supplying liquid to the inner surfaces. The surface superheat at CHF was 11 K higher for the longer test section.

Experiments completed by Launay et al. (2006) in saturation boiling of PF-5060 (identical to FC-72) at pressures from 0.46 – 1.32 bar compared the nucleate boiling results on different surfaces (including silicon pin fins, carbon nanotube coated pin fins, silicon 3-dimensional microstructure, and the 3-dimensional structure coated with carbon nanotubes) (Figure 2.11e and g). The microstructured surface was similar to those used by Ramaswamy et al (1999, 2000, 2002) and Ghiu and Joshi (2005), and had an area ratio of 6.4. The silicon surface had cylindrical pins, 70  $\mu\text{m}$  diameter, 250  $\mu\text{m}$  high, and 200  $\mu\text{m}$  pitch. The area ratio for this surface was 1.5. The surfaces with micropins coated with 100  $\mu\text{m}$  long carbon nanotubes had pins 70- $\mu\text{m}$  diameter and 100- $\mu\text{m}$  high with a pitch of 100  $\mu\text{m}$ . The reported area ratio for this structure was 2.0. They terminated all experiments either at CHF or at a surface temperature of 85  $^{\circ}\text{C}$ , whichever came first (Launay et al., 2006).

The reported results for nucleate boiling at 1 bar system pressure showed that only the microstructure surface reached CHF. All other surfaces reached a base surface temperature of 85  $^{\circ}\text{C}$  prior to reaching CHF when experiment was terminated. The maximum heat flux reported (27  $\text{W}/\text{cm}^2$ ) occurred on this 3-dimensional microstructure. The presented boiling curves for sub-atmospheric saturation boiling (0.672 bar) also showed that the microstructure surface had higher nucleate boiling heat transfer than any of the other surfaces tested, followed by the bare silicon pins.

Ujereh, Fisher, and Mudawar (2007) performed saturation boiling experiments in FC-72 on a copper surface with microstuds (0.25 x 0.25 x 0.25 mm) having a pitch of 0.5 mm (Figure 2.11h). The microstudded surface was tested bare and coated with carbon nanotubes. The surface with bare copper microstuds (area ratio 2) had a lower peak nucleate boiling heat transfer coefficient compared to plane copper surfaces, but increased CHF by 75%. The addition of carbon nanotubes (CNT) to the microstuds enhanced the nucleate boiling heat transfer coefficient, showing a near vertical boiling curve, but the CHF was lower for the surface with CNT coated microstuds (26  $\text{W}/\text{cm}^2$ )

than that with bare studs ( $32 \text{ W/cm}^2$ ), but still larger than on plane copper ( $18 \text{ W/cm}^2$ ). They explained that CHF decreased on the CNT coated microstuds because of the absence of the carbon nanotubes along the circumference of the studs and because the fin effect of the studs reduced the effectiveness of the carbon nanotubes on top of the studs (Ujereh, Fisher, and Mudawar, 2007). Near CHF, the vapor generated from the base area coalesced and engulfed the top surfaces of the microstuds.

#### **2.4.1.3 Macro-Structured Surfaces**

The enhanced structure of Ferjančič, Rajšelj, and Golobič (2006) was comprised of sintered copper spheres of 200 or 50  $\mu\text{m}$  diameter. The spheres were arranged in an array of cones 0.5 and 1.0 mm high, with the peak-to-peak distances being the same as the cone height (Figure 2.12a). Three different surface configurations were manufactured and tested: 200  $\mu\text{m}$  spheres in 1 mm cones; 50  $\mu\text{m}$  spheres in 0.5 mm cones, and 50  $\mu\text{m}$  spheres in 1 mm cones.

All three porous layer tested showed boiling incipience at a very low surface superheat ( $\Delta T_{sat} < 2 \text{ K}$ ). The highest nucleate boiling heat transfer coefficients occurred at the end of the fully developed nucleate boiling region and were  $\sim 2.0 \text{ W/cm}^2 \text{ K}$ . The reported saturation boiling CHF was  $19.5 \text{ W/cm}^2$  for the surface with the 50  $\mu\text{m}$  spheres in 0.5 mm cones,  $23.5 \text{ W/cm}^2$  for the surface with 200  $\mu\text{m}$  spheres in 1 mm cones, and  $32.5 \text{ W/cm}^2$  for the surface with 50  $\mu\text{m}$  spheres in 1 mm cones. These CHF values represent an increase of 1.34, 1.61, and 2.23 times of FC-72 saturation CHF on a plane surface ( $14.6 \text{ W/cm}^2$ ) (Ferjančič, Rajšelj, and Golobič, 2006).

Rainey and You (2000) reported results of saturation boiling of FC-72 on a surface with a 5 x 5 array of 1 mm square pins. The pins had a pitch of 2 mm and their height varied from 1 mm to 8 mm (Figure 2.12b). The authors reported that the addition of the square pins greatly enhanced the heat transfer performance up to a pin height of about 5 mm. For heights more than 5 mm, they believed that the surface temperature at the tip was too low to sustain nucleate boiling, and the effective boiling area was reduced, providing no additional enhancement due to the surface area increasing.

The presence of the pins created a resistance to the departing vapor bubbles to the returning liquid circulation, which in turn increased the residence time of the bubbles between the pins. Bubbles growing and departing coalesce with the vapor bubbles still between the pins, decreasing the nucleate boiling heat transfer rate at high surface superheats. At the surface superheat near CHF, they stated that a localized dry-out condition occurs near the base of the pins (Rainey and You, 2000). The maximum power removed from these structures increased linearly with pin height up to 4 mm. For the largest pin height of 8 mm, the power removed increased, but the increase was much less than the corresponding increase in the surface area, due to the non-boiling pin tips.

Saturation boiling experiments with FC-72 on rectangular pin arrays of copper were completed by Yu and Lu (2007). On a 10 x 10 mm surface, they had made 1 x 1 mm square pins 0.5, 1, 2, and 4 mm high, with a spacing of 0.5, 1, or 2 mm. These arrangements resulted in pin densities of 16, 25, and 49 pins per cm<sup>2</sup>, respectively (Figure 2.12c). They observed that boiling generally started on the pin tips, even though the superheat at the pin base was larger than at the tip. They stated that bubbles were trapped at the pin root, while those on the pin tips were swept away by the convective flow generated by liquid circulation between the pins. They also noted that the wall superheat at boiling incipience decreased with increasing pin height and pin density. In some cases the temperature excursion at boiling incipience was eliminated.

As the pin height increased and the pin spacing decreased, the total power removed by nucleate boiling increased, due to the increased wetted surface area available for boiling. Using the tallest pins and smallest spacing (increasing the total surface area to 8.84 times the heated footprint area), 98.3 W were removed from the 1 cm<sup>2</sup> heated footprint. However, when based on the total wetted surface area, CHF and the nucleate boiling heat transfer coefficient decreased with increasing area ratio. Smaller pin spacing and longer pins increased the hydraulic resistance to departing bubbles and the rewetting liquid. Additional resistance to departing bubbles increases the bubbles crowding and coalescence near the heated surface, which reduces the overall heat transfer rate for nucleate boiling.

## 2.4.2 Effect of Liquid Thermophysical Properties

A few studies have been performed which systematically investigated the effect of thermophysical properties of in dielectric liquids on nucleate boiling. Danielson, Tousignant, and Bar-Cohen (1987) experimentally investigated saturation boiling on a platinum wire with several different inert liquids (FC-43, FC-72, FC-75, FC-77, FC-84, FC-87, L-1402, and R-113). They discussed boiling incipience and the temperature overshoot at boiling incipience, nucleate boiling, and CHF, and compared the values with existing correlations. The results they obtained showed that temperature excursions at boiling incipience nearly always occur with these liquids. The extent of these excursions varied widely, from 24 – 47 K, and the resulting reduction in surface superheats of 15 – 30 K. Also, the nucleate boiling heat flux were predicted reasonably well using the Rohsenow (1952) correlation:

$$\frac{c_p \Delta T_b}{h_{fg}} = C_{sf} \left[ \frac{q''}{\mu_l h_{fg}} \sqrt{\frac{\sigma}{g(\rho_l - \rho_v)}} \right]^{0.33} \left( \frac{c_p \mu_l}{k} \right) \quad (2.8)$$

The results of their experiments, however, are highly dependent on the boiling surface characteristics. For example, on a particular wire, the saturation nucleate boiling curves for different inert liquids were nearly identical. However, the boiling curves differed from wire to wire, even among tests using the same liquid. For example, for saturation boiling of FC-87, the boiling curve using wire 12-1 was shifted to the left of the curve using wire 4-2, but was nearly identical to the boiling curve of FC-84 on wire 12-1. Saturation CHF, ranging from 13.5 W/cm<sup>2</sup> for FC-43 to 23.9 W/cm<sup>2</sup> for R-113, was also highly dependent on the specific wire used.

Marto and Lepere (1982) performed their pool boiling experiments with commercial boiling surfaces (Union Carbide High Flux, Figure 2.10e, Hitachi Thermoexel-E, Figure 2.10f, and Wieland Gewa-T, Figure 2.10g) and R-113 and FC-72 liquids. The superheat required to initiate boiling was about 1 – 3 K higher for R-113 than for FC-72, and the temperature excursion prior to boiling incipience for R-113 was also higher by 3 – 11 K.

The nucleate boiling heat transfer rate for R-113 on enhanced surfaces was 2 – 10 times that on the smooth surface, whereas for FC-72 it was 2 to 5 times higher.

Arik and Bar-Cohen (2001) used the thermophysical properties of HFE-7100, HFE-7200, and FC-72 to compare the theoretical heat transfer by nucleate boiling. The calculated bubble departure diameters in the Novec liquids (0.309 mm for HFE-7100 and 0.366 mm HFE-7200) were larger than for the Fluorinert liquid (0.258 for FC-72) using the expression (Mikic and Rohsenow, 1969):

$$d_d = \sqrt{\frac{\sigma 4.65 \times 10^{-4} Ja^{*5/4}}{g(\rho_l - \rho_v)}} \quad (2.9)$$

Conversely, the bubble departure frequency and the thickness of the superheated thermal boundary layer were calculated to be smaller for the HFE fluids. The calculated departure bubble diameters by Equation 2.9 are almost half of what as been observed experimentally for these dielectric liquids (Rini, Chen, and Chow, 2001; El-Genk and Bostanci, 2003a,b). No conclusions were drawn as to the comparison between the nucleate boiling heat transfer coefficients for HFE-7100, HFE-7200, and FC-72.

Using a modified form of the critical heat flux correlation proposed by Zuber (1959) (Equation 2.6), CHF values were calculated for HFE-7100, HFE-7200 and FC-72 (Arik and Bar-Cohen, 2001). The correlation predicted higher CHF values for HFE-7100 and HFE-7200 compared to FC-72. Their subsequent experimental CHF values were within  $\pm 25\%$  of the predicted values, and 50 – 90% higher than the CHF reported in the open literature for FC-72 on similar surfaces. In work done by El-Genk and Bostanci (2003a,b), El-Genk and Parker (2004a,b; 2005), Parker and El-Genk (2005, 2006b), and Priarone (2005), separate investigations compared HFE-7100 and FC-72 dielectric liquids for boiling on copper and porous graphite. Consistent with the results reported by Arik and Bar-Cohen (2001), CHF for HFE-7100 was higher than measured and found in the literature for FC-72. El-Genk and Bostanci (2003a,b) reported the saturation CHF of HFE-7100 on copper of  $24.5 \text{ W/cm}^2$ ; Priarone (2005) reported  $25.2 \text{ W/cm}^2$ . The value reported by El-Genk and Parker (2005) is  $22.7 \text{ W/cm}^2$ . The average value of saturation

CHF of FC-72 on copper and silicon as reported in the literature is  $16.3 \text{ W/cm}^2$  (O'Connor, You, and Chang, 1996; Chang and You, 1997a,b; Chang, You, and Haji-Sheikh, 1998; Rainey and You, 2000; Rainey, You, and Lee, 2003; Honda, Takamatsu, and Wei, 2002, Wei and Honda, 2003; McNiel, 1992; Watwe, Bar-Cohen, and McNiel, 1997; Z. Liu et al., 2001; O'Connor, 1994; Mudawar, Howard, and Gersey, 1997; Howard and Mudawar, 1999; Priarone, 2005; El-Genk and Parker, 2004b; Parker and El-Genk, 2005). On porous graphite saturation CHF of HFE-7100 is  $31.8 \text{ W/cm}^2$  (El-Genk and Parker, 2005). The saturation CHF value of FC-72 on porous graphite was reported as  $27.3 \text{ W/cm}^2$  (Parker and El-Genk, 2005).

### **2.4.3 Effect of Surface Orientation**

When using immersion cooling of high powered electronics, designers must take into account the type of liquid and the boiling surface to be used as well as the inclination angle of the surface. Packaging of computer components may require different orientations with respect to gravity. Several studies investigating the effect of surface inclination on boiling of dielectric liquids have been performed (Mudawar, Howard, and Gersey, 1997; Chang and You, 1996; Howard and Mudawar, 1999; Rainey and You, 2001; El-Genk and Bostanci, 2003a,b; Priarone, 2005; Parker and El-Genk, 2006a,b; Parker and El-Genk, 2008). In general, the results are the same as those obtained from non-dielectric liquids. Chang and You (1996) used saturated FC-72 and a smooth copper surface measuring  $10 \times 10 \text{ mm}$  to study the effect of surface orientation on nucleate boiling. At low surface superheats, the boiling heat transfer coefficient increased as the surface inclination increased from  $0^\circ$  (horizontal upward facing) to  $90^\circ$  (vertical). Rainey and You (2001) reported similar results for smooth copper surfaces measuring  $20 \times 20 \text{ mm}$  and  $50 \times 50 \text{ mm}$  in saturated FC-72. They reported that the nucleate boiling heat transfer rate increased for  $0^\circ < \theta < 45^\circ$ , then decreased as the angle exceeded  $90^\circ$  (vertical). The difference in the boiling heat transfer diminished as the size of the boiling surface increased from  $10 \times 10 \text{ mm}$  to  $50 \times 50 \text{ mm}$ .

Wei and Honda (2003) reported that the nucleate boiling heat transfer rate was higher for a vertical smooth silicon surface ( $10 \times 10 \text{ mm}$ ) than for the same surface in the

horizontal upward orientation in 25 K subcooled FC-72. From a 12.7 x 12.7 mm copper surface in “near saturated” FC-72, the data of Reed and Mudawar (1997) indicated that at low surface superheats, nucleate boiling heat transfer improves as the surface inclination increases. At high surface superheats, the nucleate boiling heat transfer decreases as the inclination increases.

El-Genk and Bostanci (2003a,b) performed experiments for saturated and subcooled HFE-7100 on a 10 x 10 mm copper surface. In saturation boiling, the nucleate boiling heat transfer coefficient increased as the surface inclination,  $\theta$ , increased from upward facing ( $0^\circ$ ) to downward facing ( $180^\circ$ ) at low surface superheats. The trend is reversed at high surface superheats. For subcooled liquid, they reported that for  $0^\circ < \theta < 90^\circ$ , the heat transfer coefficient decreased slightly with increased inclination angle, but increased with increased subcooling. At low surface superheats, the nucleate boiling heat transfer rate was almost the same or increased slightly as the inclination angle increased.

On surfaces with micro-porous coatings in saturated FC-72, nucleate boiling heat transfer was independent of inclination angle for all sizes of boiling surfaces tested (Chang and You, 1996; Rainey and You, 2001). However, for micro-finned surfaces with 25 K subcooled FC-72, the nucleate boiling heat transfer rate at low surface superheats was higher on the vertical than on the horizontal surfaces, and about the same or less at high surface superheats (Honda, Takamatsu, and Wei, 2002; Wei and Honda, 2003).

Despite the minor discrepancies in the angular dependence of nucleate boiling heat transfer, there is a general agreement on the effect that the inclination angle has on CHF. Reported results showed that CHF decreases slowly as the surface inclination increases up to  $90^\circ$  degrees (vertical), then rapidly decreases to its minimum value as the inclination approaches  $180^\circ$  (horizontal-downward facing) (Chang and You, 1996; Reed, 1996; Howard and Mudawar, 1999; Rainey and You, 2001; El-Genk and Bostanci, 2003a; Priarone, 2005; Parker and El-Genk 2006). CHF correlations and analytical models have been developed by El-Genk and Guo (1993), Vishnev (1974), Brusstar and

Merte (1997), Chang and You (1996), El-Genk and Bostanci (2003a), and Howard and Mudawar (1999), for dielectric and non-dielectric liquids.

In summary, the following observations can be made about the effect that the surface orientation or inclination has on nucleate boiling heat transfer and CHF: (a) at low surface superheats, the nucleate boiling heat transfer increases as inclination increases; (b) at high surface superheats, the trend is reversed and nucleate boiling heat transfer deteriorates as the inclination angle increases; (c) CHF decreases slightly as the inclination angle increases from  $0^\circ$  to  $90^\circ$  degrees, then decreases rapidly as the angle approaches  $180^\circ$ . From the reviewed data of dielectric liquids, the ratio of the CHF for downward facing surfaces to the CHF for upward facing surfaces ( $CHF_{180^\circ}/CHF_{0^\circ}$ ) is between 7% and 28% for both plain and micro-porous coated surfaces (Chang and You, 1996; Reed, 1996; Howard and Mudawar, 1999; Rainey and You, 2001; El-Genk and Bostanci, 2003a; Priarone, 2005; Parker and El-Genk 2006).

Howard and Mudawar (1999) developed a CHF model in the “near vertical” orientation using boiling data of FC-72 and PF-5052 on 12.7 x 12.7 mm copper. They identified three distinct CHF regions, which they called upward facing ( $\theta < 60^\circ$ ), near vertical ( $60^\circ < \theta < 165^\circ$ ), and downward facing ( $\theta > 165^\circ$ ). In the upward facing orientation, vapor is removed vertically from the surface by buoyancy. In the near vertical orientation, vapor moves along the boiling surface and the observed wavy liquid-vapor interface is due to the instabilities caused by the vapor movement. Bubbles growing and coalescing, covering most or all of the heated surface characterize the downward facing orientation. When bubbles reach the edge of the heated surface they slide off. Parker and El-Genk (2006) and El-Genk and Parker (2008) observed that for nucleate pool boiling near CHF at  $\theta = 180^\circ$  (downward facing), vapor masses forming on the heated surface grow into a dome and are pushed off the surface by the upward force of the liquid, which occurs at a certain frequency (Parker and El-Genk, 2006; El-Genk and Parker, 2008).

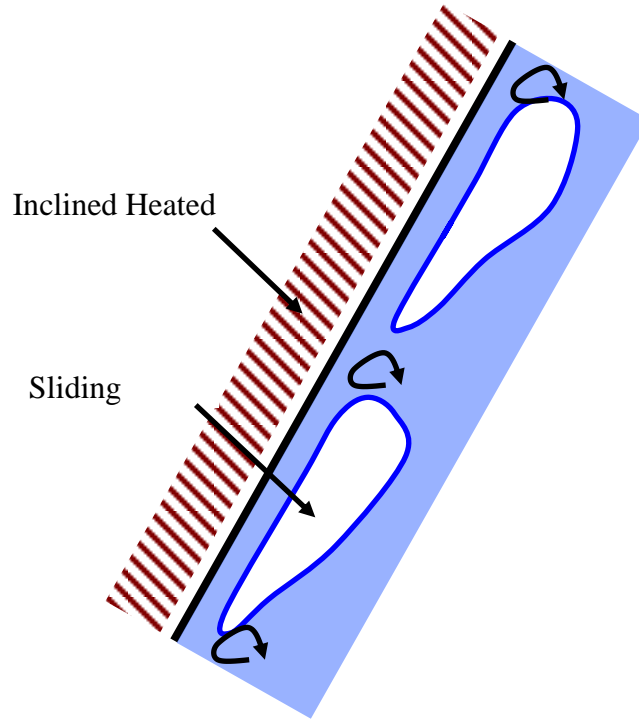
Nishikawa et al. (1984) proposed a theory regarding the nucleate boiling heat transfer from surfaces inclined  $> 90^\circ$ . The bubble movement was studied by observing injected

air bubbles moving over a downward facing non-heated surface. The film thickness between the bubble and the surface was measured with electrodes embedded in the surface. They concluded that two mechanisms are responsible for removing heat from a downward facing boiling surface. The first is the sensible heat transfer due to the elongated bubbles removing the thermal boundary layer as the bubble travels along the surface. The second effect is the latent heat of vaporization from evaporation of the thin film between the elongated bubble and the heated surface. Nishikawa et al. (1984) measured the thickness of the film between the bubble and the surfaces as a function of inclination angle. They measured the thinnest film at the highest inclination angles and increasing film thickness as the angle decreased ( $120^\circ < \theta < 175^\circ$ ) (Figure 2.13). The average residence time of a bubble was longest for larger inclination angles. Qiu and Dhir (2002) measured the velocity of bubbles on inclined downward facing surfaces in saturated and subcooled PF-5060. They reported that bubble velocities were lower at higher inclination angles, which would increase the residence time of the bubble on the heated surface. This evidence supports the claim that thin film evaporation dominates heat transfer at large inclination angles, thus increasing the heat transfer coefficient.

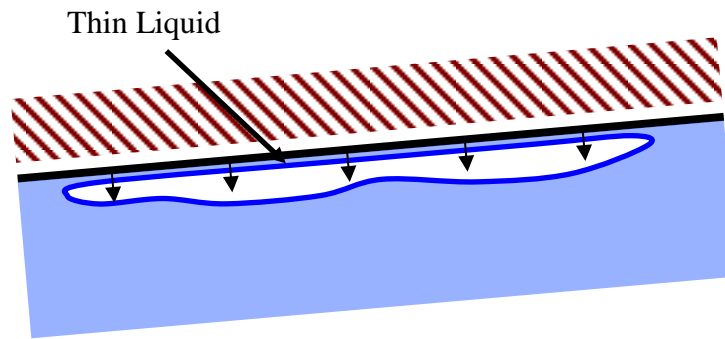
## **2.5 Summary**

With increasing power dissipation from computer chips and the expected increase in heat flux from high power electronics, different methods are needed to effectively remove the generated heat from the new generations of microprocessors while keeping the chips' junction temperature within the recommended values by the industry. Direct immersion cooling by nucleate boiling of dielectric liquids is an attractive option for the thermal management of the high power computer chips. However, because dielectric liquids such as FC-72 and HFE-7100 are highly wetting, a temperature excursion prior to boiling incipience often occurs. Pool boiling research done with FC-72 and HFE-7100 liquids has focused on reducing or eliminating the temperature excursion at boiling incipience, increasing the nucleate boiling heat transfer coefficient and CHF, as well as understanding the effect of various parameters (liquid subcooling, surface orientation, etc.) on both nucleate pool boiling and CHF.





(a) Sensible heat transfer through



(b) Liquid film

**Figure 2.13 Different modes of heat transfer during nucleate boiling for surfaces inclined  $> 90^\circ$ .**

Methods used to improve boiling heat transfer included modifying the heated surface to increase the nucleation sites density and/or increasing the wetted area in by the liquid for a given heated footprint. Increasing the nucleation site density has been done using micro-porous coatings and porous surfaces, roughened and etched surfaces, and surfaces with uniformly manufactured pits and cavities. Increasing the wetted area had been accomplished with pins and fins of various length and density. In general, using any of these surfaces for nucleate boiling of dielectric liquids reduced or eliminated the temperature excursion at boiling incipience and increased the nucleate boiling heat transfer rate and CHF. Increasing liquid subcooling also increases the removed thermal power in nucleate boiling, but at the expense of increasing the footprint temperature. CHF increases linearly with increased subcooling. Conversely, increasing the surface inclination from  $0^\circ$  (upward facing) to  $180^\circ$  (downward facing) causes CHF to decrease.

Much of the past research has focused on the effect of a single parameter on pool boiling of dielectric liquids (e.g. surface, liquid subcooling, pressure, inclination). A few have investigated the combined effects of more than one parameter. For example, El-Genk and Bostanci (2003b) reported on the combined effects of liquid subcooling and surface inclination on nucleate boiling heat transfer on smooth copper. Z. Liu et al. (2001) performed boiling experiments using smooth copper in saturated and subcooled FC-72 and HFE-7100. However, no results have been reported which included the combined effects of liquid subcooling, surface inclination, wetted area and structure (porous, micro-porous, or extended) over the range of inclination angles from  $0^\circ$  to  $180^\circ$ . Also, no experiments have been reported for pool boiling on porous or micro-porous surfaces to directly compare the performance of FC-72 and HFE-7100 dielectric liquids.

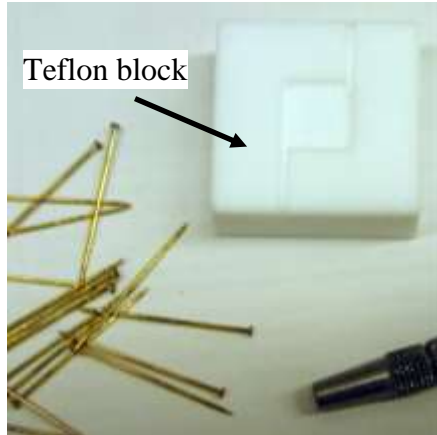
Some of the research needs are addressed in this research. The next section describes the experimental setup used in the present work. The specific objectives are listed in the Introduction section.

### 3 Pool Boiling Experiments

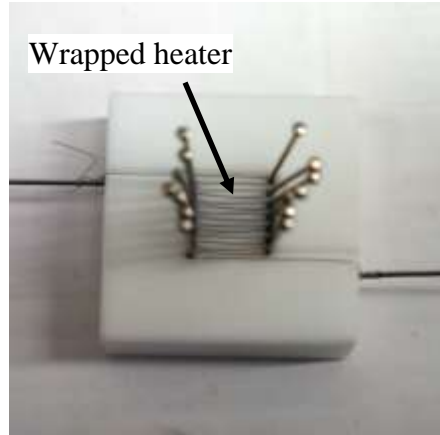
The pool boiling experiments carried out in this research are described in this chapter. The test sections, pool boiling facility, and experimental procedures are designed to minimize heat losses and uncertainties during the tests and to provide reproducible results. The experimental setup and the procedures follow those used earlier by El-Genk and Bostanci (2003a,b).

#### ***3.1 Test Section Design and Construction***

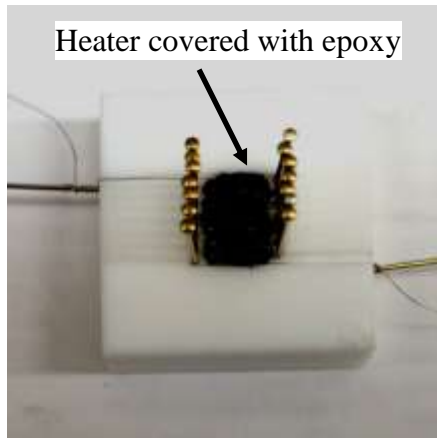
The test section consists of a Teflon block (30 x 30 x 12.7 mm) with a 1 mm deep square cavity (10 x 10 mm) machined in its center of its top surface (Figure 3.1a) to place the heating element. The heating element is covered by the surface selected for performing the pool boiling experiments. In order to minimize the interfacial resistance between the heating element and the surface for boiling, high thermal conductivity epoxy is used. The Teflon block provides thermal insulation, thus reducing side heat losses and assuring that most of the generated heat in the heating element is removed from the exposed surface by nucleate boiling. Initial experiments were performed using a wound heating element, and the latest experiments with copper surface with corner pins have used prefabricated special high heat flux heaters. Figure 3.1b shows the procedure used to wind the heating elements in the earlier experiments. Seven equally spaced holes 0.5 mm in diameter are drilled on opposite sides of the top cavity in the Teflon block, and pins are inserted and used as anchors to wind the heater using 0.125 mm diameter Nichrome wire (Figure 3.1b). The total heater resistance is  $\sim 15 \Omega$ . Thermally conducting and electrically insulating epoxy (Omegabond 200) is used to set the heater in place and insulate the wires loops from each other (Figure 3.1c). When the epoxy is set, the pins are removed and 1 mm diameter copper leads are soldered to both ends of the Nichrome wire (Figure 3.1d). The heater provides uniform heating over a  $10 \times 10 \text{ mm}^2$  area.



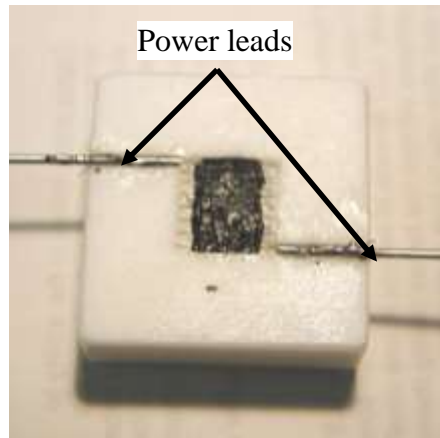
(a) Teflon with square



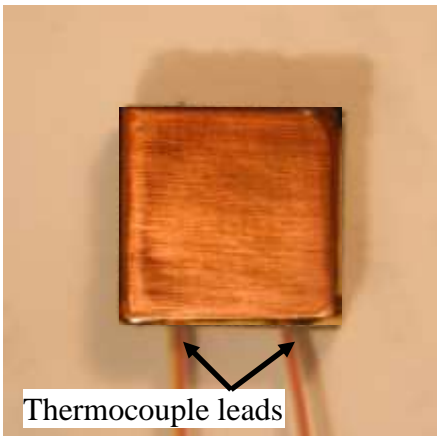
(b) Nichrome wire heater.



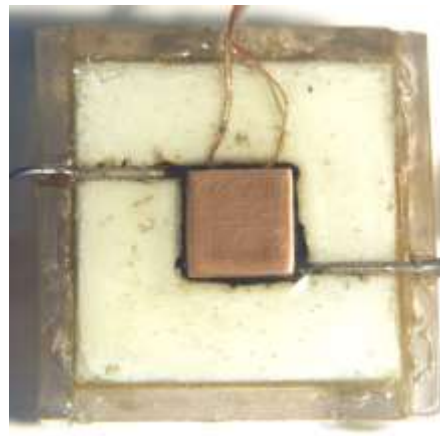
(c) Thermally conducting epoxy.



(d) Power leads soldered to heater.



(e) Plane Cu with thermocouples



(f) Fully assembled test section.

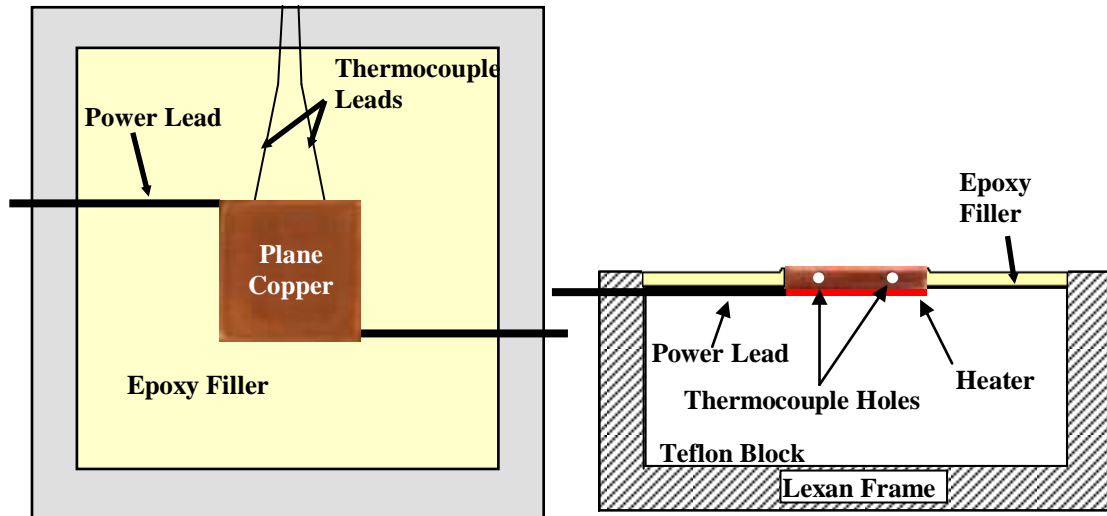
**Figure 3.1 Test section parts and assembly.**

### **3.1.1 Plane Cu Surfaces**

Prior to installing the copper or porous graphite surface on top of the heater, two K-type thermocouples are fixed into 0.6 mm diameter and 5 mm deep holes drilled in the

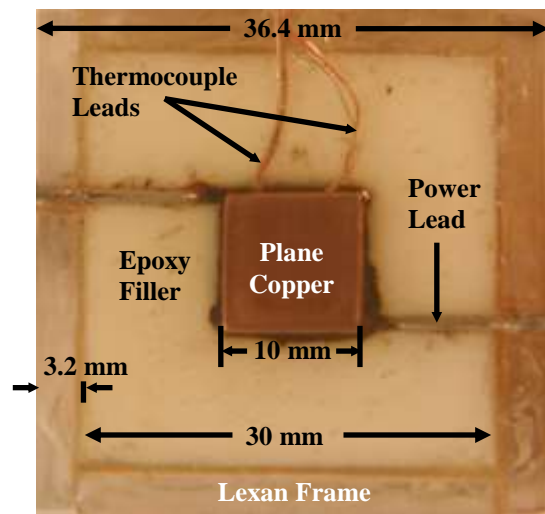
side of the block, 0.8 mm from the top surface and 2.5 mm from each edge (Figure 3.1e). The thermocouples are soldered into the copper block and attached with Omegabond 200 epoxy into the porous graphite block. The copper block (1.6 mm thick) or porous graphite (3 mm thick) is installed on top of the heater using a thin layer of Omegabond 200 epoxy. The assembled test section is encased in Lexan frame with closed bottoms (Figure 3.1f and Figure 3.2). The shallow cavity on top of the Teflon block is filled with a two-part epoxy adhesive (Scotch Weld 1839L B/A) that also seals the sides of the copper or porous graphite block, preventing any tiny grooves from forming at the edges that would act as vapor bubble nucleation sites in the experiments. Thus, extreme care is taken in applying the translucent epoxy adhesive to ensure good wetting with the sides of the copper and porous graphite blocks and the inside surface of the Lexan frame. Quick connects are crimped onto the copper leads to permit easy exchanging of test sections. It was later discovered that the Scotch Weld epoxy gradually leaches plasticizers into the liquid, skewing the results of the tests. It was replaced with a new custom-made epoxy (Masterbond Supreme 42HT(30)-2) and the leaching problem was resolved.

Before conducting the pool boiling experiments, the copper surface is prepared using consistent procedures to ensure repeatability and consistency among the different test sections used. First, the plane copper surface is sanded in even strokes using 400-grit emery (#400) paper to remove the large scratches and dents. The surface is then polished with a metal polishing liquid (Brasso) using cotton swabs, and then cleansed with water and alcohol. The final surface preparation is done using 1500-grit emery paper (#1500) by applying four consecutive strokes each in perpendicular directions (four strokes left to right, four strokes bottom to top). The 1500-grit paper produces grooves in the surface of the copper with an average width of about 1.6  $\mu\text{m}$  (Figure 3.3). The porous graphite surface was only cleansed from possible contamination that was deposited on the surface during the assembly of the test section.



(a) Plane view schematic of test section.

(b) Cross-sectional view of test section.



(c) Plane view of assembled test section.

**Figure 3.2. Cross sectional views and photograph of fully assembled plane copper test section.**

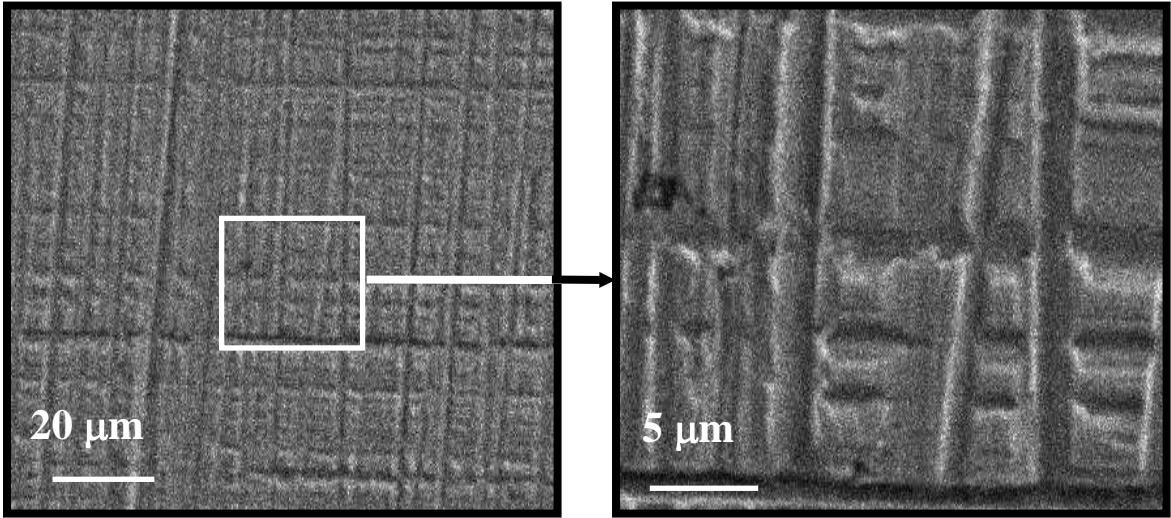


**Figure 3.3 SEM images of prepared copper boiling surface prepared using #1500 emery paper.  
Grove sizes average ~ 1.6 μm.**

### 3.1.2 Plane Porous Graphite Surface

The test sections using plane porous graphite (Figure 3.4) were constructed in the same manner as the copper test sections. The porous graphite surface in the present experiments has an open interconnected pore structure. The graphite block, measuring 10 x 10 mm and 3.0 mm thick (Figure 3.4), has a volume porosity of 60% of which 95% are open and interconnected (Poco Graphite, 2004). The randomly sized pores have non-circular openings that vary in sizes from a few to hundreds of microns (Figure 3.5). The SEM images of the porous graphite show that the re-entrant type cavities could be several hundred microns deep and have ragged, non-smooth interior surfaces. The high volume porosity of the graphite used in the present experiments entraps air, even after the liquid pool in the experiments was fully out-gassed and used for a long time in many subsequent experiments conducted without opening the test vessel. In addition, the possible formation of a thin liquid film of the very highly wetting HFE-7100 or FC-72 liquid on the interior surfaces of these cavities could increase the effective area for boiling heat transfer. Unlike copper, the porous graphite has highly anisotropic thermal conductivity. It has a high thermal conductivity (245 W/m K) out of plane and low thermal conductivity (70 W/m K) in plane at room temperature. The porous graphite is not structurally as strong as metals, but is stronger than graphite foams (Poco Graphite, 2004).

Two K-type thermocouples are inserted in two 0.6 mm diameter horizontal holes that are drilled on one side in the porous plane graphite block, ~ 0.8 mm from the surface and half way into the block (Figure 3.4). The measuring tips of these Teflon-insulated thermocouples are securely attached deep to the inside of the holes using thermally conducting epoxy (Omegabond 200). The epoxy also prevents the tips of the thermocouples from being directly exposed to liquid that may permeate through the graphite pore structure. The pores in the exposed vertical sides (~ 2.0 mm high) of the porous graphite block are also sealed with the Omegabond 200 epoxy so that they neither contribute to liquid circulation from the pool nor stimulate premature bubble nucleation during the pool boiling experiments.



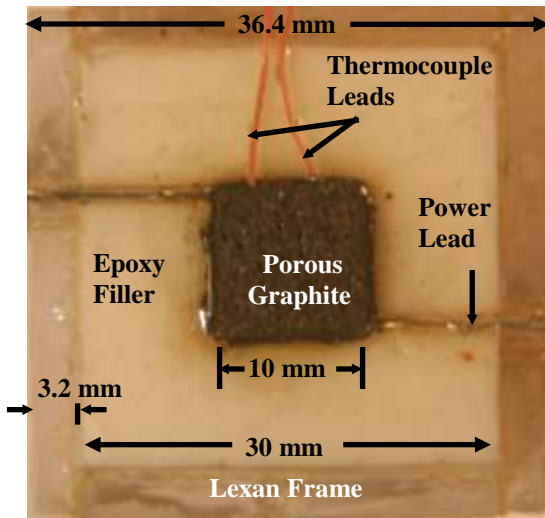
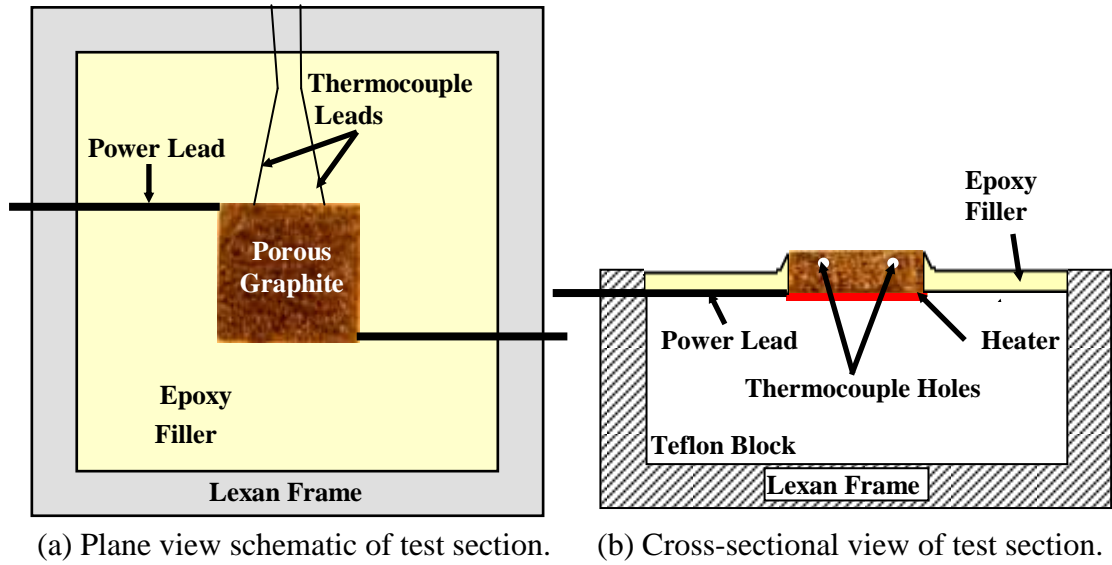


**Figure 3.4** Cross sectional views and photograph of fully assembled plane porous graphite test section.

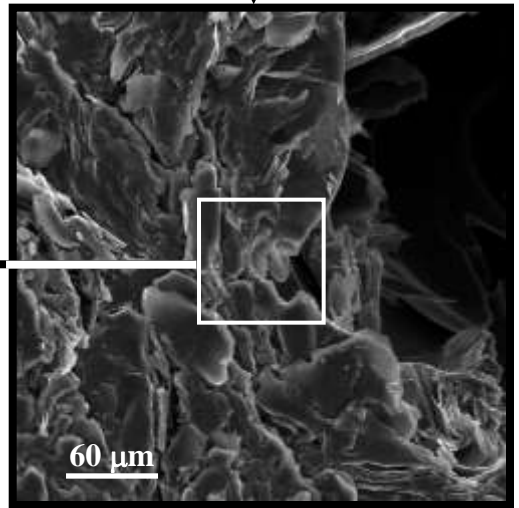
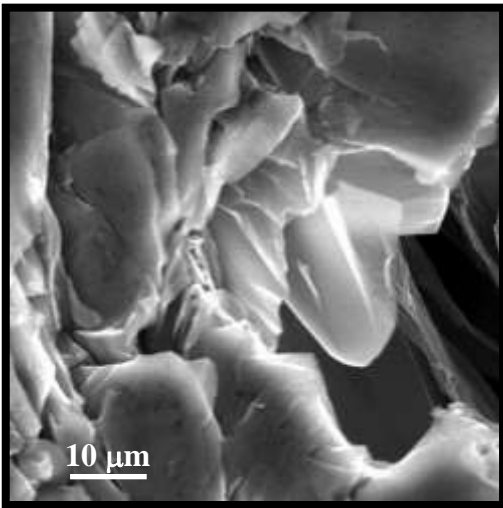
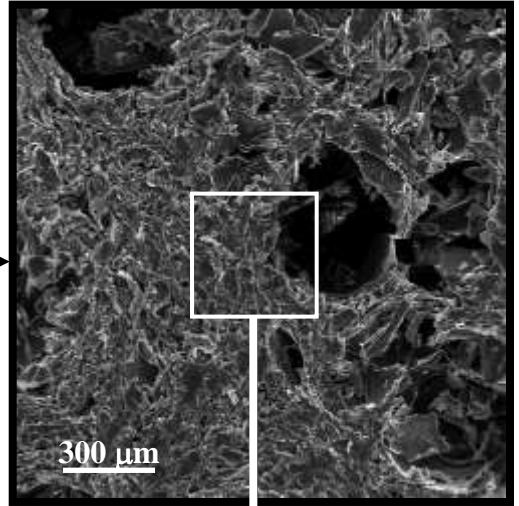
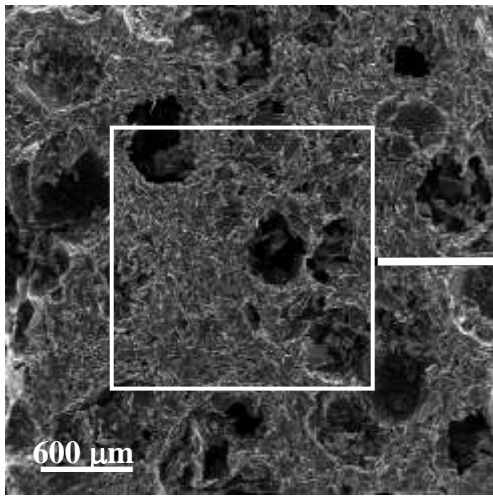


**Figure 3.5 SEM images of the plane porous graphite surface.**

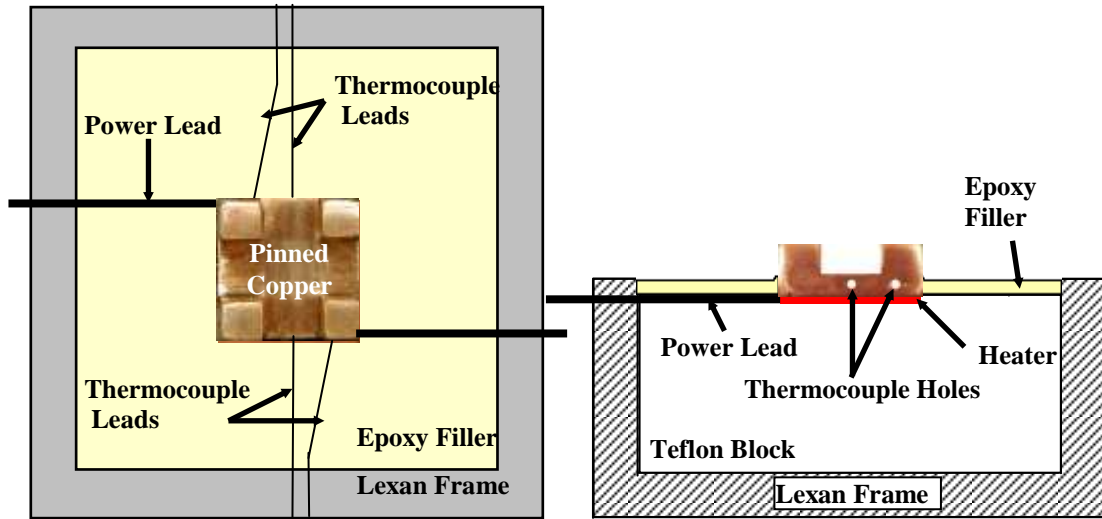
Increasing the total wetted area of the porous graphite by the addition of corner pins was attempted. However, in spite of the uniform heating of the footprint, the anisotropic thermal conductivity of the graphite led to large radial temperature gradients in the porous graphite, which cracked at high heat fluxes.

### **3.1.3 Copper with Corner Pins**

The surfaces with 3 x 3 mm square corner pins, machined from a single piece of copper, have a base of 1.6 mm thick and are 2, 3, or 5 mm tall (Figure 3.6). As the departure diameter of bubbles in saturation boiling of HFE-7100 has been measured to be  $0.55 \pm 0.07$  mm (El-Genk and Bostanci, 2003a), this test surface was designed with sufficient space between the pins (4 mm) to allow the vapor bubbles forming on the sides of the pins and on the flat area between pins to easily escape the surface. In addition, the dimensions of the corner pins (3 x 3 mm) and the height are selected to reduce the fin effects and ensure nucleate boiling from the sides and top surfaces of the pins to enhance boiling heat transfer. The cross sectional area of the pins ( $9 \text{ mm}^2$ ), which is larger than those used previously in studies of boiling on macro-pinned and structured surfaces by others (Chapter 2), help mitigate the temperature drop and fin effect in the pool boiling experiments.

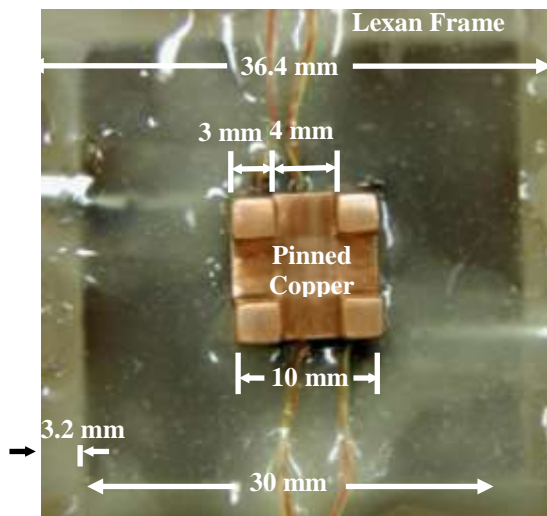
In the present pool boiling experiments, four K-type thermocouples used to measure the average temperature of the copper surfaces with corner pins are inserted and soldered into 0.6 mm diameter horizontal holes, 0.8 mm from the plane surface (Figure 3.6). Two thermocouples are inserted under pins (2 mm deep holes, 2 mm from the edge) and two inserted below the plane surface between the pins (3 mm deep holes, centered from the edges) on opposing sides (Figure 3.6). The average reading of these thermocouples, after accounting for the temperature drop due to conduction from the heating element to the root of the pins or to the plane part of the copper surface ( $< 2 \text{ K}$ ), is taken as the footprint temperature for constructing the boiling curves. To compare with results on the plane copper, the surfaces were prepared with #400 emery paper to remove the large scratches and dents in the surface. After washing with alcohol and water, the surfaces were finished with #1500 emery paper.





(a) Plane view schematic of test section.

(b) Cross-sectional view of test section.



(c) Plane view of assembled test section.

**Figure 3.6 Cross sectional views and photograph of fully assembled test section of copper with corner pins.**

When the test sections with copper with corner pins used heaters made in the same manner as for the plane copper and porous graphite test sections, the Nichrome wire heaters burned out when the heater power exceeded ~70 W. A new prefabricated, high heat flux heater was purchased and used (Component General Inc., CCR-37T-1B, 16  $\Omega$ ). This heater soldered to the bottom of the copper surfaces with corner pins is robust enough to withstand the temperatures and heat fluxes generated during the experiments.

### 3.1.4 Thermal Analysis of Test Sections

Thermal analyses were performed using ANSYS, a commercial finite element numerical analysis package, to estimate the heat losses from the test sections. The analysis balances the energy between the heat generation in the heater and the heat removed by nucleate boiling and natural convection from the exposed heated surface and through the sides of the test section in contact with the liquid. The three-dimensional heat conduction equations were solved throughout the test section:

$$q''' = -\nabla \cdot \bar{k} \nabla T, \quad (3.1)$$

subject to the heat removal boundary conditions at the exposed heated surface and the exposed sides of thermal insulation (Figures 3.2, 3.4, and 3.6):

$$k \nabla T = h(T_w - T_b). \quad (3.2)$$

The boundary condition applied to the heated surface is a temperature dependent heat transfer coefficients based on the boiling curves on the surface to be analyzed (Cu or porous graphite) and the working liquid (HFE-7100 or FC-72). Temperature dependent natural convection heat transfer coefficients are applied to the exposed the sides of the thermal insulation. Details of the analysis are in Appendix A.

Upon completion of the thermal analysis, the heat losses from the exposed faces of the thermal insulation were estimated. The total power removed as calculated by ANSYS from the exposed copper or porous graphite surface was determined by adding the values

of power removed from the individual elemental faces created during the meshing process of the analysis. The total removed power was compared to the total input power to the heater. Further analysis was done which calculated the heat loss from each exposed face of insulation. The total power lost from each face was calculated in the same manner that the thermal power removed from the heated surface: i.e. adding the values of power removed from the individual elemental mesh faces. The results of these analyses, listed in Table 3.1, showed that about 0.5% of the total thermal power generated in the heater was lost through the top of the epoxy filler, and slightly more than 1% of the total power was lost through the four vertical sides of the Lexan frame, and slightly more than 1% from the bottom of the Lexan frame (Figures 3.2 and 3.4). The total heat losses were estimated to be less than 3%.

**Table 3.1 Estimated heat losses near CHF from test sections in saturation and subcooled boiling of FC-72.**

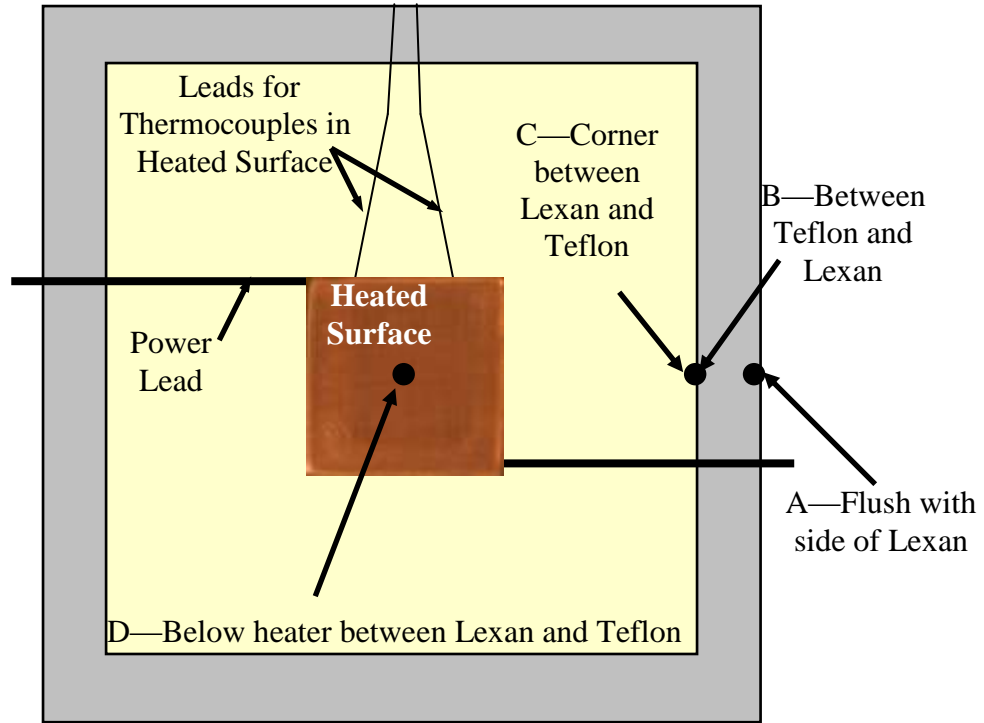
Plane Copper (Figure 4.10a boiling curves used)				
$\Delta T_{sub}$ (K)	0	10	20	30
Footprint Heat Flux ( $W/cm^2$ )	17.0	21.9	26.9	29.5
Footprint $\Delta T_{sat}$ (K)	21.3	22.9	23.5	24.9
Loss from top (%)	0.5	0.5	0.6	0.6
Loss from sides (%)	1.1	1.1	1.1	1.1
Loss from bottom (%)	1.0	1.0	1.1	1.1
Total loss (%)	2.6	2.6	2.8	2.8
Porous Graphite (Figure 4.10c boiling curves used)				
Footprint Heat Flux ( $W/cm^2$ )	27.2	39.6	49.0	57.1
Footprint $\Delta T_{sat}$ (K)	11.8	17.2	19.2	19.5
Loss from top (%)	0.5	0.5	0.5	0.5
Loss from sides (%)	1.0	1.1	1.1	1.1
Loss from bottom (%)	1.0	1.0	1.1	1.1
Total loss (%)	2.5	2.6	2.7	2.7

To validate the results of the thermal analysis, a few test sections were constructed with a thermocouple embedded within the thermal insulation, between the Lexan frame

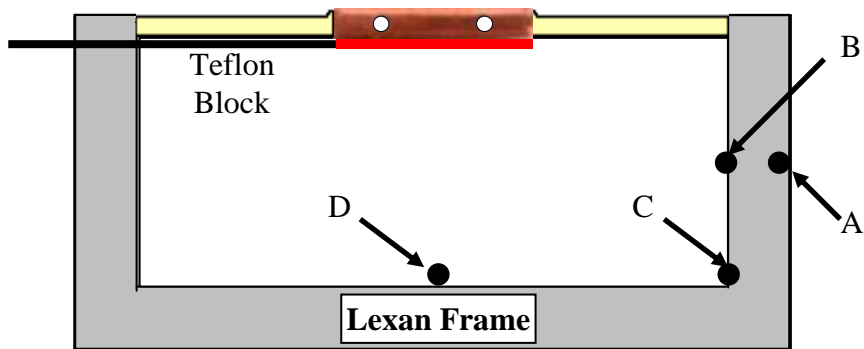
and the Teflon block. Figure 3.7 shows a plane and cross sectional view of a test section using plane copper pointing out the locations of the thermocouples. Similar test sections with porous graphite having a thermocouple embedded within the insulation were also constructed. On the side of the Lexan frame, a small pit was made and a thermocouple was set with epoxy into the pit, so as to be flush with the exposed surface (Figure 3.7, point A). Another temperature measurement was made near the same location, just inside the Lexan frame (Figure 3.7, point B). A third temperature measurement was taken at the corner edge of the Lexan frame and Teflon block (Figure 3.7, point C) and the last temperature measurement was recorded directly below the heater between the Lexan frame and the Teflon block (Figure 3.7, point D). All thermocouples were fixed in place with an epoxy having a thermal conductivity nearly the same as that of the Teflon and Lexan thermal insulation.

Figure 3.8a shows the thermal analysis completed for saturation boiling of FC-72 on plane copper near CHF, and Figure 3.8b shows the same on porous graphite near CHF. The locations labeled A, B, C, and D are the same as in Figure 3.7. Calculated temperatures for saturation boiling of FC-72 on plane copper at  $17.0 \text{ W/cm}^2$  are 325.7 K at point A, 328.4K at point B, 327.4 K at point C, and 333.8 K at point D (Figure 3.8a). The corresponding temperatures measured by the thermocouples are 326.0 K, 329.0 K, 327.0 K and 334.9 K. For saturation boiling of FC-72 on porous graphite at  $27 \text{ W/cm}^2$ , ANSYS calculated the temperatures to be 325.6 K at point A, 330.0 K at point B, 327.0 K at point C, and 337.7 K at point D, with corresponding thermocouple measurements of 325.6 K, 329.1 K, 326.3 K, and 339.0 K. The measured temperatures closely matched the temperature profile calculated by ANSYS (FIG3.8 a and 3.8b) and validated the soundness of the thermal analysis and the obtained estimates of the side heat losses (Table 3.1)

A thermal analysis modeling the copper with corner pins showed a lateral temperature gradient within the copper. Figure 3.9 displays the temperature profile of the copper with 5 mm corner pins in the plane where the thermocouples are located. The simulation in Figure 3.9 was run for saturation boiling of HFE-7100 at 55 W total thermal power (near



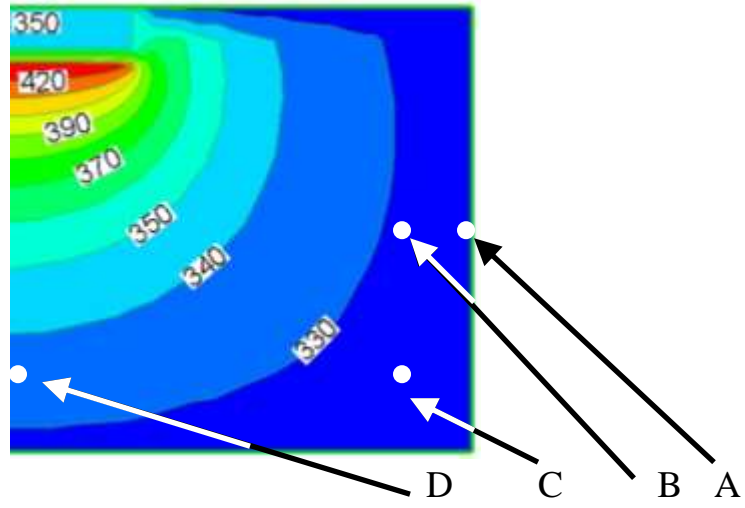
(a) Plane view of test section.



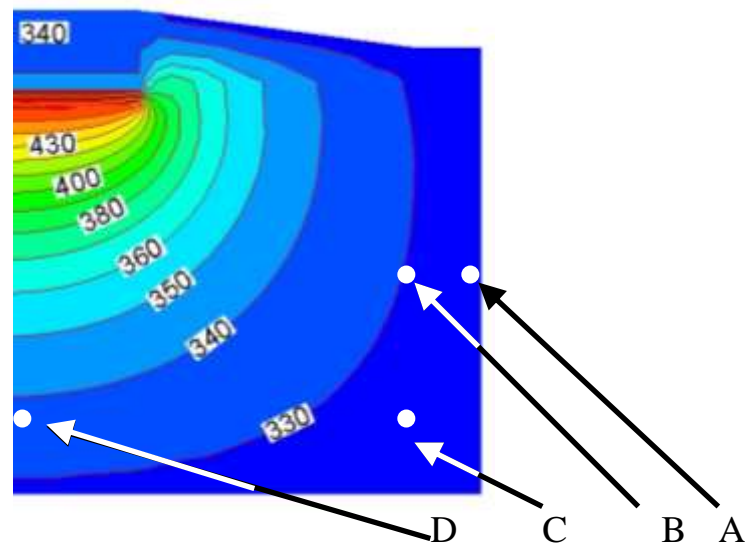
(b) Cross-sectional view of test section.

**Figure 3.7 Location of thermocouples used for thermal analysis verification for plane surfaces.**

**Error!**



(a) Plane Copper 17 W in saturation boiling of FC-72.



(b) Plane Porous Graphite 27 W in saturation boiling of FC-72.

**Figure 3.8 Numerical thermal analysis of plane copper and porous graphite test sections.**

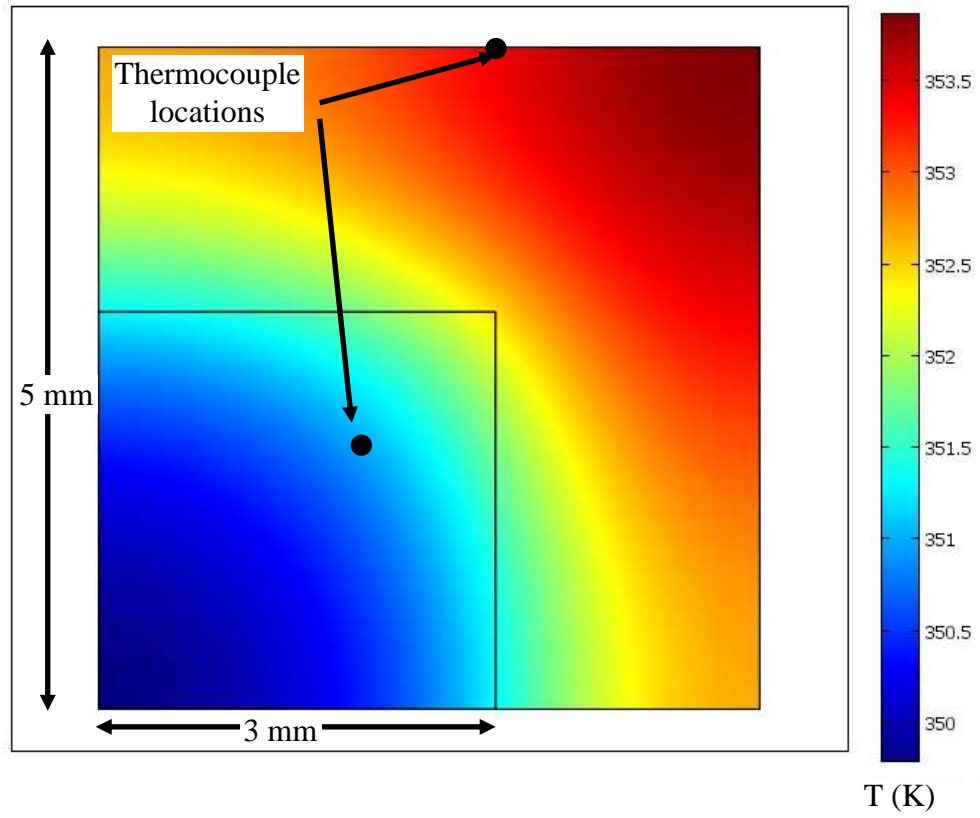


Figure 3.9. Cross sectional temperature profile of copper with 5 mm corner pins near CHF.

CHF). This analysis shows that the hottest part of the copper surface with corner pins is in the center of the heated surface (upper right hand corner of Figure 3.9) and the coolest location is on the outside corner edge of the pin (lower left hand corner of Figure 3.9). In this simulation, the maximum temperature difference is ~4 K. The temperature difference between the points where the thermocouples are located is 2 K (Figure 3.9).

### **3.2 Experimental setup**

The pool boiling facility used in the present investigations (Figures 3.10 and 3.11) is comprised of the following major components: (a) a heated water bath in an acrylic tank, (b) a polycarbonate test vessel of the dielectric liquid pool, (c) the above described assembled test section mounted on the rotation assembly, (d) equipment for controlling and monitoring the temperatures of the water bath, the dielectric liquid pool, and the boiling surface, (e) a computer controlled DC power supply to control the input power to the heating element in the test section and to monitor and record the voltage drop across and the current through the element, (f) a computer controlled data acquisition unit, and (g) a cooling water loop for the reflux condenser and a water chiller with temperature control for the two submerged coils in the test vessel. These submerged cooling coils maintain the liquid pool temperature constant at the desired values in subcooled boiling experiments.

#### **3.2.1 Test Section Holder and Rotation Assembly**

An acrylic block measuring 40 x 40 x 20 mm was used as the base to attach the test section to the submerged rotational assembly in the test vessel (Figure 3.12). A square of Superlock fastener on the top of the acrylic block and the bottom of the test section held the test section firmly in place during the experiments at all inclination angles. A 9.5 mm acrylic rod 120 mm long was inserted through the center of and welded to the acrylic block. Two wheel bearings (NTN Bearings 1L038) were placed on each end of the rod. A square piece of blue acrylic attached to the back half of the rod provided a contrasting background for the photographs and video (Figure 3.12).



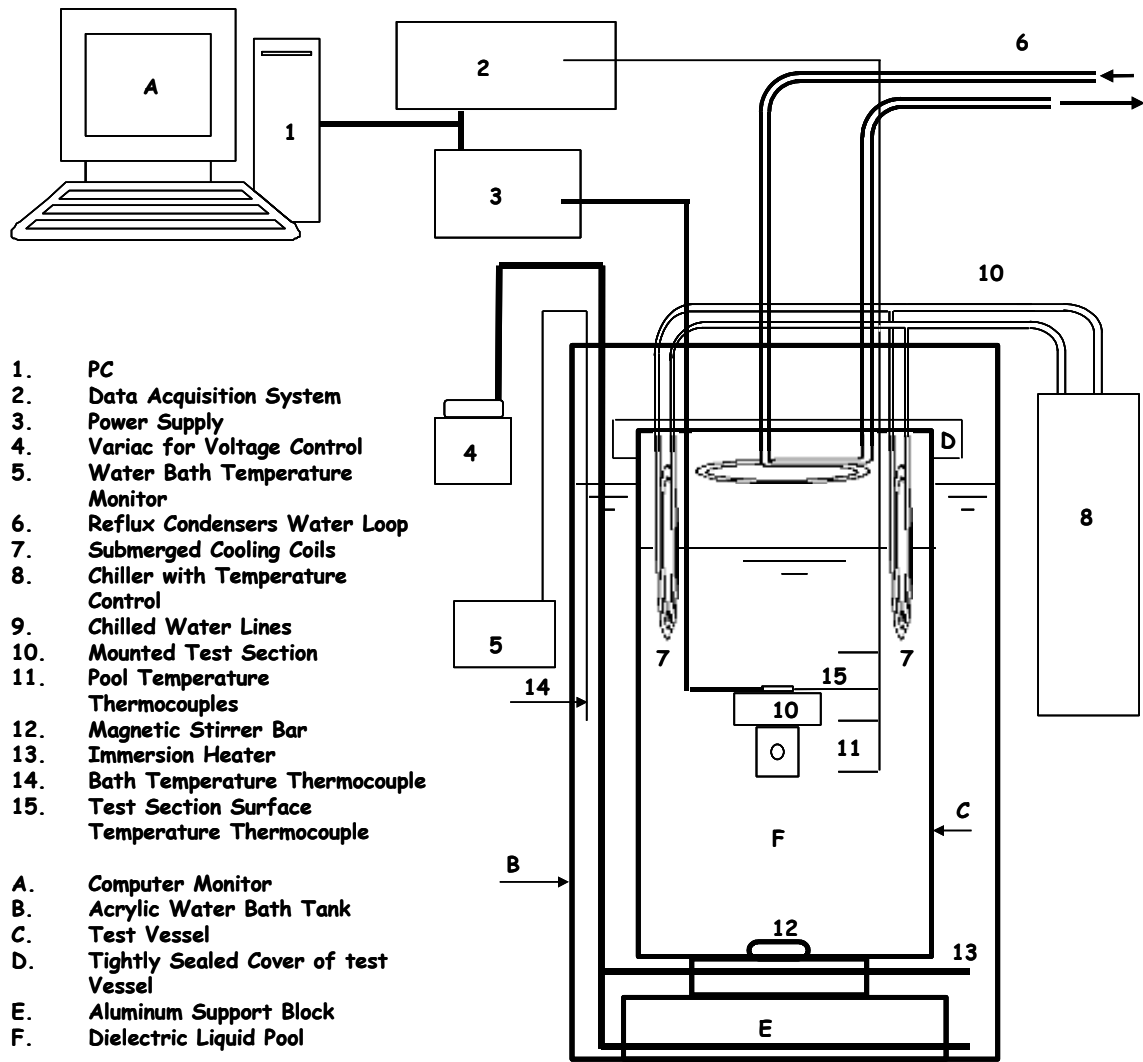


Figure 3.10 Line diagram of the pool boiling test facility.

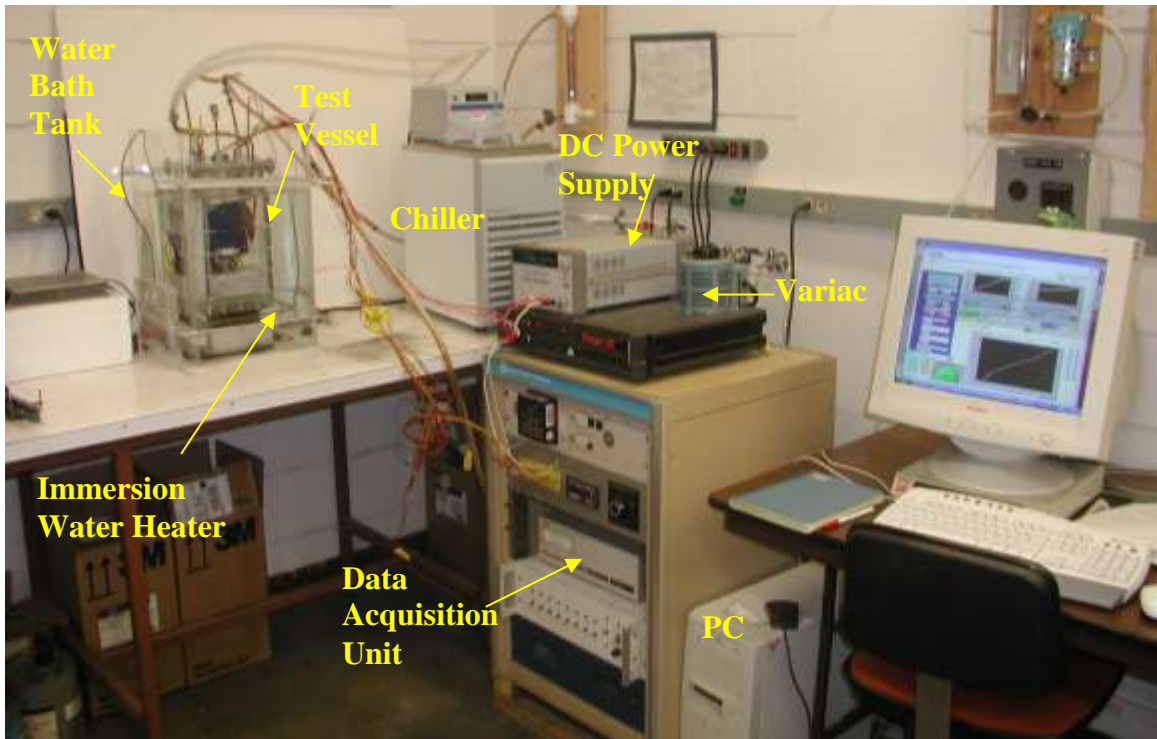
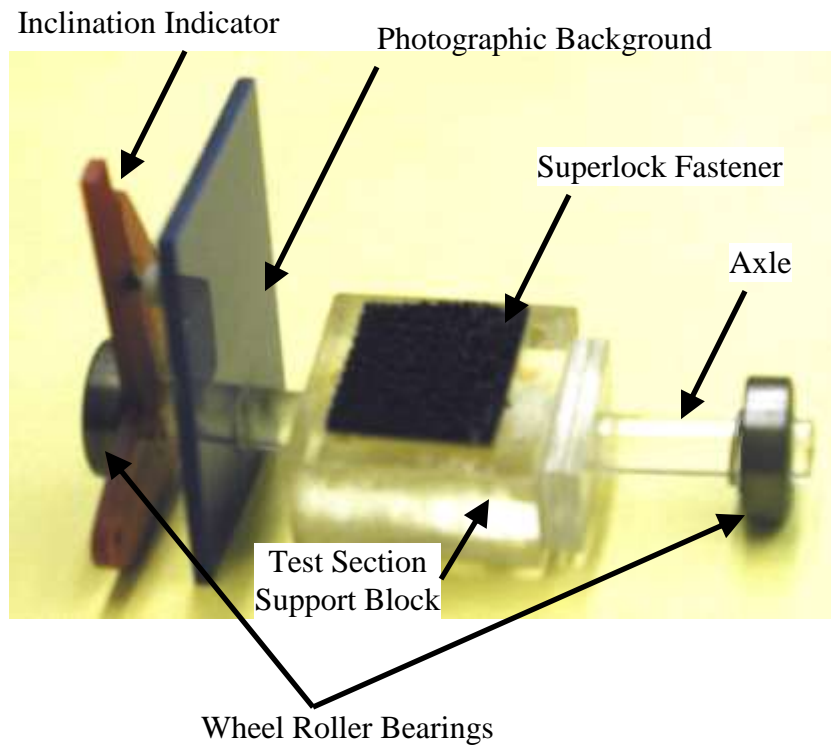


Figure 3.11 Photograph of the pool boiling facility.



**Figure 3.12 Fully assembled test section support.**

The rotation assembly consists of two arms and the angle indicator (Figure 3.13). The acrylic indicator shows the inclination angle of the test section as read from a protractor glued to the outside of the test vessel. The indicator also serves as the anchor for the arms. These arms extend through the cover of the test vessel with 1/8 inch diameter brass rods (Figure 3.13). Thus, the inclination of the test section to the desired value is adjusted using the extended arms without a need to open the test vessel (Figures 3.14a and b).

### **3.2.2 Test Vessel**

The test vessel is made of 1/2 inch Lexan with inner dimensions 290 mm high, 120 mm deep, and 140 mm wide. A lip on top of the test vessel extends 35 mm around each side (Figure 3.14c). The entire vessel is welded together using a fast curing solvent cement (IPS Corporation Weld-On 3) and secured with nylon screws, and all inside edges are sealed with a bead of the Masterbond epoxy. An O-ring fit into a groove in the lip ensures a tight seal between the vessel and its cover. Within the test vessel, there are two wheel wells in which the rotational bearings sit (Figure 3.14c). These wells are made of 1/4 inch Lexan (29 x 16 mm) with a semicircular ring (11 mm radius) cut from each. They are attached to the front and back sides of the vessel, 83 mm from the bottom and centered 57 mm from the right hand side (Figure 3.14c). The wheel wells ensure that the rod holding the test section assembly remains horizontal. Four blocks of Lexan (25 x 25 x 50 mm) are cemented to the outside of each wall, centered side to side and 240 mm from the bottom. These blocks hold stainless steel threaded rods (10 x 32) with standoffs that are used to physically stabilize the test vessel as it sits in the bath (Figure 3.14c).

The cover of the test vessel both seals the container and provides access for the power to the heating element, temperature measurements in the pool and assembled test section, the cooling coils, and for the rotation mechanism. The cover extends to the edges of the lip of the test vessel. Wires (2 for the power supply, 2 for voltage reading across the heating element) and K-type thermocouples (8 pair total) are fed through rubber stoppers in the cover of the vessel. The pool temperature, monitored by submerged thermocouples

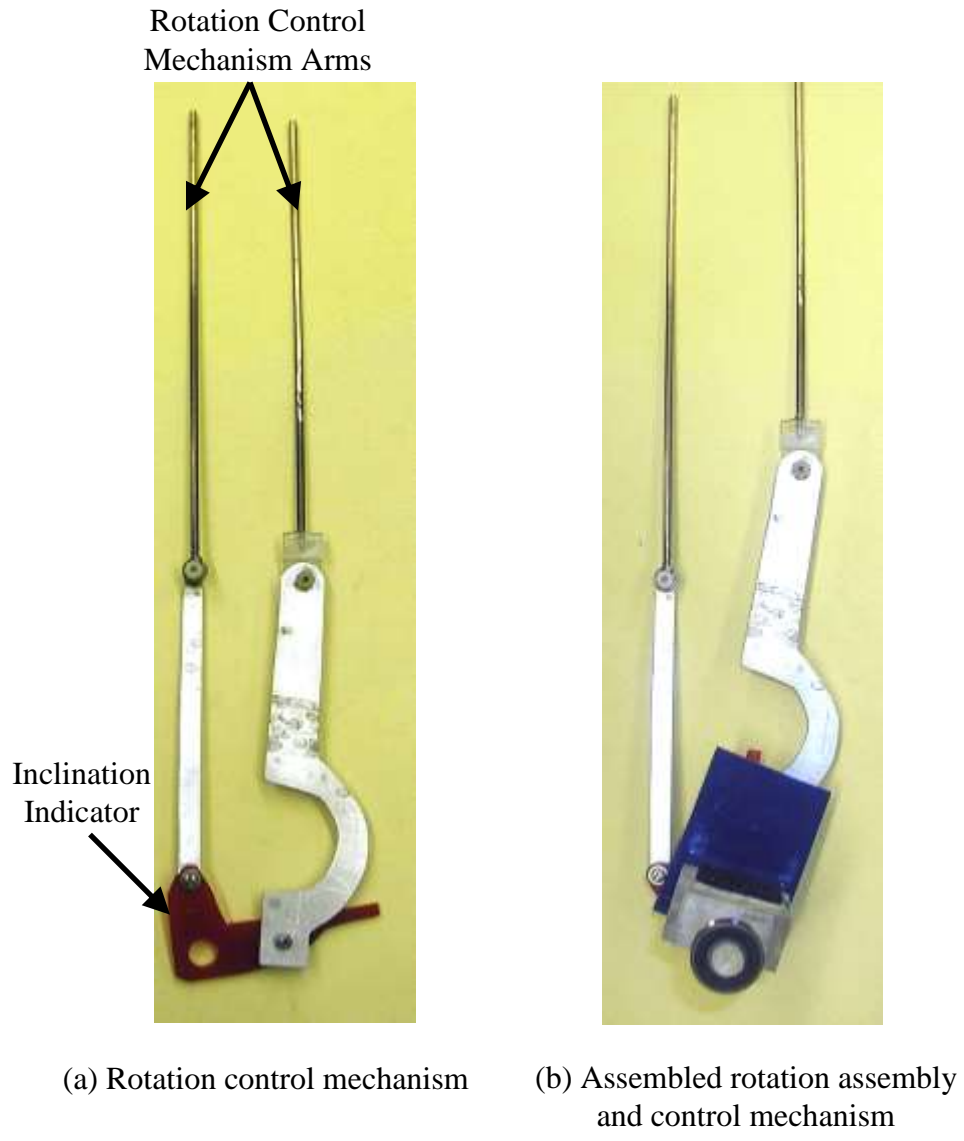


**Figure 3.13 Photographs of rotation assembly and fully assembled rotation mechanism.**

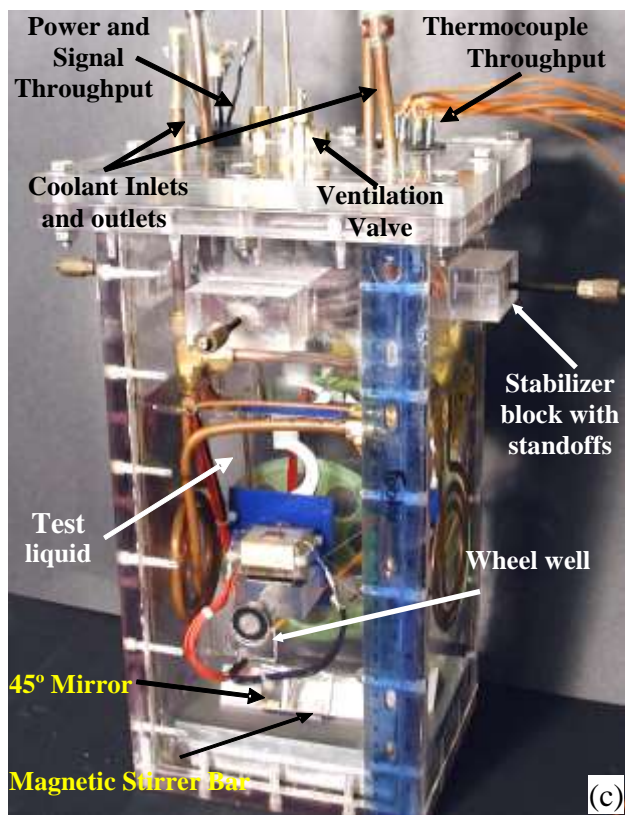
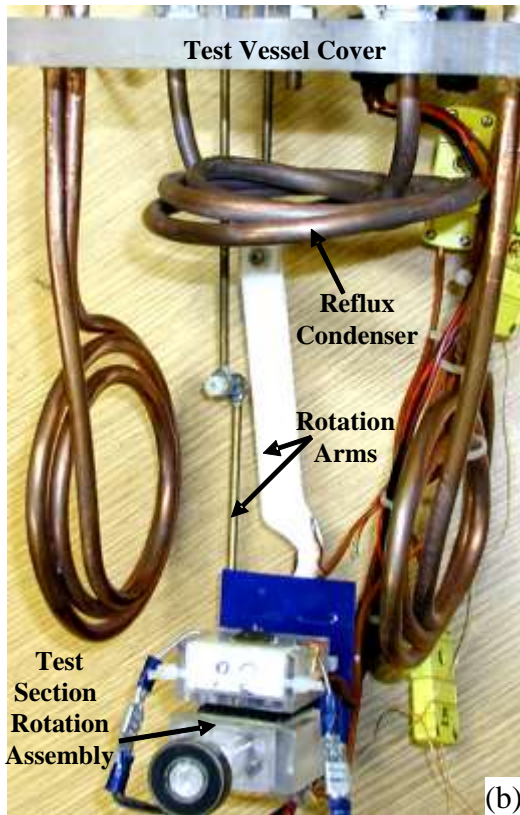
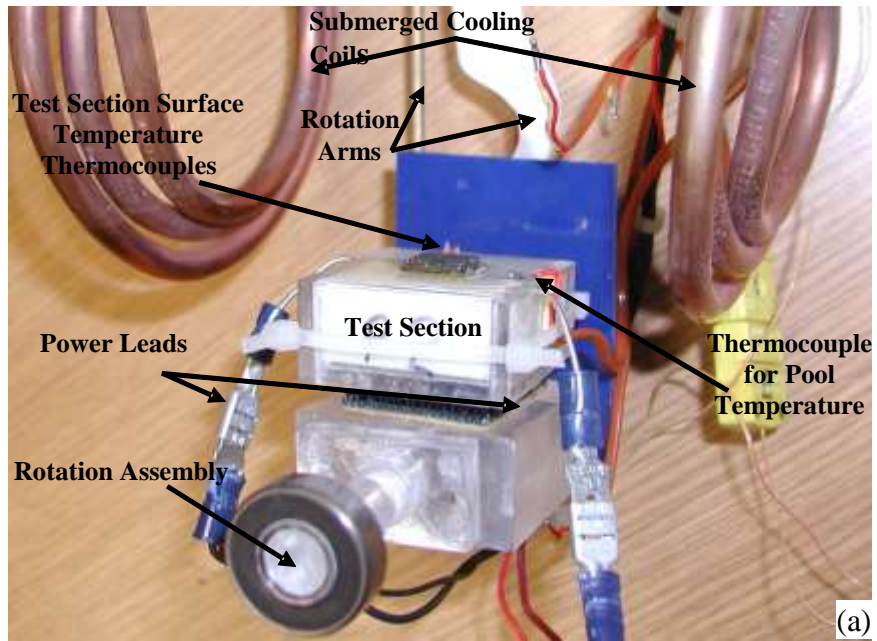


Figure 3.14 Photographs of pool boiling test vessel and assembly

suspended in the pool, is taken as the average of the readings by the two thermocouples placed 5 – 10 millimeters from the surface just above the plane of the heated surface (Figure 3.14a).

The cooling coil (or reflux condenser) on the inside of the vessel cover and the submerged cooling coils (Figure 3.14) are ¼ inch O.D. copper tubes, fed through ¼ inch holes in the cover. The coil on the inside of the cover plate effectively condenses the vapor produced in the experiments, thus maintaining a constant liquid pool height and vapor pressure in the test vessel. The submerged copper coils, also cooled with water from a chiller (Neslab RTE 7) fine tune the liquid pool temperature and remove the heat dissipated during the subcooled boiling experiments. The rotation arms pass through Swagelok fittings using Teflon ferrules. A needle valve in the center of the cover acts as a vent for the system. All throughputs are sealed both on the inside and outside with Masterbond epoxy. Because dielectric liquids have very low surface tension and are highly wetting, the test vessel must be tightly sealed to prevent liquid leakage. The cover is fixed to the test vessel with 8 quarter-inch bolts, which pass through the lip. Leak testing of the vessel is completed by slightly pressurizing it and immersing it in water. The source of any leakage observed is investigated and sealed.

### **3.2.3 Water Bath Vessel**

The test vessel sits inside a heated water bath to help maintain the dielectric liquid near the target temperature and minimize heat losses from the vessel. The water bath tank (Figures 3.10 and 3.11), made with 3/8 inch Plexiglas, has inner dimensions of 305 x 305 x 510 mm. An immersion heater sitting at the bottom of the tank (ARi Industries, model BXX19B80-17K (mod)) is powered by a Variac and used to heat the deionized water to the desired temperature (Figures 3.10 and 3.11). The water bath, together with the submerged cooling coils, maintains the liquid pool temperature to within  $\pm 0.2$  K of the desired levels in the experiments. The test vessel sits on a submersible magnetic stirrer (Cole Parmer U-04650-58 or Tri-R MS-7), which is used to accelerate degassing of the dielectric liquid.

### 3.2.4 Power and Data Acquisition

Electrical power is supplied to the heating element using a computer controlled DC power supply (Agilent E3634A), which interfaces with the controlling PC through a GPIB cable and is controlled with LabVIEW software. The LabVIEW program sets the voltage of the power supply and records the voltage drop across and the current flow through the heater as measured by the power supply. In addition, the program records the temperatures measured by the 8 thermocouples used in the experiments through a Measurement Computing Corp. USB-TC data acquisition interface.

### 3.3 *Experimental Procedures*

The test vessel is partially filled with the dielectric liquid and placed in the heated water bath tank. The assembled test section is immersed in the liquid pool in the test vessel such that the boiling surface in the upward-facing position ( $0^\circ$ ) is at least 8 cm below the free liquid surface. Owing to the high air solubility in dielectric liquids—48% by volume in FC-72 and 53% by volume in HFE-7100 (You et. al., 1995; Tuma, 2001)—out-gassing the liquid pool in the sealed test vessel is accomplished by allowing it to boil for several hours, while maintaining the temperature of the water bath 5 – 7 K above the saturation temperature of dielectric liquid (Table 1.1) and turning the magnetic stirrer at the bottom of the pool in the test vessel on (Figures 3.10 and 3.14c). The released gas is intermittently vented out by opening a release valve in the cover plate of the test vessel.

The pool boiling experiments begin by turning off the magnetic stirrer and incrementally increasing the electrical power to the heating element in the test section, via increasing the applied voltage in increments of  $< 0.2$  V. As the nucleate boiling heat flux increases, the incremental increase in the applied voltage to the heating element in the test section is adjusted down to ensure that the maximum increase in the input power to the heater is no more than 0.5 W at a time (or the increase in the surface heat flux is  $< 0.5$  W/cm<sup>2</sup>). When approaching CHF, the incremental increases in the heater's power are gradually reduced further to less than 0.05 W in each step, to accurately determine the CHF values and avoid a large temperature surge, which may burn the heating element.

Figure 3.15 shows that as the test progresses toward CHF, the voltage is adjusted downward to lower the power increments. The applied voltage to and the current through the heating element are measured simultaneously to determine the dissipation heat flux.

Following each incremental increase in the heater's power, the dissipated heat flux and footprint temperature are recorded at steady state. This is defined in the experiments as when the changes in two successive average temperature measurements are within  $\pm 0.2$  K, which is on the order of the precision of the thermocouple readings. Each of these measurements is the average of 30 subsequent readings by the two thermocouples embedded in the plane graphite or copper block, or of the four thermocouples embedded in the copper surfaces with corner pins. It usually takes 20 – 30 seconds after incrementally increasing the electrical power to the heating element to reach steady state. Figure 3.16 shows the individual temperatures measured by the thermocouples embedded in the heated surfaces of the plane copper block (Figure 3.16a), the plane porous graphite block (Figure 3.16b), and the copper block with 3 mm tall corner pins (Figure 3.16c). The solid lines represent the average of the 30 measurements of all thermocouples. Immediately after increasing the input power of the heater element, the footprint temperature increases. The average of the first 30 temperature measurements is skewed to a lower value because of the transient temperature rise following the power increase.

Of note also in Figure 3.16c is that the temperatures under the corner pins are always slightly lower than the temperatures under the flat portion of the copper block with corner pins (Figure 3.9). Figure 3.17 shows the boiling curves for saturation boiling of HFE-7100 on 5 mm Cu corner pins using the recorded average temperature readings by thermocouples in each location—underneath the pins and underneath the flat part of the heated surface. At boiling incipience the thermocouple located underneath the pin measures a temperature slightly lower than that under the plane part of the heated surface (mid), owing to the larger heat transfer area influencing the thermocouple. The boiling curves run nearly parallel to one another throughout the fully developed nucleate boiling region. However, near the end of the fully developed nucleate boiling region, the temperatures measured by each thermocouple begin to diverge as bubble crowding between the pins becomes important and starts to impede boiling heat transfer from the

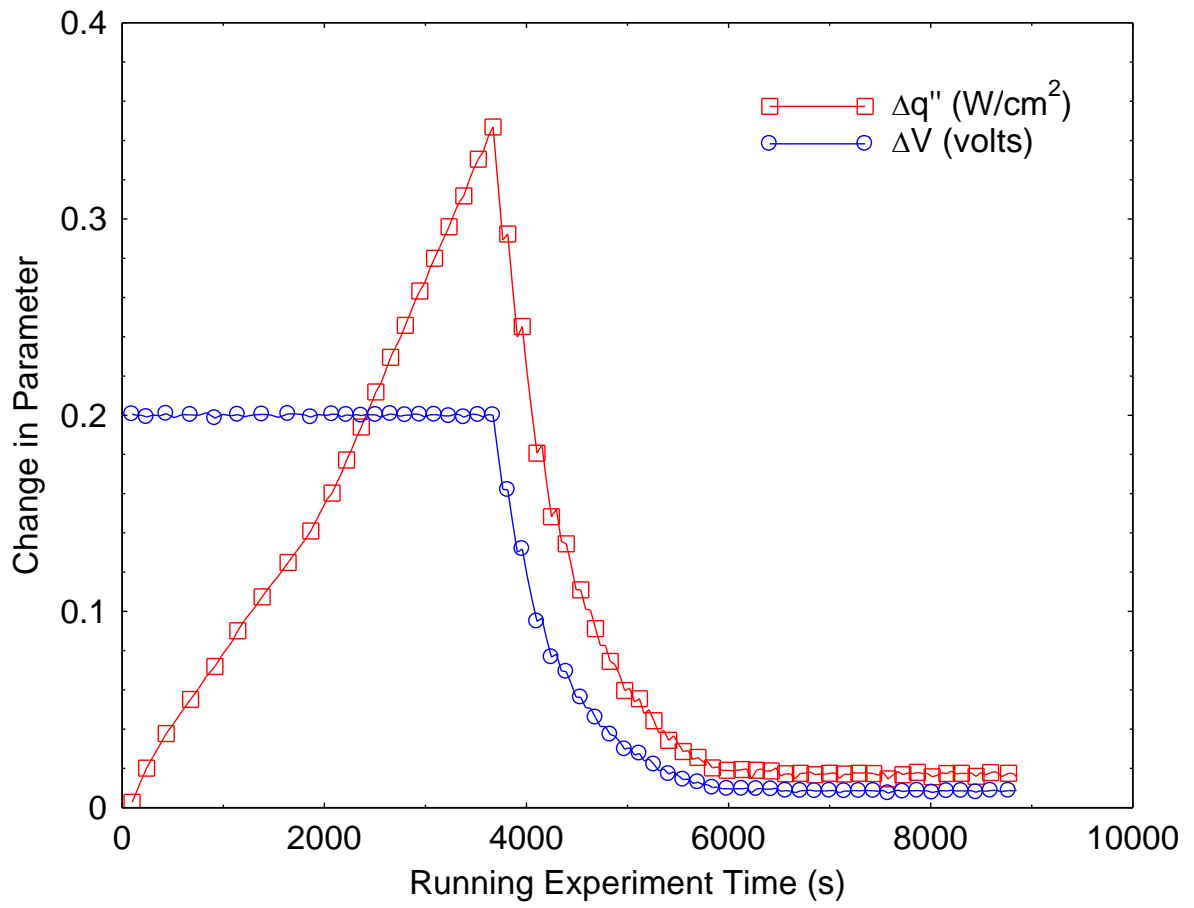


Figure 3.15 Voltage and power adjustment during the pool boiling experiments.

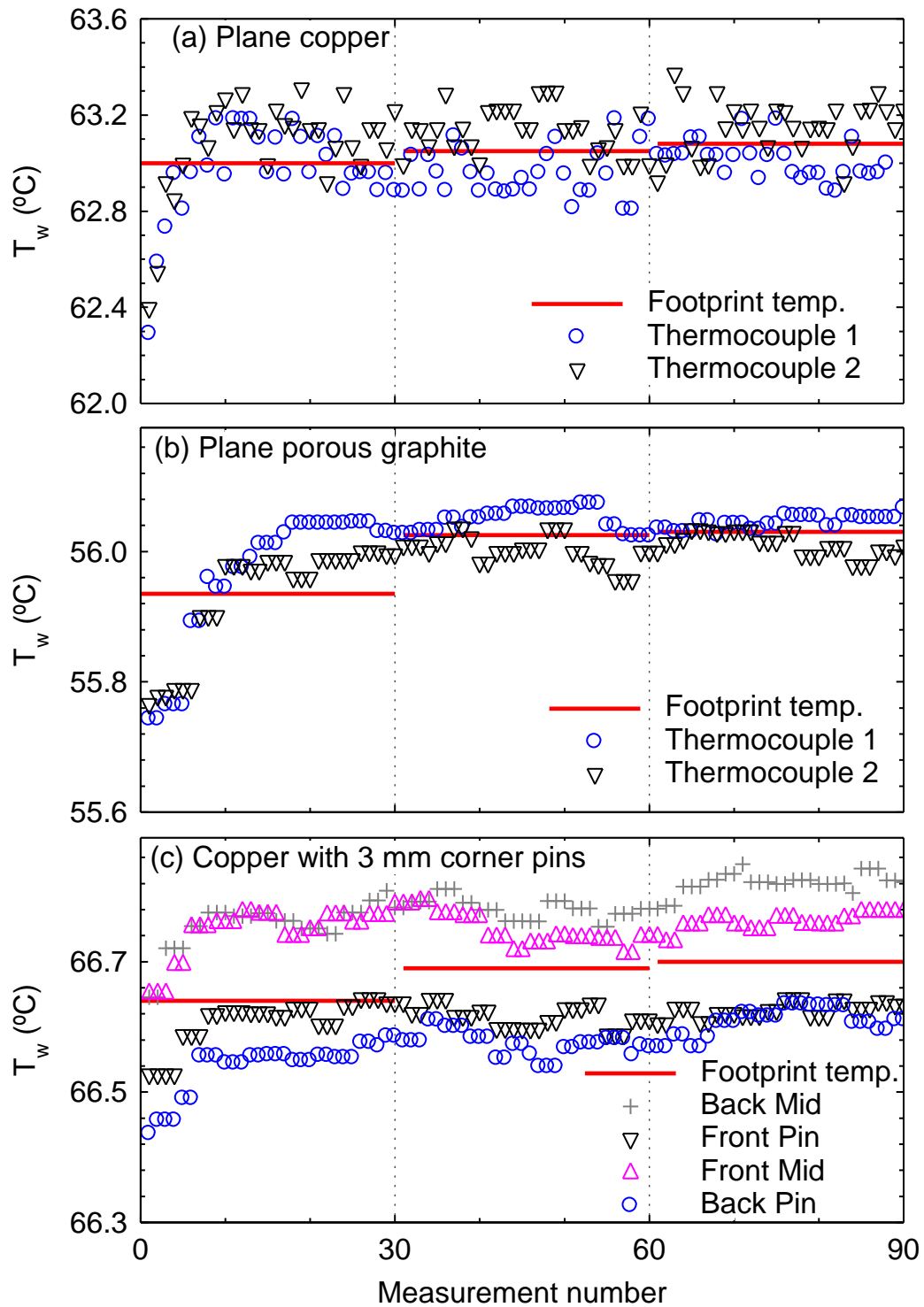
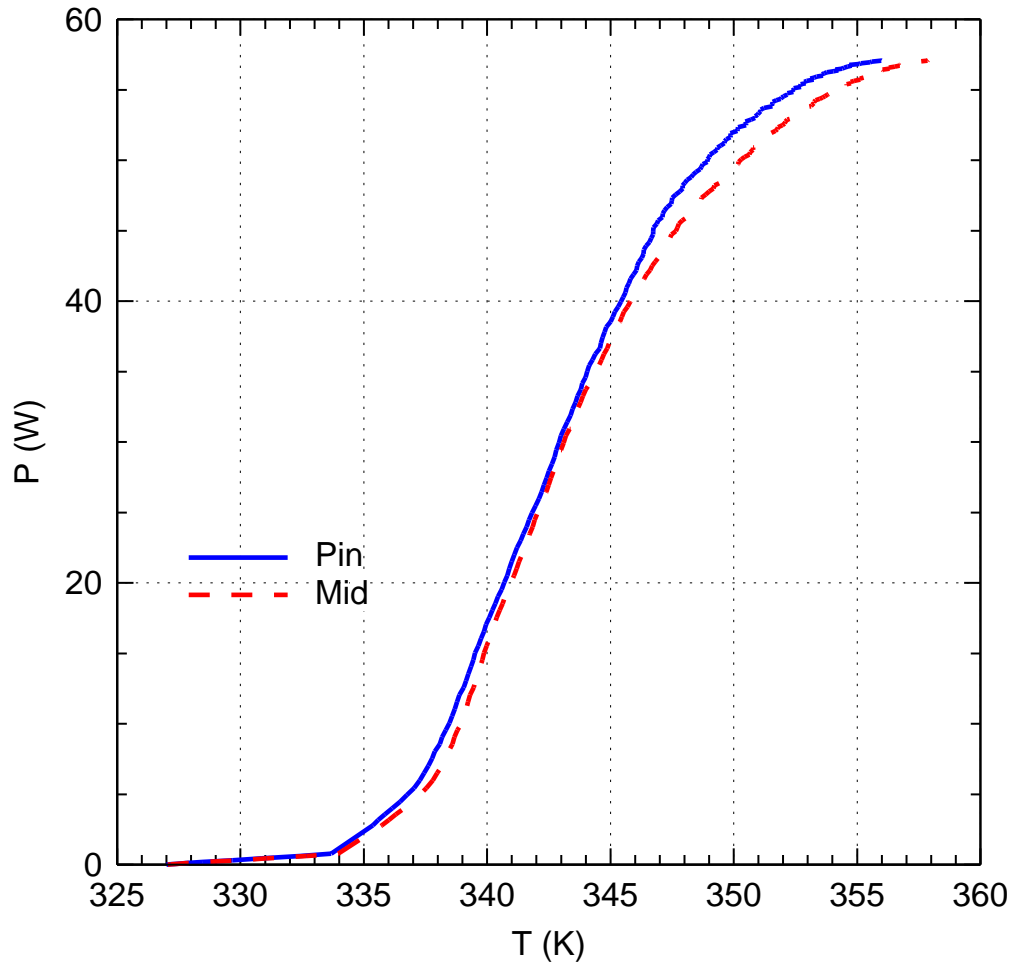


Figure 3.16. Temperature measurements of the thermocouples embedded in the heated surfaces.



**Figure 3.17. Saturation boiling curves on 5 mm corner pins using thermocouples under the pin and the middle or flat part of the heated surface.**

plane part of the heated surface. At CHF, the temperature difference between the measurements of the two thermocouples is about 2 K, which matches well with the results of the thermal analysis (Figure 3.9). To make comparisons with the plane surfaces, the boiling curves presented in Chapter 5 on copper with corner pins used the average of all four thermocouples, corrected for the temperature drop due to conduction to the base of the pins ( $< 2$  K).

To avoid burning the heating element at CHF, when any surface thermocouple detects an increase of 30 K or more over the last steady state average surface temperature, it is considered an indication of reaching CHF, and the experiments are terminated. The LabVIEW program that executes the test procedures is capable of terminating the experiments within 40 ms upon sensing CHF according to the above procedures, hence protecting the heating element in the test section. At the point where the CHF criteria are met, the heater power shuts off and the test section rapidly cools down.

Figure 3.18 shows an example of how the surface temperature of the test section changes with time during the boiling experiments. Initially, the heat transfer is by natural convection (Section 2.1). The wall temperature continues to increase until boiling initiates. On plane copper, there is a temperature excursion prior to boiling incipience. At incipient boiling, the wall temperature sharply drops and heat transfer is by nucleate boiling. All three of the nucleate boiling regimes are represented in Figure 3.18 (Section 2.2.2). At a low surface superheat is the region of discrete bubbles, where not all of the potential active nucleation sites on the surface are active, but their number increase with increased surface temperature. The fully developed nucleate boiling region occurs at higher surface superheat and has a higher density of active nucleation sites. Near the end of this region, bubbles coalesce and hinder the heat removal from the surface. The region of lateral coalescence extends from the end of the fully developed nucleate boiling region to CHF. In this region, the incremental increases in the heater's power are gradually reduced to accurately determine the CHF values and avoid a large temperature surge, which may burn the heating element (Figure 3.15). When a temperature surge of more

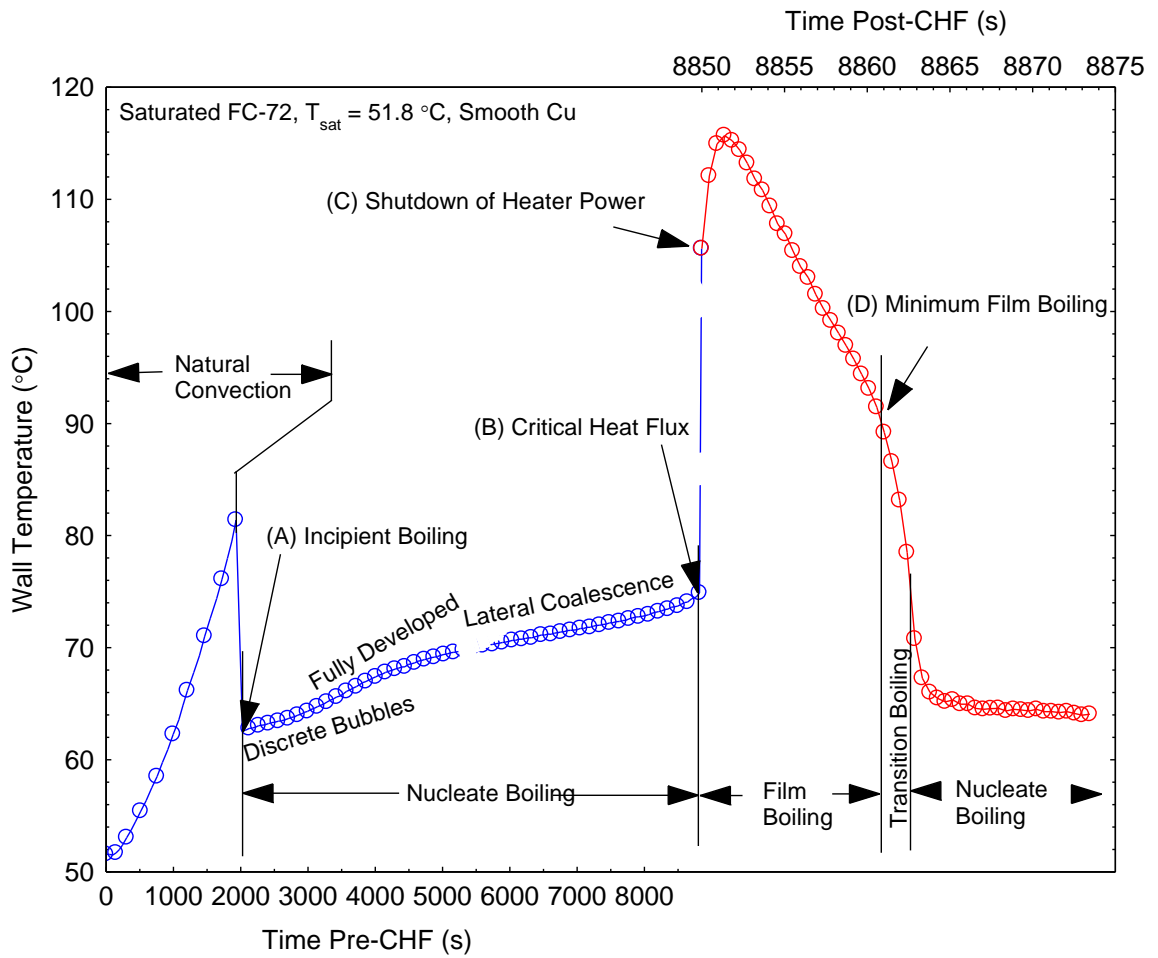


**Figure 3.18. Temporal boiling curve of saturated FC-72 on copper.**

than 30 K over the last steady state surface temperature is measured, the power is shut off and the test section cools (Figure 3.18).

The experimental uncertainties are determined from the manufacturers' stated uncertainties for each piece of equipment used and the random uncertainties associated with the measurements. These are combined to estimate the uncertainty for each individual parameter and the overall uncertainty of the boiling curves in the experiments. The details of the uncertainty analysis are given in Appendix B. The estimated experimental uncertainties are  $\pm 1.0$  K in the measured temperatures and  $\pm 3\%$  in the steady state surface heat flux measurements. Near CHF, the slope of the boiling curve is shallow and small increases in power can result in large temperature increases. In addition, the hydrodynamic instability of the liquid-vapor interface near CHF can cause blanketing of the surface at many points near CHF. The resultant uncertainty in the CHF measurement can be larger (additional  $\pm 3\%$  in experimental values) and the variation in the surface superheat at CHF can be as much as 4 K.

## 4 Pool Boiling on Plane Surfaces

Improvements of the boiling heat transfer can be realized by increasing the nucleation site density on the heated surface and/or the surface area wetted by the boiling liquid. The porous graphite provides a significant increase in the nucleation site density over a plane copper surface, and thus enhances the boiling heat transfer. This chapter presents and discusses the results of pool boiling experiments on plane surfaces with FC-72 and HFE-7100 dielectric liquids (on copper and porous graphite). The results show both the effect of liquid properties and subcooling and the surface orientation on both nucleate boiling and CHF. For comparison purposes, the pool boiling curves for a flat or plane copper surface are used because it is a common reference surface in boiling heat transfer experiments with FC-72 and HFE-7100 by many investigators (Chang and You, 1997; Rainey and You, 2000; Z. W. Liu et al., 2001; El-Genk and Bostanci, 2003a,b; Ujereh, Fisher, and Mudawar, 2007; Priarone, 2005). The comparisons of the nucleate boiling heat transfer and CHF are made in reference to the obtained values for plane copper

### 4.1 Reproducibility and Hysteresis of Boiling Curves

The experimental procedures set forth in the previous chapter are used to consistently ensure that the data obtained are reproducible. A sample of the obtained pool boiling curves for saturation and subcooled boiling of HFE-7100 and FC-72 liquid on different surfaces at different inclinations in two sequential tests conducted at the same conditions are shown in Figures 4.1a – 4.1c. These boiling curves demonstrate excellent reproducibility of the data in the pool boiling experiments for different surfaces, boiling liquid and liquid subcooling, and inclination angle. Figure 4.1a shows saturation boiling curves for HFE-7100 on the plane copper surface in the upward facing orientation ( $\theta = 0^\circ$ ). Subcooled boiling ( $\Delta T_{\text{sub}} = 20 \text{ K}$ ) curves of FC-72 on plane porous graphite at  $\theta = 0^\circ$  is shown in Figure 4.1b. Figure 4.1c presents the subcooled boiling ( $\Delta T_{\text{sub}} = 10 \text{ K}$ ) curves of HFE-7100 on the copper surface with 5 mm tall corner pins in the vertical orientation ( $\theta = 90^\circ$ ).

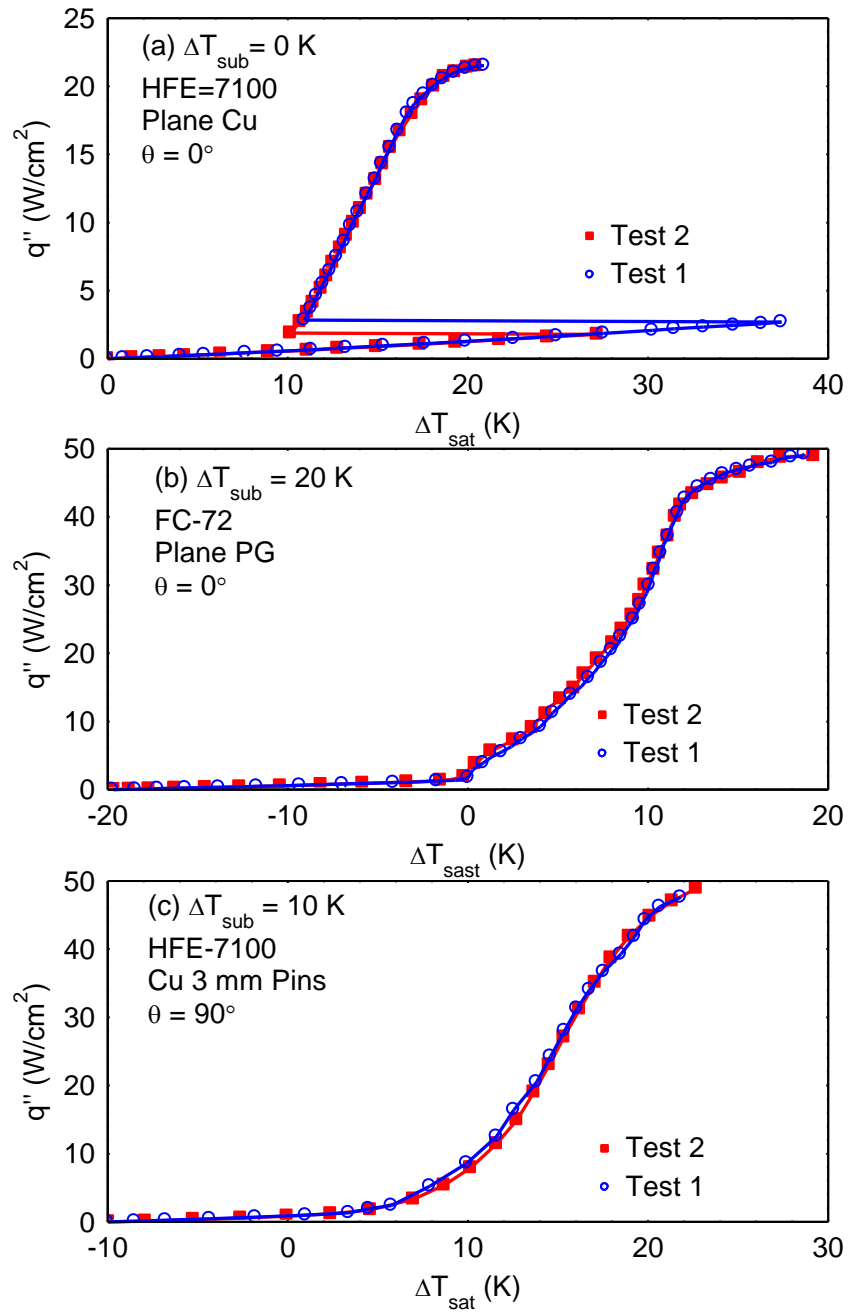


Figure 4.1 Reproducibility of boiling curves.

All pool boiling experiments are conducted under increasing heat flux conditions, as described in Chapter 3. Because heat flux increases with time in the experiments, some portions of the boiling surface activate later than others. The portions starting boiling earlier stimulate nucleate boiling in neighboring nucleation sites. Under decreasing heat flux conditions, the nucleation sites generally deactivate uniformly on the heated surface. A boiling hysteresis can occur in this case. With dielectric liquids, the surface tension is low and as such flood the surface crevices, which delays the onset of nucleate boiling to higher surface superheats (see Sections 1.1 and 2.1). Boiling curves generated with decreasing heat flux follow the same data as those of increasing heat flux except in the region of low heat fluxes (Rini, Chen, and Chow, 2001; El-Genk and Bostanci, 2003a). Figure 4.2 presents the obtained saturation boiling curves of HFE-7100 on a copper surface with 5 mm tall corner pins with both increasing and decreasing heat flux. The low heat flux region is where the temperature excursion prior to boiling incipience occurs. The uneven boiling curve shown in Figure 4.2 for increasing heat flux is caused by the nucleate boiling on individual pins being partially activated separately and thus reducing the average footprint temperature in steps.

## **4.2 Typical Pool Boiling Curve**

Figures 4.3a – 4.3c present the obtained saturation and subcooled ( $\Delta T_{\text{sub}} = 10, 20,$  and  $30 \text{ K}$ ) boiling curves of FC-72 on porous graphite. Figures 4.3d -4.3f present the respective boiling curves on plane copper. The horizontal arrows labeled “NC” indicate the extent of the natural convection region, prior to boiling incipience. The boiling curves of the dielectric liquids have three distinct nucleate boiling regions in addition to the natural convection region. Figure 4.4 shows the saturation boiling curve for FC-72 on porous graphite with embedded photographs of the boiling process in each of the three boiling regions.

Region I, the region of *discrete bubbles*, is that of low-superheat nucleate boiling. Not all of the potential active nucleation sites are active, but their number increases with increased heat flux. Region II, the region of *fully developed nucleate boiling*, occurs at

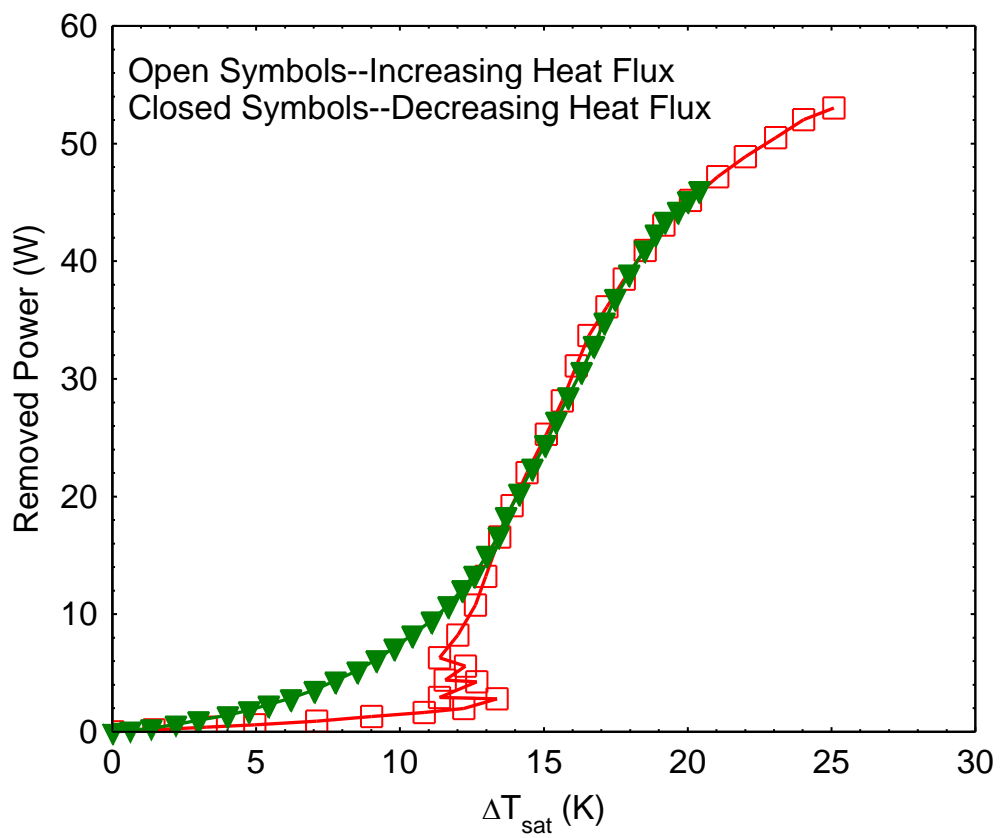


Figure 4.2 Boiling curve hysteresis.

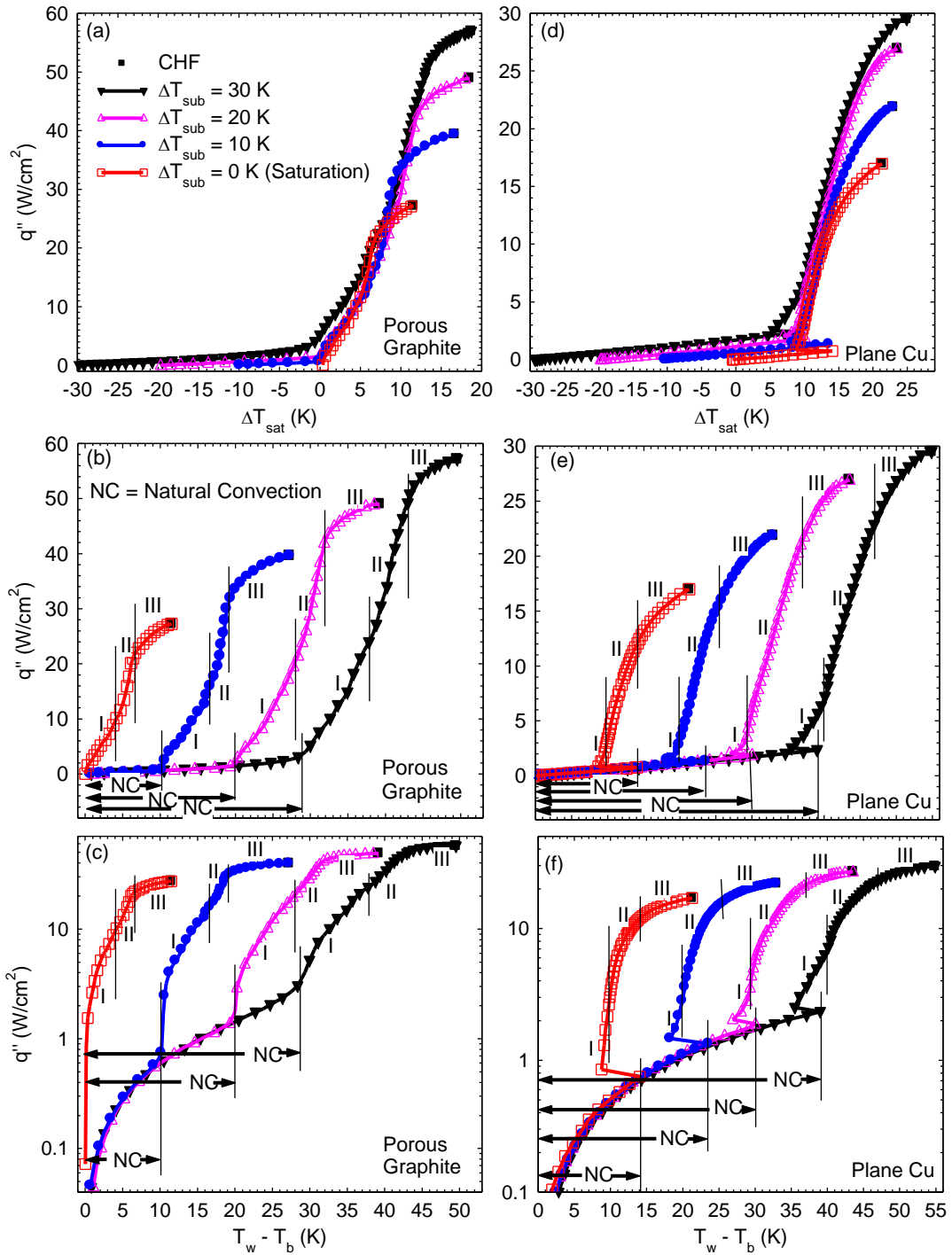


Figure 4.3 Boiling regimes of FC-72 on porous graphite and copper

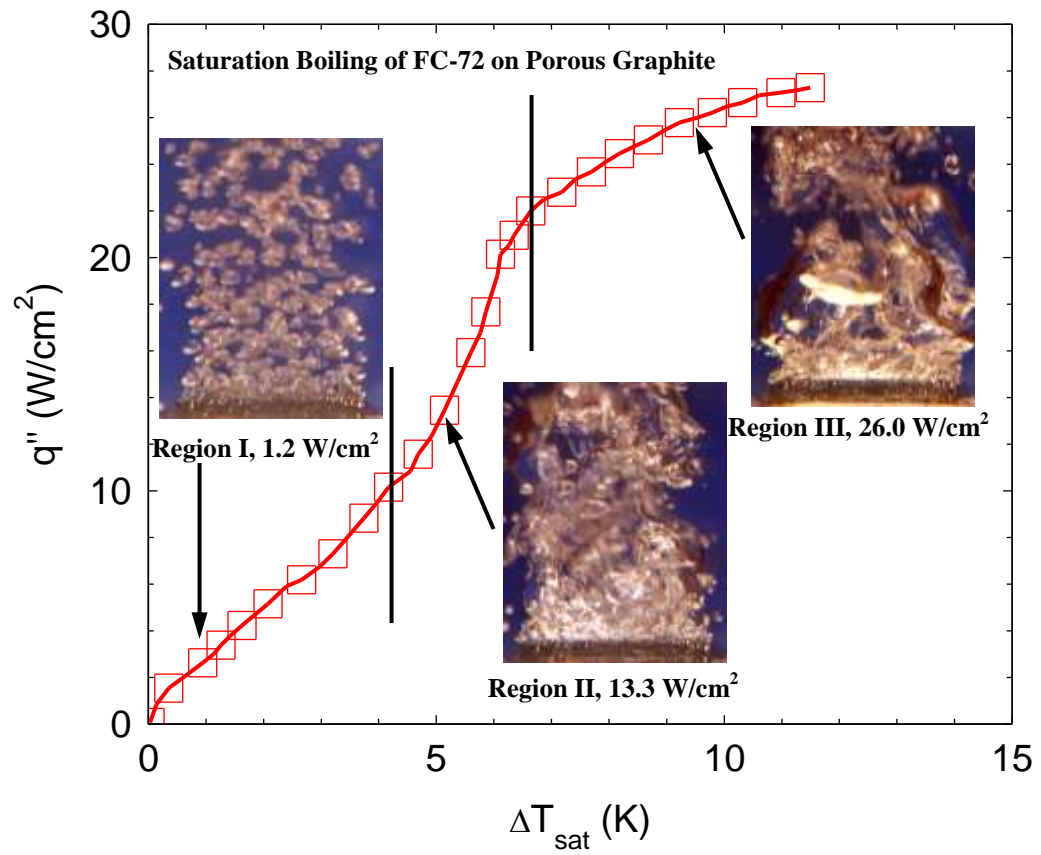


Figure 4.4 Photographs of different boiling regimes of FC-72 on porous graphite.

higher heat flux than in the discrete bubble region and is characterized by a steep slope of the boiling curve. The steep slope is indicative of the high density of active nucleation sites on the surface. Departing bubbles from the surface cause mixing in the boundary layer, which further enhances the heat transfer. In addition to the high density of the active nucleation sites on the surface, lateral coalescence among growing and departing vapor bubbles is negligible, but increases with increasing heat flux. Near the end of this region, lateral bubbles coalesce and hinder the heat removal from the surface as indicated by the decrease of slope of the boiling curve, making the beginning of the next region of lateral coalescence.

When the departing bubbles begin to coalesce and form vapor globules near the boiling surface, nucleate boiling transitions to Region III, of *lateral bubble coalescence*. In this region, the gradually decreasing slope of the boiling curves is caused by the increased lateral coalescence of the growing and departing bubbles, forming large vapor masses in the pool near the boiling surface. Consequently, the rate of increase in the nucleate boiling heat flux in region III with increasing surface superheat is significantly lower than those in regions I and II. Region III extends to CHF, marked in Figures 4.3a – 4.3f by a solid square symbol. The above classification of the boiling regions is confirmed by visual observations and the recorded digital photographs and video of the boiling processes (Figure 4.4). However, they should be considered as approximations.

### **4.3 Natural Convection**

The natural convection region for FC-72 and HFE-7100 on porous graphite only exists in subcooled boiling and extends to incipient boiling when the surface temperature is a only fraction of a degree above the liquid's saturation temperature. Natural convection begins when the surface temperature,  $T_w$ , is higher than that of the bulk liquid,  $T_b$ . On plane copper, the natural convection region exists in both subcooled and saturation boiling because the surface temperature could be as much as 35 K above the liquid saturation temperature prior to boiling incipience. Since the surface in the experiments is uniformly heated, the dissipated heat removal rate in the natural convection region is proportional to  $(T_w - T_b)^{1.2}$ . The present natural convection data for

both FC-72 and HFE-7100, on porous graphite and plane copper, and those reported by other investigators for FC-72 on micro-porous coatings, micro-fined surfaces and surfaces with micro-reentrant cavities (Kubo, Takamatsu, and Honda, 1999; Chang and You, 1996; Rainey, You, and Lee, 2003) are shown in Figures 4.5a and 4.5b. The data in these figures are correlated as:

$$(a) \quad q_{NC} = 0.0353(T_w - T_b)^{1.2}, \text{ on porous and micro-structured surfaces} \quad (4.1a)$$

$$(b) \quad q_{NC} = 0.0314(T_w - T_b)^{1.2}, \text{ on plane smooth surfaces.} \quad (4.1b)$$

Equations 4.1a and 4.1b fit the data in Figures 4.5a and 4.5b to within  $\pm 10\%$  and  $\pm 7\%$ , respectively. These figures show that the dissipated heat flux in natural convection on porous and micro-structured surfaces is  $\sim 12\%$  higher than that on plane copper and silicon. The enhancement in natural convection of dielectric liquids on porous graphite, compared to that on copper, is attributed to the tiny air bubbles released from the porous graphite surface in the experiments, enhancing the mixing in the thermal boundary layer. This may also explain the similarity in the heat transfer rate in natural convection on micro-porous and structured surfaces from which bubbles of entrapped air could have also been released prior to boiling incipience. In the present work, no air bubbles are released from the copper surface in natural convection region. As indicated earlier, for consistency, the dielectric liquids in the present experiments were degassed.

#### **4.4 Nucleate Boiling**

The natural convection regime ends at boiling incipience. On plane copper (Figures 4.3a – 4.3c) there is usually a temperature excursion prior to boiling incipience which extends the natural convection region. On porous graphite, there is no temperature excursion prior to boiling incipience in the experiments. Thus, natural convection ends when the surface temperature just exceeds the saturation temperature of the liquid (Figures 4.3d – 4.3f). When nucleate boiling ensues, there is a rapid increase in the dissipated heat flux as the surface superheat increases.



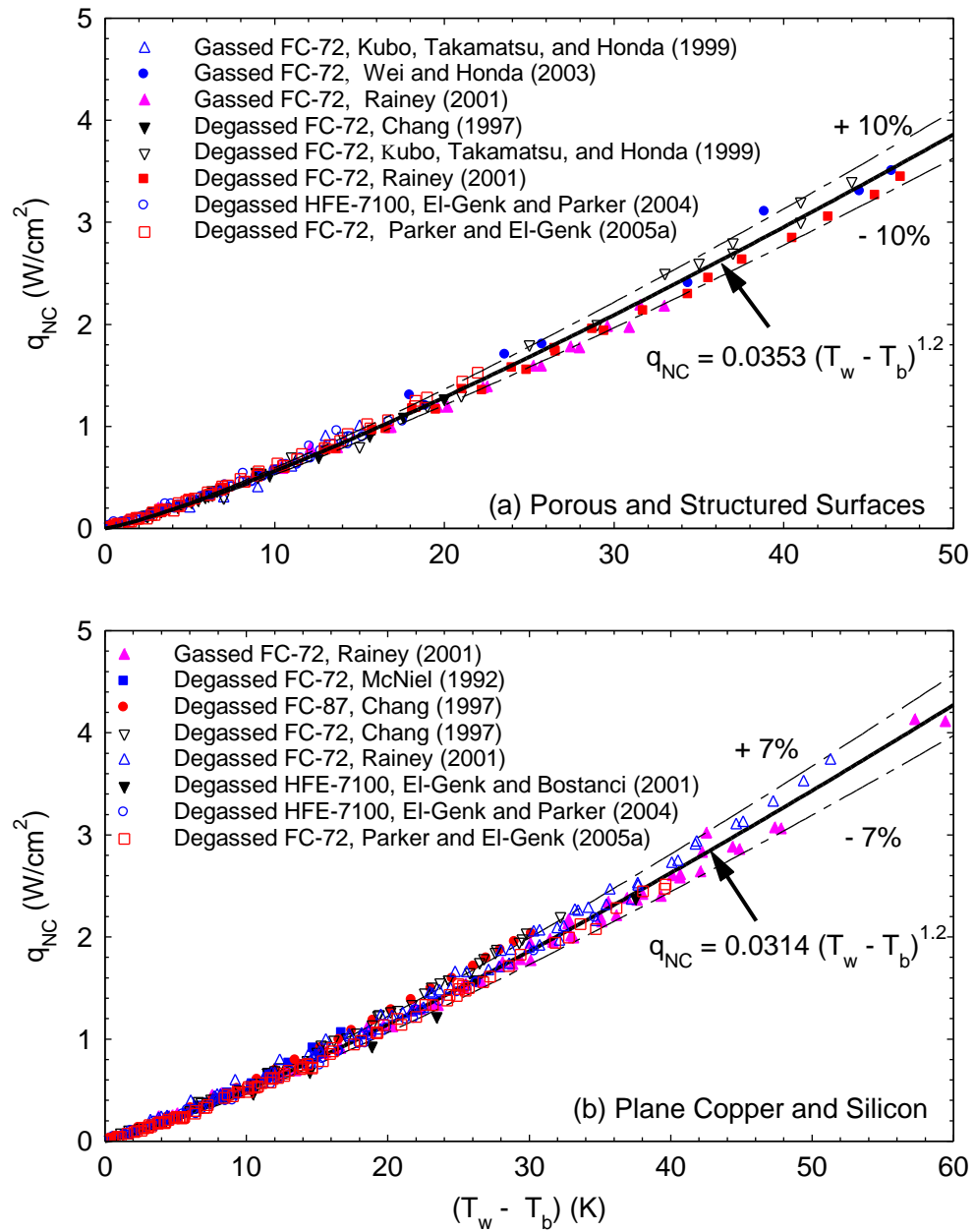
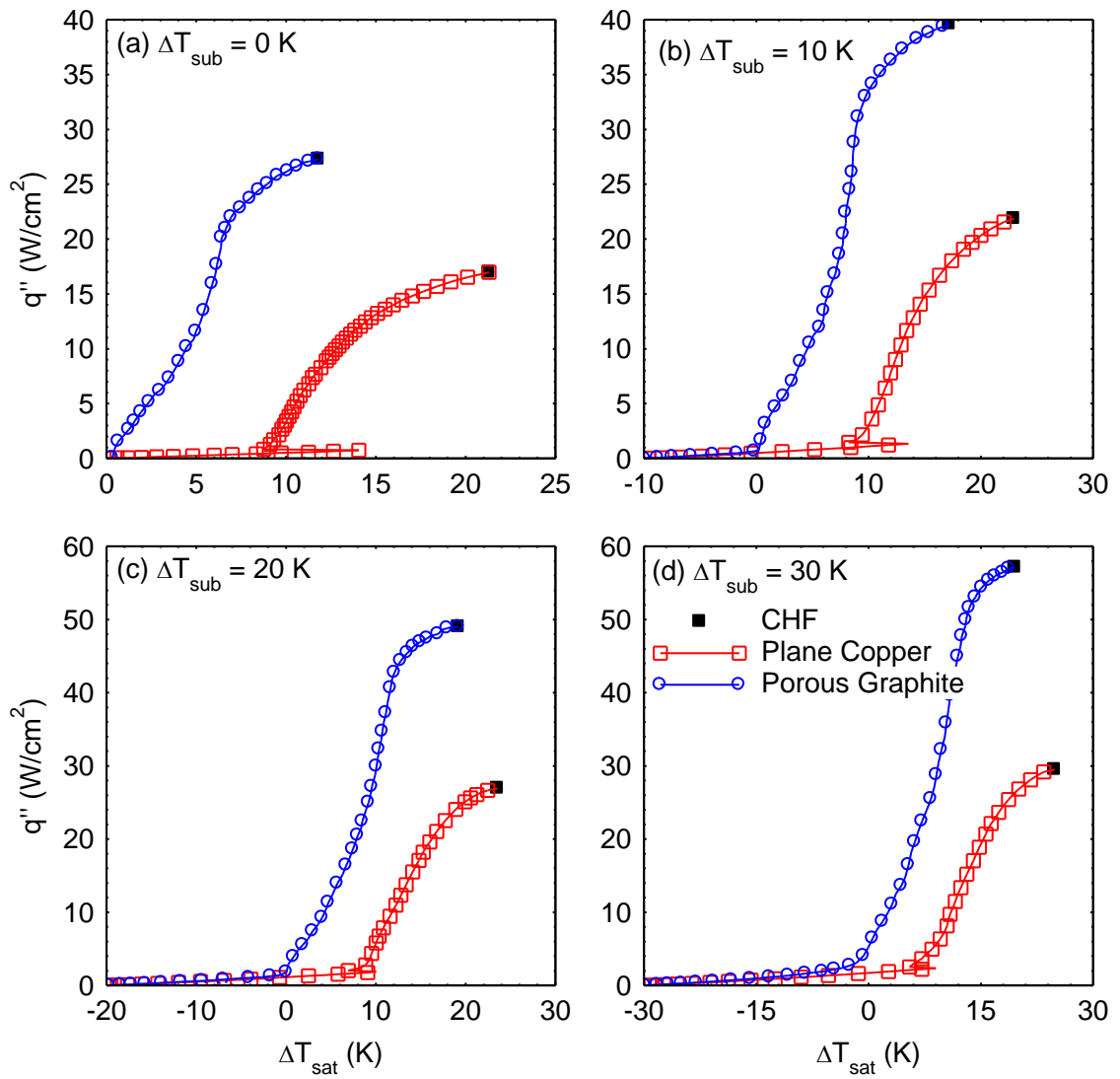


Figure 4.5 Natural convection data of dielectric liquids on smooth, porous, micro-structured, and micro-porous surfaces

Figures 4.6 and 4.7 compare the obtained saturation and subcooled boiling curves of HFE-7100 and FC-72 on plane porous graphite and copper surfaces. These figures show that there are no temperature excursions prior to boiling incipience on porous graphite and nucleate boiling starts when the surface temperature is only a fraction of a degree higher than the liquid's saturation temperature (because of the high elevation of Albuquerque, NM, ambient pressure of  $\sim 0.085$  MPa the saturation temperature of FC-72 is  $\sim 51.8$  °C and  $\sim 54.0$  °C for HFE-7100). The absence of temperature excursions at boiling incipience on porous graphite is attributed to the air entrapped in the tiny and interconnected pores and re-entrant cavities at the surface. Because of the low surface tension of dielectric liquids the pores with mouth diameters  $< \sim 13$   $\mu\text{m}$  are not readily wetted and entrap air which promotes bubble nucleation. The larger pores and re-entrant cavities, however, are likely filled with liquid, but some of the interconnecting pores to these cavities could be too small to be wetted, and thus entrap air. In addition, boiling ensues on the porous graphite surfaces at very low surface superheats. Conversely, the temperature excursions prior to boiling incipience on plane copper varied from 9 K to 14 K for FC-72 and from 18 K to 36 K for HFE-7100.

Figures 4.6 and 4.7 show that the nucleate boiling heat transfer rate and CHF for porous graphite are both much larger than for boiling on the copper surface in both liquids. Also, the surface superheat at CHF on porous graphite is lower than on plane copper. Table 4.1a lists the present values of CHF and superheat at CHF and some saturation and subcooled nucleate boiling heat fluxes and the corresponding superheats in saturation and subcooled boiling of FC-72 on porous graphite and copper (Figure 4.6). Table 4.2b lists similar values for boiling of HFE-7100 (Figure 4.7). The measured increase in the nucleate boiling heat flux and the decrease in the corresponding surface superheat for dielectric liquids on porous graphite translate into lower junction temperatures and, hence, longer operation life and lower frequency of thermally induced failures of computer chips (Peterson, 1994). In addition, the absence of temperature excursions at boiling incipience on porous graphite is an attractive feature for cooling CPU chips at low heat fluxes at which the chips are expected to operate the longest period of time.



**Figure 4.6 Saturation and subcooled pool boiling curves of FC-72 on porous graphite and plane copper.**

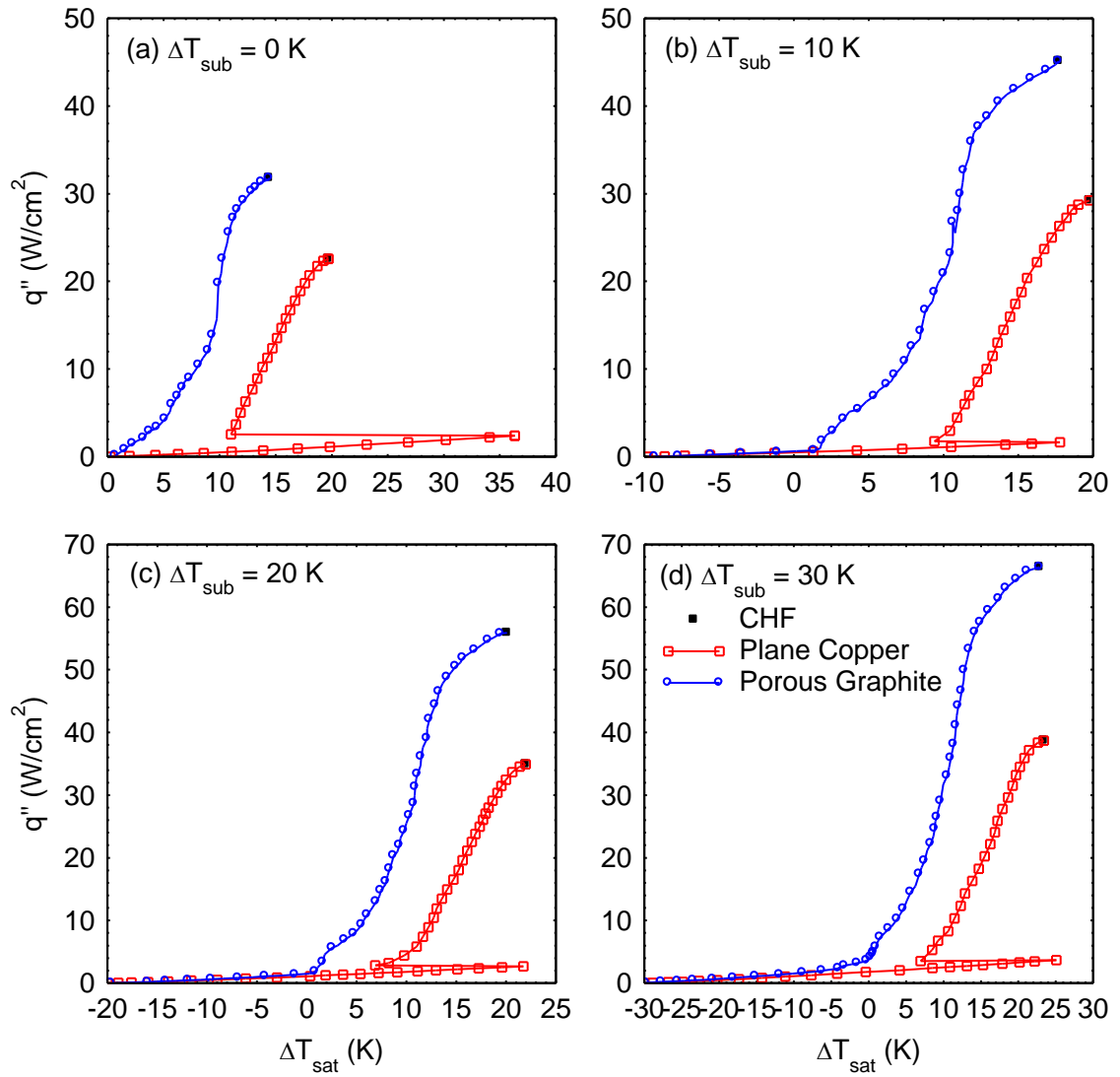


Figure 4.7 Saturation and subcooled pool boiling curves of HFE-7100 on porous graphite and plane copper

**Table 4.1. Comparison of boiling data for FC-72 and HFE-7100**

**(a) FC-72**

Parameter	on Porous Graphite				on Plane Copper			
	0 K	10 K	20 K	30 K	0 K	10 K	20 K	30 K
Liquid subcooling, $\Delta T_{\text{sub}}$ (K)								
$\Delta T_{\text{sat,ex}}$ (K)	None	None	None	None	14.0	13.5	10.0	9.0
$\Delta T_{\text{sat,inc}}$ (K)	$\leq 1.0$	$\leq 1.0$	$\leq 1.0$	$\leq 1.0$	$\leq 8.8$	$\leq 8.2$	$\leq 6.9$	$\leq 5.5$
CHF ( $\text{W}/\text{cm}^2$ )	27.3	39.6	49.0	57.1	16.9	21.9	26.9	29.5
$\Delta T_{\text{sat,CHF}}$ (K)	11.8	17.2	19.2	19.5	21.3	22.9	23.5	24.9
$q_{\text{NB}}$ ( $\text{W}/\text{cm}^2$ )								
@ $\Delta T_{\text{sat}} = 11$ K	27.1	35.1	36.8	40.0	6.3	5.2	8.3	9.9
@ $\Delta T_{\text{sat}} = 14$ K	N/A	38.0	45.9	52.7	11.9	13.0	15.3	17.0
@ $\Delta T_{\text{sat}} = 17$ K	N/A	39.5	48.1	56.0	14.8	17.5	21.4	23.1

**(b) HFE-7100**

Parameter	Porous Graphite				Copper			
	0 K	10 K	20 K	30 K	0 K	10 K	20 K	30 K
Liquid subcooling, $\Delta T_{\text{sub}}$ (K)								
$\Delta T_{\text{sat,ex}}$ (K)	None	None	None	None	39.3	36.6	34.1	7.5
$\Delta T_{\text{sat,inc}}$ (K)	$\leq 1.0$	$\leq 1.0$	$\leq 1.0$	$\leq 1.0$	$\leq 11.9$	$\leq 10.9$	$\leq 9.5$	$\leq 7.5$
CHF ( $\text{W}/\text{cm}^2$ )	31.8	45.1	55.9	66.4	22.7	28.8	37.1	41.5
$\Delta T_{\text{sat,CHF}}$ (K)	14.4	17.7	20.1	22.8	23.3	25.0	25.7	26.7
$q_{\text{NB}}$ ( $\text{W}/\text{cm}^2$ )								
@ $\Delta T_{\text{sat}} = 11$ K	29.0	36.9	39.1	44.3	3.1	5.1	6.8	10.5
@ $\Delta T_{\text{sat}} = 14$ K	31.4	40.9	48.7	55.1	9.4	10.3	11.1	13.7
@ $\Delta T_{\text{sat}} = 17$ K	N/A	44.2	53.3	60.7	16.7	18.8	21.1	21.4

#### 4.4.1 Effect of Liquid Properties

Because of the different thermophysical properties of FC-72 and HFE-7100, nucleate boiling heat transfer rates and CHF for each liquid on the same surface differ. Figure 4.8 compares the saturation boiling curves of the two liquids on porous graphite (Figure 4.8a) and plane copper (Figure 4.8b). The nucleate boiling heat transfer rate is higher for FC-

72 than with HFE-7100 on both surfaces, but the CHF for FC-72 is lower. With FC-72,

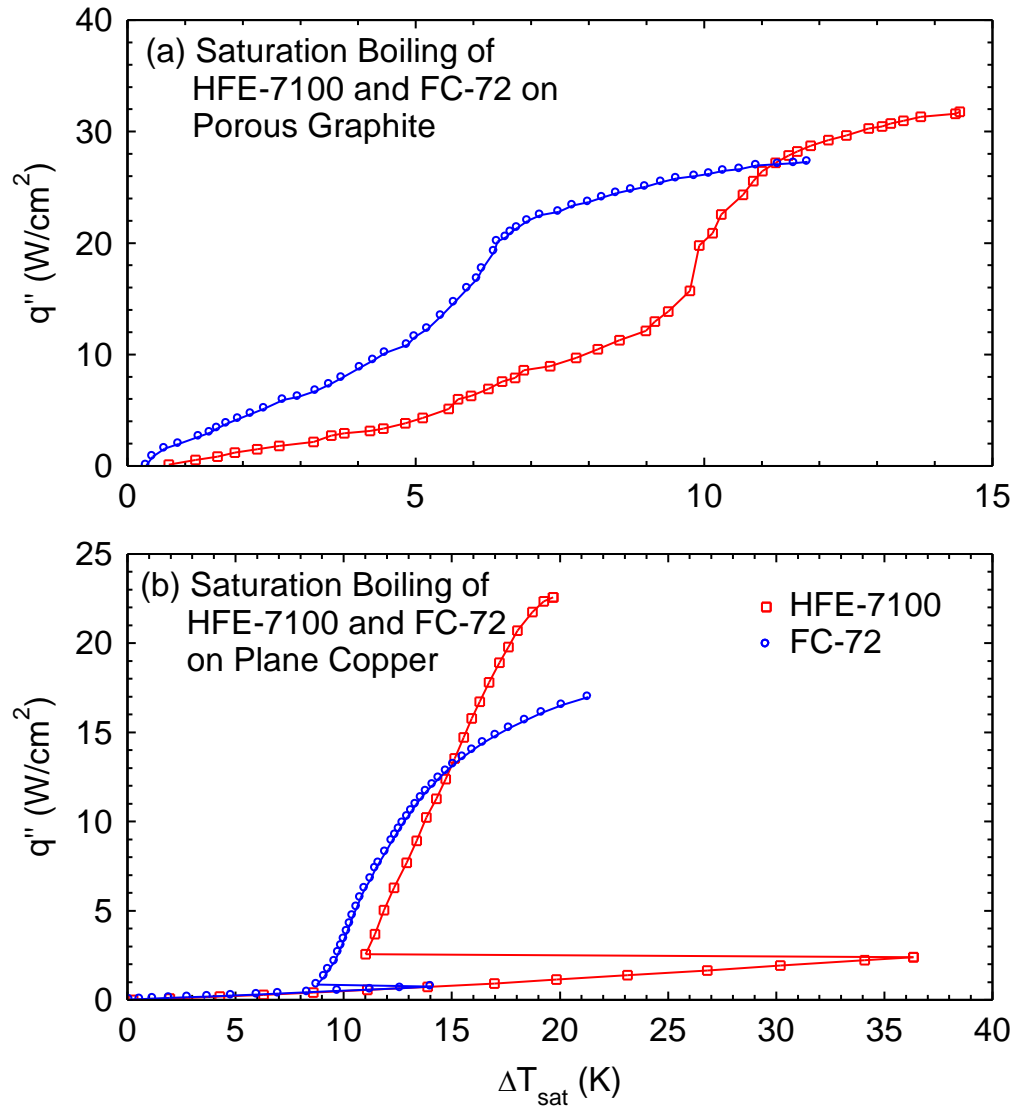


Figure 4.8 Comparison of boiling curves for HFE-7100 and FC-72 on porous graphite and copper.

there is a larger range of active cavity sizes than with HFE-7100 (Figure 2.4). In addition, the cavities with mouths of the same size are activated at a lower superheat with FC-72 than with HFE-7100. These factors combined increase nucleate boiling heat flux in FC-72 more than HFE-7100 at the same surface superheat on the same heated surface.

For example, at a nucleate boiling heat flux of  $5.0 \text{ W/cm}^2$ , the surface superheat in saturation boiling of FC-72 on porous graphite is 2.3 K, while with HFE-7100,  $\Delta T_{sat} = 5.5 \text{ K}$  (Figure 4.8a). At a surface superheat of 5.5 K, the dissipated heat flux in nucleate boiling of FC-72 is  $13.8 \text{ W/cm}^2$  compared to  $5.0 \text{ W/cm}^2$  in HFE-7100, representing an increase of 2.8 times in the nucleate boiling heat transfer coefficient. Similarly, on plane copper (Figure 4.8b), at  $5.0 \text{ W/cm}^2$ , the surface superheat with FC-72 is 10.5 K and with HFE-7100 is 11.8 K. At a superheat of 11.0 K, the nucleate boiling heat flux with FC-72 is  $6.2 \text{ W/cm}^2$  compared to only  $2.6 \text{ W/cm}^2$  with HFE-7100, which is an increase of 2.4 times in the nucleate boiling heat transfer rate. Conversely, CHF for HFE-7100 is higher than that for FC-72 by 12 – 14% on porous graphite and by 24 – 29% on plane copper (Table 4.1).

Nucleation sites activate at a lower surface superheat in FC-72 than HFE-7100 (Figure 2.4). Figures 4.9a and 4.9b show photographs of nucleate boiling of FC-72 and HFE-7100 on porous graphite at 1.4 K superheat and  $3.0 \text{ W/cm}^2$  and  $0.8 \text{ W/cm}^2$ , respectively. Figures 4.9c and 4.9d show boiling on the porous graphite at  $\sim 3\text{K}$  superheat and  $6.7 \text{ W/cm}^2$  (FC-72) and  $2.0 \text{ W/cm}^2$  (HFE-7100). On plane copper at a superheat of  $\sim 11 \text{ K}$ , the photographs in Figures 4.9e and 4.9f are at a nucleate boiling heat flux of  $7.0 \text{ W/cm}^2$  for FC-72 and  $2.9 \text{ W/cm}^2$  for HFE-7100. It is clear that with FC-72, more nucleation sites activate at lower surface superheats than for HFE-7100. This helps to explain the higher heat transfer rate with FC-72 than HFE-7100 on both porous graphite and plane copper. However, at higher surface superheats, the boiling heat transfer rate is higher with HFE-7100. With more active nucleation sites and thus more bubble generation, the region of lateral bubble coalescence occurs at lower heat fluxes with FC-72 than HFE-7100 (Figures 4.8a and 4.8b). HFE-7100 has a higher latent heat of vaporization (Table 1.1), resulting in a higher CHF than FC-72.



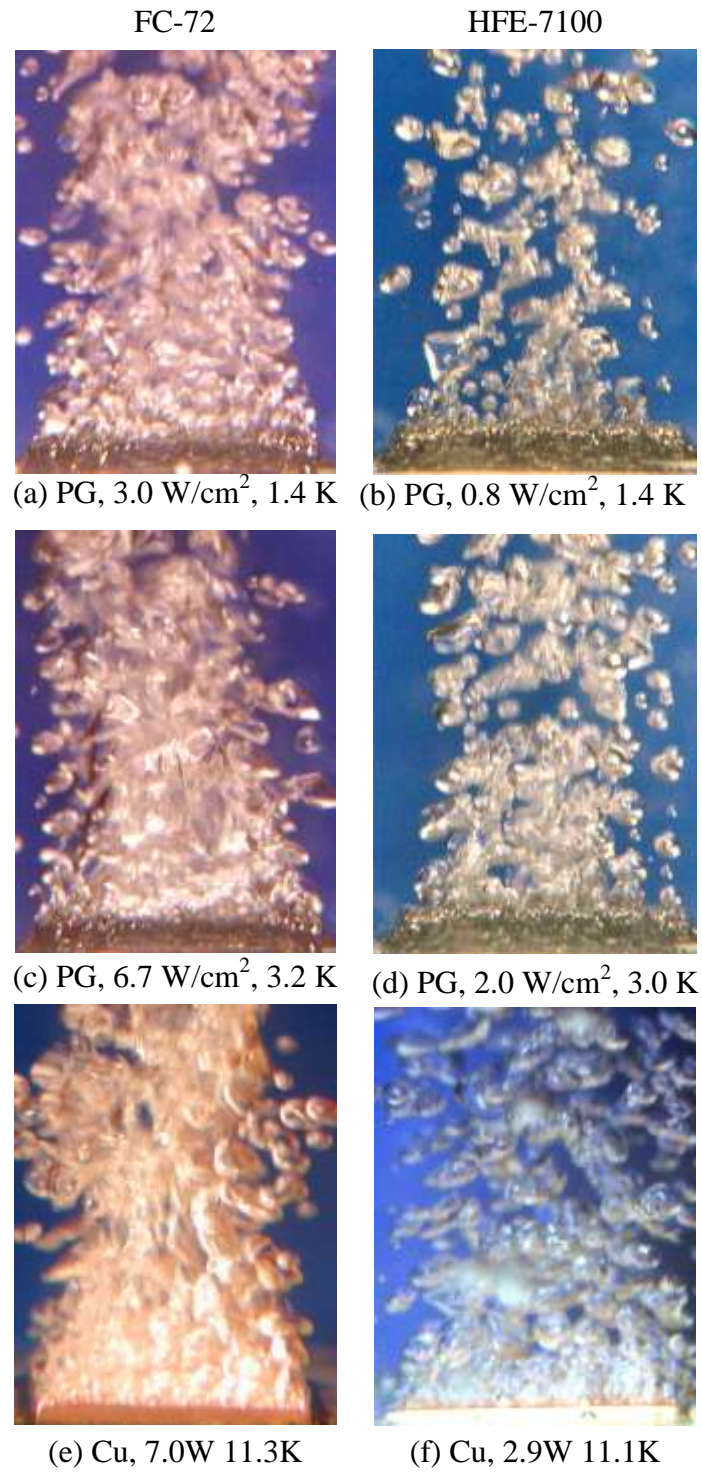


**Figure 4.9** Photographs of boiling of FC-72 and HFE-7100 on porous graphite and plane copper at similar surface superheats.

#### 4.4.2 Effect of Liquid Subcooling

The pool boiling curves shown in Figures 4.10a – 4.10d ( $\Delta T_{sub} = 0$  K, 10 K, 20 K, and 30 K) demonstrate the effect of liquid subcooling on pool boiling of the dielectric liquids on porous graphite and plane copper. The CHF values increase with increased subcooling and so does the corresponding surface temperature or superheat,  $\Delta T_{sat}$ . For HFE-7100 on porous graphite at  $\Delta T_{sub} = 30$  K and HFE-7100, CHF is as much as 66.4 W/cm<sup>2</sup>, compared to only 31.8 W/cm<sup>2</sup> for saturation boiling. The corresponding superheat at CHF is 22.8 K and 14.4 K for 30 K subcooled and saturation boiling, respectively (Figure 4.10b). Similar increases in CHF and the surface superheat at CHF are observed in FC-72 boiling experiments (Table 4.1).

For a consistent comparison, the ratios of the nucleate boiling heat transfer coefficient of FC-72 and HFE-7100 on porous graphite and copper at the same  $\Delta T_{sat}$  are plotted in Figures 4.11a and 4.11b for saturation and subcooled boiling. At  $\Delta T_{sat} \simeq 9$  K, the saturation nucleate boiling heat flux of FC-72 on porous graphite is ~ 30 times that on copper, and with HFE-7100 this ratio is about 17. The saturation nucleate boiling heat flux ratio decreases exponentially with increased surface superheat for both FC-72 and HFE-7100, eventually approaching asymptotes of ~ 1.8 and 1.56, respectively, which are approximately 11% higher than the saturation critical heat flux ratio ( $CHF_{PG} / CHF_{Cu}$ ) for both liquids. For 10, 20, and 30 K subcooled boiling of FC-72, the nucleate boiling heat flux ratios are constant at 17.0 up to  $\Delta T_{sat} = 9.0$  K, 8.8 up to  $\Delta T_{sat} = 8.5$  K, and 6.4 up to  $\Delta T_{sat} = 6.5$  K, respectively. Beyond these surface superheats, the ratios of nucleate boiling heat flux decrease exponentially with increasing surface superheat, approaching the same asymptote as the saturation nucleate boiling heat flux ratio (~1.8) (Figure 4.11a). Similarly, for 10, 20, and 30 K subcooled boiling of HFE-7100, the values of the nucleate boiling heat flux ratios are constant at 11.4 up to  $\Delta T_{sat} = 10.0$  K, 5.5 up to  $\Delta T_{sat} = 11.0$  K, and 3.7 up to  $\Delta T_{sat} = 13.0$  K, respectively, beyond which the ratios also decrease exponentially with increasing surface superheat, asymptotically approaching saturation nucleate boiling heat flux ratio (~1.56) (Figure 4.11b).

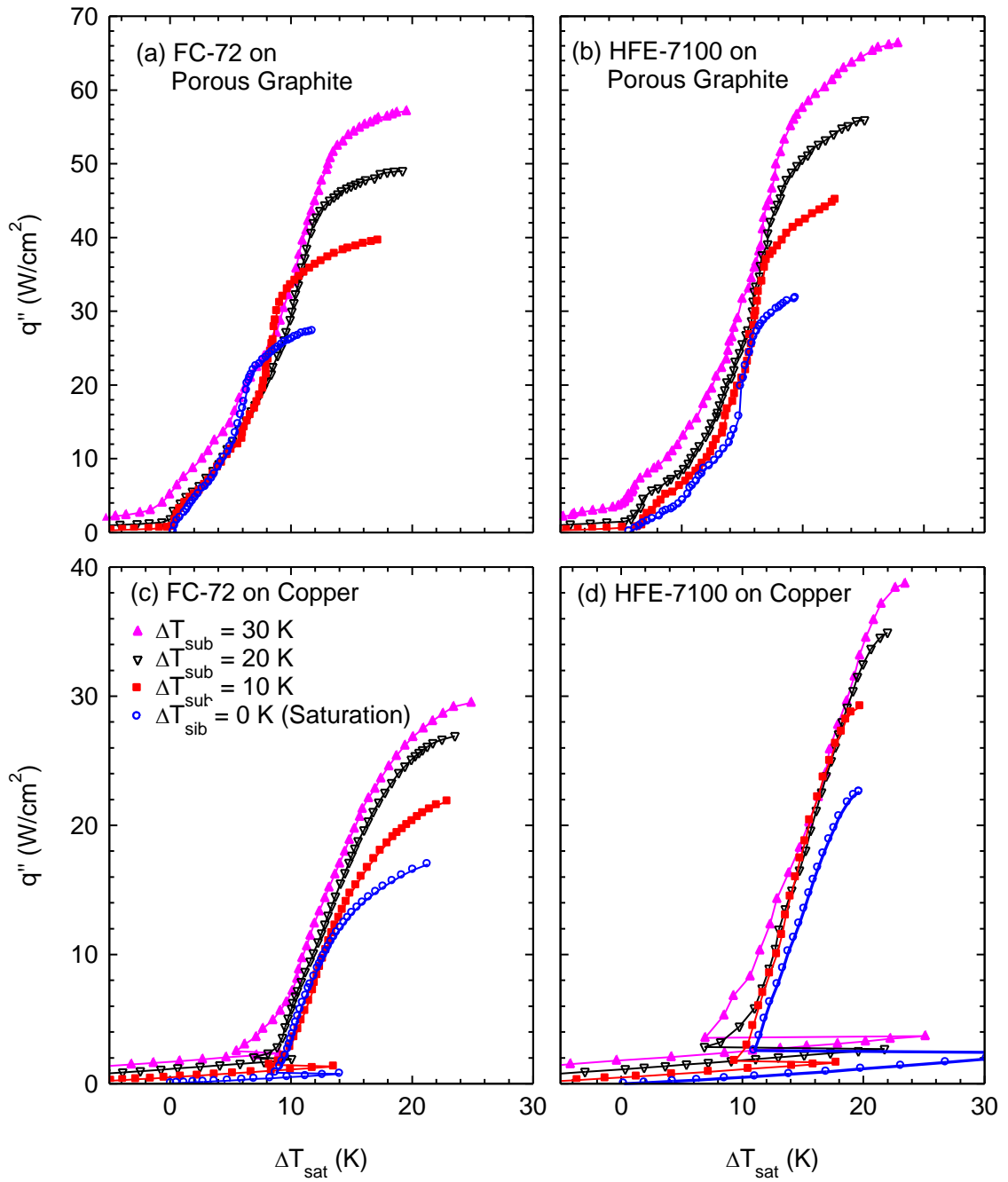
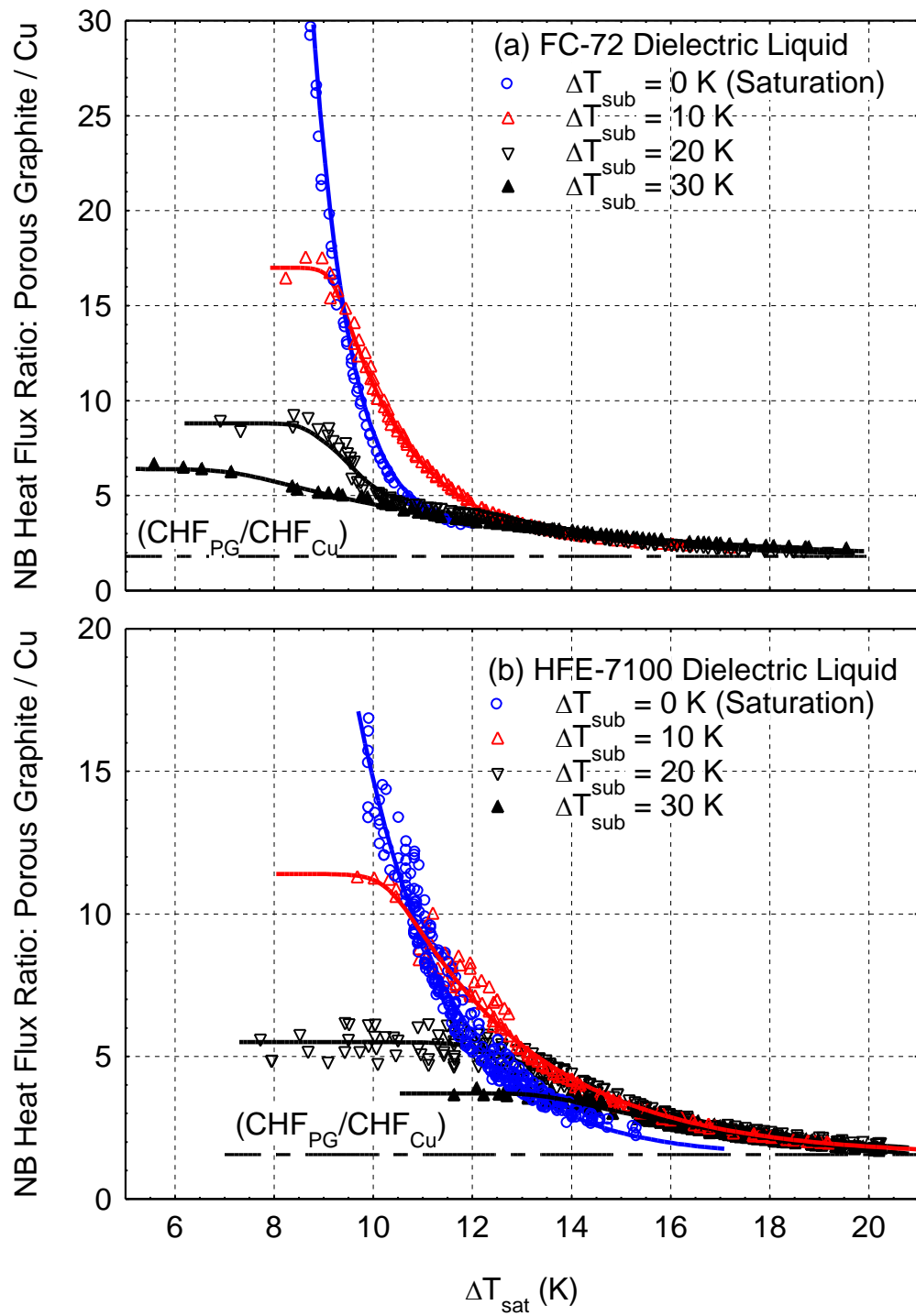


Figure 4.10 Effect of subcooling on pool boiling of HFE-7100 and FC-72 on copper and porous graphite.

Figure 4.11 Ratio of nucleate boiling heat transfer coefficient on porous graphite to copper.



### 4.4.3 Liquid Aging Effect

The presented results on porous graphite in the following section at different surface inclinations are for previously used or aged dielectric liquid. The aged FC-72 or HFE-7100 liquid has been used for ~ 50 days during which more than 165 hours of boiling in 50 tests at different liquid subcoolings are conducted. The fresh liquid, whose results are reported in the previous sections, has been used only 10's of hours in less than 10 boiling tests. For each level of liquid subcooling, the presented pool boiling curves are highly reproducible for both fresh and aged liquid. In general, the nucleate boiling heat fluxes from the aged liquid are lower and the corresponding surface superheats are higher than those measured using the fresh liquid. This difference is pronounced at and near CHF but decreases with decreased nucleate boiling heat flux, becoming insignificant at low surface superheats (Figure 4.12).

Though inert, a possible cause for the apparent aging of the dielectric liquid could be the leaching of plasticizers into the liquid from the epoxy used as a thermal insulator and filler in the test section assembly (3M Scotch-Weld 1836-L B/A). Chang (1997) has reported that over time the increased level of plasticizers in the liquid caused CHF to increase slightly at a significantly higher superheat in saturation boiling of FC-72 liquid on micro-porous coatings. Such mixing of the leached plasticizers with the boiling dielectric liquids could increase their surface tension, reducing the nucleate boiling heat flux and shifting the boiling curve to higher surface superheats, which is consistent with the present results and those of Chang (1997). The above causes could also be responsible for the measured shift in the boiling curves, the decrease in the nucleate boiling heat fluxes, and the higher CHF values for the dielectric liquids on porous graphite in the present experiments when using aged liquid. After discovering the source of this problem, a new epoxy was obtained (Masterbond Supreme 42HT(30)) and used for the subsequent tests using extended copper surfaces (Chapter 6). The results showed no aging effect on the pool boiling curves.

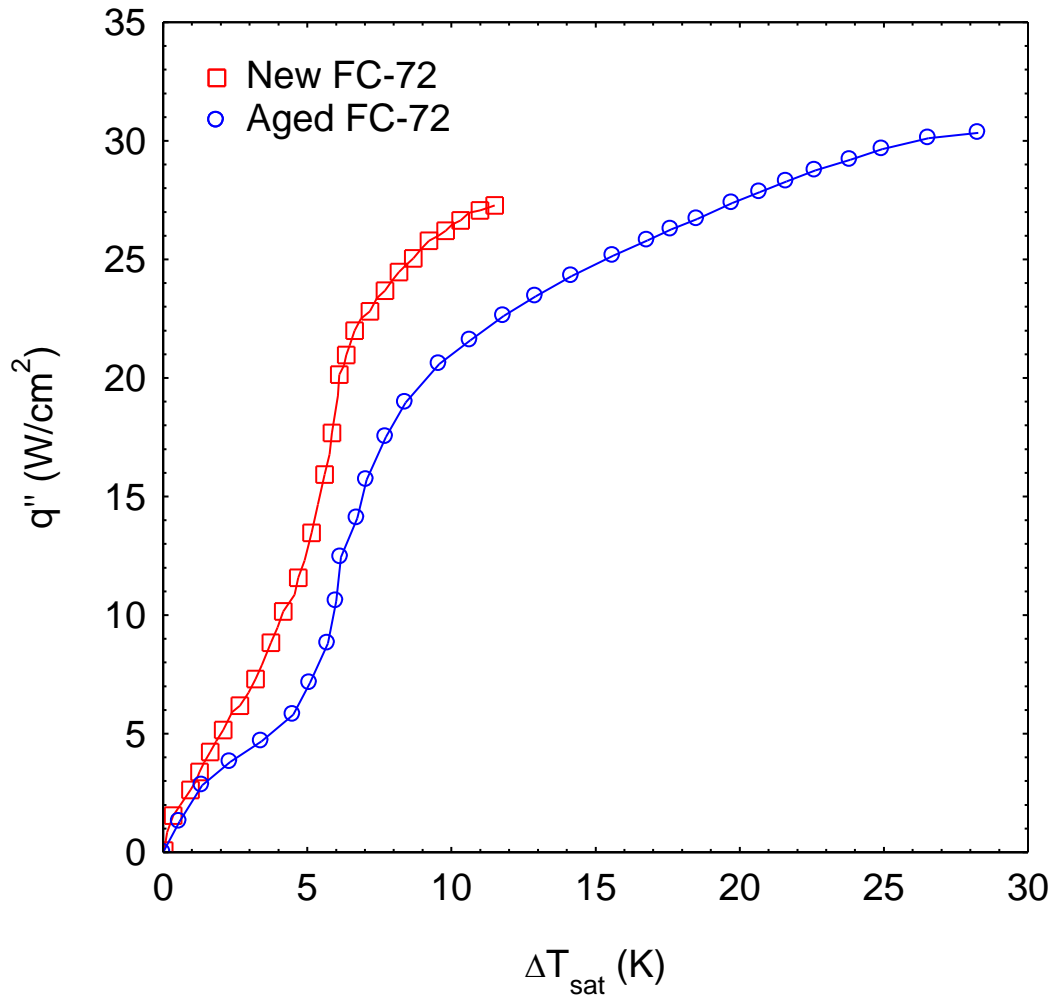


Figure 4.12 Effect of aging on pool boiling of FC-72 on porous graphite.

#### 4.4.4 Effect of Surface Orientation

As with liquid subcooling, the orientation of the boiling surface with respect to gravity also influences the pool boiling heat transfer. The effect of this parameter is systematically investigated. The results of the effect of surface inclination on nucleate boiling and CHF of dielectric liquids on porous graphite and plane copper are consistent with those previously published by other investigators with dielectric and non-dielectric liquids. Generally, increasing the surface inclination decreases the nucleate boiling heat flux at high surface superheat and decreases CHF. Conversely, at low surface superheats, the nucleate boiling heat flux increases slightly with increases surface inclination. The lowest CHF values are those for the downward facing inclination.

Figures 4.13a-d and 4.13e-h present the measured pool boiling curves for saturation and subcooled boiling of FC-72 and HFE-7100, respectively, on porous graphite at inclination angles of  $0^\circ$  (upward-facing),  $60^\circ$ ,  $90^\circ$ ,  $120^\circ$ ,  $150^\circ$ , and  $180^\circ$  (downward-facing). Excluding the  $180^\circ$  inclination, in saturation boiling of FC-72 when the surface superheats are  $< 6$  K and  $< 8$  K for HFE-7100, the nucleate boiling heat transfer rates are is generally larger for higher as the inclination angle increases, but decrease with increasing inclination at higher surface superheats. Consistent with previously reported data, CHF decreases as the surface inclination increases, and increases as liquid subcooling increases. In general, the surface superheat at CHF decreases slightly as surface inclination increases, however, due to the method of determining CHF there is a large scatter in the data of surface superheat at CHF. As stated earlier, CHF is higher for both saturation and subcooled boiling of HFE-7100 than for FC-72.

Nishikawa et al. (1984) have proposed two mechanisms for nucleate boiling heat removal from inclined and downward facing surfaces. The first is sensible heat transfer due to the mixing of the thermal boundary layer as the bubbles slide along the surface. The second is the latent heat of vaporization from the evaporating thin film between the sliding bubbles and the heated surface. Nishikawa et al. (1984) measured the thickness of the water film between a heated surface and an injected air bubble at different surface inclinations. The thinnest film ( $44 \mu\text{m}$ ) occurred at the highest inclination angle

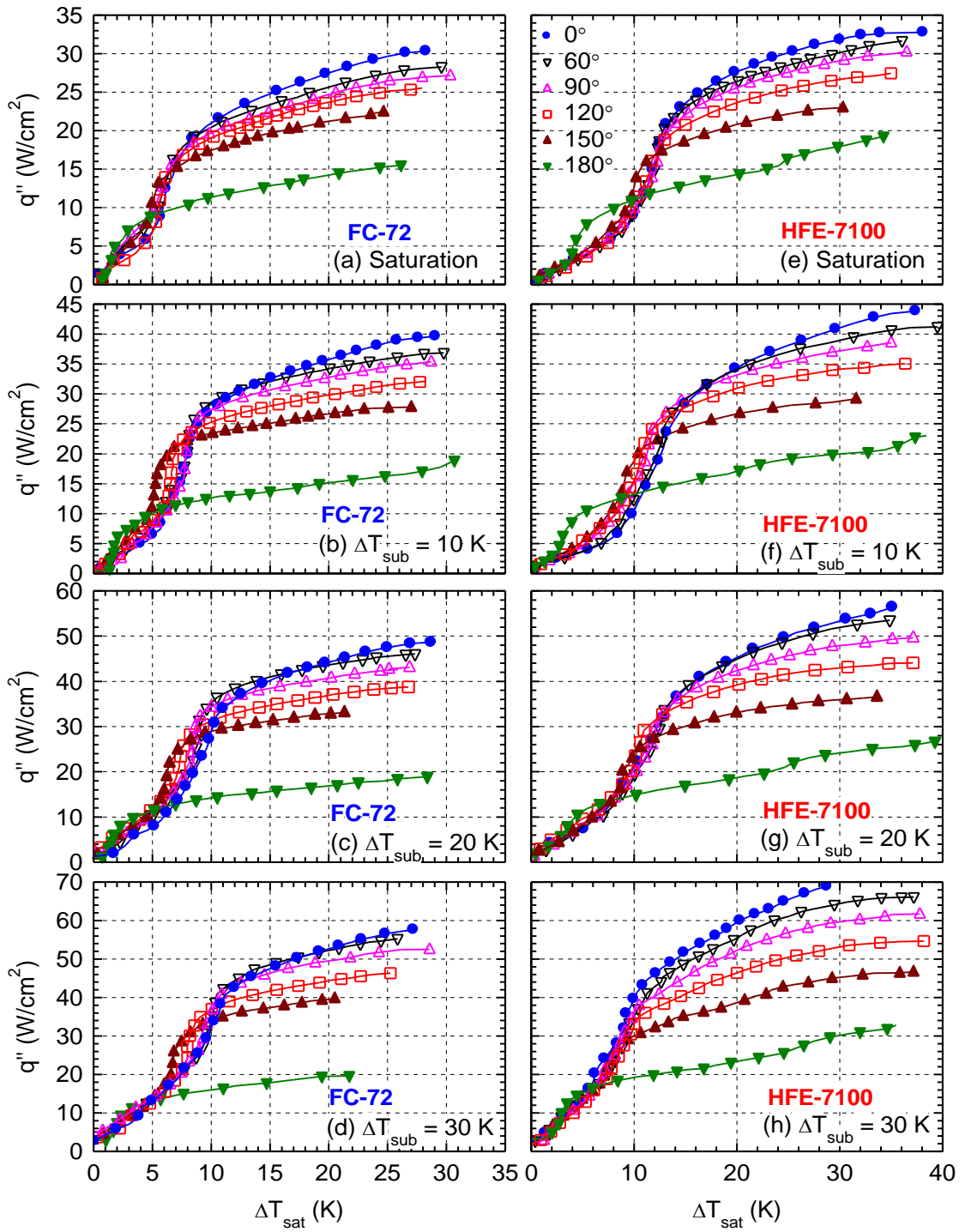


Figure 4.13 Effect of inclination angle on saturation and subcooled pool boiling of FC-72 on porous graphite.

considered ( $175^\circ$ ). As the inclination angle decreased, the measured film thickness between the sliding air bubble and the surface increased to  $78\ \mu\text{m}$  at  $165^\circ$ ,  $145\ \mu\text{m}$  at  $150^\circ$ , and  $401\ \mu\text{m}$  at  $120^\circ$ . They also measured a longer residence time of the bubbles near the surface at higher inclination angles. In experiments using PF-5060 dielectric liquid, Qiu and Dhir (2002) observed a decrease in the sliding bubble velocities as the surface inclination increased beyond  $120^\circ$ . Since the residence time of the bubbles is longer at higher inclinations and the liquid film is thinner, Nishikawa et al. (1984) concluded that the contribution to the heat transfer by thin film evaporation increases with increasing inclination.

To further quantify the enhancement of nucleate pool boiling of HFE-7100 and FC-72 on porous graphite in the present experiments, comparisons are made with the obtained results of these liquids on a smooth copper surface. Figure 4.14 compares the measured saturation pool boiling curves of FC-72 and HFE-7100 liquids on plane copper at inclination angles of  $0^\circ$ ,  $60^\circ$ ,  $90^\circ$ ,  $120^\circ$ ,  $150^\circ$ , and  $180^\circ$ . The plane copper surfaces show the same trend as the surface inclination increases—nucleate boiling heat transfer at low superheats increases with increased inclination, but decreases at higher superheats. CHF also decreases as the surface inclination increases (Figure 4.14).

The saturation pool boiling curves of FC-72 on plane copper and porous graphite at  $0^\circ$ ,  $60^\circ$ ,  $90^\circ$ ,  $120^\circ$ ,  $150^\circ$ , and  $180^\circ$  inclinations are compared in Figures 4.15a - 4.15f, respectively. The curves for HFE-7100 at the same inclination angles are compared in Figures 4.16a - 4.16f. CHF values of these dielectric liquids on porous graphite are higher than those measured on plane copper, with the largest difference the downward-facing orientation ( $180^\circ$ ). In this orientation, CHF of FC-72 on porous graphite is 6.4 times that on copper but lower at lower inclinations of  $150^\circ$ ,  $90^\circ$ , and  $0^\circ$  where it is  $\sim 4.14$ ,  $1.69$ , and  $1.67$  times that on copper, respectively. With HFE-7100, the differences in CHF with increasing surface inclination are slightly smaller. CHF for HFE-7100 in the downward facing orientation is 4.0 times larger on porous graphite than on copper. At inclinations of  $150^\circ$ ,  $90^\circ$ , and  $0^\circ$ , the CHF ratios decrease to  $1.62$ ,  $1.55$ , and  $1.45$ , respectively. The surface superheat at CHF on porous graphite is also higher than on

plane copper, particularly in the downward facing orientation (Figures 4.15f and 4.16f).

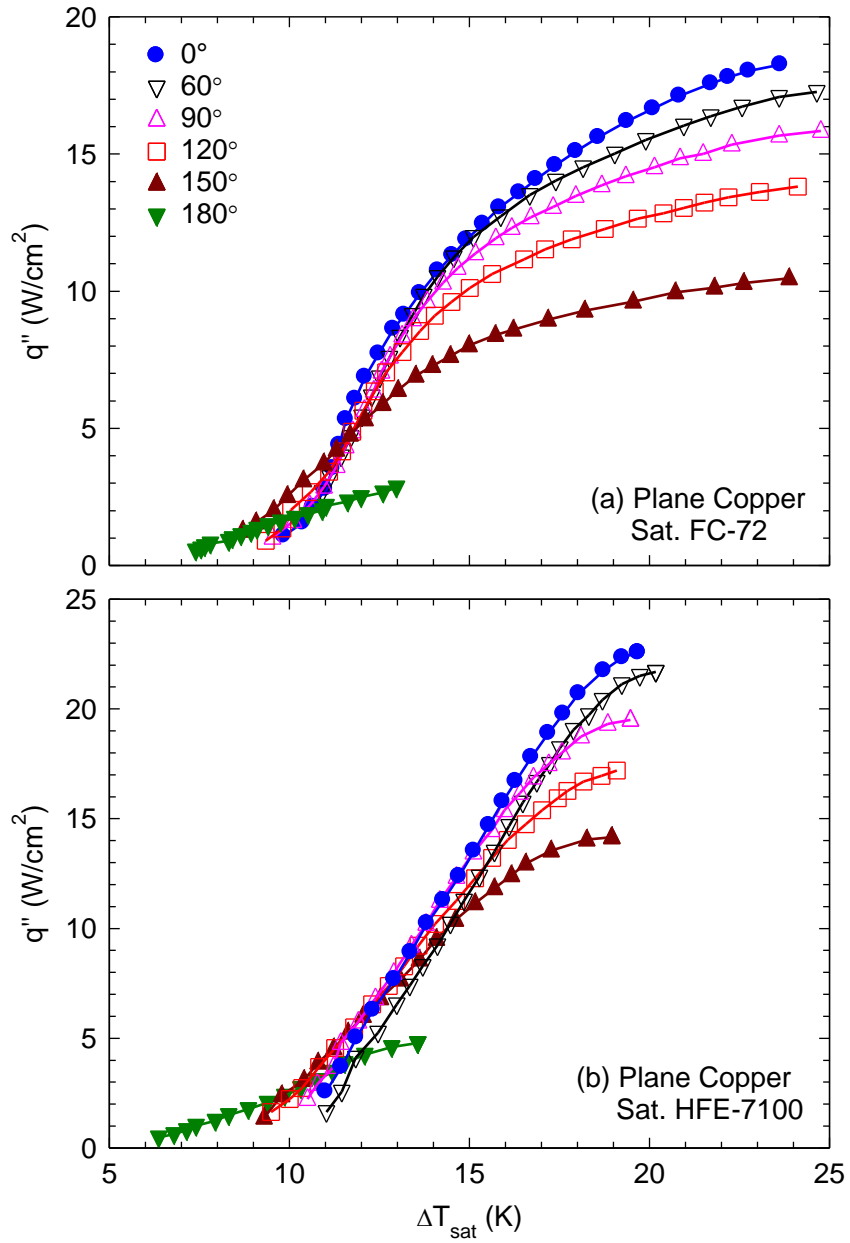


**Figure 4.14 Comparison of saturation pool boiling curves of FC-72 and HFE-7100 at different inclinations on smooth copper.**

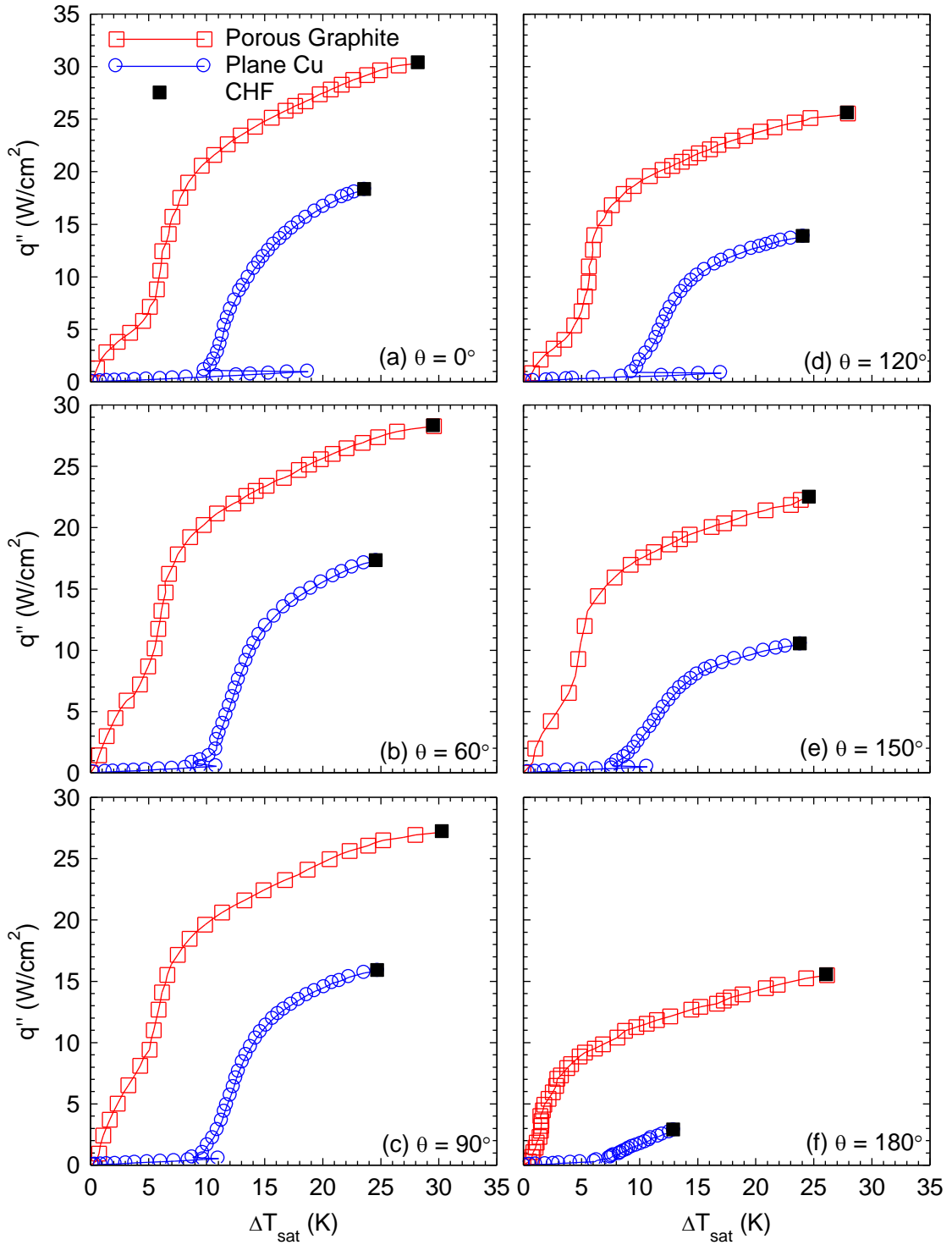
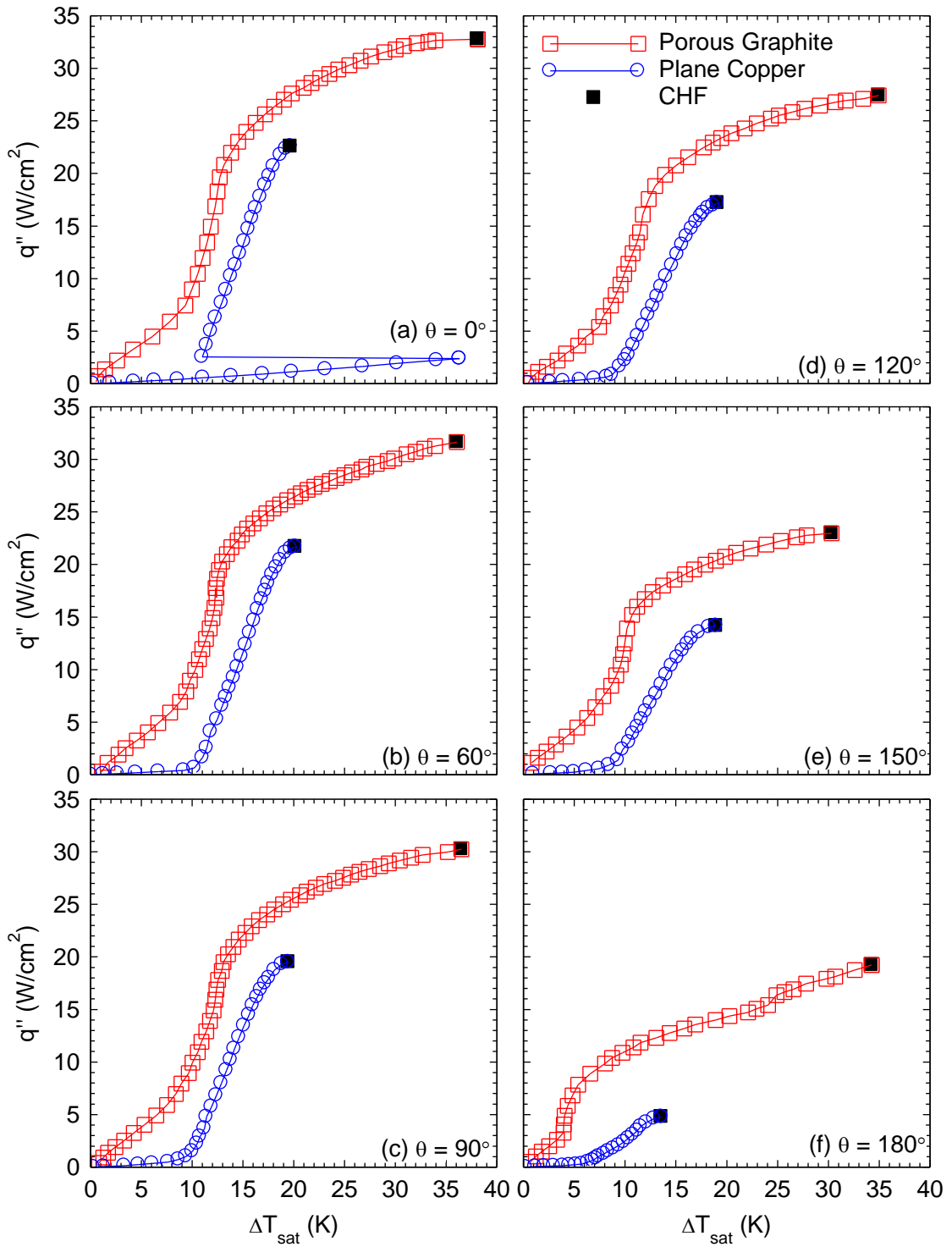


Figure 4.15 Saturation boiling curves of FC-71 and copper at different inclinations.



**Figure 4.16 Saturation boiling curves of HFE-7100 on porous graphite and copper at different inclinations.**

#### 4.4.5 Nucleate Boiling Heat Transfer Coefficient

The heat transfer coefficient is obtained from the measured pool boiling curves by dividing the nucleate boiling heat flux by the corresponding  $\Delta T_b$ , the difference between the measured surface temperature,  $T_w$ , and that of the liquid pool near the heated surface,  $T_b$ , in the experiments. Figures 4.17a and 4.17b plot the saturation nucleate boiling heat transfer coefficient,  $h$ , of FC-72 versus surface superheat at different orientations of the porous graphite and the plane copper surface, respectively. At the same surface superheats, the values of  $h$  of FC-72 and HFE-7100 on porous graphite are typically 1.5 – 3 times those on plane copper (Figures 4.15 – 4.17). On both porous graphite and plane copper, the saturation nucleate boiling heat flux and nucleate boiling heat transfer coefficient at higher surface superheats decrease with increased surface inclination. On both plane copper and porous graphite,  $h$  increases with increased surface superheat reaching a maximum then decreases with further increase in the surface superheat (Figures 4.17a and 4.17c). Such dependence of  $h$  on surface superheat is also true on copper, but the rate of change in its value with decreasing wall superheat is much milder than on porous graphite (Figures 4.17b and 4.17d).

As delineated in Figures 4.17 – 4.17, at the same surface superheat the saturation nucleate boiling heat flux of the dielectric liquids on porous graphite is higher than on copper, which explains the significantly higher nucleate boiling heat transfer coefficient on porous graphite. In the upward facing orientation ( $\theta = 0^\circ$ ), the maximum  $h$  of FC-72 on porous graphite is  $\sim 2.25 \text{ W/cm}^2 \text{ K}$  and occurs at a surface superheat of 8 K, compared to only  $0.85 \text{ W/cm}^2 \text{ K}$  and 18 K on copper, respectively. Similarly, in the downward facing orientation ( $\theta = 180^\circ$ ), the maximum  $h$  of FC-72 on porous graphite is  $2.75 \text{ W/cm}^2 \text{ K}$  and the corresponding wall superheat is only 1.5 K, compared to only  $0.19 \text{ W/cm}^2 \text{ K}$  and as much as 13 K on copper (Figures 4.17a and 4.17b). For HFE-7100, the respective values of  $h$  and  $\Delta T_{sat}$  in the upward facing orientation are  $\sim 1.6 \text{ W/cm}^2 \text{ K}$  at 14 K on porous graphite and  $1.16 \text{ W/cm}^2 \text{ K}$  at 19 K on plane copper. In the downward facing orientation, the maximum  $h$  on porous graphite of  $1.45 \text{ W/cm}^2 \text{ K}$  occurs at 5.4 K superheat and on plane copper it is  $0.35 \text{ W/cm}^2 \text{ K}$  and occurs at 13.6 K superheat. The high values of the maximum  $h$  on porous graphite reflects the higher nucleate boiling heat

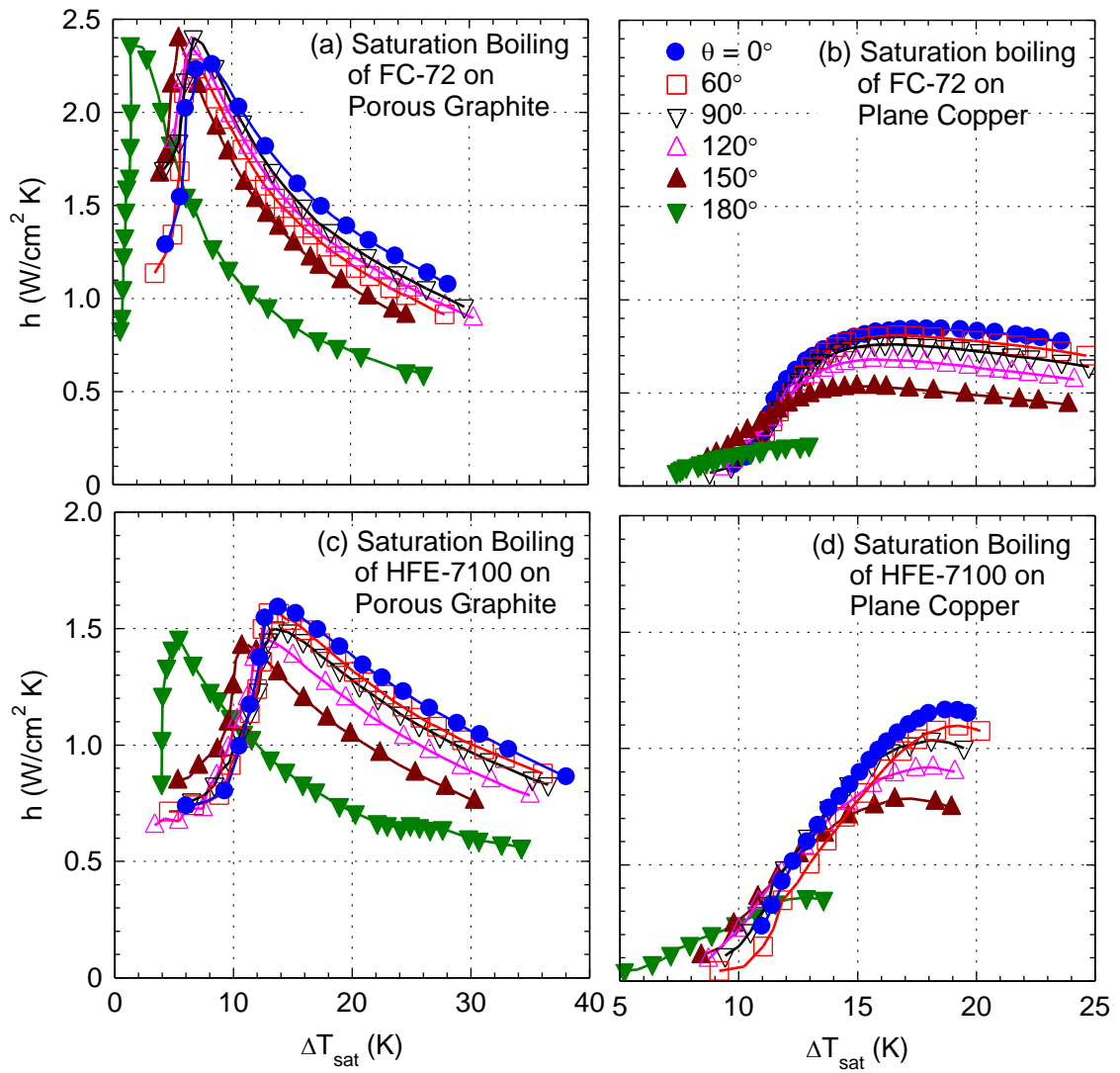


Figure 4.17 Saturation nucleate boiling heat transfer coefficient for FC-72 and HFE-7100 on porous graphite and plane copper.

flux and the smaller surface superheats, compared to plane copper where the nucleate boiling heat fluxes are much lower and the corresponding surface superheats are higher. For electronic cooling applications, operating at the maximum nucleate boiling heat transfer coefficient not only enhances the cooling processes but also decreases the junctions' temperature of the chips.

Figure 4.18 plots the ratios of the measured saturation nucleate boiling heat transfer coefficients of FC-72 on porous graphite to that on plane copper versus the surface superheat for the different inclination angles investigated in this work. Except for the 180° inclination, the ratio of the saturation nucleate boiling heat transfer coefficients decreases with increased inclination angle when the surface superheats is  $< \sim 12$  K, but increases with increased inclination angle at higher surface superheats. When  $\Delta T_{\text{sat}} < 12$  K, the ratio of the saturation nucleate boiling heat transfer coefficient on porous graphite to that on copper is in excess of  $\sim 3.5$  and as much as 20-24 at lower surface superheats, with the highest values being those for 0° inclination (upward-facing). Conversely, when  $\Delta T_{\text{sat}} > 12$  K, the ratios of the saturation nucleate boiling heat transfer coefficients increase with increased inclination angle, with the lowest values being those at 0° inclination. They approach  $\sim 1.67$  at 24 K surface superheat, which is near CHF. In the downward-facing orientation (180° inclination), the ratio of the saturation nucleate boiling heat transfer coefficients decreases from as much as 20 at  $\Delta T_{\text{sat}} = 7$  K to  $\sim 4.0$  at surface superheat of  $\sim 13$  K, which is close to that at CHF.

#### 4.4.6 Boiling Resistance

The boiling resistance,  $r_B$ , equals the rise in the surface temperature,  $T_w$ , relative to that of the boiling liquid in the pool above the surface,  $T_b$ , divided by the total thermal power removed from surface,  $P$ . In another word, it is a measure of the temperature budget for cooling by nucleate boiling of the dielectric liquids per unit thermal power dissipated by the underlying chip and removed by the boiling liquid. This resistance is expressed as:

$$r_B = \Delta T_b / P. \quad (4.2)$$

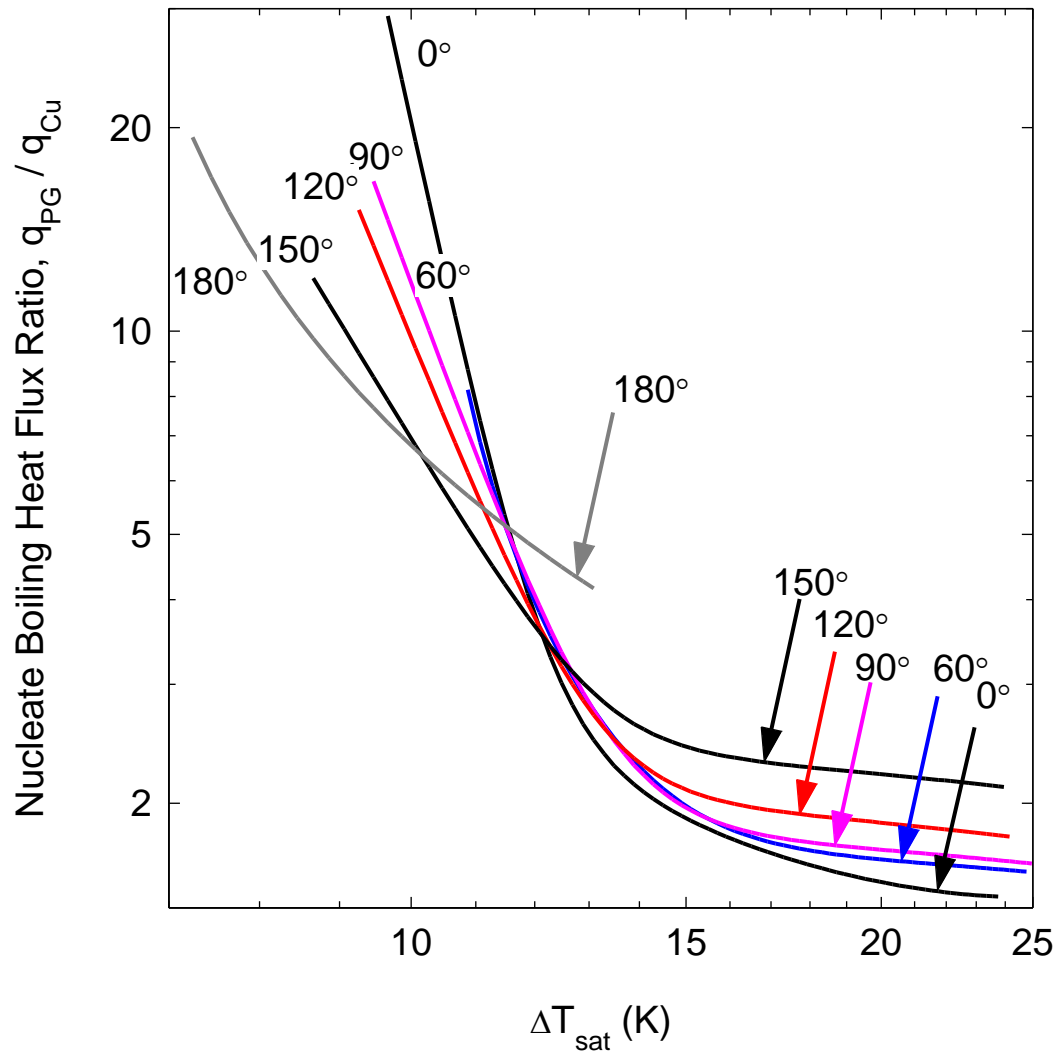


Figure 4.18 Ratios of saturation FC-72 nucleate boiling heat transfer coefficient on porous graphite and plane copper.

Figures 4.19a – 4.19d present the obtained curves of the boiling resistance for FC-72 and Figures 4.19e – 4.19h for HFE-7100 liquid on porous graphite. The lowest resistances are those of saturation boiling of FC-72 and HFE-7100 (Figures 4.19a and 4.19e). The boiling resistance decreases with increased surface superheat,  $\Delta T_{sat}$ , to a minimum and then increases with further increase in surface superheat. The minimum values in these figures of  $\sim 0.4$  K/W and  $\sim 0.6$  K/W for FC-72 and HFE-7100, respectively, correspond to the maximum nucleate boiling heat transfer coefficient (Figures 4.17a – 4.17b).

At low surface superheats, the boiling resistances decrease with decreased surface inclination, but increase with increased inclination at high surface superheats. Figures 4.19a – 4.19h also show that increasing liquid subcooling increases the boiling resistances at all surface inclinations. At surface superheats  $\Delta T_{sat} > 10 - 12$  K, the lowest total boiling resistances are those in the upward facing orientation ( $\theta = 0^\circ$ ). It is important to note that since computer chips will be overlaid by a heat spreader made of high thermal conductivity materials and cooled with nucleate boiling, the actual total thermal resistances to the spreader surface would be much smaller than indicated in Figures 4.19a – 4.19h (El-Genk, Saber, and Parker, 2005, 2007; El-Genk and Saber, 2006).

#### **4.5 Critical Heat Flux Correlation**

The previous sections discussed the enhancements in natural convection and nucleate boiling heat transfer of FC-72 and HFE-7100 dielectric liquids on porous graphite and plane copper surfaces. This section focuses on the Critical Heat Flux (CHF), which is the maximum heat flux dissipated by nucleate boiling. Although CHF corresponds to a lower nucleate boiling heat transfer coefficient than the peak value, which occurs at the end of the fully developed nucleate boiling region, knowledge of the CHF values is important to identify the upper limits of safe operation. Saturation CHF values on a plane surface at  $\theta = 0^\circ$  can be predicted using the form suggested by both Kutateladze (1952) and Zuber (1959), as previously noted in Equation 2.6 and repeated here:

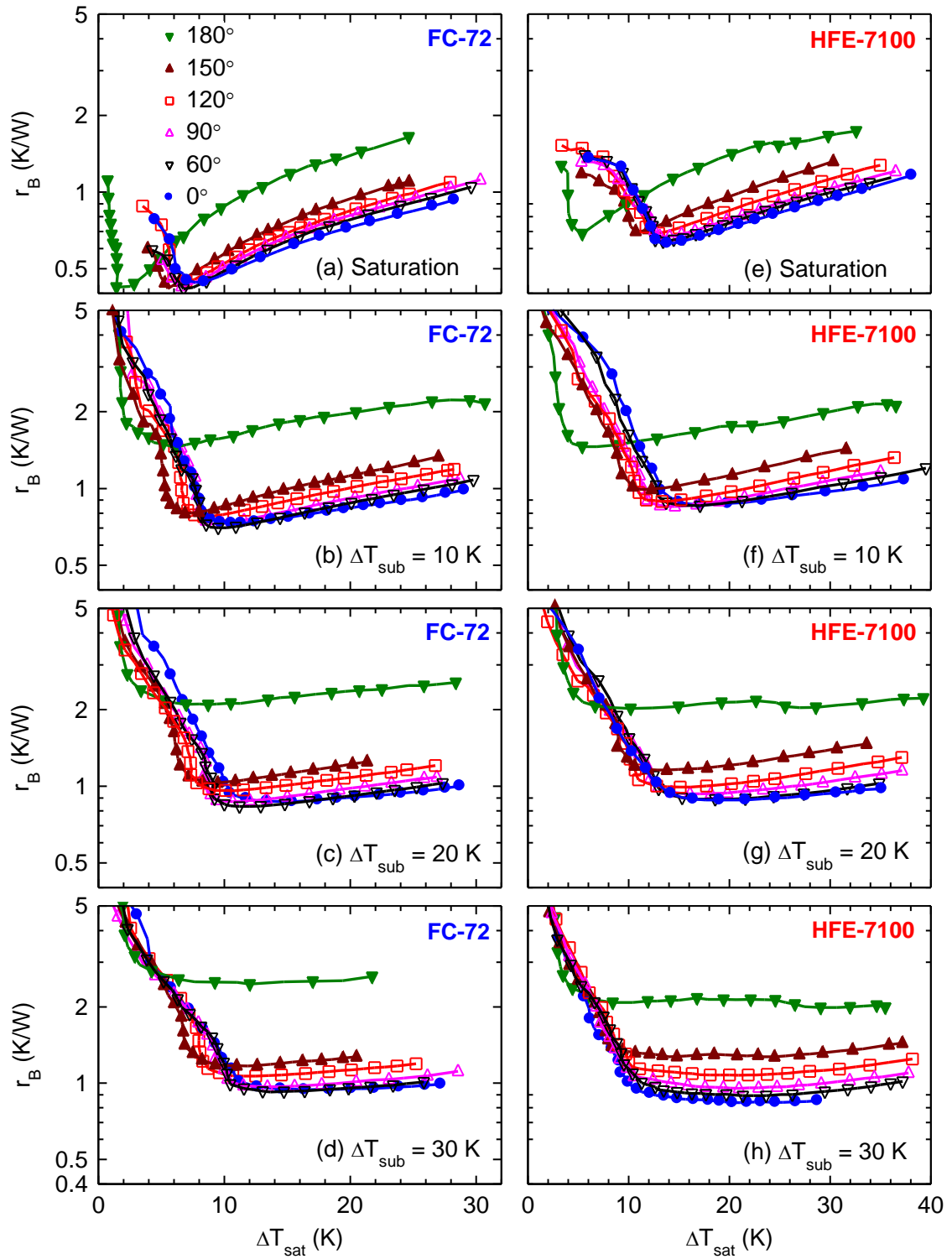


Figure 4.19 Boiling resistance for saturated and subcooled FC-72 and HFE-7100 on porous graphite at different inclination angles.

$$CHF_{sat} = C_{CHF} \rho_v^{0.5} h_{fg} [\sigma g (\rho_l - \rho_v)]^{0.25} \quad (4.3)$$

The liquid and vapor properties, ( $h_{fg}$ ,  $\sigma$ ,  $\rho_l$ ,  $\rho_v$ ) in this correlation are evaluated at the saturation temperature. The critical heat flux coefficient,  $C_{CHF}$ , however, is a function of the type and nature of surface, the surface orientation,  $\theta$ , and the liquid subcooling,  $\Delta T_{sub}$ . Thus, the coefficient  $C_{CHF}$  may be expressed as a multiplication of three terms as

$$C_{CHF}(\theta, \Delta T_{sub}) = C_{CHF,sat}(0^\circ) R(\theta) F_{sub}(\theta, \Delta T_{sub}) \quad (4.4)$$

In this equation, the first term on the right hand side,  $C_{CHF,sat}(0^\circ)$  is the CHF coefficient for saturation boiling at  $0^\circ$ . The second term,  $R(\theta)$ , represents the relative effect of surface orientation,  $\theta$ , on the saturation CHF values. The third term,  $F_{sub}(\theta, \Delta T_{sub})$ , represents the effect of liquid subcooling on CHF at different surface orientations. These terms are determined empirically based on the present CHF values and those reported by other investigators for HFE-7100 and FC-72 on various surfaces.

#### 4.5.1 Effect of Surface Characteristics and Liquid Properties on CHF

The values of  $C_{CHF,sat}(0^\circ)$  determined for FC-72 liquid on porous graphite and plane copper are presented in Figure 4.20a. As shown in this figure, the best fit of the present values of  $C_{CHF,sat}(0^\circ)$  on copper is 0.166, which agrees with those obtained from the reported CHF data by other investigators on plane copper and silicon (Rainey and You, 2000; Rainey, You, and Lee, 2003; Honda, Takamatsu, and Wei, 2002; Z. W. Liu et al, 2001; O'Connor, 1994; McNiel, 1992; Priarone, 2005; Howard, 1999) to within + 6% and -10%. Similarly, the best fit of the present values of  $C_{CHF,sat}$  for FC-72 on porous graphite is 0.263. This value is 58% higher than that on plane surfaces (0.166) and within + 5% and -7% of the obtained values from the reported CHF data by other investigators for FC-72 on micro-porous coatings (Rainey and You, 2000; Rainey, You, and Lee, 2003; Chang and You, 1997; O'Connor, 1994) and micro-finned silicon surfaces (Wei and Honda, 2003). The data in Figure 4.20a also indicate that the surface superheats at CHF on smooth surfaces vary from 12 K to 35 K, while that on porous,

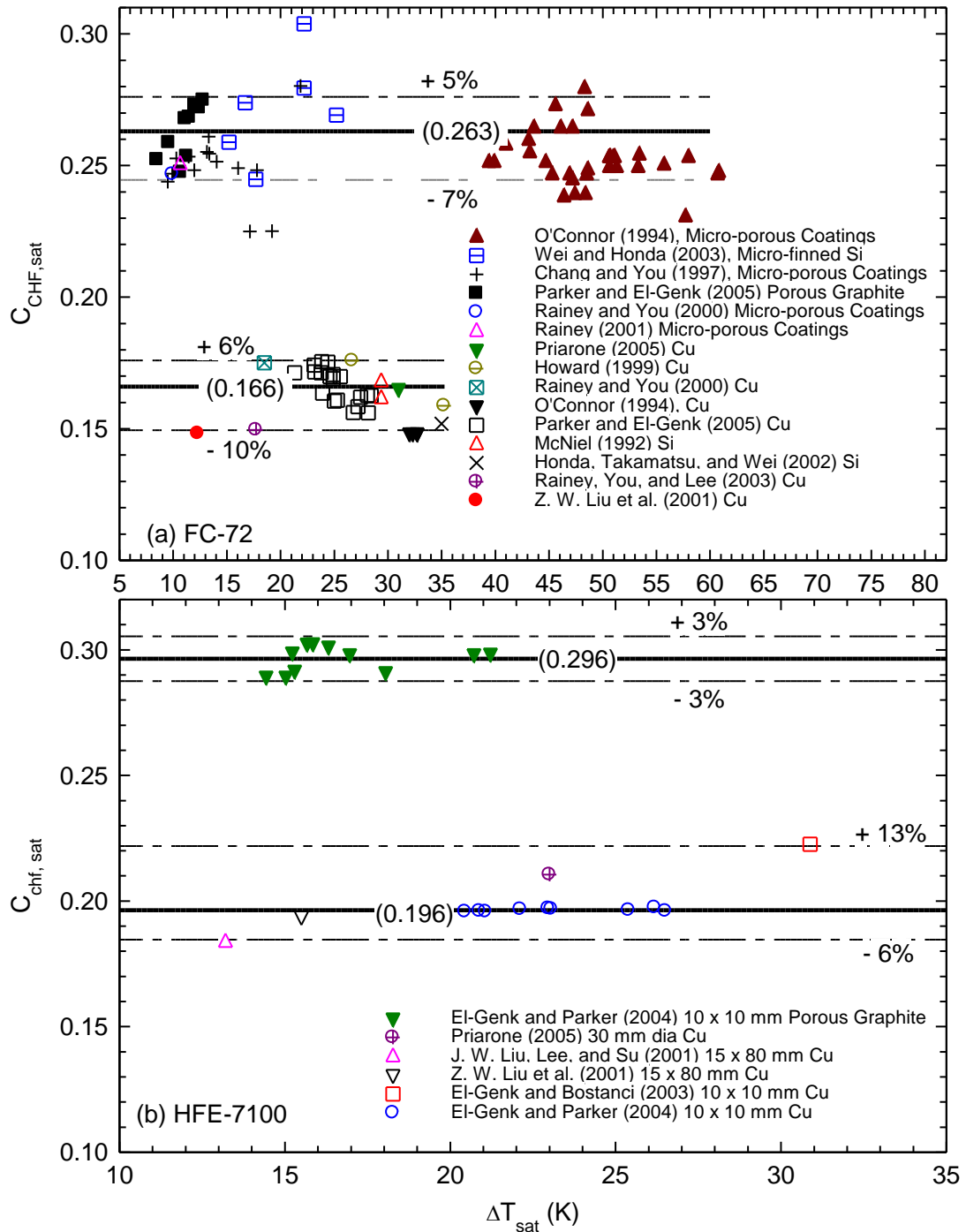


Figure 4.20 Saturation CHF coefficients for FC-72 and HFE-7100 of different surfaces.

micro-finned, and micro-porous surfaces vary from as little as 8 K to as much as 63 K. The highest surface superheats at CHF are those of O'Connor (1994) on micro-porous coatings (39 to 61 K), which may be attributed to a potential contamination of the FC-72 liquid in the experiments with plasticizers, which have the effect of producing a “tail effect” near CHF (Chang, 1997).

Figure 4.20b presents the data obtained for saturation boiling of HFE-7100 in this research on plane copper and porous graphite. The value of  $C_{CHF,sat}(0^\circ)$  is 0.196 for HFE-7100 boiling on copper (Parker and El-Genk, 2005b; El-Genk and Parker, 2004; Z. W. Liu et al., 2001; Z. W. Liu et al., 2001 El-Genk and Bostanci, 2003a; Priarone, 2005), and is 18% larger than for FC-72. Similarly, the value for HFE-7100 boiling on porous graphite is 0.296, which is 13% higher than the average values obtained for FC-72 boiling on porous graphite, micro-porous coatings, and micro-finned silicon ( $C_{CHF,sat}(0^\circ) = 0.263$ ). For HFE-7100,  $C_{CHF,sat}$  on porous graphite is 67% larger than for plane copper. As seen in Figure 4.20a and 4.20b, using a porous graphite or other enhanced boiling surfaces increases the critical heat flux over the CHF obtained on plane surfaces. These results confirm that the properties of the boiling liquid as well as the characteristics of the heated surface strongly affects saturation CHF in pool boiling.

#### **4.5.2 Effect of Surface Orientation on CHF**

In Figures 4.21a and 4.21b, the saturation CHF values for HFE-7100 and FC-72 versus inclination angle on porous graphite are shown with those reported on copper (Reed and Mudawar, 1997; Howard and Mudawar, 1999; Mudawar Howard, and Gersey, 1997; Chang and You, 1996; Rainey and You, 2001; Priarone, 2005; Parker and El-Genk, 2005a; El-Genk and Bostanci, 2003a) and with the CHF values of micro-porous coatings in saturated FC-72 (Chang and You, 1996). Note that the data presented in Figures 4.21a and 4.21b are for 10 mm x 10 mm, 12.7 mm x 12.7 mm plane surfaces, and circular surfaces 30 mm in diameter. The highest saturation CHF values for HFE-7100 and FC-72 are those measured in the present work on porous graphite, followed by those reported on micro-porous coatings, then on copper. For example, in the upward-facing orientation (or  $0^\circ$  inclination), the saturation CHF of FC-72 on porous graphite ( $30 \text{ W/cm}^2$ ) is  $\sim 12 \%$

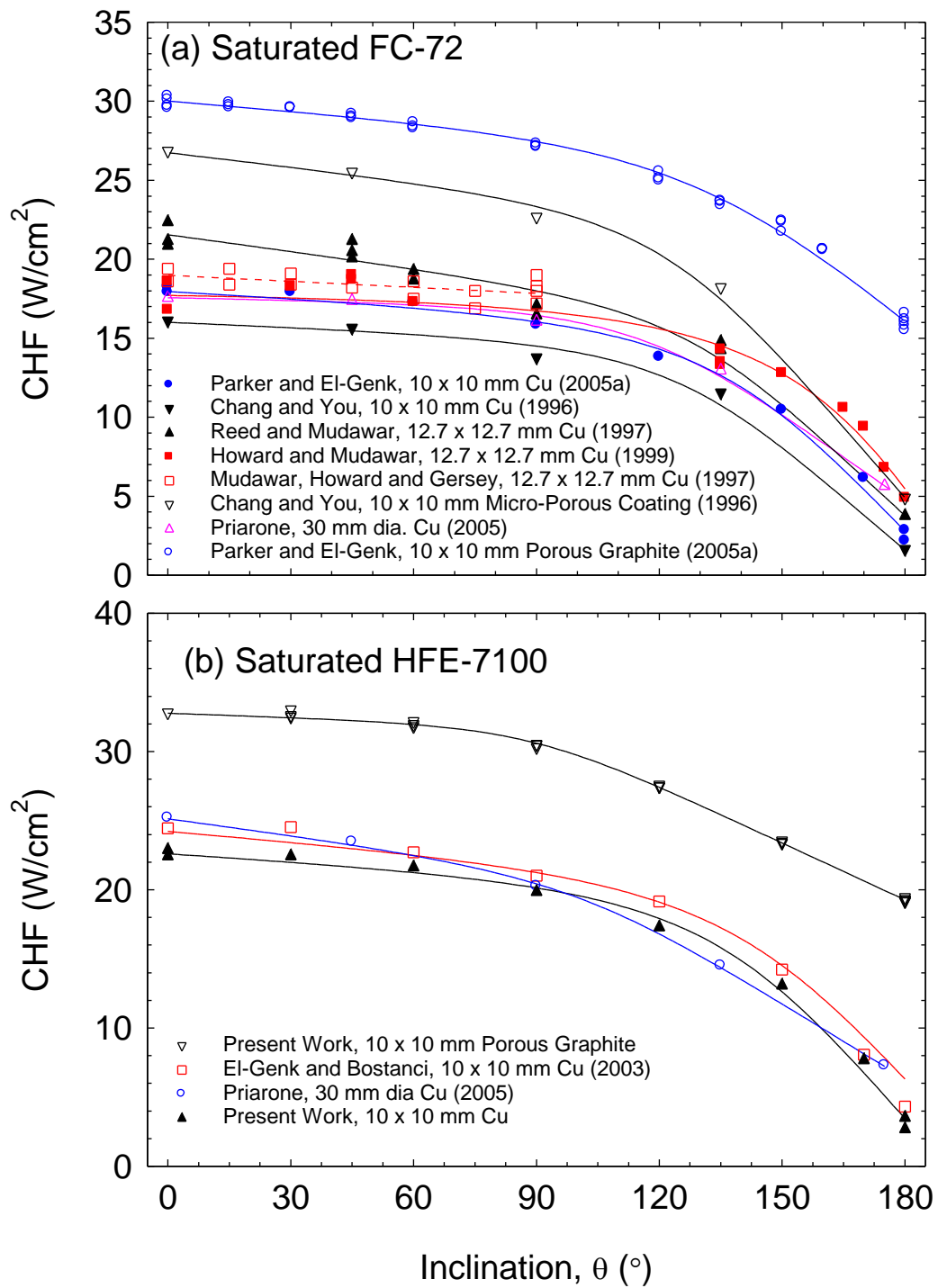


Figure 4.21 Effect of surface inclination on saturation CHF of FC-72 and HFE-7100 on different surfaces.

higher than that reported by Chang and You (1996) on micro-porous coatings ( $26.8 \text{ W/cm}^2$ ), and  $\sim 57\%$  higher than the average values on plane copper ( $\sim 19.1 \text{ W/cm}^2$ ). The FC-72 CHF values in the present work on plane copper and those reported by other of investigators on similar surfaces range from  $16.1 \text{ W/cm}^2$  to  $22.4 \text{ W/cm}^2$  (Chang and You 1996; Mudawar, Howard, and Gersey 1997; Reed and Mudawar 1997; Howard and Mudawar 1999; Priarone, 2005).

As delineated in Figure 4.21a, there is a relatively large scattering in the reported values of saturation CHF of FC-72 on plane copper by the different investigators at the various surface orientations, including  $180^\circ$  (downward-facing). The reported CHF values on plane copper for this inclination varied from  $1.6 \text{ W/cm}^2$  (Chang and You 1996) to as much as  $4.9 \text{ W/cm}^2$  (Howard and Mudawar 1999); the value measured in the present work is  $\sim 2.5 \text{ W/cm}^2$ . Such variations are indicative of the sensitivity of the measured CHF to the adjustment of the surface in the downward-facing position.

In general, CHF decreases slowly with increased surface inclination up to  $90^\circ$  and then decreases much faster with increased inclination angle beyond  $90^\circ$  to its lowest value at  $180^\circ$ . Figures 4.21a and 4.21b show that the rate of decrease in saturation CHF for FC-72 with inclination angle up to  $90^\circ$  is very similar to that on porous graphite, micro-porous coatings, and plane copper. Beyond  $90^\circ$  inclination, however, the rate of decrease in the measured CHF for saturation boiling on porous graphite with increased inclination in the present work is much smaller than those reported on micro-porous coatings, but the CHF values on the former are consistently higher (El-Genk and Parker 2004a,b, 2008; Parker and El-Genk 2005). When the inclination angle is  $> 150^\circ$ , the saturation boiling CHF values of FC-72 on porous graphite are at the upper range of those measured in the present work and reported by other investigators on plane copper. For example, the measured CHF on porous graphite in the  $180^\circ$  orientation (downward-facing) of  $16 \text{ W/cm}^2$  is  $\sim 53\%$  of that measured in the upward-facing orientation ( $0^\circ$ ), while that reported on micro-porous coatings of  $4.9 \text{ W/cm}^2$  is only  $18\%$  of that reported for the upward-facing orientation (Chang and You, 1996).

The values of CHF are plotted in Figure 4.22 versus  $\theta$  at the different values of liquid subcooling. They show that the CHF values of HFE-7100 on porous graphite are 5-15% higher than those for FC-72. These results are consistent with those reported in the open literature, which reported that CHF values of HFE-7100 are higher than those for FC-72 (El-Genk and Bostanci, 2003a; Arik and Bar-Cohen, 2001; Parker and El-Genk, 2005b; Priarone, 2005). For saturation and subcooled boiling of the dielectric liquids, CHF decreases slowly with increasing inclination angle up to  $90^\circ$ , then beyond  $90^\circ$  the CHF decreases rapidly to its lowest value at  $180^\circ$ .

Empirical correlations have been published that describe the effect of surface inclination on CHF for FC-72 and HFE-7100 dielectric liquids (Chang and You, 1996; El-Genk and Bostanci, 2003a; Priarone, 2005). The correlations are based on CHF data in saturation boiling of FC-72 on plane copper (Priarone, 2005; Chang and You, 1996) and micro-porous coatings (Chang and You, 1996) and saturation boiling of HFE-7100 on copper (El-Genk and Bostanci, 2003a, Priarone, 2005). These published correlations are as follows:

***Chang and You (1996):***

$$R(\theta) = [1 - 0.0012 \theta \tan(0.414 \theta) - 0.122 \sin(0.318 \theta)] \quad (4.5a)$$

***El-Genk and Bostanci (2003):***

$$R(\theta) = \left[ (1 - 0.00127 \theta)^{-4} + (3.03 - 0.016 \theta)^{-4} \right]^{-0.25} \quad (4.5b)$$

***Priarone (2005) ( $0^\circ \leq \theta \leq 175^\circ$ )***

$$R(\theta) = 1 - 0.001117\theta + 7.79401 \times 10^{-6} \theta^2 - 1.37678 \times 10^{-7} \theta^3 \quad (4.5c)$$

As seen in Figure 4.23a, the correlations given by Equations 4.5a, 4.5b, and 4.5c fit the reported and present saturation CHF data for FC-72 and HFE-7100 on plane copper to within + 20% and - 10%. These correlations also fit the reported saturation FC-72 CHF

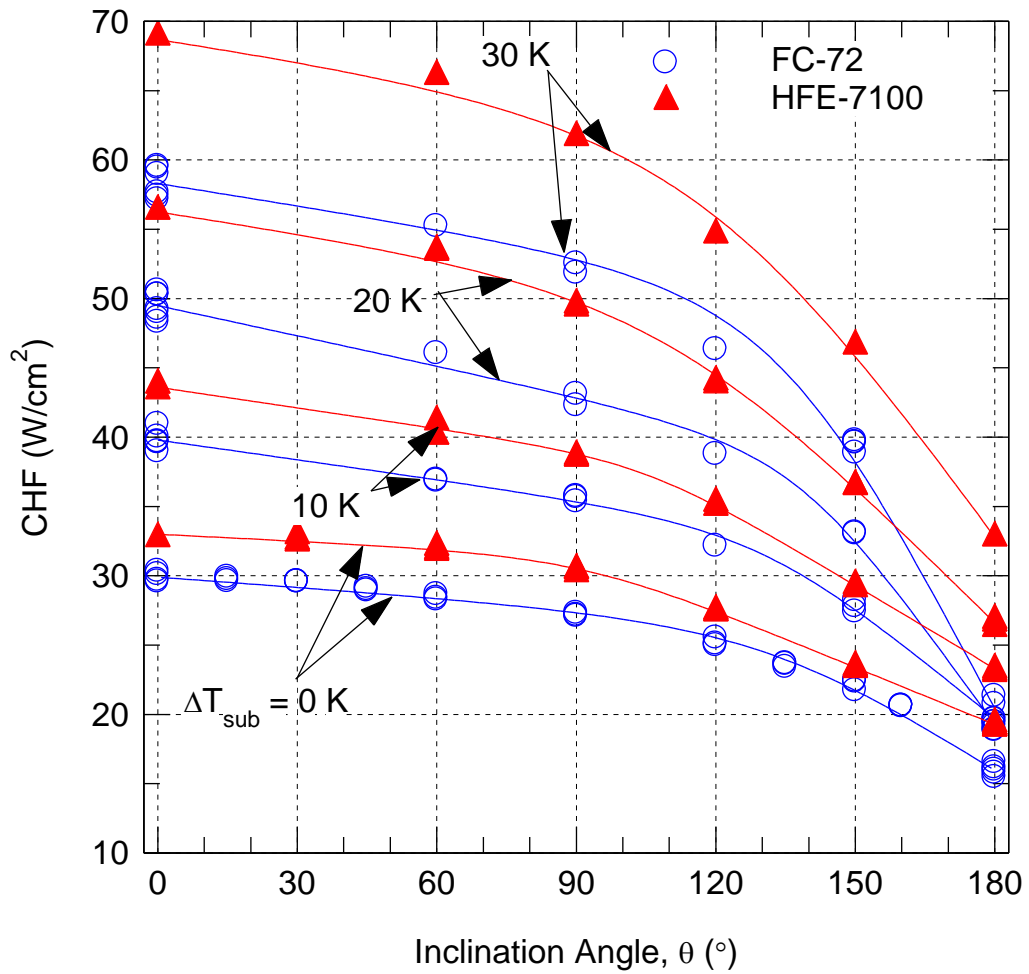


Figure 4.22 Effect of inclination on and liquid subcooling on CHF of FC-72 and HFE-7100 boiling on porous graphite.

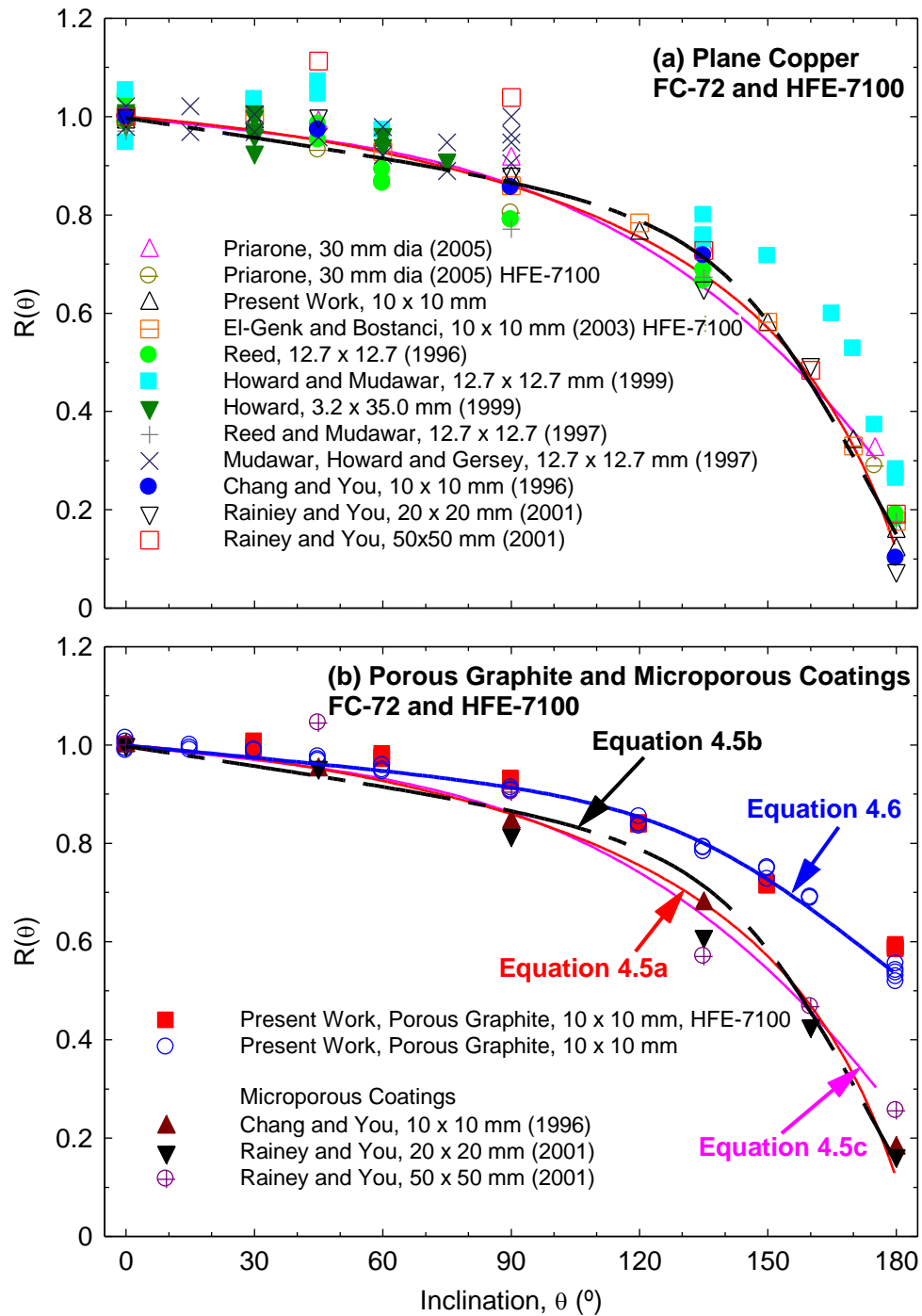


Figure 4.23 Relative decrease in saturation CHF of dielectric liquids on plane copper, micro-porous coatings, and porous graphite.

data on micro-porous coatings by Chang and You (1996) and Rainey and You (2001) to within + 10% and -15%.

For the present saturation CHF values of FC-72 and HFE-7100 on porous graphite, the following relationship for  $R(\theta)$  is obtained from the least square fit of the data shown in Figure 4.23b as:

$$R(\theta) = \left[ (1 - 0.000796\theta)^{-4} + (1.8 - 0.00703\theta)^{-4} \right]^{-0.25} \quad (4.6)$$

Equation 4.6 fits the present CHF data on porous graphite to within  $\pm 5\%$  for an inclination of  $180^\circ$  and to within +3% to -2%, otherwise (Figure 4.23b). Figures 4.23a and 4.23b compare Equations 4.5a, 4.5b, 4.5c, and 4.6 for  $R(\theta)$  and clearly shows that the values of  $R(\theta)$  on porous graphite are significantly higher than those on either plane copper or micro-porous coatings, particularly at higher inclinations. As stated earlier and delineated in Figures 4.23a and 4.23 b,  $R(180^\circ)$  for FC-72 on porous graphite is 0.54 versus only 0.15 on plane copper and on micro-porous coatings. Similarly, at lower inclinations of  $150^\circ$  and  $90^\circ$ ,  $R(\theta)$  on porous graphite is  $\sim 0.73$  and  $\sim 0.9$  versus  $\sim 0.56$  and 0.84 on either plane copper or micro-porous coatings, respectively.

It should be noted, however, that although  $R(\theta)$  for dielectric liquids on plane copper (El-Genk and Bostanci, 2003a; Priarone, 2005; Chang and You, 1996) and micro-porous coatings (Chang and You, 1996) are similar, the actual CHF values on the latter are significantly higher than on the former. To illustrate this difference, the reported values of the saturation CHF for FC-72 on micro-porous coatings (Chang and You, 1996; Rainey and You, 2001) and the present measurements on porous graphite are divided by those measured in the present work for the same dielectric liquids on plane copper. The normalized values are plotted in Figure 4.24 versus the inclination angle of the surface. This figure indicates that saturation CHF of FC-72 on porous graphite is  $\sim 1.65$  times that on plane copper. It remains constant up to  $60^\circ$ , then increases precipitously with further increase in inclination angle to its highest value of  $\sim 6.4$  times that on copper in the downward-facing orientation ( $180^\circ$ ).

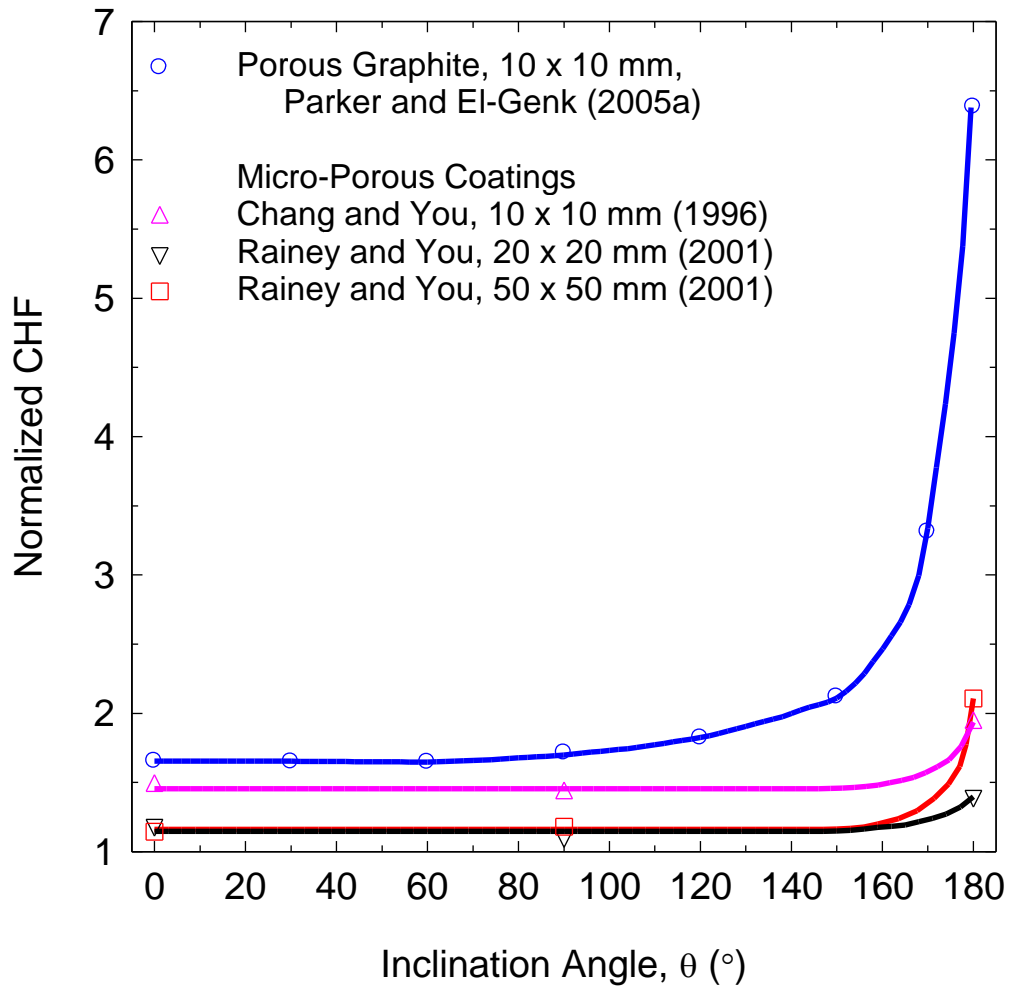


Figure 4.24 Ratios of saturation CHF of FC-72 on porous graphite and micro-porous coatings to that measured on copper.

For 20 x 20 mm and 50 x 50 mm surfaces, the normalized CHF values on micro-porous coatings (Rainey and You 2001) are identical and constant, ~15% higher than those measured on plane copper in the present work up to an inclination of 150°. They increase rapidly to ~ 40% to 210% higher than those on plane copper at 180°. The reported CHF values by Chang and You (1996) on micro-porous coatings (10 x 10 mm) behave similarly, but are much higher than those reported by Rainey and You (2001) on 20 x 20 and 50 x 50 mm surfaces. No comparable data are available for boiling of HFE-7100 on micro-porous coatings.

### 4.5.3 Effect of Liquid Subcooling

Increasing the liquid subcooling linearly increases CHF. The values of the critical heat flux in subcooled boiling,  $CHF_{sub}$ , are correlated in terms of  $CHF_{sat}$  (Equation 4.3) and  $\Delta T_{sub}$  using the linear relationship given below in Equation 4.7. This relationship has been used successfully by many investigators for dielectric and non-dielectric liquids (Ivey and Morris, 1966, El-Genk and Bostanci, 2003b; Rainey, You, and Lee, 2003; Watwe, Bar-Cohen, and McNiel, 1997; McNiel, 1992):

$$CHF_{sub} = CHF_{sat} (1 + C_{CHF,sub} \Delta T_{sub}) \quad (4.7)$$

The subcooling coefficient,  $C_{CHF,sub}$ , in Equation 4.7 is obtained from the least squares fit of the CHF values at various liquid subcoolings. As with the coefficient  $C_{CHF,sat}$ , the value of  $C_{CHF,sub}$  also depends on the characteristics of the surface as well as the thermophysical properties of the boiling liquid (El-Genk and Bostanci, 2003b; Ivey and Morris, 1966). For FC-72 on porous graphite,  $C_{CHF,sub} = 0.041$  and Equation 4.7 fits the data to within + 5% and - 4% (Figure 4.25a). The ratio of CHF values reported by a number of investigators for both gassed and degassed FC-72 liquid on etched silicon, Cu, and etched SiO<sub>2</sub> surfaces (O'Connor, You, and Chang, 1996; Honda, Takamatsu, and Wei, 2002; Wei and Honda, 2003; Z. W. Liu, et al. 2001; Watwe, Bar-Cohen, and McNiel, 1997); micro-porous coatings (Rainey, You, and Lee, 2003; O'Connor, You, and Chang, 1996), and micro-finned silicon (Honda, Takamatsu, and Wei, 2002; Wei and Honda, 2003) are presented versus  $\Delta T_{sub}$  in Figures 4.25b, 4.25c, and 4.25d, respectively.

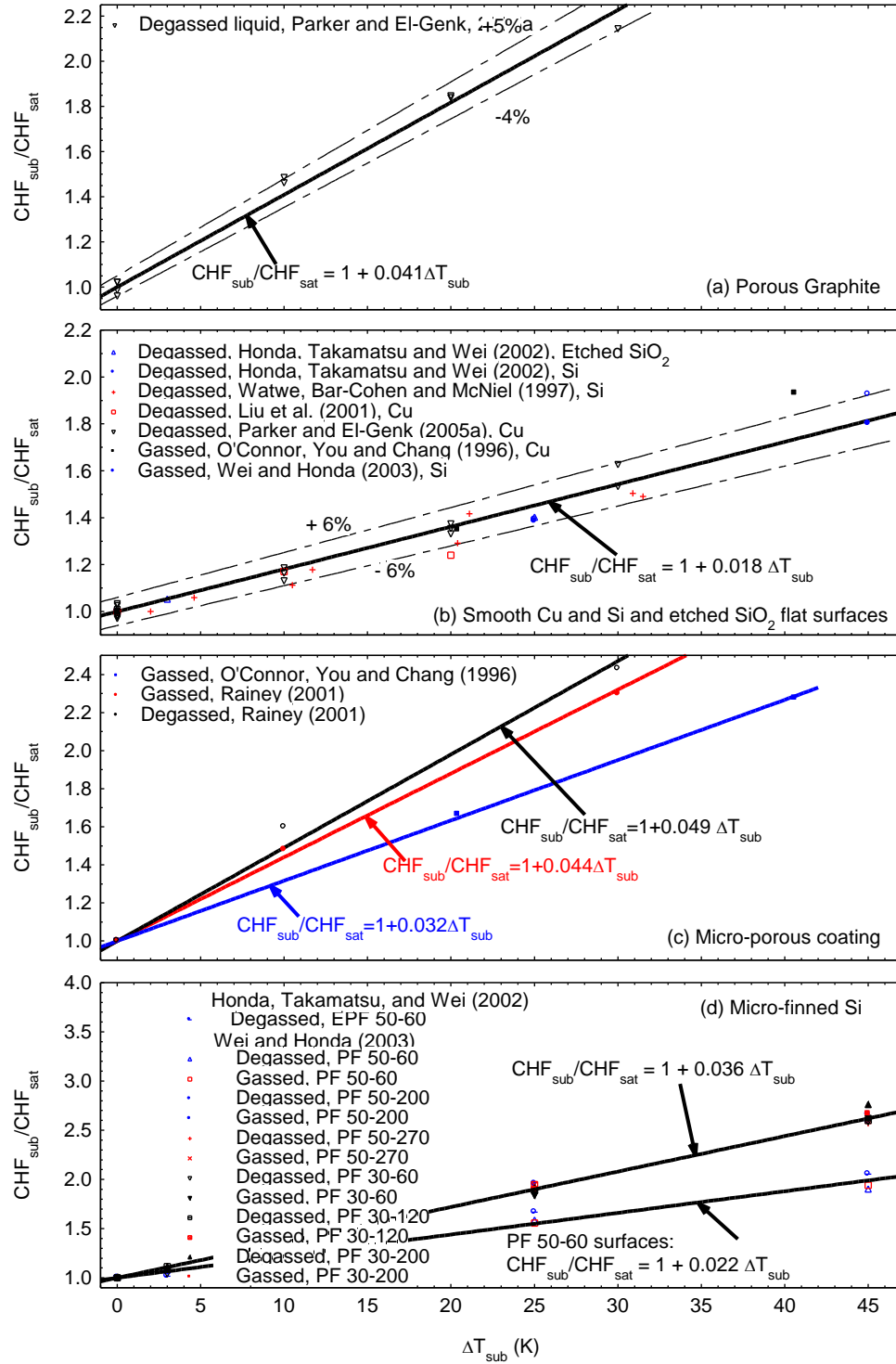


Figure 4.25 Effect of liquid subcooling on CHF of FC-72 on different surfaces.

The coefficient  $C_{CHF,sub}$  for FC-72 on smooth surfaces of 0.018 is within  $\pm 6\%$  of the data (Figure 4.25b). The obtained values based on the reported CHF data on micro-porous coatings for gassed (0.044) and degassed (0.049) FC-72 liquid are close (Rainey, You, and Lee, 2003), while that for gassed liquid on the micro-porous coating used by O'Connor, You, and Chang (1996) is much smaller (0.032) (Figure 4.25c).

Rainey, You, and Lee (2003) used micro-porous coatings of aluminum particles, 1 - 20  $\mu\text{m}$  in size, mixed with epoxy and a solvent, while O'Connor, You, and Chang (1996) used a micro-porous coating of diamond particles, ranging in size from 8 – 12 $\mu\text{m}$ , mixed with epoxy and solvent. The data on micro-finned silicon surfaces showed almost no difference between gassed and degassed liquids, but rather a strong of CHF dependence on the surface characteristics. For the boiling on PF 50-60 micro-finned surface (50  $\mu\text{m}$  square fins that are 60  $\mu\text{m}$  tall) (Honda, Takamatsu, and Wei, 2002; Wei and Honda, 2003)  $C_{CHF,sub} = 0.022$ , but for all other surfaces with micro-fins of different dimensions (Wei and Honda, 2003)  $C_{CHF,sub} = 0.036$ , ~64% higher (Figure 4.25d).

The critical heat flux for HFE-7100 also increases linearly with increased liquid subcooling. Figures 4.26a and 4.26b show the increase of CHF with increasing subcooling. For HFE-7100 boiling on smooth surfaces, the coefficient  $C_{CHF,sub}$  is 0.024 (El-Genk and Bostanci, 2003b; Liu et al., 2001; Arik and Bar-Cohen, 2001; El-Genk and Parker, 2005). On porous graphite, this value is 0.036 and fits the data to  $\pm 4\%$  (Figure 4.26a). The results of applying Equation 4.7 to the present and reported subcooled CHF data are summarized in Figure 4.27a. Figure 4.27b plots the ratio of the subcooled boiling CHF values of FC-72 liquid on structured and porous surfaces ( $CHF_E$ ) and the values obtained on smooth surface ( $CHF_S$ ). The largest enhancements in subcooled boiling CHF are those reported for gassed and degassed FC-72 on micro-porous coatings (Rainey, You, and Lee, 2003), followed by the present values on porous graphite, then those for gassed and degassed liquid on micro-finned surfaces (Honda, Takamatsu, and Wei, 2002; Wei and Honda, 2003).

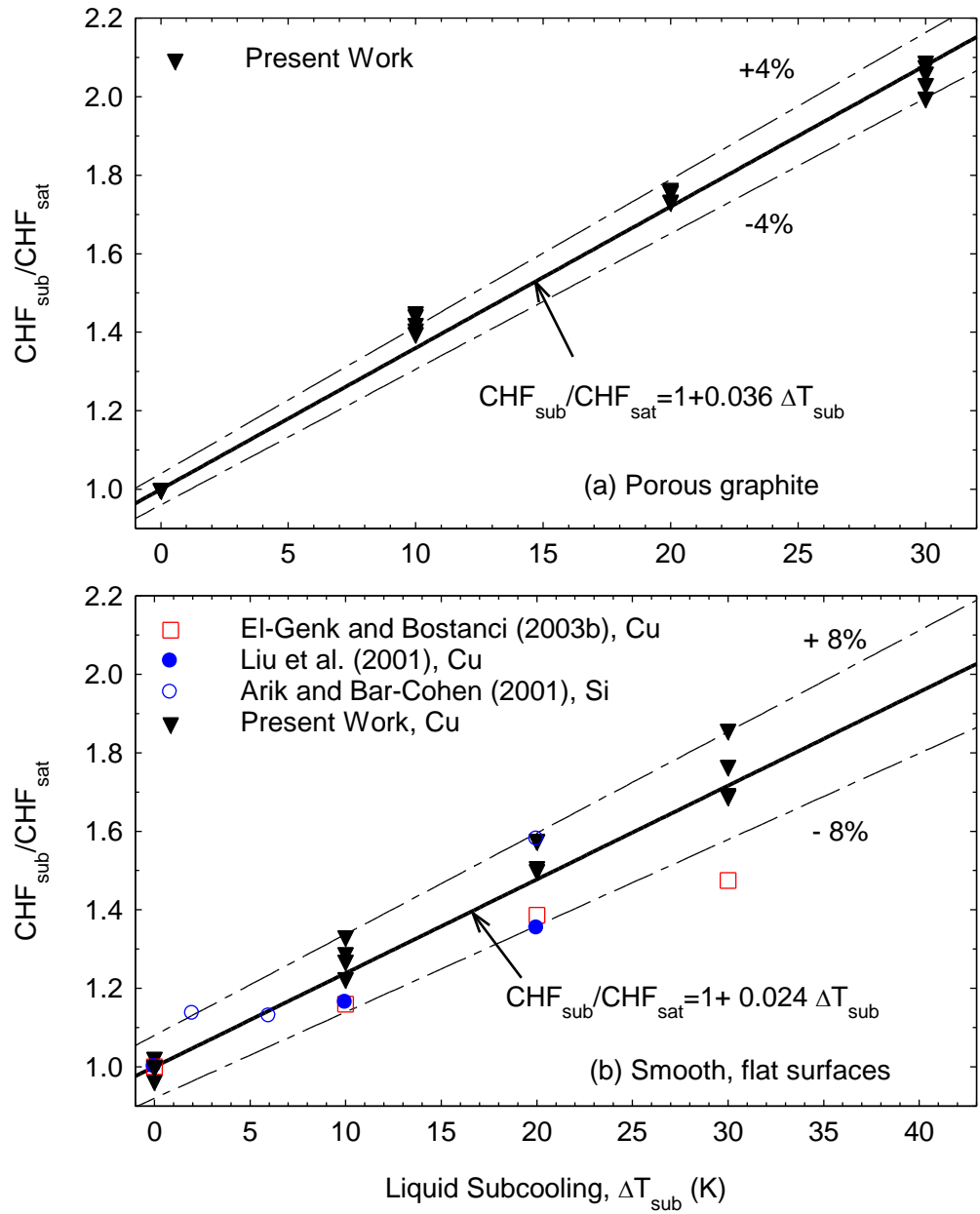


Figure 4.26 Effect of liquid subcooling on CHF of HFE-7100 on different surfaces.

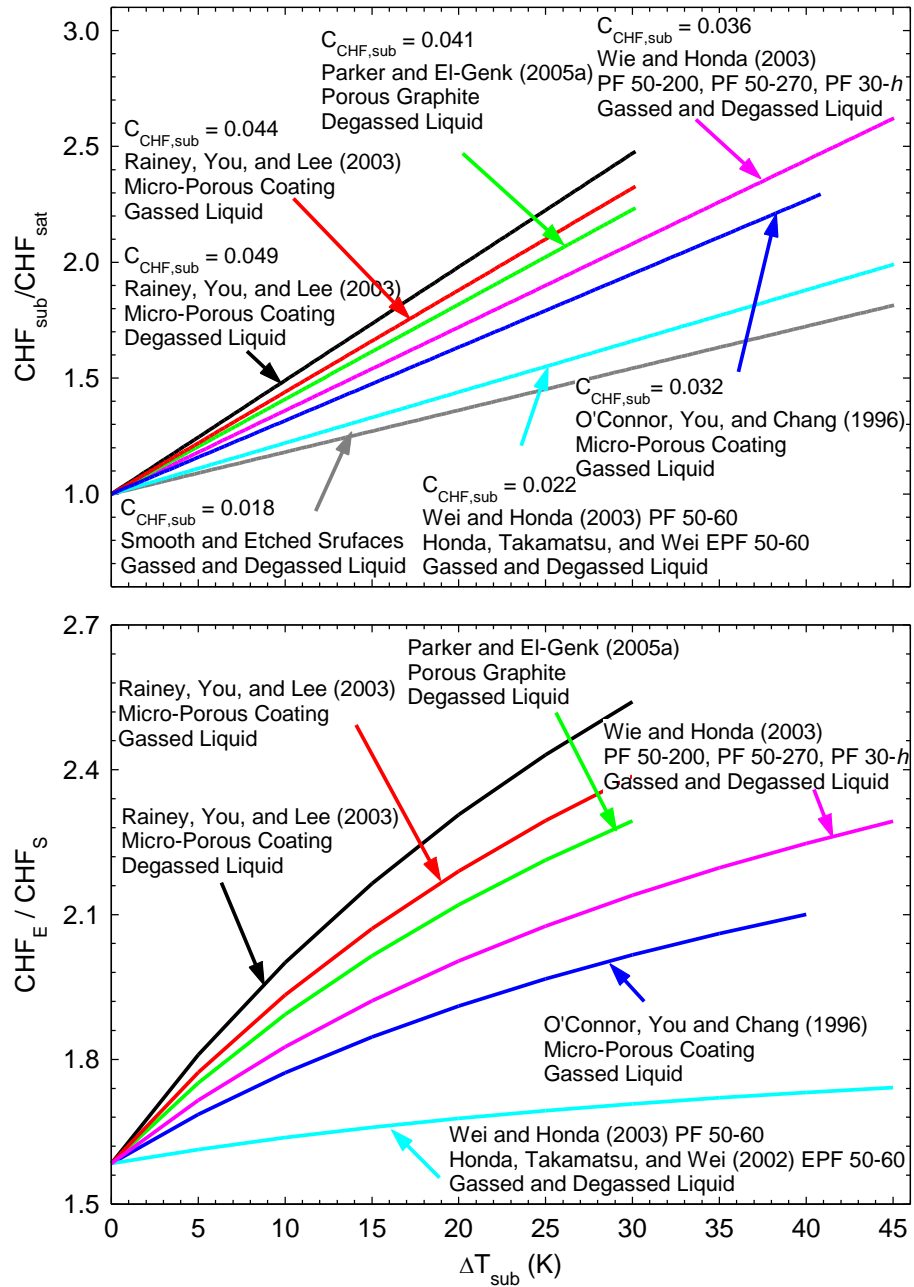


Figure 4.27 Summary of the effect of liquid subcooling and surface characteristics on CHF of FC-72.

#### 4.5.4 Combined Effect of Subcooling and Surface Orientation on CHF

The previous section presented results on the effect of liquid subcooling on CHF in the upward facing orientation ( $\theta = 0^\circ$ ). In this orientation, CHF values for dielectric liquids of FC-72 and HFE-7100 increase linearly with increased liquid subcooling, consistent with those reported for water (Ivey and Morris, 1966) and dielectric liquids on copper, Si, micro-finned silicon, and micro-porous coatings (Figures 4.25 and 4.26). The linear increase in CHF with increased liquid subcooling occurs at all surface orientations ( $0^\circ - 180^\circ$ ). However, the rate of increase in CHF with increased liquid subcooling depends on the surface type (porous graphite or copper), the liquid type (FC-72 or HFE-7100), and the surface inclination. The relative increase in CHF with increased liquid subcooling and inclination angle is given by the function  $F_{sub}$  expressed as

$$F_{sub}(\theta, \Delta T_{sub}) = 1 + C_{sub}^*(\theta) \Delta T_{sub}. \quad (4.8)$$

The angular dependence of the subcooling coefficient  $C_{sub}^*(\theta)$  replaces the equivalent subcooling coefficient in Equation 4.7,  $C_{CHF,sub}$ , which is identical to  $C_{sub}^*(0^\circ)$ . Figures 4.28a – 4.28f show the obtained values of  $F_{sub}(\theta, \Delta T_{sub})$  for FC-72 and HFE-7100 CHF on porous graphite at different inclination angles. As shown in Figure 4.28a,  $C_{sub}^* = 0.036 \text{ K}^{-1}$  and  $0.032 \text{ K}^{-1}$  for HFE-7100 and FC-72, respectively, in the upward facing orientation. The subcooling coefficient of porous graphite in HFE-7100 and FC-72 dielectric liquids decreases with increasing inclination.  $C_{sub}^*$  at  $90^\circ$  is  $0.032 \text{ K}^{-1}$  for HFE-7100 and  $0.03 \text{ K}^{-1}$  for FC-72 (Figure 4.28c); it is as little as  $0.021 \text{ K}^{-1}$  for HFE-7100 and  $0.011 \text{ K}^{-1}$  for FC-72 respectively in the downward facing orientation ( $\theta = 180^\circ$ ) (Figure 4.28f). Figures 4.29a – 4.29f show the values of  $F_{sub}(\theta, \Delta T_{sub})$  for HFE-7100 on plane copper at different surface orientations. The value of  $C_{sub}^*$  increases as the inclination angle of the surface increases from  $0^\circ$  to  $180^\circ$ . In the upward facing orientation,  $C_{sub}^* = 0.024 \text{ K}^{-1}$  and increases to  $0.029 \text{ K}^{-1}$  at  $90^\circ$ . The subcooling coefficient is highest at  $\theta = 180^\circ$ ,  $C_{sub}^* = 0.032 \text{ K}^{-1}$ .

Figure 4.30 plots the subcooling coefficient  $C_{sub}^*$  versus the inclination angle. For FC-72 and HFE-7100 on porous graphite,  $C_{sub}^*$  decreases slowly with increased

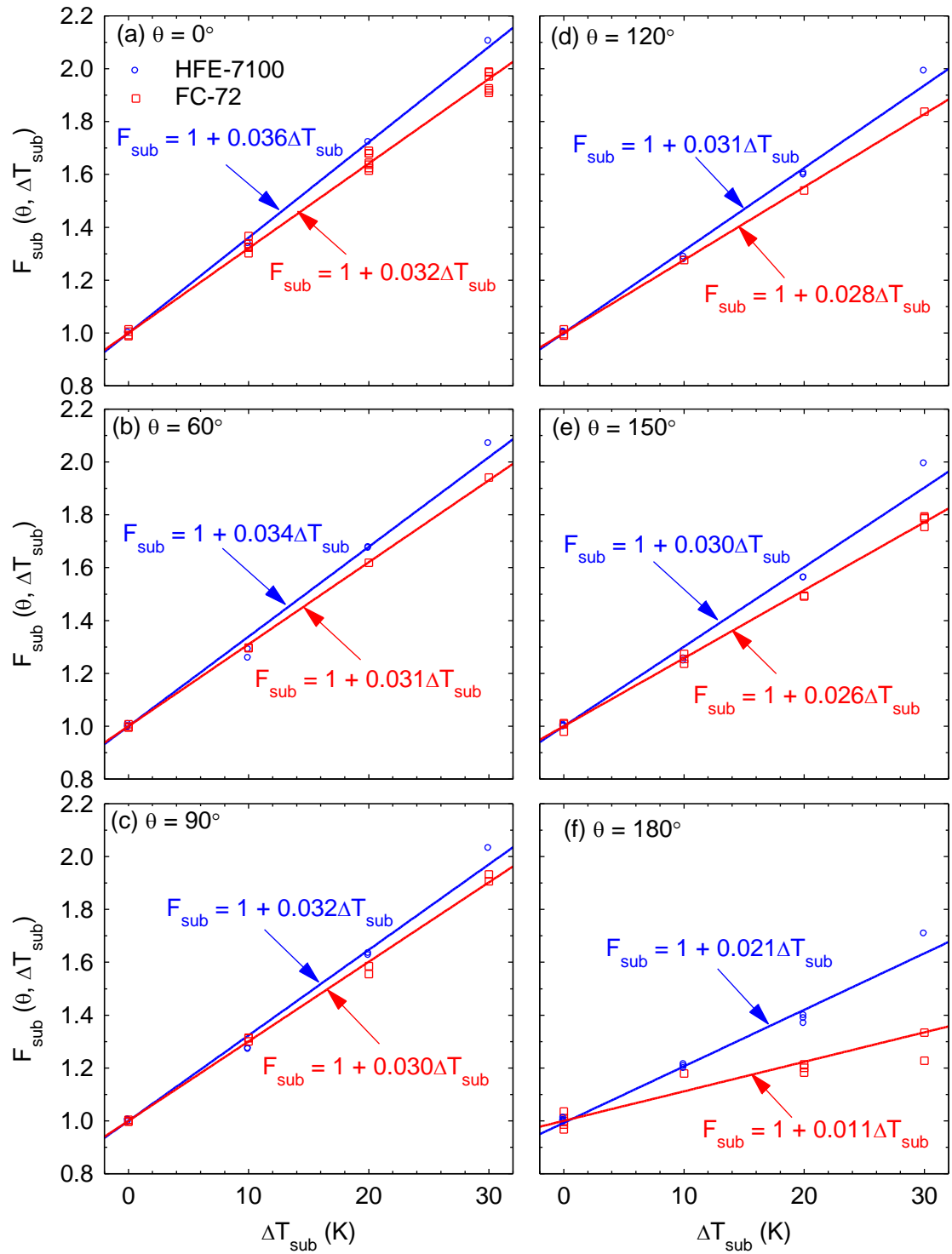


Figure 4.28 Effect of surface inclination on subcooled CHF coefficient for porous graphite.

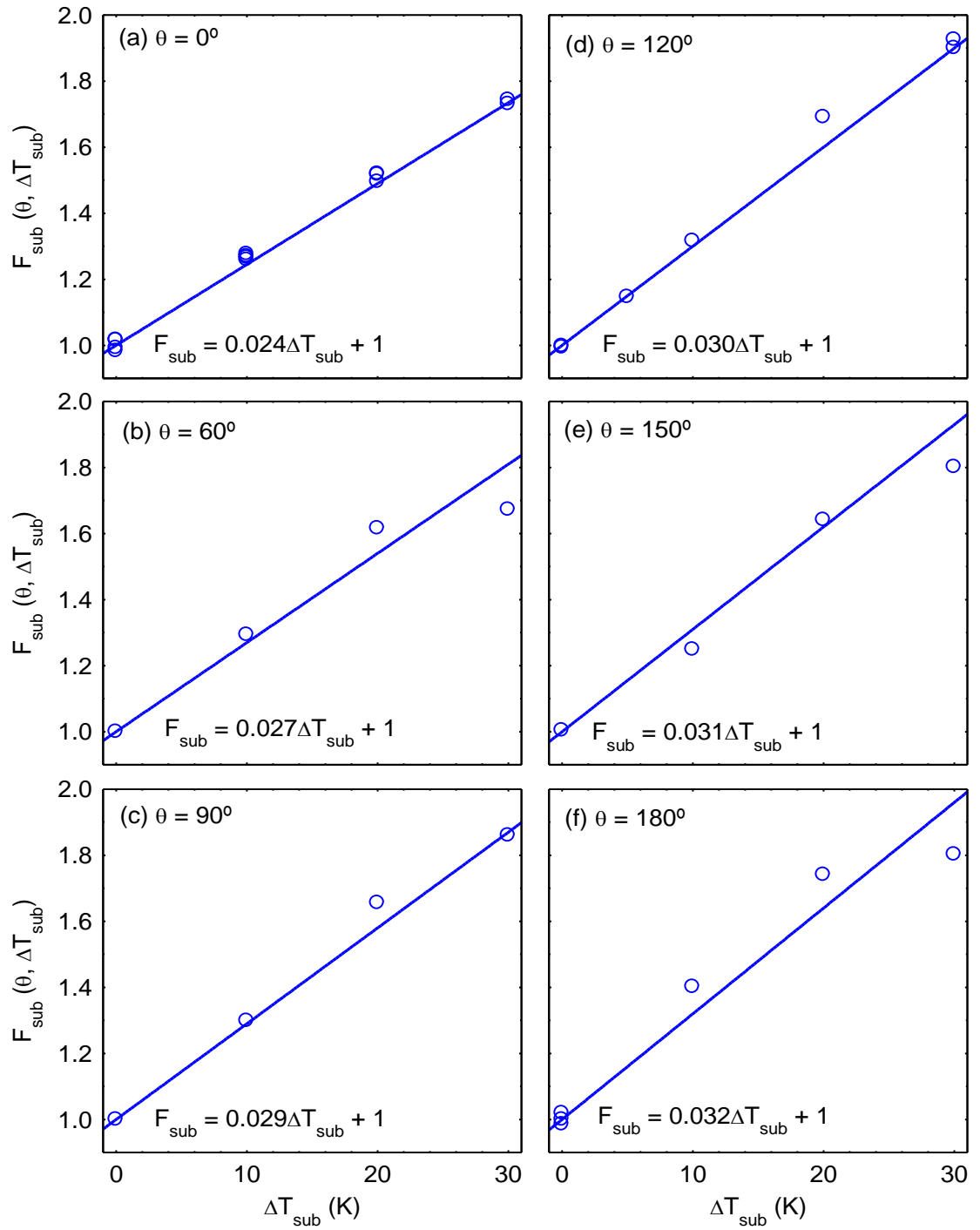


Figure 4.29 Effect of surface inclination on subcooled HFE-7100 CHF coefficient for copper.

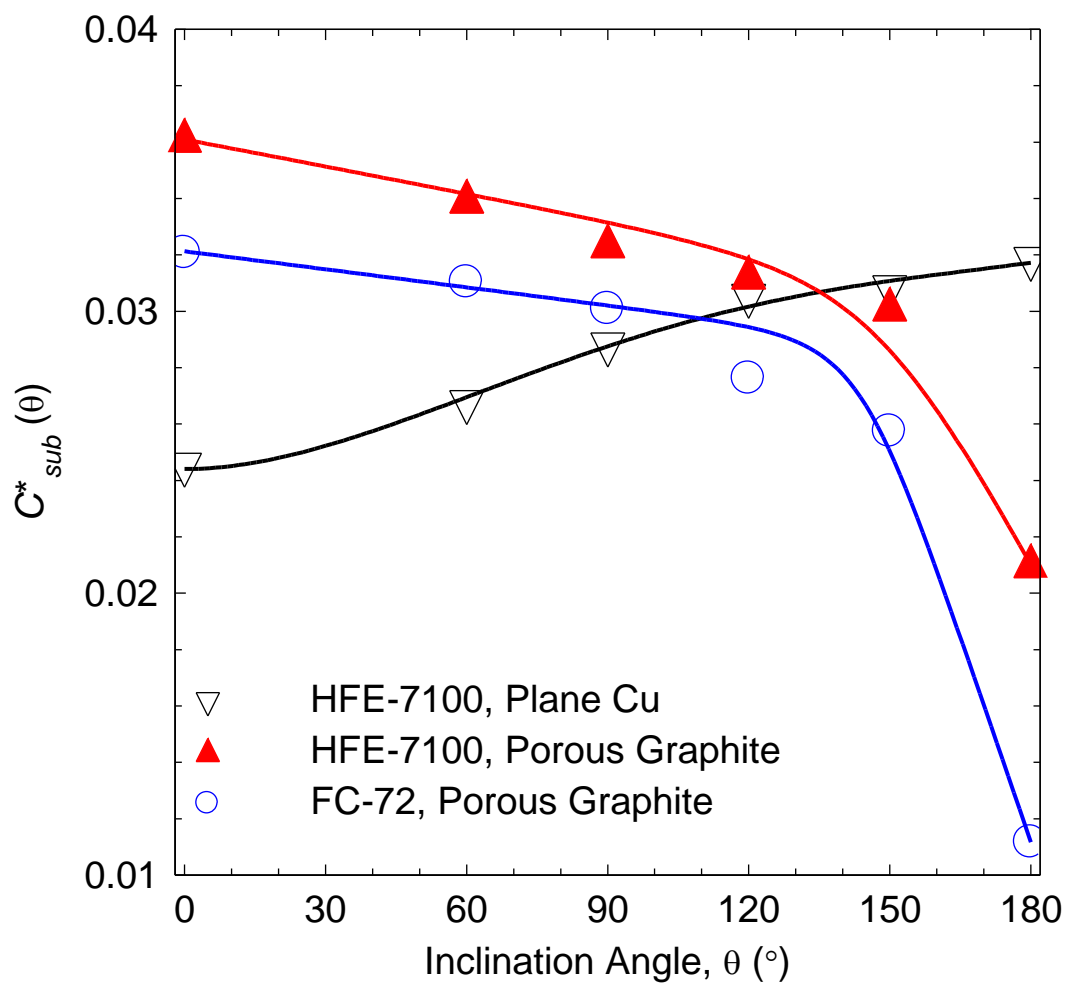


Figure 4.30 CHF subcooling coefficient on plane porous graphite and copper as a function of inclination angle.

inclination to  $\sim 120^\circ$  and then decreases faster at higher inclinations. The value of  $C_{sub}^*$  for HFE-7100 on porous graphite is about 10% higher than for FC-72 up to an inclination of  $150^\circ$ , then at  $180^\circ$  it is about twice as high. For HFE-7100 on copper,  $C_{sub}^*$  increases slowly with increased inclination at both low and high inclination angles, and increases fastest around  $90^\circ$  (vertical).

Combining the appropriate forms of Equations 4.3 – 4.8 gives the following CHF correlation:

$$CHF(\theta, \Delta T_{sub}) = C_{CHF, sat}(0^\circ) R(\theta) \left[ 1 + C_{sub}^*(\theta) \Delta T_{sub} \right] \left[ h_{fg} \sqrt{\rho_v} (\sigma g (\rho_l - \rho_v))^{1/4} \right]. \quad (4.9)$$

This correlation accounts for the effects of liquid properties and subcooling and the inclination angle and characteristics of the heated surface. Such general CHF correlation for dielectric liquids is reported for the first time. Figure 4.31 compares the prediction of the CHF correlation in Equation 4.9 with the current CHF data for both FC-72 and HFE-7100 dielectric liquids at different surface orientations ( $0^\circ - 180^\circ$ ) and liquid subcoolings up to 30 K. The CHF correlation fits the data to within +6% and -7%.

#### **4.6 Discussion on Nucleate Boiling of Dielectric Liquids**

Nucleate boiling of the dielectric liquids FC-72 and HFE-7100 ensues on porous graphite at a surface superheat just above the saturation temperature of the liquid ( $\Delta T_{sat} < \sim 1$  K). Figure 4.32a shows a photograph of saturation boiling of HFE-7100 on porous graphite at as little as  $0.2 \text{ W/cm}^2$  and  $\Delta T_{sat} \sim 0.8$  K. At this low superheat, bubbles are seen coming from the porous graphite. On plane copper, the mode of heat transfer at these surface superheats is always natural convection.

SEM images of the porous graphite show that there are pores and re-entrant cavities with openings ranging from  $< 1 \mu\text{m}$  to  $> 100 \mu\text{m}$  diameter (Figure 3.5). If the radius of the cavity opening,  $r$ , is sufficiently small that the liquid's surface tension,  $\sigma$ , would withstand the pressure head of the liquid above the cavity, and the liquid will not enter and flood the cavity:

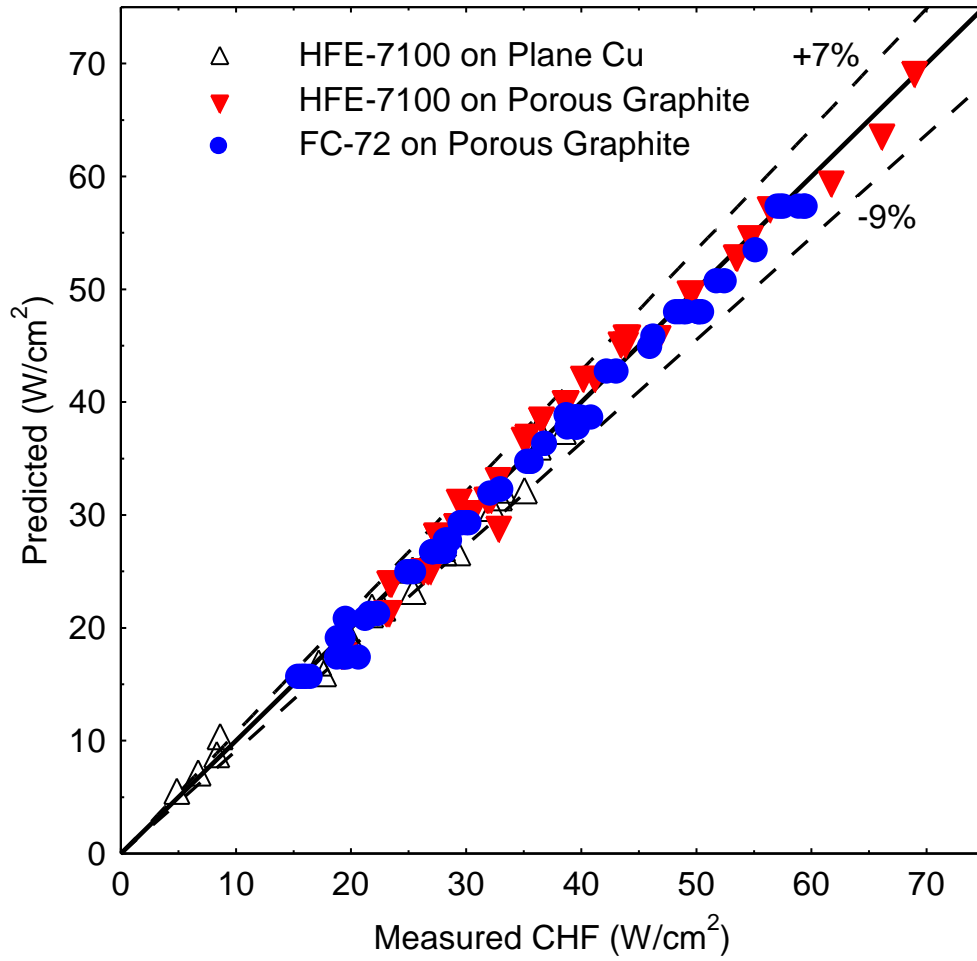
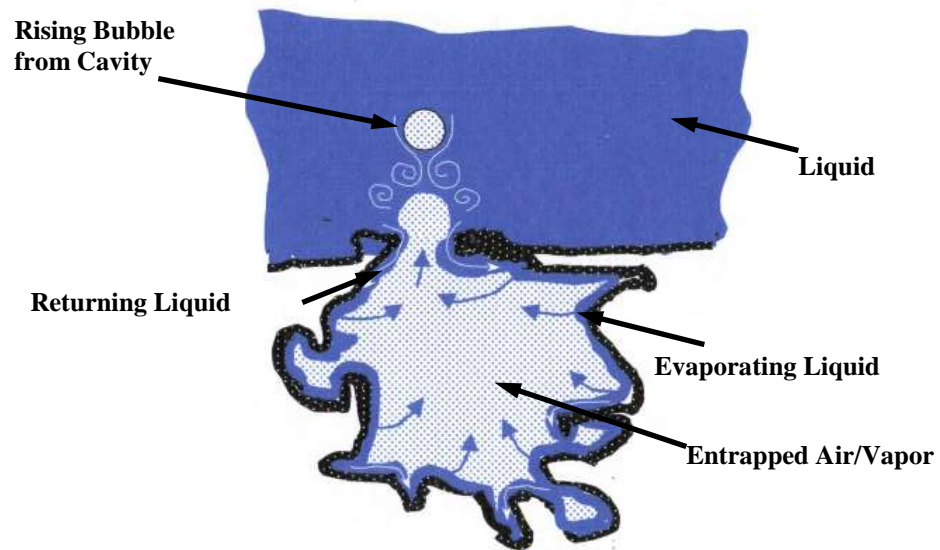


**Figure 4.31 Predicted and measured CHF values for saturation and subcooled boiling on porous graphite and plane copper.**



(a)  $0.2 \text{ W/cm}^2$



(b) Enhanced heat transfer from porous graphite at low power

Figure 4.32 Photograph and sketch of low heat flux heat transfer in porous graphite.

$$r_{\min} < 2\sigma/(\rho_l gH), \quad (4.10)$$

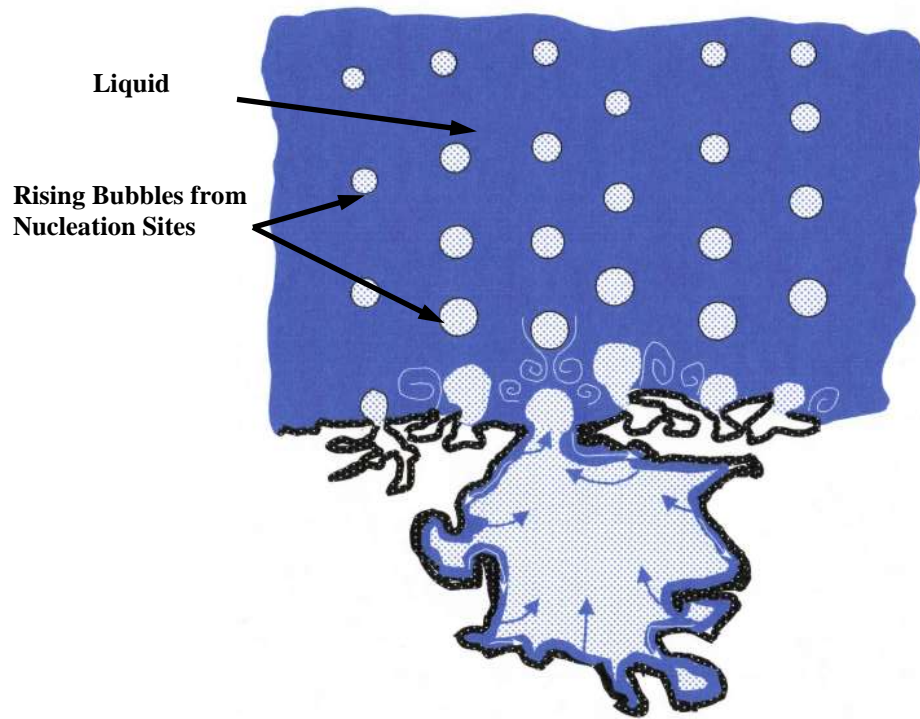
The value of  $r_{\min}$  for HFE-7100 and FC-72 with 8 cm of liquid above the porous graphite is  $\sim 13 \mu\text{m}$ . Even though the liquid cannot flood the cavity, it may creep down the edges of the opening and coat the cavity's inner walls with a thin film (Figure 4.32b). When the temperature of the cavity wall approaches the saturation temperature of the liquid, thin film evaporation within the cavity ensues and the accumulated vapor is released through the open mouth of the cavity onto the liquid pool, which is observed in the experiments. As the thin liquid film evaporates, it is continuously replenished from the pool. Figure 4.33a shows saturation boiling of HFE-7100 at  $10 \text{ W/cm}^2$  (boiling region II). In addition to the active nucleation sites on the surface, the thin film evaporation inside the cavity enhances the overall heat transfer (Figure 4.33b).

#### **4.7 Selected Photographs of Nucleate Boiling**

Figures 4.34a – 4.34d present photographs of saturation and subcooled ( $\Delta T_{\text{sub}} = 10 \text{ K}$ ,  $20 \text{ K}$ , and  $30 \text{ K}$ ) boiling of HFE-7100 on porous graphite and plane copper at nearly the same heat fluxes. Close examination of the photographs in the figures reveals that at almost the same heat fluxes, nucleate boiling of HFE-7100 on the porous graphite is more vigorous than on plane copper, resulting in much lower surface superheats. Such observation is more prevalent in subcooled boiling (Figures 4.34b – 4.34d). In saturation boiling on porous graphite at  $5.4$  and  $9.8 \text{ W/cm}^2$ , the surface superheats are  $6.0 \text{ K}$  and  $8.6 \text{ K}$ , respectively (Figure 4.34a), while the corresponding values on smooth copper, at almost the same heat fluxes of  $5.2$  and  $10.0 \text{ W/cm}^2$ , are much higher;  $11.6 \text{ K}$  and  $13.5 \text{ K}$ , respectively. These results are also applicable to subcooled boiling (Figures 4.34b – 4.34d). The intense nucleation on the porous graphite results in relatively more coalescence of departing vapor bubbles near and above the surface (Figures 4.34a – 4.34d), compared to those on smooth copper. However, the lower surface superheats of the porous graphite delay blanketing the surface with vapor, hence resulting in higher CHF values, compared to those on smooth copper.



(b) 10.0 W/cm<sup>2</sup>



(b) Enhanced heat transfer from porous graphite at moderate power

Figure 4.33 Photograph and sketch of moderate heat flux heat transfer in porous graphite.

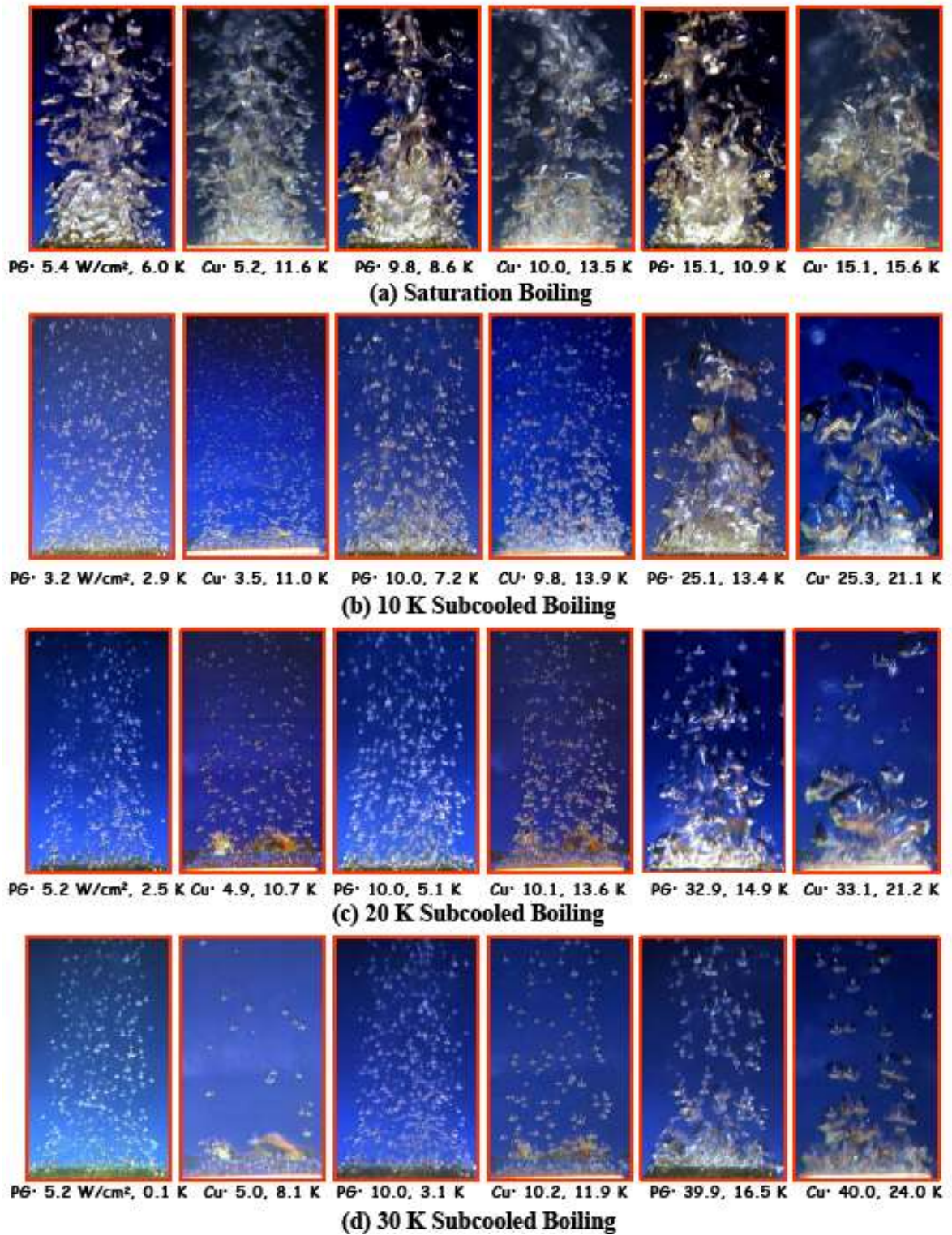


Figure 4.34 Photographs of saturation and subcooled nucleate boiling on porous graphite and smooth copper at similar heat fluxes.

Figures 4.35 – 4.39 compare the photographs of saturation nucleate boiling of FC-72 liquid on porous graphite and on plane copper at inclination angles of 60°, 90° (vertical), 120°, 150°, and 180° (downward facing). For each figure, the first photograph compares the boiling process at similar heat fluxes in boiling region I (discrete bubble region), followed by photographs near 5 W/cm<sup>2</sup>, then photographs in region II (fully developed nucleate boiling region). The last image in each figure is the last photograph taken prior to CHF (Figures 4.35 – 4.39). These photographs clearly show the higher density of bubble nucleation on the porous graphite, which explains the higher nucleate boiling heat transfer coefficient and CHF, compared to those on smooth copper. The photographs in Figures 4.36a of nucleate boiling on porous graphite in the vertical orientation show that the thickness of the two-phase flow boundary layer next to the surface increases with increased heat flux. Also, the instability of the interface of the boundary layer with the surrounding liquid in the pool becomes more apparent and wavier. The mixing in this two-phase boundary layer by the vapor bubbles rolling upward intensifies. Also, as the vapor bubbles are released, the growth and collapse of the two-phase boundary layer becomes more pulsating as the heat flux increases. Similar observations are made of nucleate boiling on copper (Figure 4.36b), but with less intensity than on porous graphite.

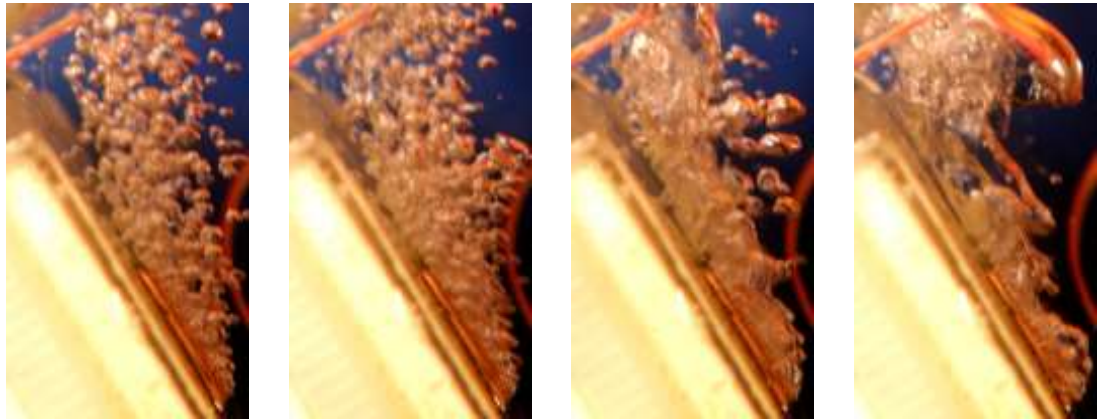
Figures 4.35 ( $\theta = 60^\circ$ ), 4.37 ( $\theta = 120^\circ$ ), and 4.38 ( $\theta = 150^\circ$ ), show similar trends. As the heat flux increases, the thickness of the two-phase region next to the surface increases. The mixing in the two-phase region is more intense on the porous graphite (Figures 4.35a, 4.37a, and 4.38a) than on the plane copper (Figures 4.35b, 4.37b, and 4.38b). This is clearly apparent for the 150° inclination (Figure 4.38), where near CHF (22.6 W/cm<sup>2</sup> on porous graphite, 11.0 W/cm<sup>2</sup> on copper), the thickness of the two phase flow region is thicker, whereas on copper, it appears to be nearly flat.

In the downward facing orientation (Figure 4.39), the detachment of the vapor bubbles from the surface is aided by the inertial force of the vapor generation at the base of the bubbles with the surface prior to detachment. The detached bubbles coalesce with others near the surface forming flat vapor globules under the effect of the upward gravity force acting on the surface. These vapor globules continue to grow with additional



3.2 W/cm<sup>2</sup>, 1.5 K    5.1 W/cm<sup>2</sup>, 2.8 K    10.5 W/cm<sup>2</sup>, 5.6 K    27.9 W/cm<sup>2</sup>, 26.6 K

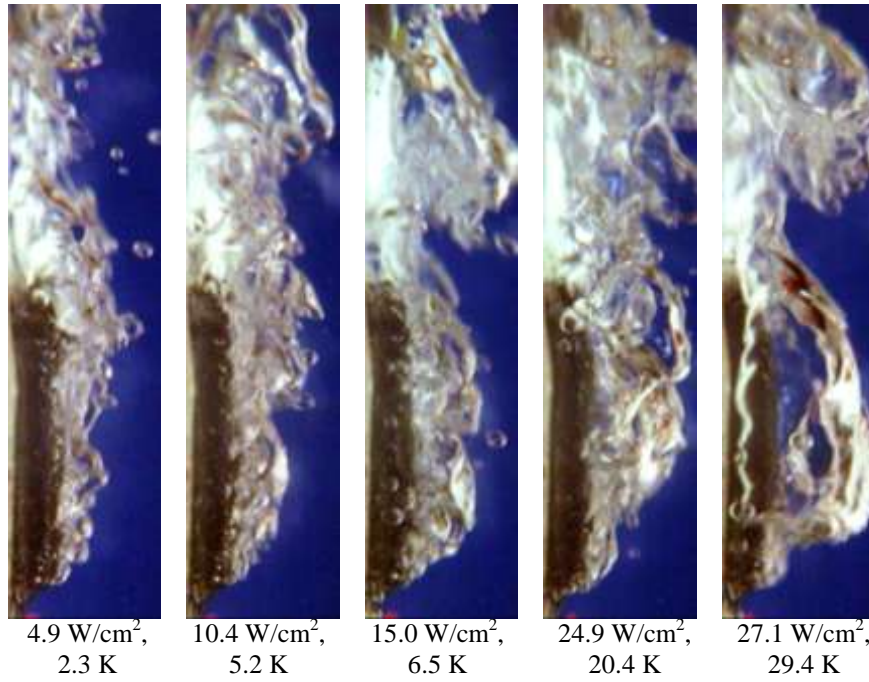
**(a) Photographs of nucleate boiling on porous graphite at inclination angle of 60°**



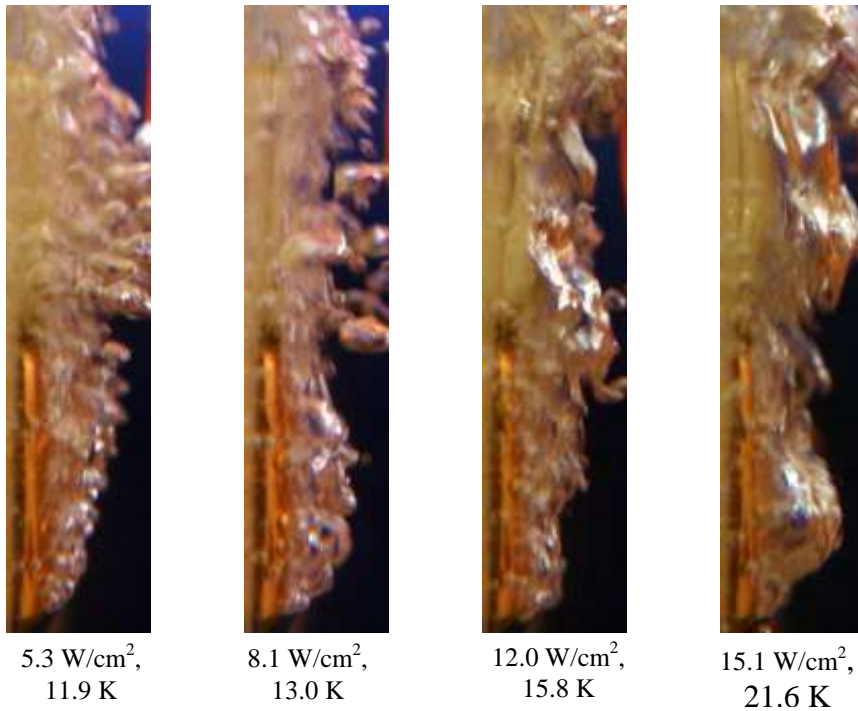
3.1 W/cm<sup>2</sup>, 11.1 K    4.9 W/cm<sup>2</sup>, 11.8 K    10.0 W/cm<sup>2</sup>, 13.8 K    15.1 W/cm<sup>2</sup>, 19.1 K

**(b) Photographs of nucleate boiling on copper at inclination angle of 60°**

**Figure 4.35 Photographs of FC-72 saturation boiling on porous graphite and copper ( $\theta = 60^\circ$ ).**

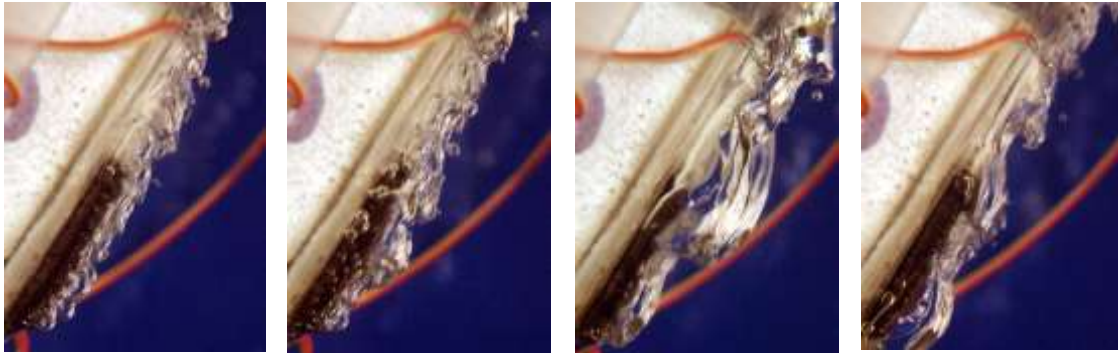


**(a) Photographs of nucleate boiling on porous graphite at inclination angle of 90°**



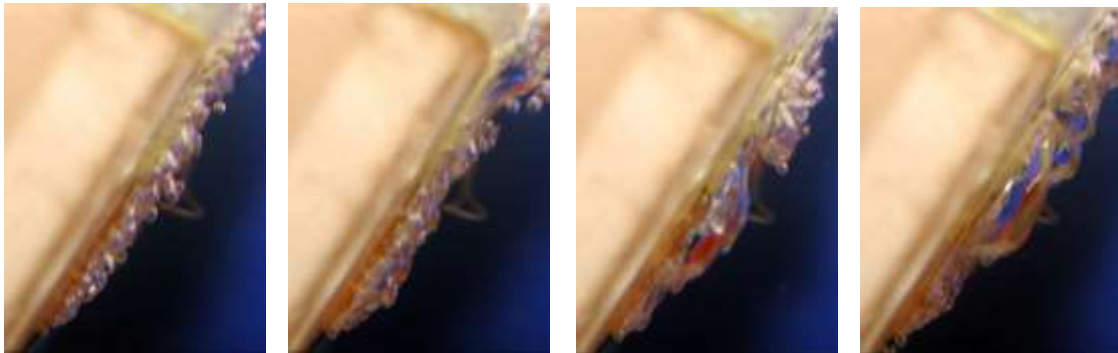
**(b) Photographs of nucleate boiling on copper at inclination angle of 90°**

**Figure 4.36 Photographs of FC-72 saturation boiling on porous graphite and copper ( $\theta = 90^\circ$ ).**



3.4 W/cm<sup>2</sup>, 2.8 K      7.2 W/cm<sup>2</sup>, 5.1 K      20.0 W/cm<sup>2</sup>, 11.6 K      25.2 W/cm<sup>2</sup>, 25.3 K

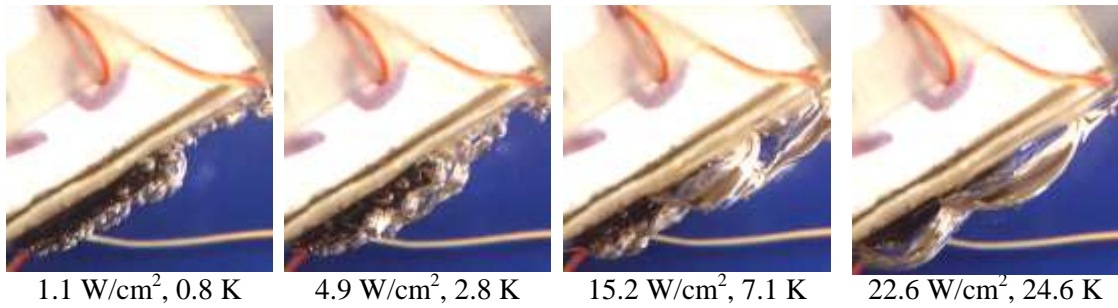
**(a) Photographs of nucleate boiling on porous graphite at inclination angle of 120°**



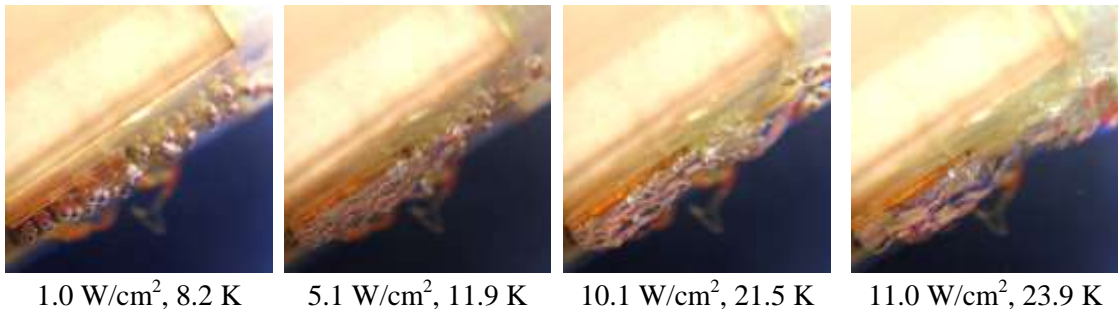
3.0 W/cm<sup>2</sup>, 10.8 K      7.9 W/cm<sup>2</sup>, 13.2 K      10.1 W/cm<sup>2</sup>, 14.9 K      12.9 W/cm<sup>2</sup>, 20.4 K

**(b) Photographs of nucleate boiling on copper at inclination angle of 120°**

**Figure 4.37 Photographs of FC-72 saturation boiling on porous graphite and copper ( $\theta = 120^\circ$ ).**



**(a) Photographs of nucleate boiling on porous graphite at inclination angle of 150°**



**(b) Photographs of nucleate boiling on copper at inclination angle of 150°**

**Figure 4.38 Photographs of FC-72 saturation boiling on porous graphite and copper ( $\theta = 150^\circ$ ).**

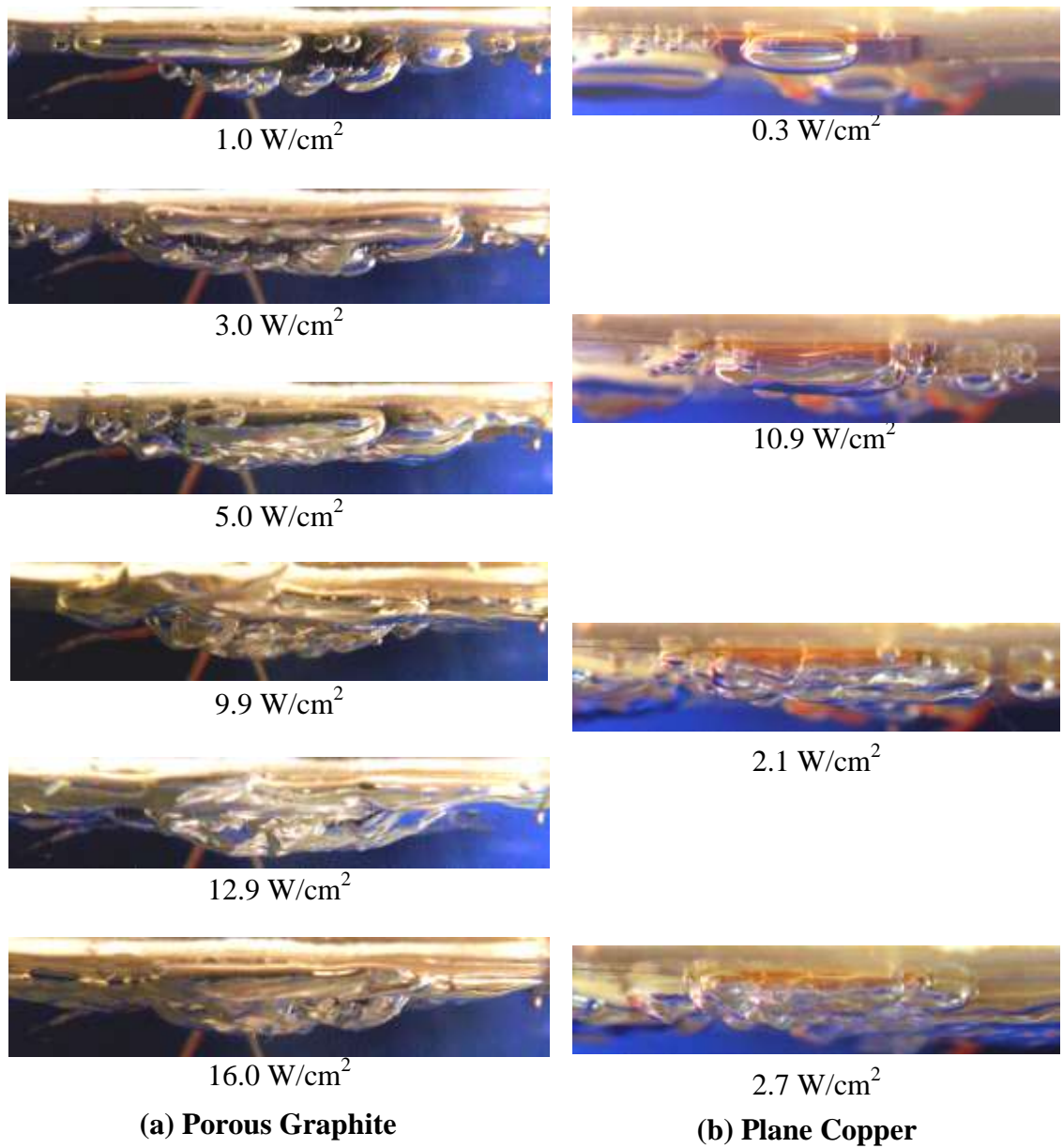


**Figure 4.39 Photographs of FC-72 saturation boiling on porous graphite and copper ( $\theta = 180^\circ$ ).**

evaporation caused by the heat transfer across a very thin liquid film that separates these globules from the heated surface. As the size of the vapor globules increases they are swept away from the surface and to the side and eventually released from the edge of the test section. This process of the detachment of vapor bubbles, the formation and growth of flat vapor globules, and the sweeping of these globules from the surface occur repetitively with certain frequency, which increases as the surface heat flux increases. Visual observation indicate that the frequency of vapor slug formation and removal from the porous graphite are typically much higher than those associated with the copper surface. Such a cyclical process has been observed in all orientations, but at slightly higher frequencies. Table 4.2 lists some selected values of the frequency of vapor slug formation and release at different surface inclinations and heat fluxes for saturation boiling of HFE-7100 on porous graphite and plane copper.

Figure 4.40 shows a sequence of still photographs and corresponding sketches illustrating the pulsating release of vapor during saturation boiling of FC-72 on porous graphite in the downward facing orientation ( $\theta = 180^\circ$ ). These photographs are taken at a

**Table 4.2. Frequency of formation and rise of vapor slugs in saturation boiling of HFE-7100.**

Surface	Inclination, $\theta$ ( $^\circ$ )	Heat flux, $q''$ ( $\text{W}/\text{cm}^2$ )	Frequency, (Hz)
Plane Copper	0	14.7	12
	0	20.0	13
	180	3.5	3
	180	4.1	5
	180	4.5	6
Porous Graphite	0	20.3	14
	0	30.0	15
	90	20.1	12
	90	30.1	14
	180	10.4	10
	180	18.1	13

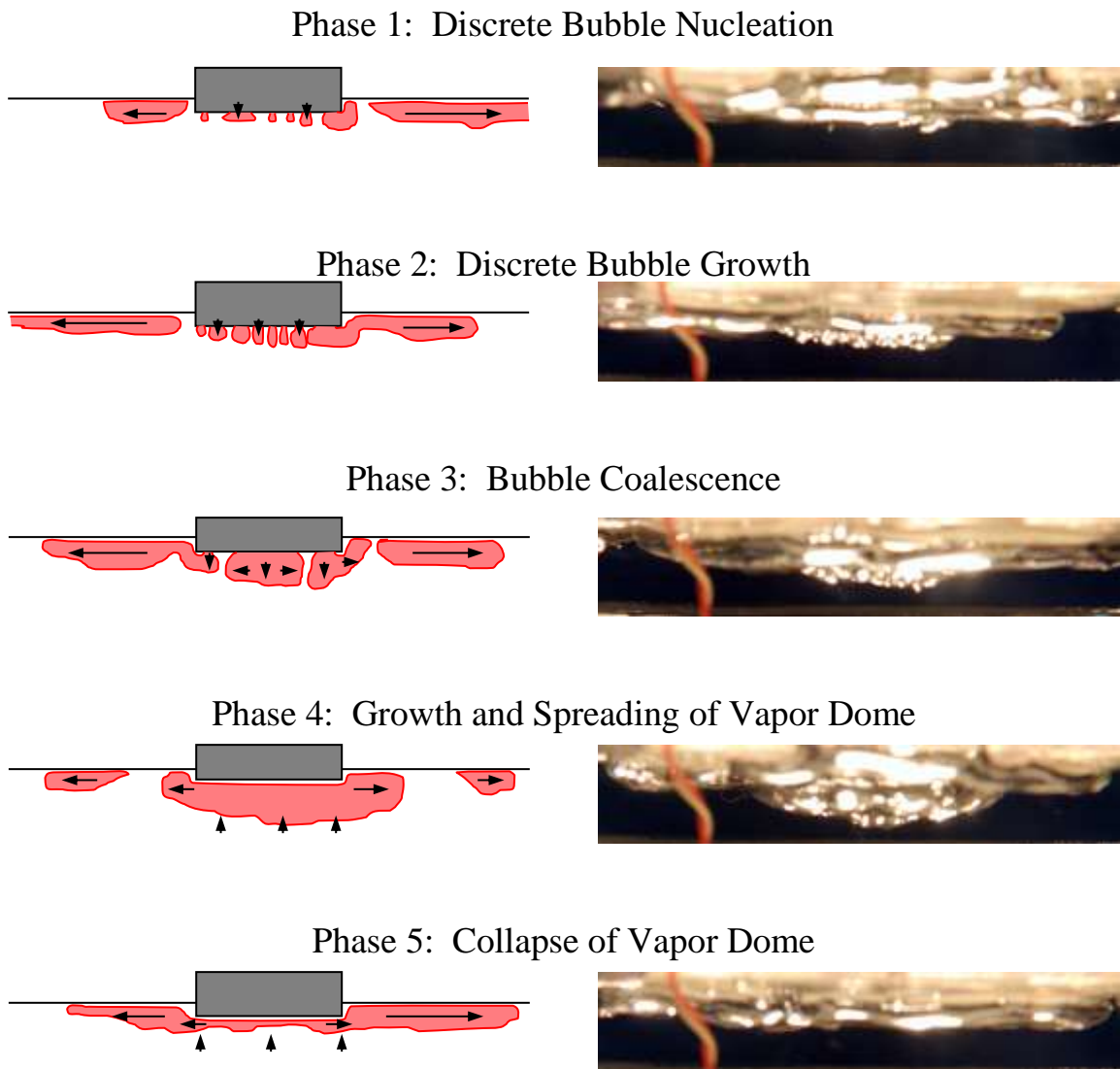


**Figure 4.40** Pumping action during saturation boiling of FC-72 on porous graphite at  $\theta = 180^\circ$  ( $q'' = 11.9 \text{ W/cm}^2$ ,  $\Delta T_{sat} = 11.7 \text{ K}$ ).

heat flux of  $11.9 \text{ W/cm}^2$  and a superheat of  $11.6 \text{ K}$ . The sequence shown is divided into several successive phases or steps, namely:

- (1) Discrete bubbles nucleation (Figure 4.40a), when bubbles form on the surface at discrete and isolated sites;
- (2) Discrete bubbles lateral growth (Figure 4.40b), by the evaporation of the thin liquid film separating them from the heated surface;
- (3) Bubbles coalescence (Figure 5.40c), when the growing bubbles on the surface begin to detach and coalesce with their neighbors; this coalescence begins to form a swelling two-phase dome;
- (4) Growth and spreading of the vapor dome (Figure 4.40d), when the vapor dome grows rapidly by evaporation of the liquid film separating the vapor from the heated surface;
- (5) Collapse of the vapor dome, when upward force of the liquid pushes the vapor to the sides, thus replenishing the supply of liquid to the heated surface.

For this case at  $q'' = 11.9 \text{ W/cm}^2$ , and  $\Delta T_{sat} = 11.7 \text{ K}$  the growth and release cycle repeats about every  $0.08 \text{ s}$  ( $\sim 12 \text{ Hz}$ ).

## **4.8 Summary**

The work presented in this chapter investigated saturation and  $10$ ,  $20$ , and  $30 \text{ K}$  subcooled boiling of FC-72 and HFE-7100 dielectric liquids on porous graphite and plane copper at inclination angles  $\theta = 0^\circ$  (upward facing) to  $\theta = 180^\circ$  (downward facing) and compared the boiling curves and nucleate boiling heat transfer coefficients. At low surface superheats ( $< \sim 12 \text{ K}$ ), increasing the surface inclination,  $\theta$ , increases the nucleate boiling heat flux, while, at higher superheats, the nucleate boiling heat flux decreases with increased  $\theta$  (Figures 4.13 and 4.14). Although increasing liquid subcooling increases the nucleate boiling heat flux and CHF (Figure 4.10), it decreases the nucleate boiling heat transfer coefficient, thus increasing the boiling resistance (Figure 4.19).

The nucleate boiling heat transfer coefficients of FC-72 on porous graphite are

significantly (up to 52.7%) higher than those on HFE-7100. At surface superheats below those at the peak nucleate boiling heat transfer coefficient, occurring at or near the end of the fully developed nucleate boiling region, the nucleate boiling heat transfer coefficient increases with increased surface orientation or inclination angle. At higher surface superheats, however, increasing the surface orientation decreases the nucleate boiling heat transfer coefficient (Figure 4.17).

Increasing liquid subcooling,  $\Delta T_{sub}$ , decreases the nucleate boiling heat transfer coefficient (increasing the boiling resistance) but increases CHF. CHF decreases slowly with increasing inclination angle from  $0^\circ$  to  $90^\circ$  then rapidly to  $180^\circ$ . The relative decrease in CHF of dielectric liquids on copper and micro-porous coatings with increased  $\theta$  are almost identical, but they are smaller on porous graphite. Actual CHF values on porous graphite are higher than those on micro-porous coatings, and CHF values on micro-porous coatings are higher than those on copper. CHF increases linearly with increased liquid subcooling. CHF for HFE-7100 on porous graphite is consistently higher than that for FC-72. At  $180^\circ$  inclination, saturation CHF on porous graphite for HFE-7100 is  $19.2 \text{ W/cm}^2$  and for FC-72 is  $15.9 \text{ W/cm}^2$ . On plane copper, the CHF values are  $4.8 \text{ W/cm}^2$  and  $2.5 \text{ W/cm}^2$ , respectively. The developed CHF correlation for FC-72 and HFE-7100 dielectric liquids on porous graphite and other surfaces, as a function of the boiling surface, liquid subcooling, and inclination angle, fits the present and reported data by other investigators to within  $\pm 10\%$ .

Nucleate boiling heat transfer can be improved by increasing the nucleation site density on the heated surface and/or the surface area wetted by the boiling liquid. The work in this chapter focused on the results obtained in experiments of boiling on plane copper and porous graphite surfaces. The next chapter presents results of experiments of saturation and subcooled nucleate boiling heat transfer in dielectric liquids using copper surfaces with square corner pins.

## 5 Pool Boiling on Surface with Corner Pins

The previous chapter focused on investigating the effects of liquid subcooling, surface orientation, and liquid thermophysical properties on nucleate pool boiling on plane copper and porous graphite. The results showed that using porous graphite eliminates the temperature excursion at to boiling incipience and increases the nucleate boiling heat transfer coefficient and the critical heat flux. This chapter presents and discusses the results of saturation and subcooled boiling heat transfer experiments performed using copper surfaces with square corner pins of different heights. The motivation of these experiments was to increase the total thermal power dissipated by the underlying 10 x 10 mm chip and heat removal from the copper surface. The increase in the removed thermal power in nucleate boiling would be a function of the increase in the wetted surface area by the boiling dielectric liquid.

The results would show the effect of the height of the corner pins on the total power removed by nucleate boiling and on CHF at different orientations from upward-facing ( $\theta = 0^\circ$ ) to downward-facing ( $\theta = 180^\circ$ ). The obtained results in the natural convection regime in the upward-facing orientation are also presented and discussed. All experiments are conducted using the HFE-7100 dielectric liquid. The square corner pins (3 x 3 mm) have a cross sectional area of 9 mm<sup>2</sup>, with the heights of 2, 3, and 5 mm, increasing the total wetted surface 1.96, 2.44, and 3.4 times that of plane copper of the same footprint (10 x 10 mm). Results for the copper surface with corner pins are presented later, while the next section discussed those for porous graphite.

### 5.1 Results for Porous Graphite with Corner Pins

Experiments are conducted using porous graphite with square corner pins having 3 x 3 mm cross section and 2, 3, and 5 mm tall. Figure 5.1a shows a boiling curve obtained for saturation boiling of HFE-7100 on porous graphite with 5 mm tall corner pins in the horizontal ( $\theta = 0^\circ$ ) orientation. Note that the scale of the x-axis is temperature ( $^\circ\text{C}$ ) rather than superheat. Figure 5.1a shows that the thermal power removed at CHF porous (79.8 W) was 2 ½ times that at CHF on a plane porous graphite surface at CHF (31.7 W).

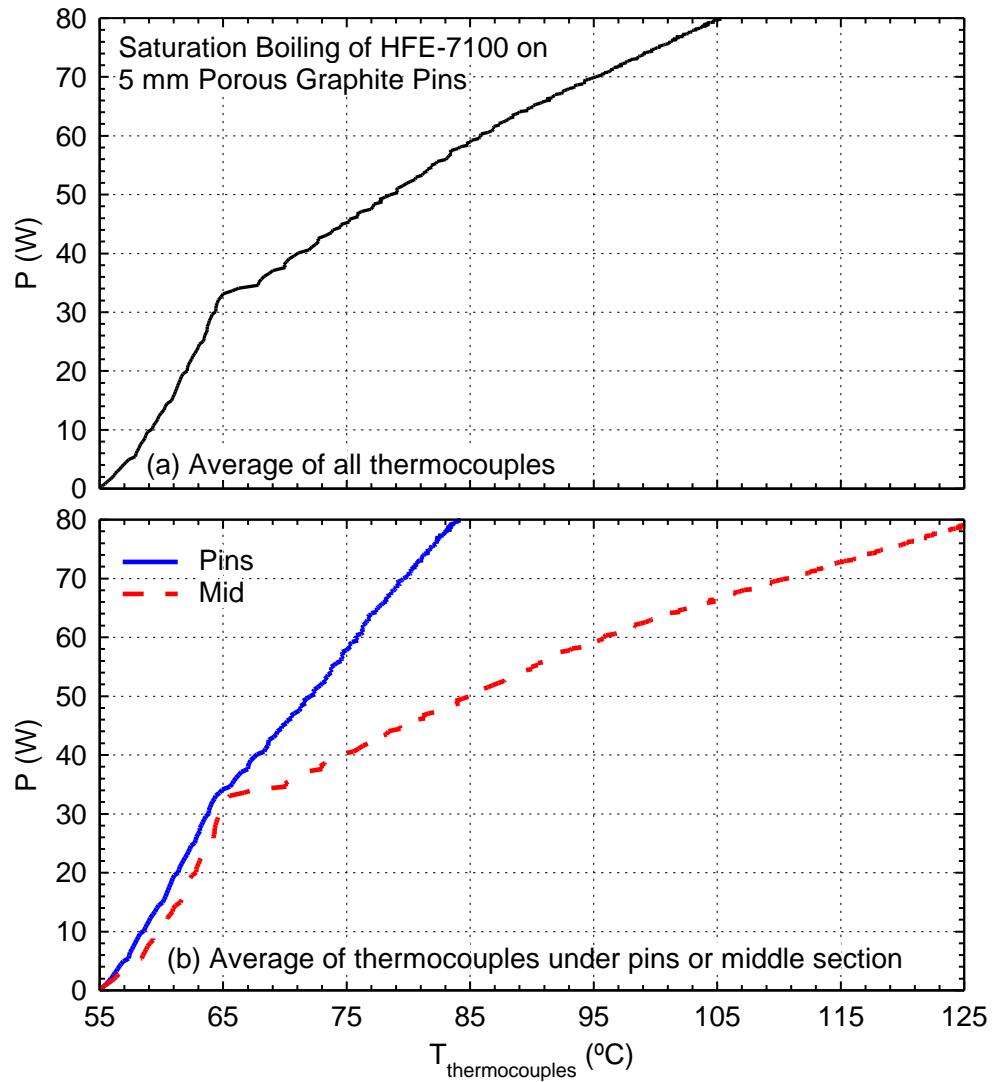


Figure 5.1 Saturation boiling curve for HFE-7100 on porous graphite with 5 mm tall corner pins.

However, the average temperature measurements of the thermocouples embedded in the porous graphite of 105 °C is much more than allowable for standard electronics cooling applications (~85 °C), but less than the limit for more robust high temperature electronics (~150 °C). Further data analysis revealed that in spite of the uniform heating of the footprint area, a large temperature difference existed between the thermocouples located underneath the corner pins and the flat portion of the boiling surface. Figure 5.1b shows a boiling curve constructed with the total power removed versus the average temperature measured by the two thermocouples underneath the corner pins and another using the measurements from the thermocouples underneath the middle or flat section. The temperatures measured by the thermocouples underneath the corner pins are always lower than that measured by those under the flat section for the same total power removed. At about 30 W, the measurements start to diverge rapidly. When the thermal power removed reaches 79.9 W, the difference between the pin and middle thermocouples was about 40 K. Such large temperature gradients could be harmful to electronics.

A thermal analysis conducted using ANSYS calculated the temperature profile inside the porous graphite with 5 mm tall corner pins. The case shown in Figures 5.2a and 5.2b is for 65 W dissipated power in saturation boiling of HFE-7100. Figure 5.2a Displays the temperature profile in the plane of the thermocouples and Figure 5.2b shows the temperature profile in a cutaway view through the pins. The calculated temperatures at the thermocouple locations underneath the corner pins and the flat portion are ~353 K (80 °C) and ~373 K (100 °C). The measured temperatures at those locations were 77 °C and 103 °C (Figure 5.1b).

The thermal conductivity of the porous graphite is anisotropic, with the thermal conductivity in the lateral direction about 30% of that in the axial direction (Poco Graphite, 2004). Underneath the corner pins, the heat is conducted through the pins and removed by boiling at the wetted surface of the pins. Under the flat portion of the porous graphite surface, although there is less thermal resistance from the thermocouple location to the wetted surface, the actual surface area is small and fewer nucleation sites per unit heated area are available. Bubble crowding between the pins also increases the local

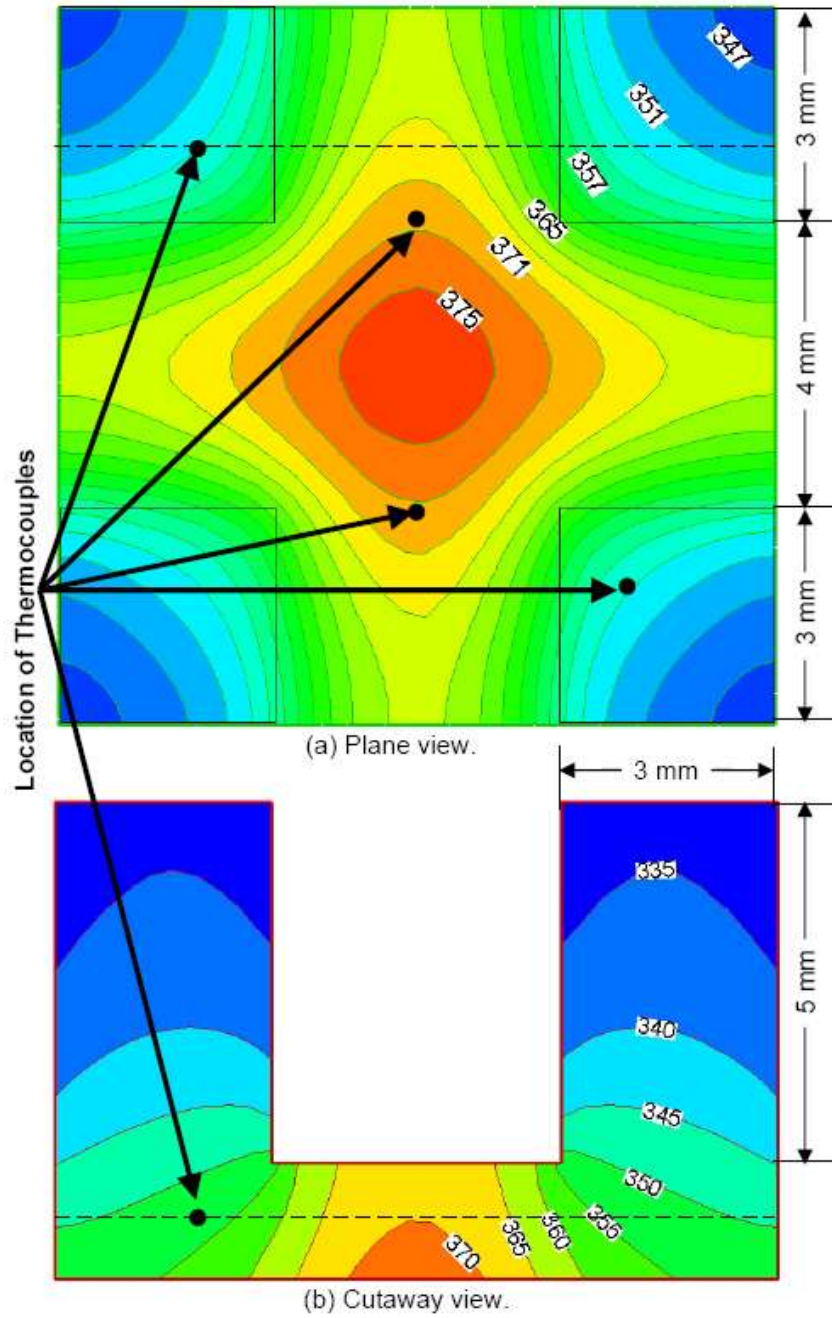


Figure 5.2 Thermal analysis of porous graphite with 5 mm corner pins at 65 W.

boiling thermal resistance in the flat portion of the porous graphite surface. Due to the relatively low lateral thermal conductivity of the porous graphite, the heat conduction toward the pins is driven by a large temperature gradient. Another concern with the porous graphite is that the section with corner pins bowed and cracked under these high thermal stress conditions (Figures 5.3a and 5.3b). Without the assistance of an additional high conductivity heat spreader (El Genk, Saber, and Parker 2005, 2007; El-Genk and Saber 2006), the use of the corner pins on porous graphite for electronics cooling is not appropriate and therefore was not investigated further. The focus in the remainder of this chapter, therefore, is on boiling heat transfer using copper surfaces with corner pins.

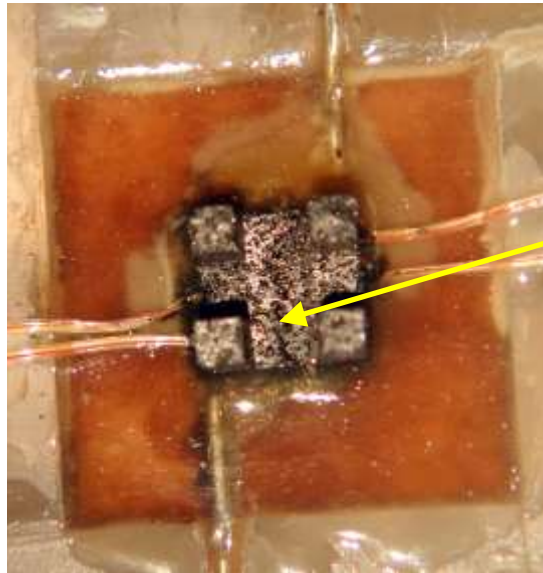
## 5.2 Natural Convection

Prior to boiling incipience, natural convection is the dominant mode of heat transfer for removing the dissipated power from the copper surface in the experiments. Since the footprint area (10 x 10 mm) of the plane copper surfaces is uniformly heated, natural convective heat flux is proportional to  $\Delta T_b^{1.2}$ . Figure 5.4 compares the natural convection data in the upward facing orientation ( $\theta = 0^\circ$ ) for the copper surfaces with corner pins with that for plane copper surface in this work and reported for plane Si and Cu surfaces by others (McNiel 1992; Chang and You 1996; Chang, You, and Haji-Sheikh 1998; Kubo, Takamatsu, and Honda 1999; Rainey, You, and Lee 2003; Wei and Honda 2003; El-Genk and Bostanci 2003; El-Genk and Parker 2005; Parker and El-Genk 2005).

For plane copper and silicon, the removed power by natural convection has been correlated as:

$$P_{NC} = 0.0314 \Delta T_b^{1.2} . \quad (5.1)$$

Figure 5.4 confirms the dependence of the power removed by natural convection on  $\Delta T_b^{1.2}$ . For the Cu surfaces with corner pins, both the actual surface area wetted by the liquid and the total thermal power removed by natural convection increase as the height of the corner pins increases. The fin effect, which increases the temperature drop along the corner pins, also increases with the pin height. This causes the total surface averaged



**Crack in surface**

(a) Top view



**Non-parallel pins**

(b) Plane view

**Figure 5.3 Photograph of test porous graphite with corner pins after tests.**

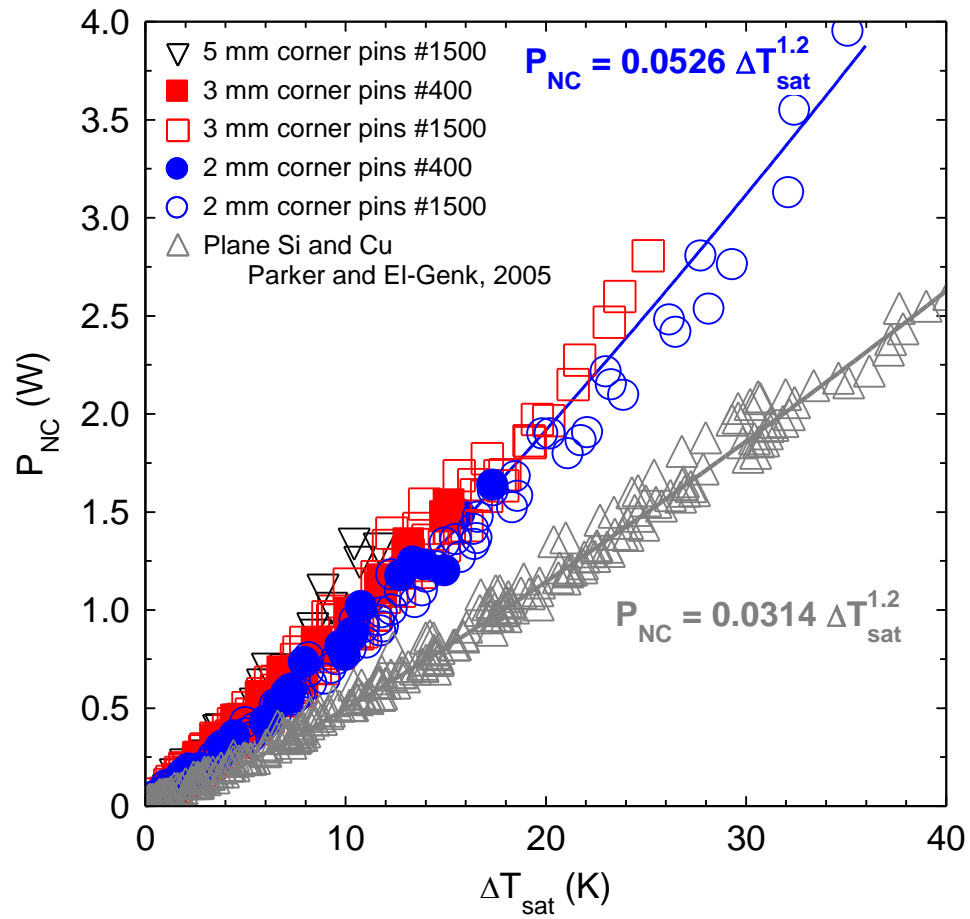


Figure 5.4 Natural convection data of plane Cu and Cu surface with corner pins

heat flux to decrease as the height of the corner pins increases. However, for consistency and since the footprint area of the copper surface with corner pins is uniformly heated, the present data for natural convection power removal, or the heat flux based on the footprint area, is also correlated (Figure 5.4) in terms of the footprint surface superheat raised to the 1.2 power as:

$$P_{NC} = 0.0526 \Delta T_b^{1.2}. \quad (5.2)$$

This correlation is within  $\pm 12\%$  of the present natural convection data for Cu surface with corner pins of different heights.

Although the total thermal power removed by natural convection from the surfaces with 3 x 3 mm corner pins are on average 67.5% higher than from the plane surfaces of the same foot print area (10 x 10 mm) at the same surface superheat,  $\Delta T_p$ , the actual total surface average heat flux decreases as the height of pins increases. For the 2 mm, 3 mm and 5 mm pins, the actual surface area is 96%, 144% and 240% higher than the footprint area (1 cm<sup>2</sup>).

The correlations given by equations (5.1) and (5.2) would be useful in cooling applications of computer chips while in the standby or sleeping mode, in which the thermal power removal requirement is typically < 3 W. At such low thermal power, the Cu surfaces with corner pins would be more that 20 K cooler than plane surfaces (Figure 5.4), resulting in a much lower junction temperatures. For the same surface superheat, there is a 68% increase in removed power from the surfaces with corner pins compared to plane surfaces (Figure 5.4).

### **5.3 Nucleate Boiling**

The saturation boiling curve delineated in Figure 5.5 shows the three distinct boiling regimes, as discussed earlier for plane surfaces (Section 4.2). The embedded photographs show that in the discrete bubbles regime (Region I) there is little coalescence of departing bubbles. Because not all potential nucleation sites are active, there is a larger increase in the superheat of the footprint surface as the input power increases,

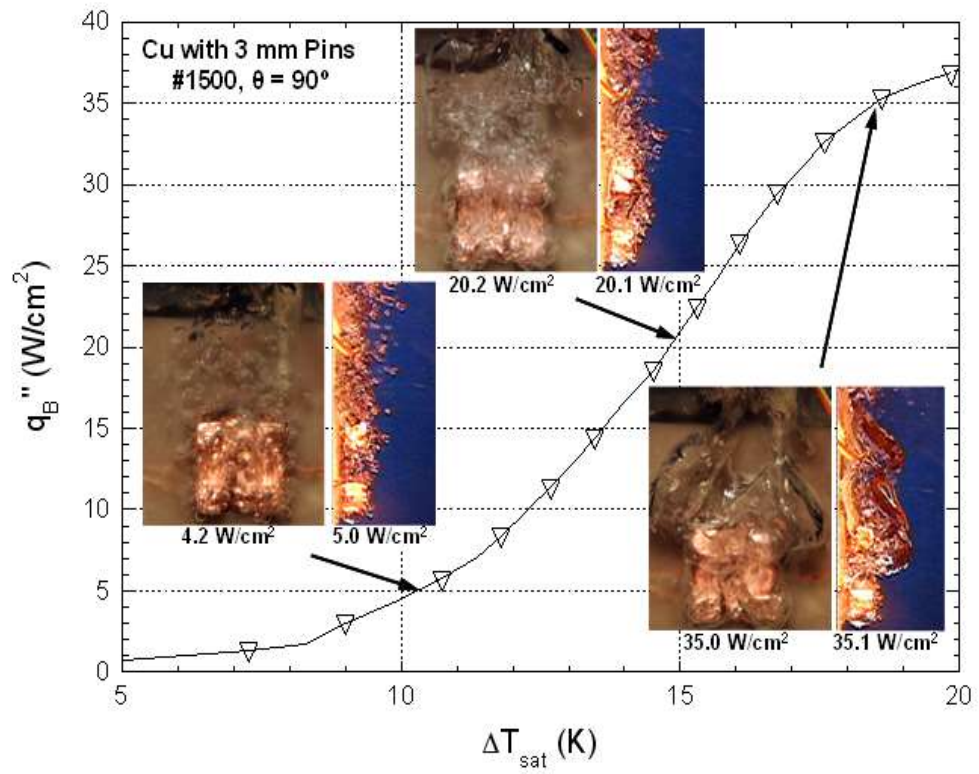


Figure 5.5 Saturation boiling curve for a Cu surface with 3 mm corner pins at  $\theta = 90^\circ$

compared to the subsequent regime of fully developed nucleate boiling (Region II). Near the end of this regime (II), all potential nucleation sites are active and the increase in surface superheat is small as the input power increases. In Region III, lateral coalescence of departing bubbles becomes increasingly more intense as the input power increases, resulting in a relatively larger increase in the surface superheat than in the discrete bubbles regime (II).

Figure 5.6a compares the obtained saturation pool boiling curves on plane and extended copper surfaces in the upward facing orientation. The indicated enhancements in the power removed from the copper surfaces with corner pins are mostly due to the increase in the total surface area wetted by the liquid and increase linearly with the height of the pins, while other effects also influence boiling from the surfaces with corner pins. Since the pins effectively function as fins, increasing the pin height lowers the fin efficiency and results in a smaller increase in the total thermal power removed by nucleate boiling. Furthermore, nucleate boiling on the vertical sides of the pins is less effective than on the flat top and in the area between the pins, reducing the rate of increase in the removed power as the height of the pins increases. Conversely, departed and growing bubbles enhance mixing as they pass near the pins' surfaces, reducing the thermal boundary layer and increasing the convective heat transfer. The net result of these competing effects as well as of increasing the wetted surface area as the height of the corner pins increases is reflected in the boiling curves in Figure 5.6a.

This figure shows that for the same superheat of the footprint surface, increasing the height of the corner pins increases the total power removed. The removed thermal power at CHF (the last data point of the boiling curves) also increases, but at a higher superheat of the footprint surface. There is a 36.5 K excursion in the temperature of the plane copper surface prior to boiling incipience (Figure 5.6a and 5.6b), versus little or no temperature excursion on the surfaces with corner pins. It is worth noting that nucleate boiling heat flux and CHF, when based on the total area of the Cu surfaces with corner pins, are significantly lower than on the plane Cu surface (Figure 5.6b).

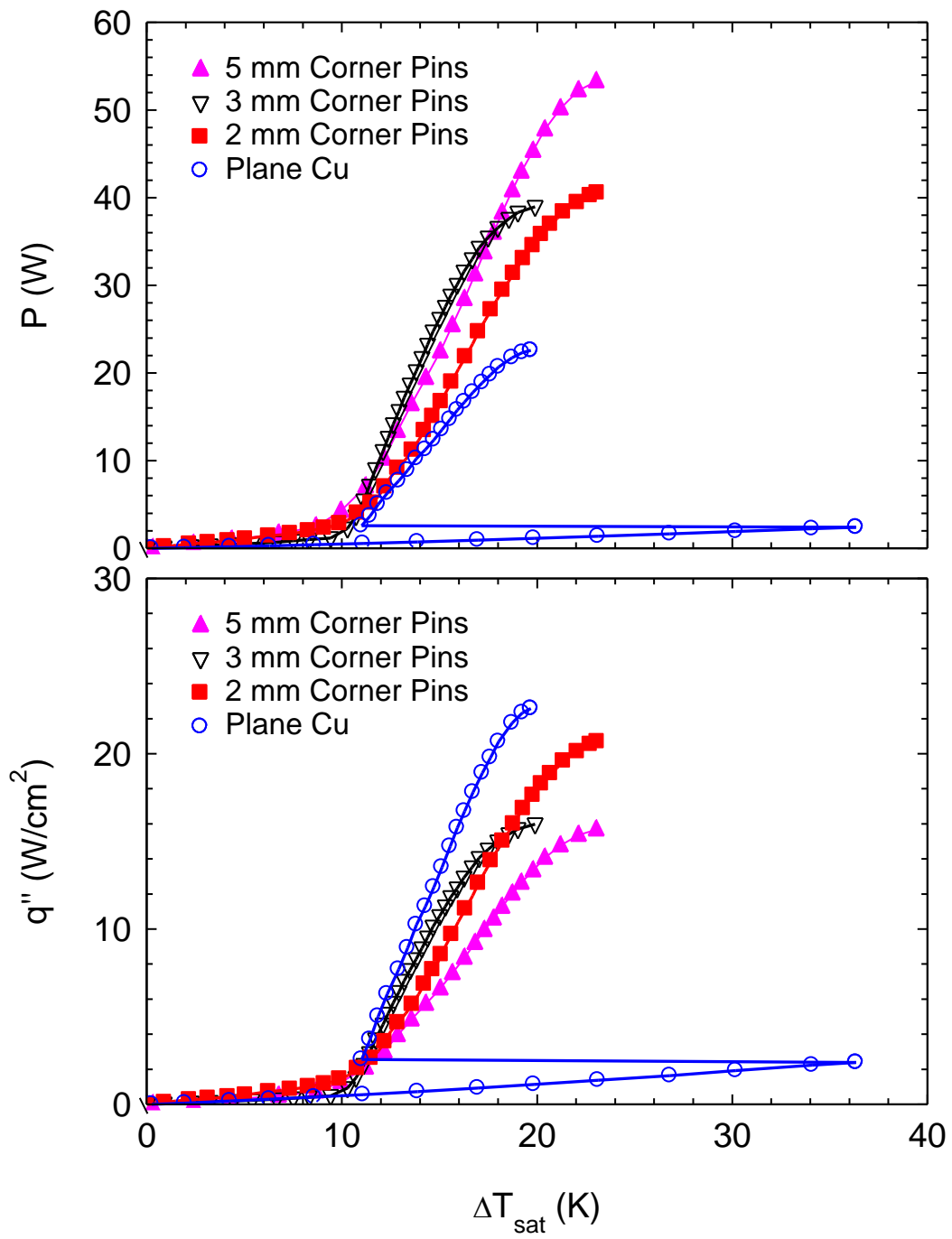


Figure 5.6 Effect of pin height on saturation boiling of HFE-7100 on plane Cu and Cu surfaces with corner pins.

### 5.3.1 Effect of Surface Orientation

The saturation pool boiling curves on plane and extended copper at different orientations are compared in Figure 5.7. From this figure, it is evident that the presence of corner pins affects saturation boiling heat transfer in HFE-7100. For all surface inclinations, the corner pins enhance the removed thermal power by nucleate boiling, mostly because of the increase in surface area wetted by the liquid. For the plane surface (Figure 5.7a), at low surface superheat ( $< \sim 12$  K) the boiling heat transfer rate is higher at high inclination angles. For high surface superheats, boiling heat transfer rates increase as the surface inclination increases. The same trend is observed for surfaces with 2 mm and 3 mm tall corner pins (Figures 5.7b and 5.7c). For the surface with 5 mm tall pins, (Figure 5.7d), there is no clear trend for the changes in the nucleate boiling heat transfer rate at low surface superheats as the surface orientation changes. However, at high superheats, the nucleate boiling heat transfer rate is lower for higher inclination angles.

The presence of corner pins reduces the penalty of increasing the surface inclination on the nucleate boiling heat transfer rate and CHF. For example, on the plane copper surface, the power removed by nucleate boiling at 18 K superheat is 20.6 W in the upward facing orientation, 18.6 W for the vertical orientation, and 13.9 W for  $\theta = 150^\circ$ , representing a decrease in the removed power of 14% and 36%, respectively. For the surface with 5 mm tall corner pins, the removed power by nucleate boiling at 18 K superheat is 37.2 W in the upward facing orientation, 35.5 W for  $90^\circ$  (4% decrease), 31.4 for  $150^\circ$  (15% decrease), and for the downward facing orientation, the decrease in removed power by nucleate boiling is only to 30.1 W (19% decrease).

### 5.3.2 Nucleate Boiling Heat Transfer Coefficient

Figure 5.8 presents the obtained results of the nucleate boiling heat transfer coefficient that is based on the heated footprint ( $h_B$ ) and shows the effect of surface inclination on  $h_B$ . The values of  $h_B$  are calculated by dividing the total power removed during nucleate boiling by the quantity of the temperature difference between the wall and the bulk pool ( $T_w - T_b$ ) and the heated footprint area ( $1 \text{ cm}^2$ ). On all surfaces and at

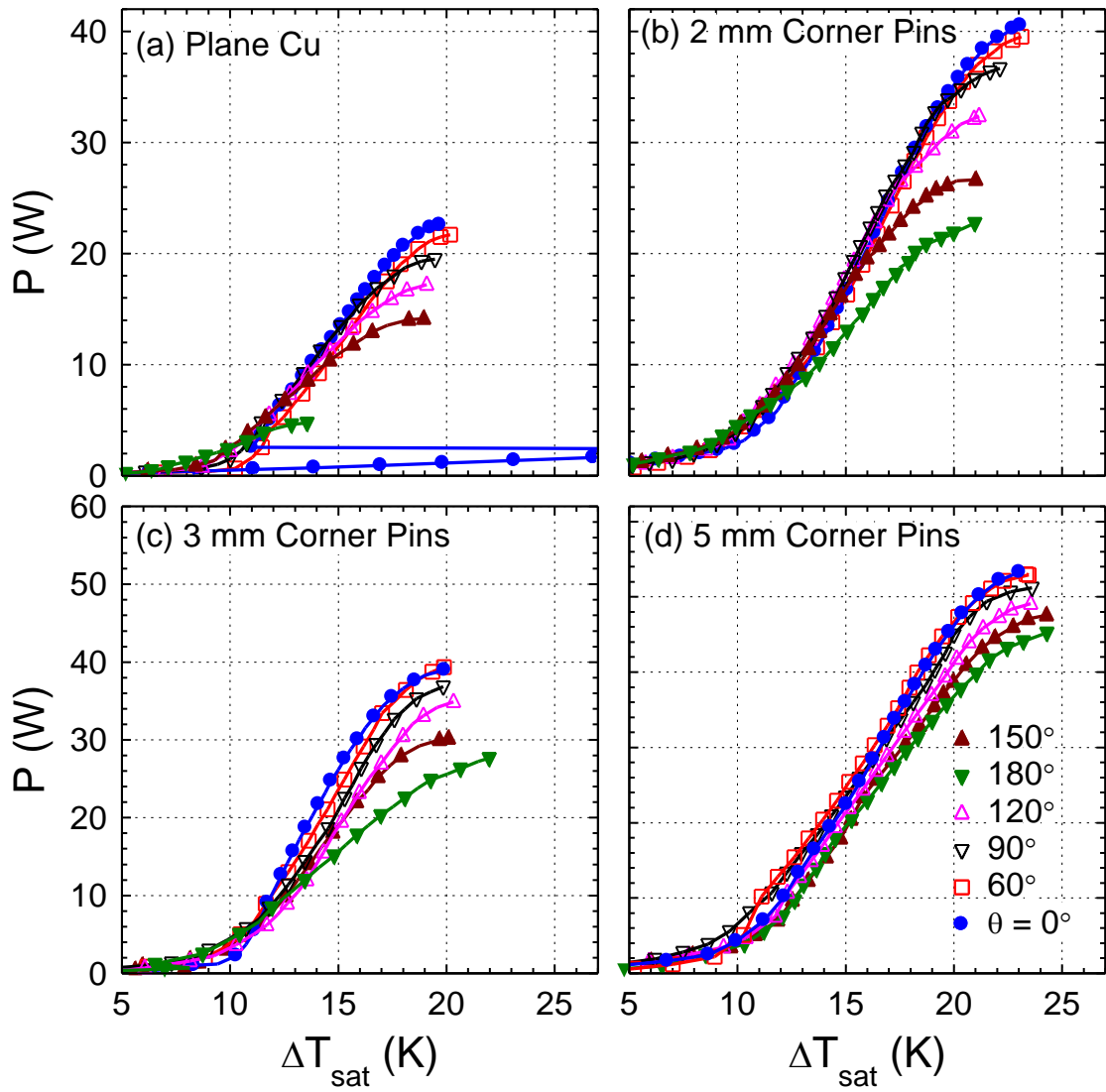


Figure 5.7 Saturation boiling curves for HFE-7100 at different surface inclinations.

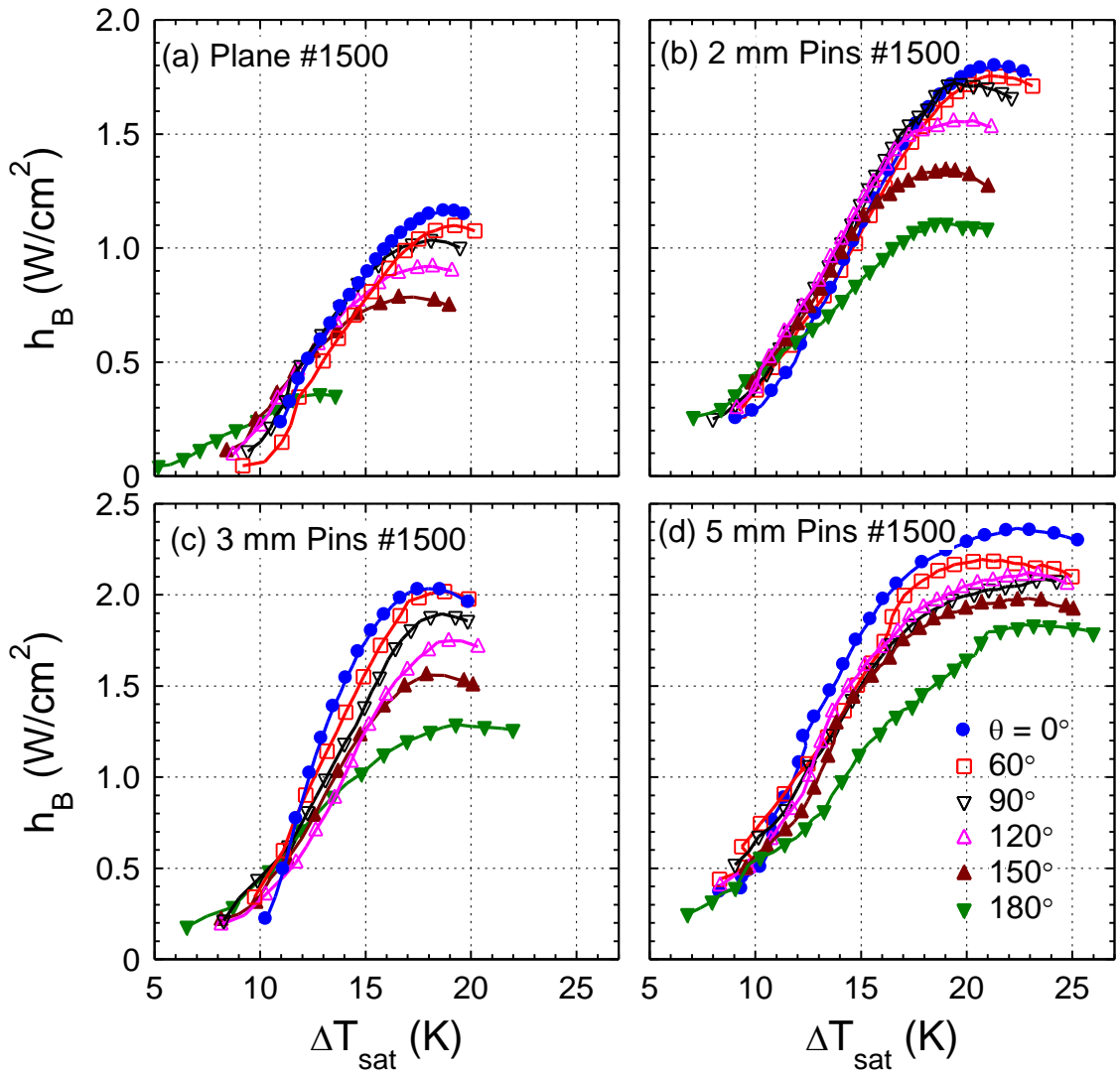


Figure 5.8 Effect of surface orientation on nucleate boiling heat transfer coefficient for saturation boiling of HFE-7100 on copper corner pins.

all inclination angles, the nucleate boiling heat transfer coefficient increases with increasing surface superheat till it reaches a peak, then gradually decreases until CHF. The peak nucleate boiling heat transfer coefficient,  $h_B^*$  occurs near the transition from boiling region II (fully developed nucleate boiling) to boiling region III (region of lateral bubble coalescence). At this point, bubbles begin to coalesce near the heated surface and reduce the nucleate boiling heat transfer rate.

For the plane surface, increasing the orientation angle significantly decreases both  $h_B^*$  and the corresponding surface superheat (Figure 5.8a), particularly for  $\theta > 90^\circ$ . On the surfaces with corner pins, the decreases in  $h_B^*$  with increased inclination angle are much smaller and the changes in the corresponding surface superheat are within a few degrees (Figure 5.8b – d). In the upward facing orientation,  $h_B^*$  on the plane surface is 1.18 W/cm<sup>2</sup> K, compared to 1.85, 2.02, and 2.38 W/cm<sup>2</sup> K on the surfaces with 2, 3, and 5 mm tall corner pins. In the downward-facing orientation,  $h_B^*$  decreases to 0.35 W/cm<sup>2</sup> K (~ 70% decrease), while those on the surfaces with the 2, 3, and 5 mm tall corner pins decrease only to 1.15, 1.3, 1.9 W/cm<sup>2</sup> K (a decrease of ~ 38%, 36%, and 20%, respectively). These results clearly demonstrate the advantage of the surfaces with corner pins. They not only increase the total power removed from the underlying computer chips, but also reduce the penalty of increasing the orientation angle of the CPU, in terms of decreasing the total power dissipated and increasing the surface temperature (< 10 K).

Figures 5.9a - c compare the obtained curves for  $h_B$  on plane and pinned surfaces at inclination of 0°, 90°, and 180°, and show that increasing the pin height increases  $h_B$  and  $h_B^*$ , and generally decreases the surface temperature corresponding to the later, by a few degrees. For the surfaces with corner pins, the nucleate boiling heat transfer coefficient based, on the total wetted area by the liquid,  $\bar{h}$ , are lower than those on plane copper, and decrease as the pin height increases (Figures 5.9d – f). The values of  $\bar{h}$  are calculated using the wetted surface area (1.96 cm<sup>2</sup> for 2 mm pins, 2.44 cm<sup>2</sup> for 3 mm pins, and 3.4 cm<sup>2</sup> for 5 mm pins), instead of the heated footprint area (1 cm<sup>2</sup>). Figure 5.9a shows that for a given surface superheat,  $h_B$  increases with increasing pin height. Conversely, Figure 5.9d shows that  $\bar{h}$  is lowest for the surfaces with the tallest corner

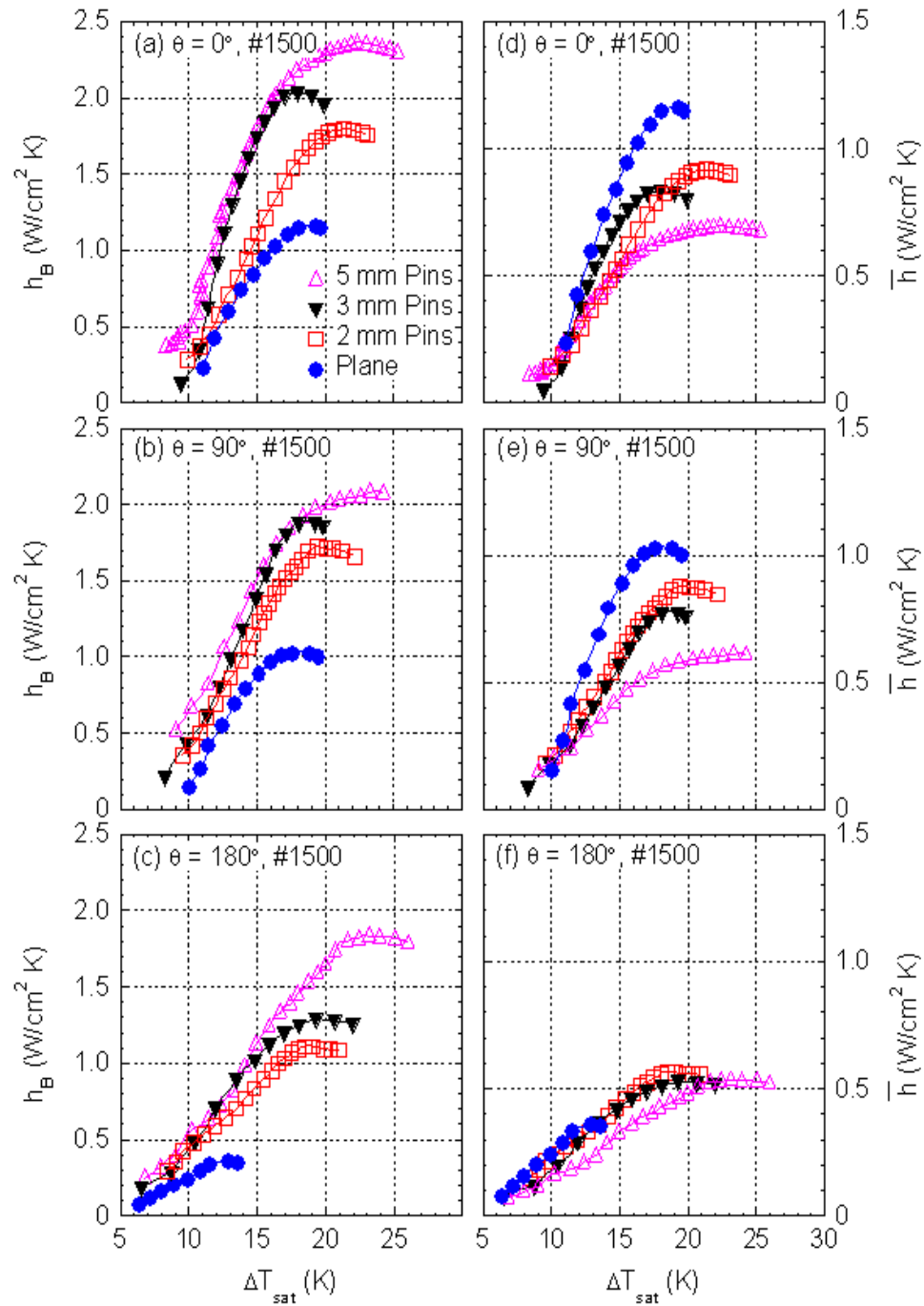
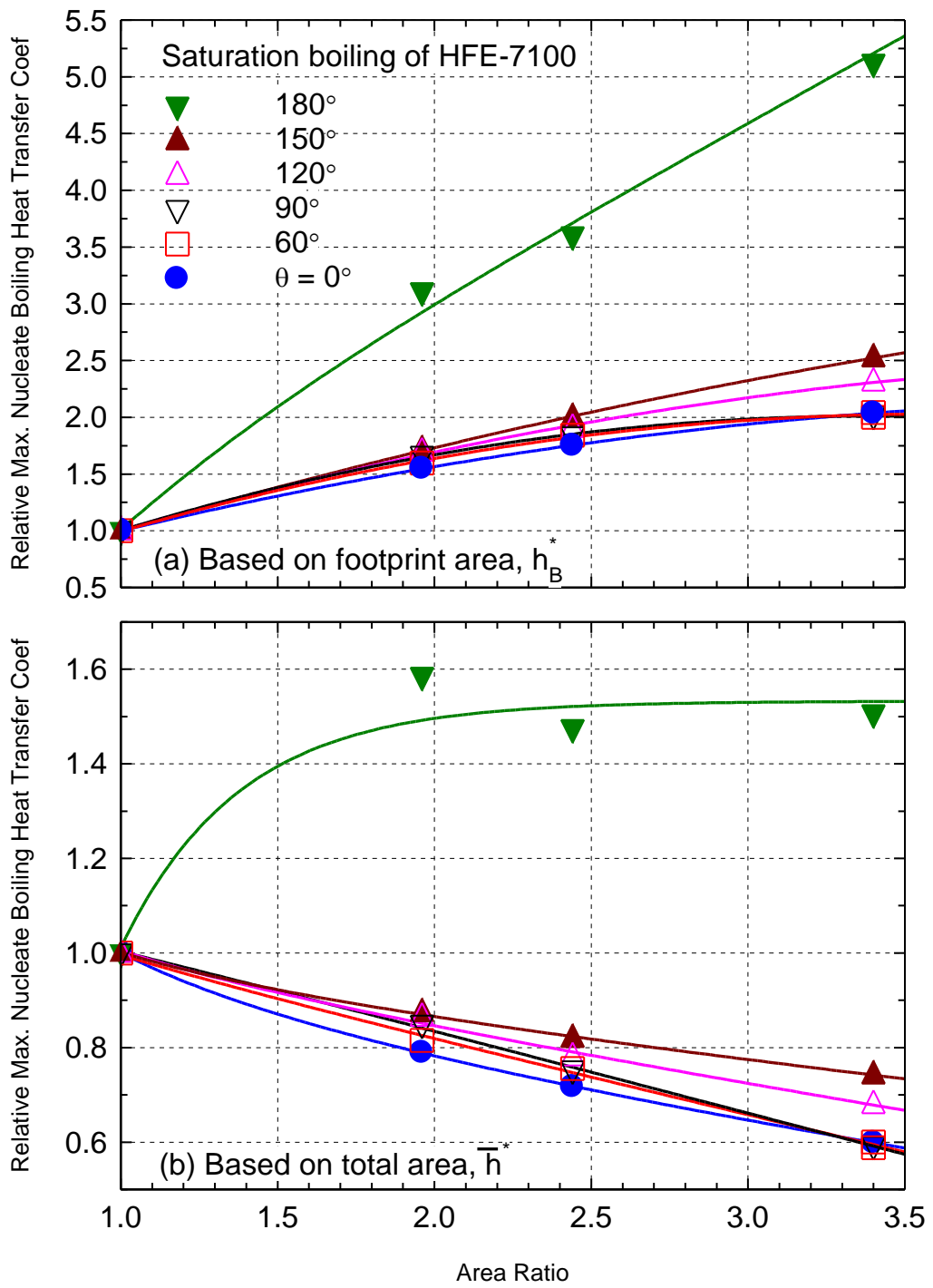


Figure 5.9 Effect of pin height and orientation on the nucleate boiling heat transfer coefficient.

pins. Although the total power removed by nucleate boiling increases as the height of the corner pins increases, the low values of  $\bar{h}$  could be caused by the fin effect of the pins, less efficient boiling on the vertical sides of pins, and bubble interference from the rising bubbles past the pins. The bubbles departing from the pins' sides interfere with those departing from the plane portion of the surface between the pins. This effect is most prominent in the upward facing orientation. On the other hand, this same effect increases mixing on the inclined surfaces, causing the nucleate boiling heat transfer coefficient to decrease less with increased surface inclination.

Figure 5.10 compares the changes in the peak values of the saturation nucleate boiling heat transfer coefficients based on both the heated footprint,  $h_B^*$ , and the wetted area,  $\bar{h}^*$ , on the copper surfaces with corner pins. The results are plotted relative to those on the plane copper surface at the same surface inclination versus the ratio of the wetted area. An area ratio of 1.0 represents the plane copper surface. The area ratio increases as the height of the corner pins increases. As shown in Figure 5.10a,  $h_B^*$  increases monotonically with increased height of the corner pins or the wetted area ratio. In the upward facing orientation ( $0^\circ$ ) it is as much as 2 times that on the plane surface. Increasing the inclination to  $90^\circ$  insignificantly changes  $h_B^*$ , but at a  $150^\circ$   $h_B^*$  for the Cu surfaces with 3 and 5 mm tall corner pins is 1.9 and 2.5 times that on the plane surface. The largest increases in  $h_B^*$  with increased pin height occur in the downward facing orientation ( $180^\circ$ ). In this orientation,  $h_B^*$  for the surfaces with 2 and 5 mm tall corner pins is  $\sim 3$  and 5 times that on the plane surface.

Conversely, for all angles, except  $180^\circ$ ,  $\bar{h}^*$  decreases as the height of the corner pins increases (Figure 5.10b); the decrease in  $\bar{h}^*$  is most significant in the upward facing orientation ( $\theta = 0^\circ$ ). In this orientation,  $\bar{h}^*$  for the copper surfaces with 2, 3, and 5 mm tall pins is 79%, 72% and 60% of that for the plane surface. In the  $150^\circ$  inclination,  $\bar{h}^*$  for the copper surfaces with 2, 3, and 5 mm tall corner pins is 87%, 82%, and 74% of that on the plane surface. In the downward facing orientation, however,  $\bar{h}^*$  for the surfaces with corner pins of different heights is about 1.5 times of that on the plane surface.



**Figure 5.10** Effect of the corner pin height on saturation nucleate boiling heat transfer coefficients based on footprint and total area.

The peak saturation nucleate boiling heat transfer coefficients, based on the footprint and the total wetted area, are compared in Figure 5.11a versus inclination. Those normalized to the measured values in the upward facing orientation are presented in Figure 5.11b. For both the plane and extended surfaces used in the present work,  $h_B^*$  decreases with increased inclination to its lowest value in the downward facing orientation. Increasing the height of the corner pins reduces the fractional decrease in  $h_B^*$  with increased inclination. Figure 5.11b indicates that  $h_B^*$  for the surface with 5 mm corner pins in the downward facing orientation, ( $\theta = 180^\circ$ ) is 79% of that in the upward facing orientation ( $\theta = 0^\circ$ ), compared to only 31% for the plane surface. Although the values of  $h_B^*$  differ for the different pin heights (Figure 5.11a), the relative decrease with increasing inclination is nearly identical between the surfaces with 2 mm tall corner pins and 3 mm tall corner pins (Figure 5.11b).

### 5.3.3 Effect of Surface Roughness

A study of the effect of surface roughness on nucleate boiling on copper surfaces with corner pins is conducted using surfaces prepared with #400 emery paper (average groove width  $\sim 6 \mu\text{m}$ ) and #1500 emery paper (average groove width  $\sim 1.7 \mu\text{m}$ ). SEM images of surfaces prepared with each grade of emery paper are shown in Figures 5.12a and 5.12b. Figure 5.13 compares the results of the effect of roughness on the boiling curves for the surface with 3 mm tall corner pins at three inclinations. The nucleate boiling heat transfer rate and CHF on the coarse surfaces prepared with #400 emery papers are slightly higher than for the surfaces with a finer finish, prepared with #1500 emery papers. The difference increases as the inclination angle increases, and is largest in the downward-facing orientation ( $180^\circ$ ). Figures 5.14a and 5.14b show that the peak nucleate boiling heat transfer coefficient,  $h_B^*$ , for the surfaces with 2 mm and 3 mm tall pins and prepared with #400 paper are consistently  $\sim 12$  to 25% higher than for the finer finish surfaces. Surface roughness, however, does not appear to affect the decreases in  $h_B^*$  relative to those in upward facing orientation (Figure 5.14c and d). Such decreases are smaller for the surface with 3 mm tall pins than for the surface with the 2 mm tall corner pins.

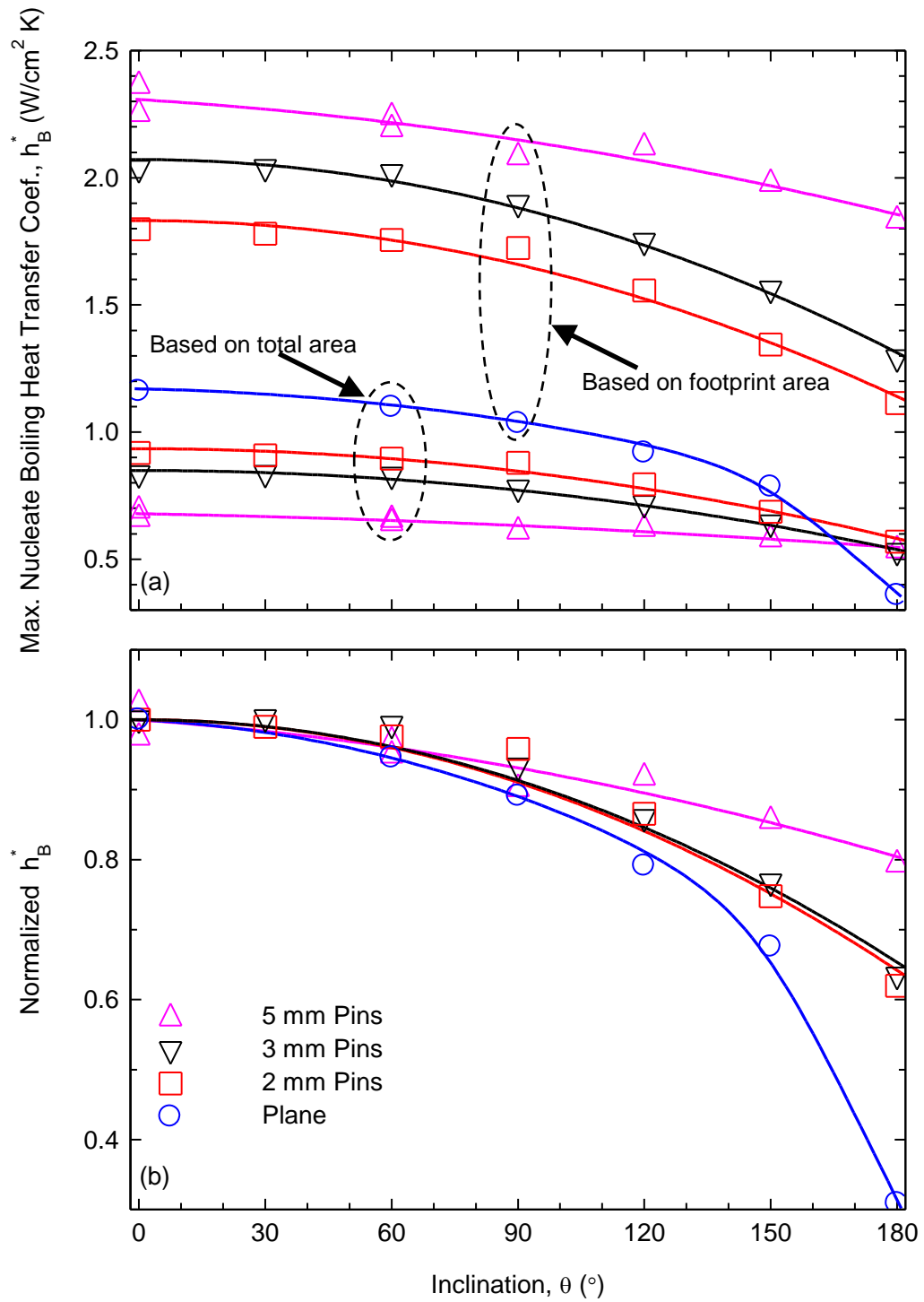
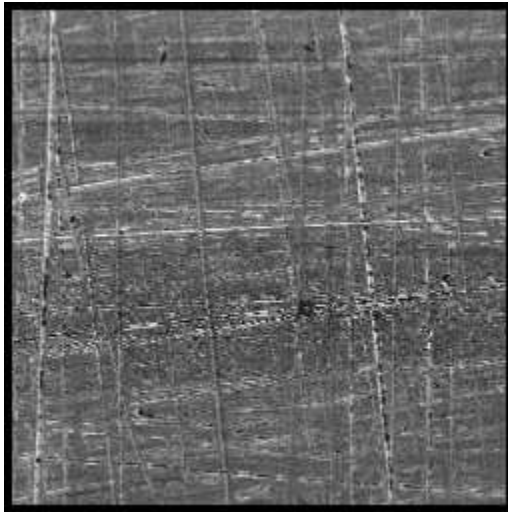
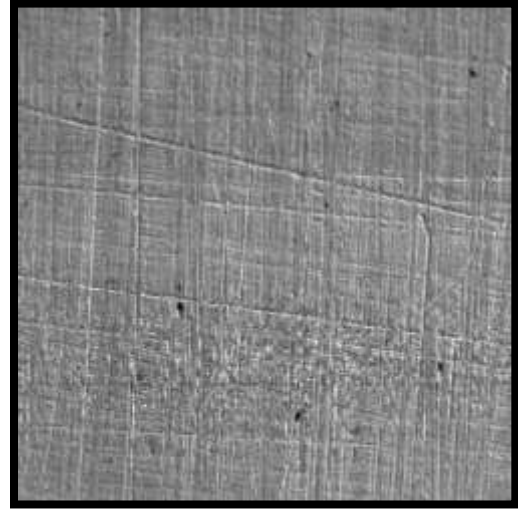


Figure 5.11 Effect of surface orientation on  $h^*$  based on footprint and total area.



(a) Prepared with #400 Emery Paper.



(b) Prepared with #1600 Emery Paper.

**Figure 5.12 SEM images of copper surfaces.**

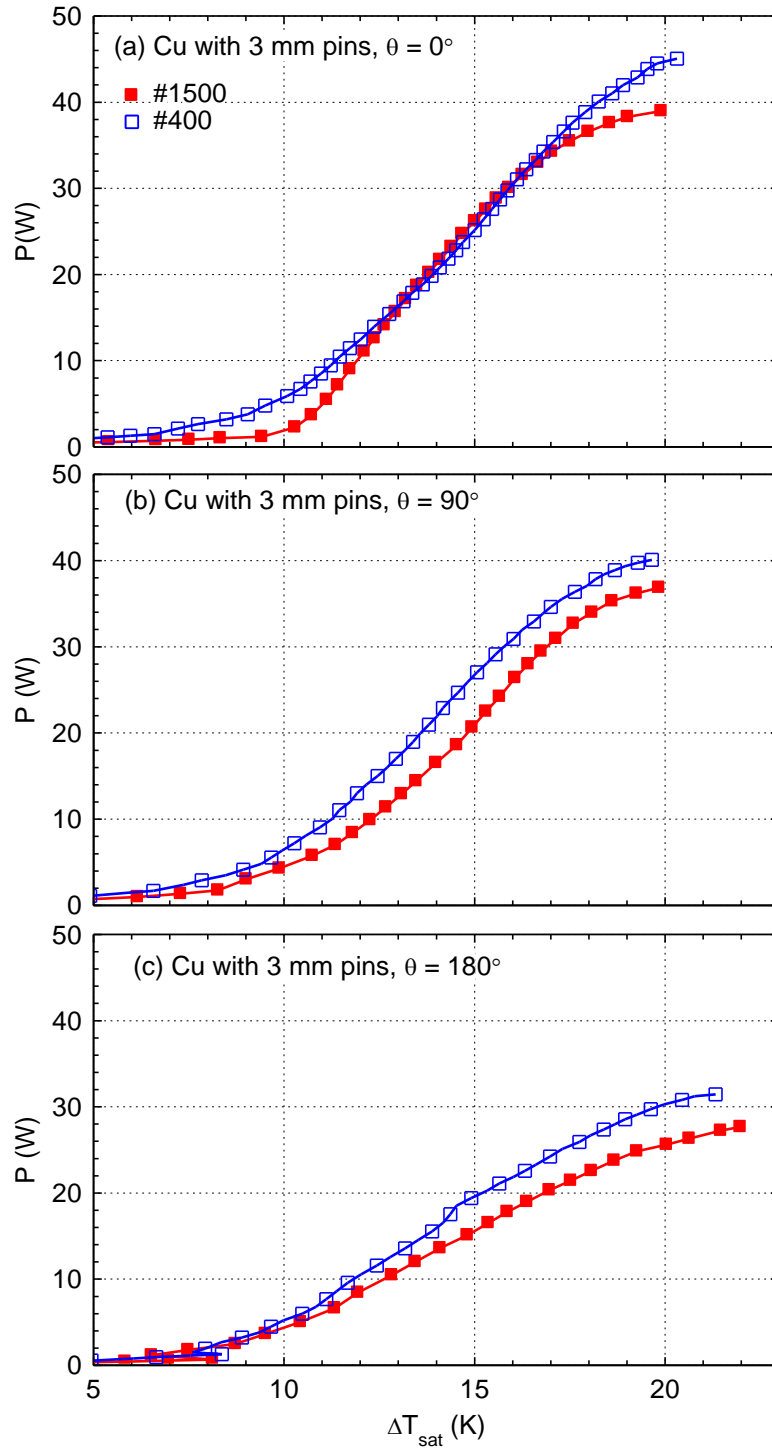


Figure 5.13 Effect of surface roughness on nucleate boiling on Cu surfaces with corner pins.

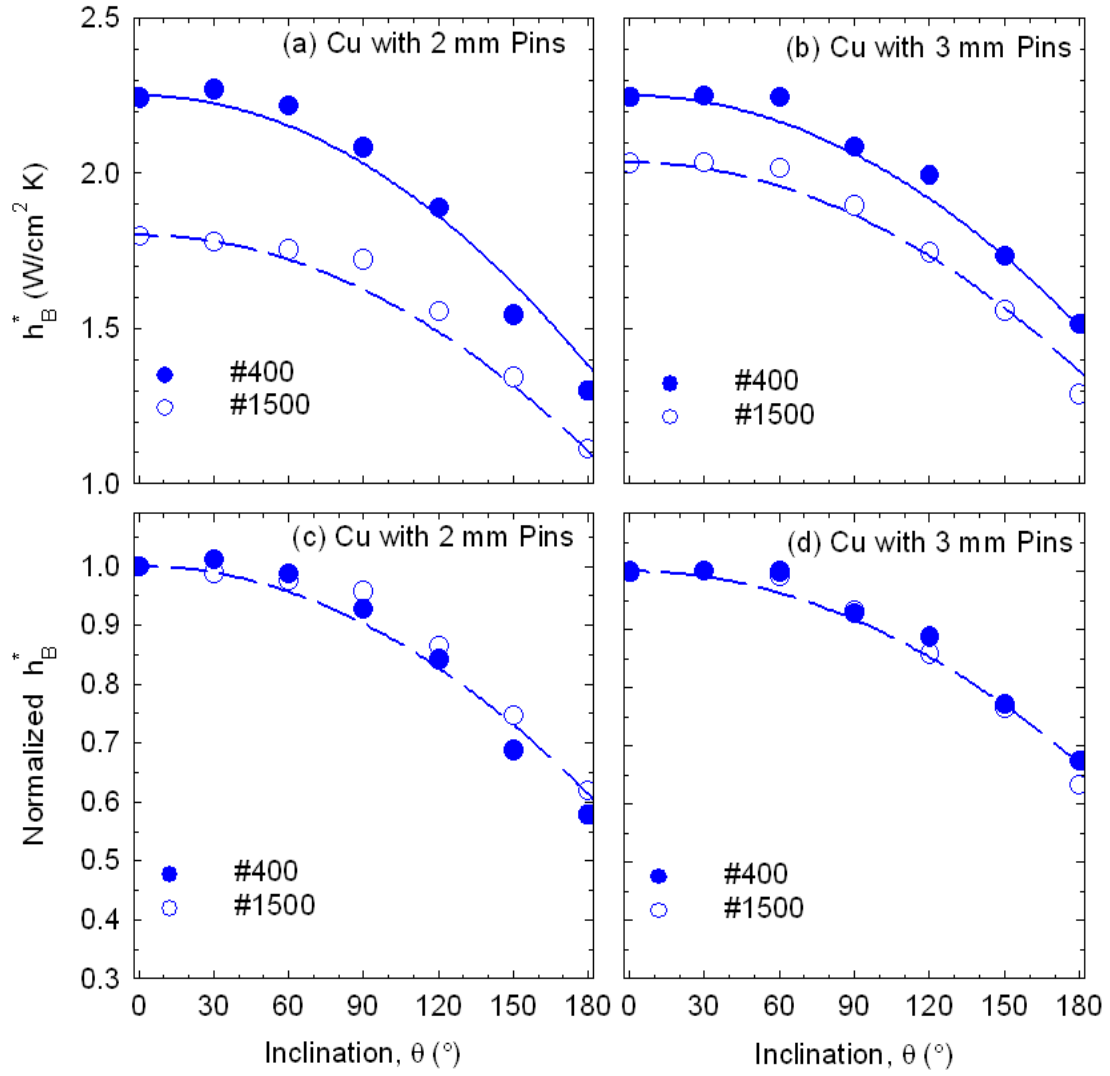


Figure 5.14 Effect of surface orientation and surface roughness on  $h^*$ .

### 5.3.4 Effect of Liquid Subcooling on Nucleate Boiling

On plane surfaces, nucleate boiling heat transfer of dielectric liquids is affected by the liquid subcooling (Sections 4.2.1 and 4.3.1). Subcooled HFE-7100 liquid on both plane copper and porous graphite shifted the boiling curves toward lower surface superheats and substantially increased the critical heat flux. These trends were observed for all surface orientations. A series of experiments are performed with subcooled HFE-7100 on plane and extended copper surfaces. The liquid subcooling is 10 K, 20 K, and 30 K and the tests are conducted at surface inclinations of  $\theta = 0^\circ, 60^\circ, 90^\circ, 120^\circ, 150^\circ,$  and  $180^\circ$ .

Figure 5.15 compares the boiling curves for the plane copper and the copper surface with 5 mm corner pins in saturation and 30 K subcooled boiling at  $\theta = 0^\circ, 90^\circ, 150^\circ,$  and  $180^\circ$ . As the liquid subcooling increases, the removed thermal power at CHF increases, as does the superheat at CHF. For the surface with 5 mm pins, the thermal power removed at CHF is as much as 93 W at  $\Delta T_{\text{sub}} = 30$  K, compared to only 53 W for saturation boiling. As indicated earlier, there is little or no excursion in the footprint temperature prior to boiling incipience.

The presence of the corner pins greatly reduces the penalty of increasing inclination on the reduction in both the nucleate boiling heat transfer coefficient and CHF. Generally, the removed thermal power by nucleate boiling at low surface superheats increases slightly with increased surface inclination; the highest values are for the downward facing orientation ( $\theta = 180^\circ$ ). For the copper surface with 5 mm tall corner pins, the thermal power removed at CHF of 30 K subcooled HFE-7100 decreases from 93 W at  $0^\circ$  to only 86 W at  $180^\circ$ . Conversely, at higher surface superheats, the thermal power removed by nucleate boiling increases with decreased inclination; the highest is in the upward-facing orientation ( $\theta = 0^\circ$ ). The thermal power removed at CHF increases with decreased surface inclination and is highest at  $\theta = 0^\circ$ . The corresponding surface superheat is sensitive to the surface orientation, with a relatively large uncertainty of  $\pm 4$  K. Considering such uncertainties, the results in Figure 5.15 suggest that the surface temperature at CHF changes slightly with surface inclination, but increases as the height

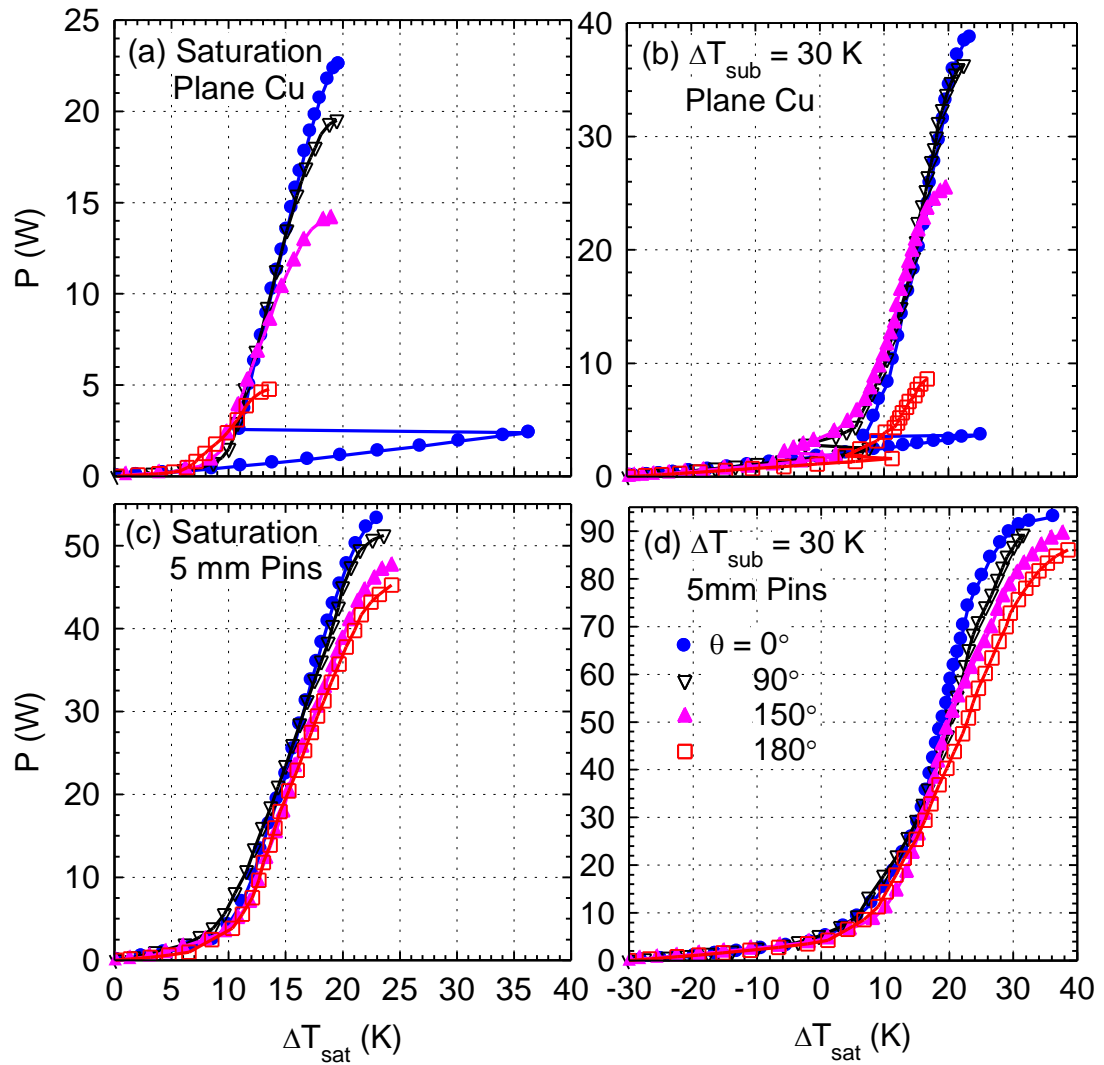


Figure 5.15 Saturation boiling curves for HFE-7100 on copper with different lengths of corner pins and at different inclinations.

of the corner pins increases; the same is also true for CHF. Increasing the liquid subcooling also increases the average temperature of the footprint area at CHF by  $\sim 3 - 5$  K for the plane copper surface and by as much as 15 K for the surface with 5 mm tall corner pins.

The effect of liquid subcooling on nucleate boiling on the surfaces with corner pins is more clearly seen in representative samples of the data, shown in Figure 5.16. All of the boiling regimes, namely; the discrete bubble regime, the fully developed nucleate boiling regime, and the regime of bubble coalescence, are distinctly shown in the boiling curves. Figures 5.16a – d show the boiling curves for plane copper and the copper surfaces with corner pins 2 mm, 3 mm, and 5 mm tall in the upward facing orientation ( $0^\circ$ ). Figures 5.16e – h show the corresponding pool boiling curves for the vertical orientation ( $90^\circ$ ). As liquid subcooling increases, the fully developed nucleate boiling regime extends to higher heat fluxes and increased total thermal power removed. Bubbles detaching from the surface pass through the superheated thermal boundary layer and upon entering the subcooled liquid pool condense and eventually disappear. This in turn reduces the bubble crowding and allows liquid replenishment on the surface, and delays the onset of CHF in subcooled boiling.

The values of CHF and the corresponding superheats increase with increased pin height and liquid subcooling. For  $\theta = 0^\circ$ , CHF on the plane surface (Figure 5.16a) for  $\Delta T_{sub} = 0^\circ$  is  $22.6 \text{ W/cm}^2$  at a superheat of 19.7 K. With a liquid subcooling of 20 K CHF increases to  $34.9 \text{ W/cm}^2$  and the corresponding footprint superheat increases slightly to 22.0 K. In the vertical orientation (Figure 5.16e), the values of CHF and  $\Delta T_{sat}$  at CHF for saturation and 20 K subcooled boiling of HFE-7100 are  $19.5 \text{ W/cm}^2$  and 19.5 K and  $32.3 \text{ W/cm}^2$  and 22.3 K, respectively. Similar results are shown for the other copper surfaces with corner pins. For example, for the surface with 3 mm corner pins facing upward (Figure 5.16c), CHF for saturation and 20 K subcooled boiling are  $39.0 \text{ W/cm}^2$  ( $\Delta T_{sat} = 19.9 \text{ K}$ ) and  $57.6 \text{ W/cm}^2$  ( $\Delta T_{sat} = 24.8 \text{ K}$ ), respectively. Increasing the inclination angle to  $90^\circ$  decreases CHF to  $36.9 \text{ W/cm}^2$  ( $\Delta T_{sat} = 19.8 \text{ K}$ ) and  $57.0 \text{ W/cm}^2$  ( $\Delta T_{sat} = 26.3 \text{ K}$ ). Increasing the liquid subcooling to 30 K increases the footprint superheat at CHF

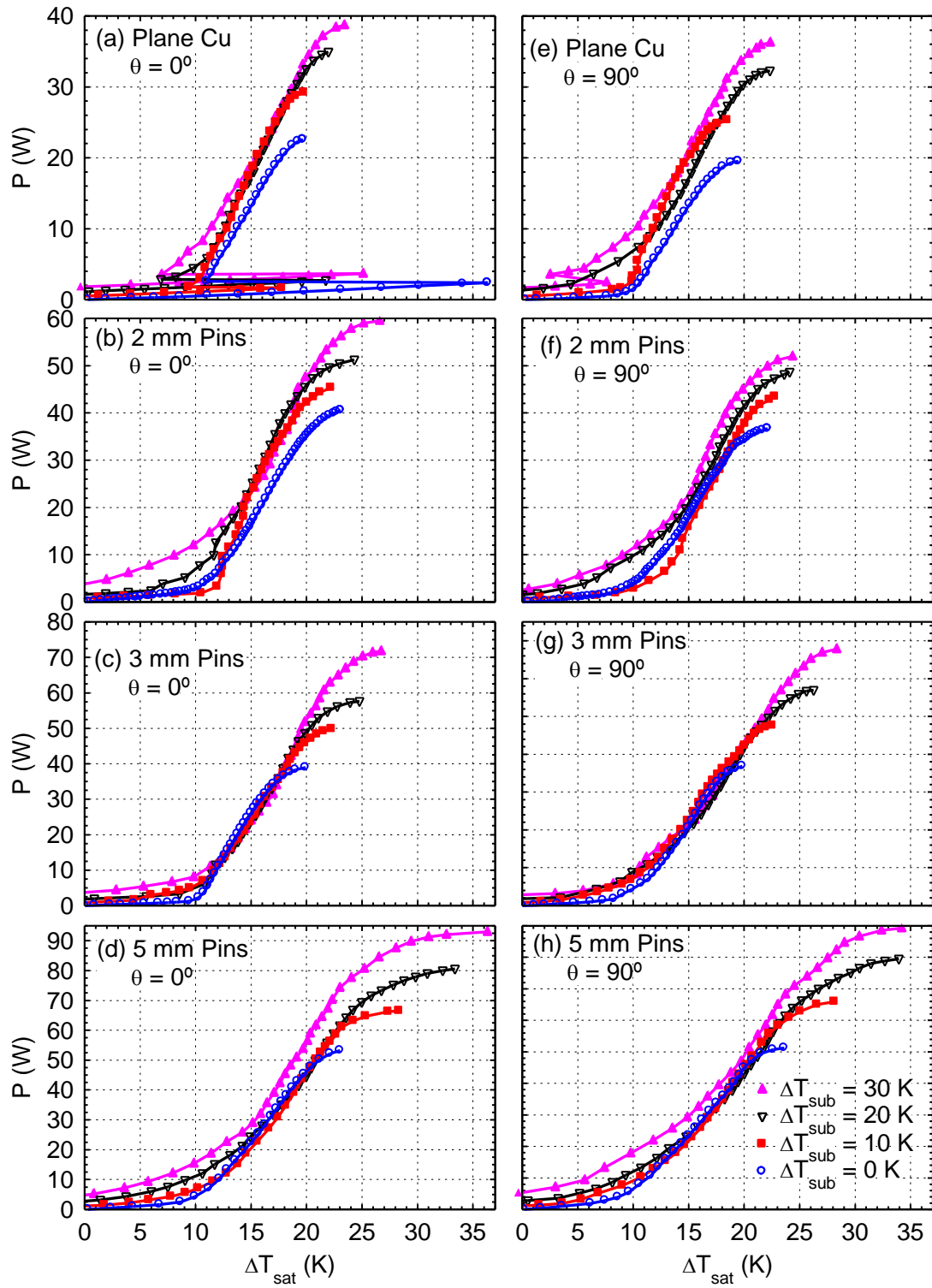


Figure 5.16 Effect of liquid subcooling on boiling of HFE-7100 on inclined extended copper surfaces.

by  $\sim 3 - 4$  K compared to saturation boiling. On the copper surfaces with corner pins,  $\Delta T_{sat}$  at CHF could vary by as much as 13 K (Figure 5.16d and 5.16h), mostly due to the relatively larger uncertainties in the measurements of the footprint temperature in subcooled boiling experiments.

### 5.3.5 Boiling Resistance

The boiling resistance,  $r_B$ , equals the rise in the footprint surface temperature, relative to that of the boiling liquid in the pool above the surface ( $\Delta T_b = T_w - T_b$ ), divided by the total thermal power removed by nucleate boiling ( $P$ ). In another word, it is a measure of the temperature budget for cooling by nucleate boiling of HFE-7100 per unit thermal power dissipated by the underlying chip and removed by the boiling liquid. This boiling resistance is expressed as:

$$r_B = \Delta T_b / P. \quad (5.3)$$

The minimum boiling resistance (Figure 5.17) occurs near the end of the fully developed nucleate boiling region (II), corresponding to the peak nucleate boiling heat transfer coefficient (Figure 5.8). The boiling resistances for the copper surfaces with corner pins are markedly lower than for plane copper, at the same liquid subcooling, but the corresponding footprint temperature is typically a few to several degrees higher. The minimum boiling resistance is lowest in the upward-facing orientation ( $\theta = 0^\circ$ ) and increases with increased surface inclination or liquid subcooling. The results in Figures 5.17a and 5.17b for plane copper, show the minimum boiling resistance for saturation boiling is 0.86 K/W at  $\theta = 0^\circ$ , and increases to 2.8 K/W at  $\theta = 180^\circ$  (Figure 5.17a). These values increase to as much as 1.4 K/W and 5.4 K/W for 30 K subcooled boiling of HFE-7100 liquid (Figure 5.17b). On the copper surface with 5 mm tall corner pins, the minimum boiling resistance for saturation boiling of HFE-7100 is 0.42 K/W at  $\theta = 0^\circ$  and 0.52 K/W at  $\theta = 180^\circ$  (Figure 5.17c). It increases to 0.66 K/W and 0.78 K/W for 30 K subcooled boiling (Figure 5.17d).

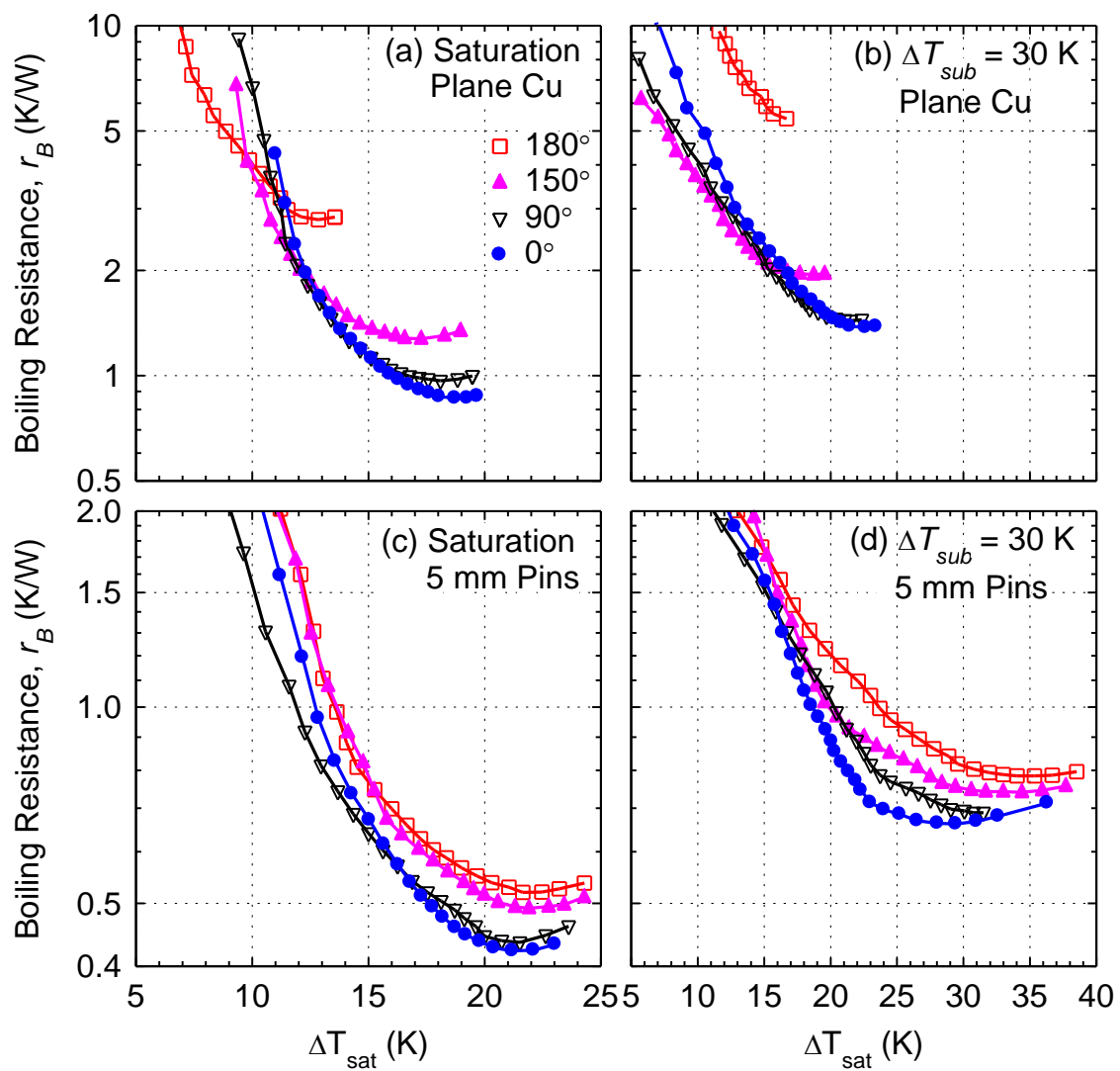


Figure 5.17 Effect of surface orientation and subcooling on boiling resistance.

## 5.4 Critical Heat Flux

Figure 5.18 compares the obtained values of the thermal power removed at CHF by saturation boiling of HFE-7100 on Cu surfaces with corner pins with those reported for HFE-7100 and FC-72 on surfaces with different dimension pins and micro-fins versus the wetted area ratio (Rainey and You, 2000; Wei and Honda 2003; Al-Hajri et al., 2005, Misale et al., 1999; Launay et al., 2006, Yu and Lu, 2007; Ujereh, Fisher, and Mudawar, 2007; Parker and El-Genk, 2007). For saturation pool boiling of FC-72 on a micro-finned silicon surface (Wei and Honda, 2003), the power removed at CHF increases as the wetted area increases to  $\sim 30$  W at an area ratio of  $\sim 7$ . These values are significantly lower than those reported by Rainey and You (2000) and Yu and Lu (2007) for FC-72 on Cu surfaces with square pins (Figure 5.18). The values of the thermal power removed at CHF in saturation boiling of PF-5060 on the silicon microstructure of Launay et al. (2006) are in the range of those reported by Wei and Honda (2003). For saturation boiling of HFE-7100 on the micro-finned surface of Al-Hajri et al. (2005), the thermal power removed at CHF is  $\sim 41$  W and almost independent of the wetted area ratio. This CHF value is much lower than that measured in the present work for a wetted area ratio of 3.4 ( $\sim 53$  W). No CHF values were reported by Al-Hajri et al. (2005) for saturation boiling on plane Cu and micro-finned surfaces with wetted area ratios less than 4.

The width and the pitch of the square pins used by Misale et al. (1999) are smaller than those used by Rainey and You (2000) and in the present work, but the pitch is larger than for the micro-pinned and micro-finned surfaces by Wei and Honda (2003) and Al-Hajri et al., (2005). The reported saturation boiling CHF values by Misale et al. (1999) are lower than those of Rainey and You (2000), but higher than those for micro-structured silicon (Launay et al., 2006), silicon with micro-pins (Wei and Honda, 2003), and copper with micro-fins (Al-Hajri et al., 2005). Increasing the wetted area ratio from 4.75 to 8.5 increases the total thermal power removed reported by Misale et al. (1999) by only 20%.

The reported CHF for FC-72 by Rainey and You (2000) for saturation boiling of FC-72 on a machine roughened, plane Cu surface is  $18.8 \text{ W/cm}^2$ , and that reported by Yu and

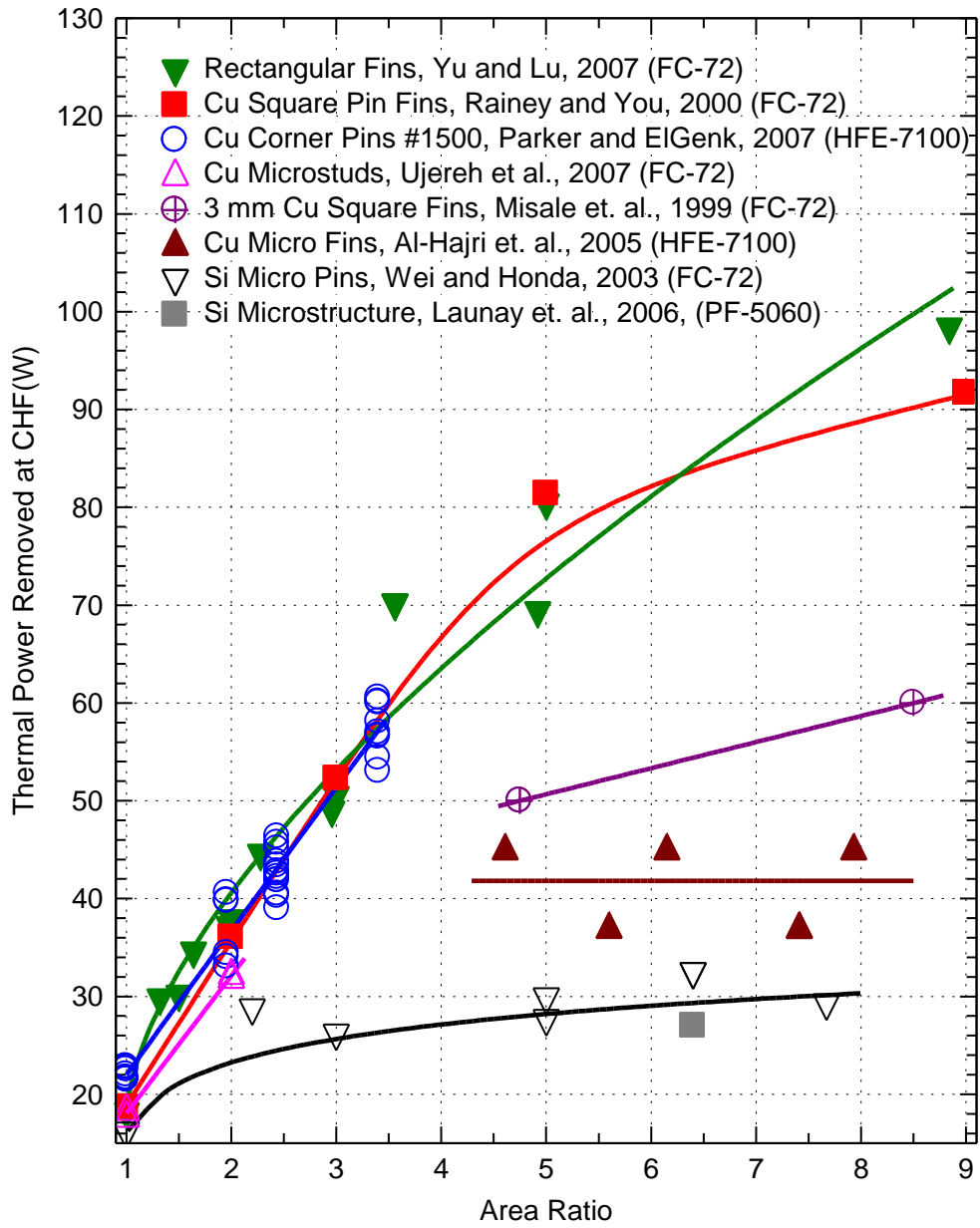


Figure 5.18 Power removal at CHF of saturation boiling of dielectric liquids on extended surfaces in the upward facing orientation.

Lu (2007) is  $18.1 \text{ W/cm}^2$ . These values are about 18% lower than the present value for HFE-7100 on a plane Cu surface prepared with #1500 emery paper. It is interesting to note that for the same wetted area ratio, the total thermal power removed, as reported by Yu and Lu (2007) and Rainey and You (2000) in saturation boiling of FC-72 on Cu surfaces with square pins, are very close to the present values for HFE-7100 on Cu surfaces with four corner pins. The three data sets in Figure 5.18 show that the thermal power removed at CHF increases linearly as the wetted area ratio increases up to 5, and at a significantly higher rate than reported by both Wei and Honda (2003) and Al-Hajri et al. (2005). The reported values of the thermal power removed at CHF by Ujereh, Fisher, and Mudawar (2007) on a surface with micro-studs follow the same trend as those in the present work and reported by Rainey and You (2000) and Yu and Lu (2007), even though the surface structures and spacing are much smaller. On these surfaces, the length scale is much smaller than the departure bubble diameter for saturation boiling of FC-72 and HFE-7100 liquids ( $\sim 0.55 \text{ mm}$ ), increasing the resistance to detaching bubbles from the surface.

#### 5.4.1 CHF correlation for extended surfaces

A correlation for the critical heat flux is developed in this section following the same method used for the correlating CHF for plane surfaces (Section 4.5). The obtained CHF values for saturation boiling of HFE-7100 on plane copper in the upward-facing orientation ( $\theta = 0^\circ$ ) are correlated, using the general form suggested by Kutateladze (1952) and Zuber (1959):

$$CHF_{sat}(0^\circ) = C_{CHF,sat}(0^\circ) \rho_v^{0.5} h_{fg} [\sigma g (\rho_\ell - \rho_v)]^{0.25}. \quad (5.4)$$

The coefficient,  $C_{CHF,sat}(0^\circ)$ , determined from the least squares fit of the present CHF values and those reported earlier by others on plane Cu and silica surfaces, is 0.196 for HFE-7100 (Parker and El-Genk, 2006; El-Genk and Parker, 2004; J. Liu et al., 2001; Z. Liu et al., 2001; El-Genk and Bostanci, 2003a; Priarone, 2005), and 0.166 for FC-72 (Parker and El-Genk 2005, 2006; Priarone, 2005; Howard, 1999; Rainey and You, 2000;

O'Connor, 1994; Rainey, You, and Lee, 2003; Z. Liu et al., 2001; McNiel, 1992; Honda, Takamatsu, and Wei, 2002) dielectric liquids (Figure 5.19). To account for the effect of surface inclination and area ratio, the following expression is suggested for predicting saturation CHF on plane surfaces:

$$CHF_{sat}(\theta, AR) = CHF_{sat}(0^\circ) R_{sat}(\theta) F_{sat}(AR, 0^\circ). \quad (5.5)$$

The coefficient,  $F_{sat}(AR, 0^\circ)$ , which accounts for the effect of the extended surface features on the saturation CHF is unity for plane surfaces. This coefficient for the Cu surfaces with square corner pins is determined from the least square fit of the present CHF data for saturation boiling of HFE-7100 in the upward-facing orientation ( $0^\circ$ ) in Figure 20a as:

$$F_{sat}(AR, 0^\circ) = 0.655 + (0.348/AR). \quad (5.6a)$$

This expression is within  $\pm 5\%$  of the present CHF data for saturation boiling of HFE-7100 dielectric liquid (Figure 5.20a). Similarly, the values reported for saturation boiling of FC-72 by Yu and Lu (2007) and Rainey and You (2000) on surfaces with square pins and rectangular fins (Figure 5.20b) are correlated as:

$$F_{sat}(AR, 0^\circ) = 0.868 + (0.139/AR) \quad (5.6b)$$

This expression is within  $\pm 3\%$  of the reported CHF data for saturation boiling of FC-72 dielectric liquid by Yu and Lu (2007) and Rainey and You (2000) (Figure 5.20b).

The coefficient  $R_{sat}(\theta)$  in equation (5.5) accounts for the effect of the inclination angle on saturation boiling CHF. The following expressions are obtained from the least square fit of the present saturation boiling CHF data on plane Cu and Cu surfaces with corner square pins as:

$$R_{sat}(\theta) = 1 - 6.31 \times 10^{-5} \theta - 4.97 \times 10^{-7} \theta^2 - 1.25 \times 10^{-7} \theta^3, \text{ for plane Cu (AR = 1)}. \quad (5.7a)$$

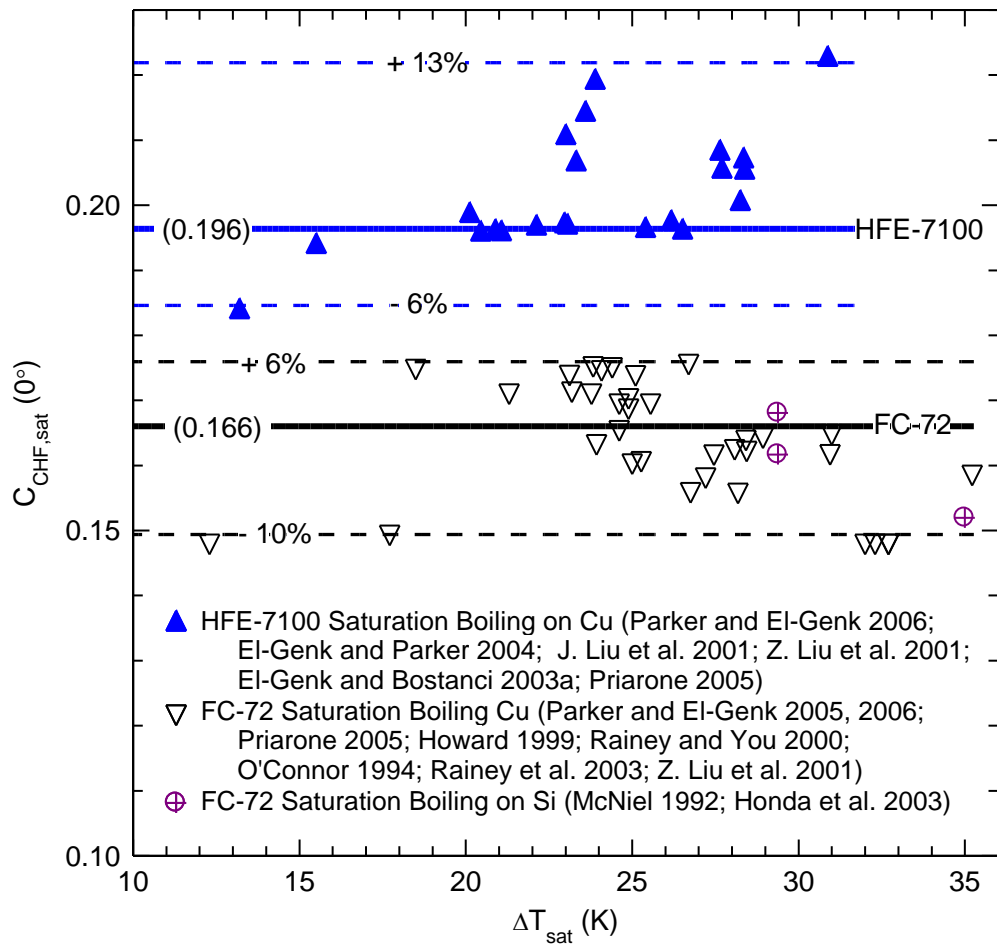


Figure 5.19 Saturation CHF coefficient in the upward facing orientation  $C_{CHF,sat}(0^\circ)$ .

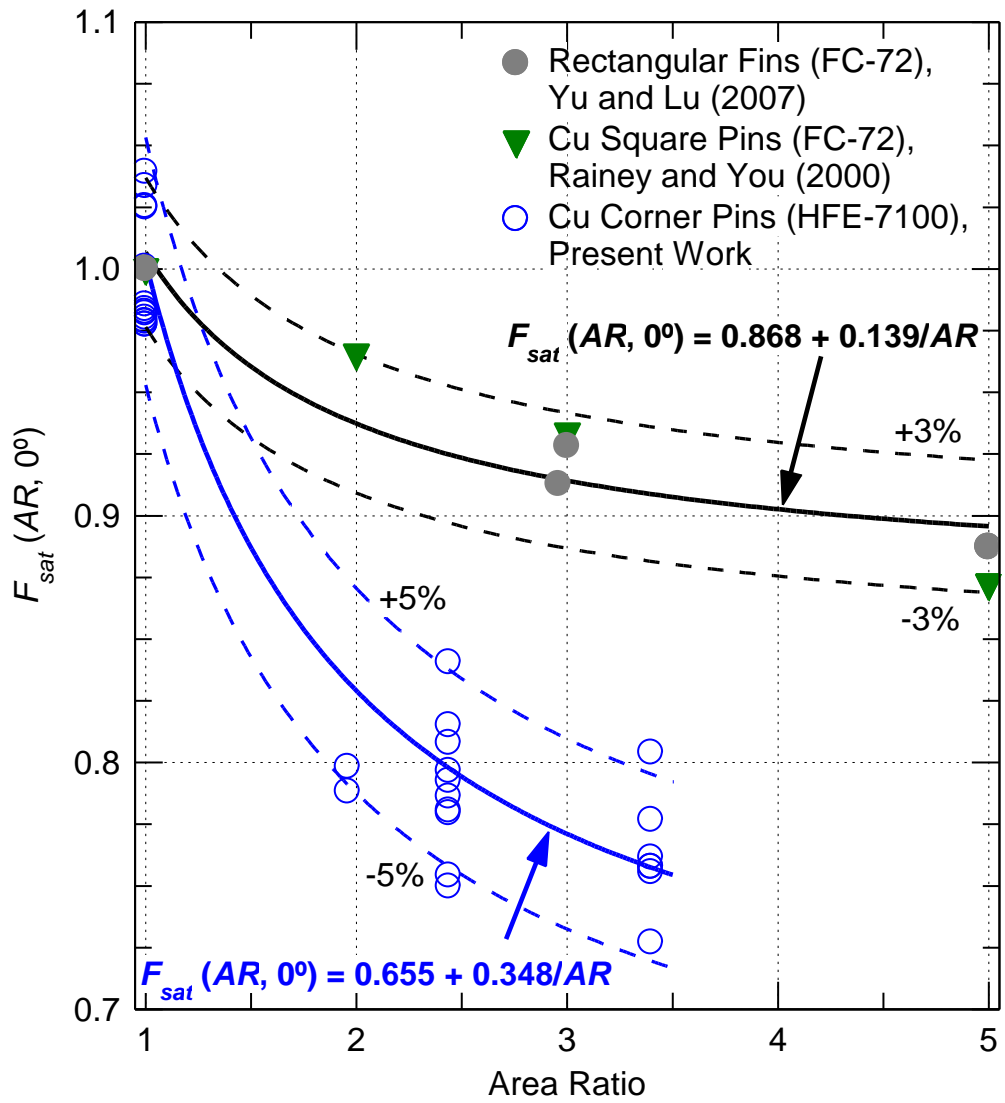


Figure 5.20 Effect of area ratio on saturation CHF in the upward facing orientation.

$$R_{sat}(\theta) = 1 - 8.27 \times 10^{-11} \theta - 8.26 \times 10^{-6} \theta^2 - 3.42 \times 10^{-8} \theta^3, \text{ for Cu with 2 mm pins.} \quad (5.7b)$$

$$R_{sat}(\theta) = 1 - 4.03 \times 10^{-5} \theta - 5.12 \times 10^{-6} \theta^2 - 2.51 \times 10^{-8} \theta^3, \text{ for Cu with 3 mm pins.} \quad (5.7c)$$

$$R_{sat}(\theta) = 1 - 1.22 \times 10^{-7} \theta - 4.76 \times 10^{-6} \theta^2 - 1.59 \times 10^{-11} \theta^3, \text{ for Cu with 5 mm pins.} \quad (5.7d)$$

As delineated in Figure 5.21, these expressions are in reasonable agreement with the present data. When the expressions in Equations (5.6) and (5.7) are incorporated into equation (5.5), the resulting correlation can be used to predict the saturation CHF of HFE-7100 on plane surfaces and Cu surfaces with 3 x 3 square corner pins. However, in order to extend this correlation to other macro-structured surfaces additional data is needed for validation.

#### 5.4.2 Subcooled Boiling Critical Heat Flux

For subcooled boiling, CHF data are correlated in terms of the saturation value (Equation 5.5) and the liquid subcooling as:

$$CHF(\theta, AT, \Delta T_{sub}) = CHF_{sat}(\theta, AR) F_{sub}(\theta). \quad (5.8)$$

The data in Figures 5.22a – 5.22h show that the subcooled boiling CHF values for HFE-7100 dielectric liquid in the 0° and 90° orientations increase linearly with increased liquid subcooling and  $F_{sub}(\theta)$  can be expressed as (El-Genk and Bostanci, 2003b; Parker and El-Genk, 2006; El-Genk and Parker, 2008a,b):

$$F_{sub}(\theta) = 1 + C_{sub}(\theta) \Delta T_{sub} \quad (5.9)$$

Similar results are obtained for the other orientations. In equation (5.9), the value of the CHF subcooling coefficient for the upward-facing orientation,  $C_{sub}(0^\circ)$ , depends on the surface conditions. For subcooled boiling of HFE-7100 dielectric liquid on plane Cu, the present data is in excellent agreement with that reported by Arik and Bar-Cohen (2001) on plane Cu (Figure 5.22a). For this surface  $C_{sub}(\square 0^\circ) = 0.0255 \text{ K}^{-1}$ , that is CHF

increases by 2.55% as the liquid subcooling,  $\Delta T_{sub}$ , increases one degree Celsius or Kelvin. The

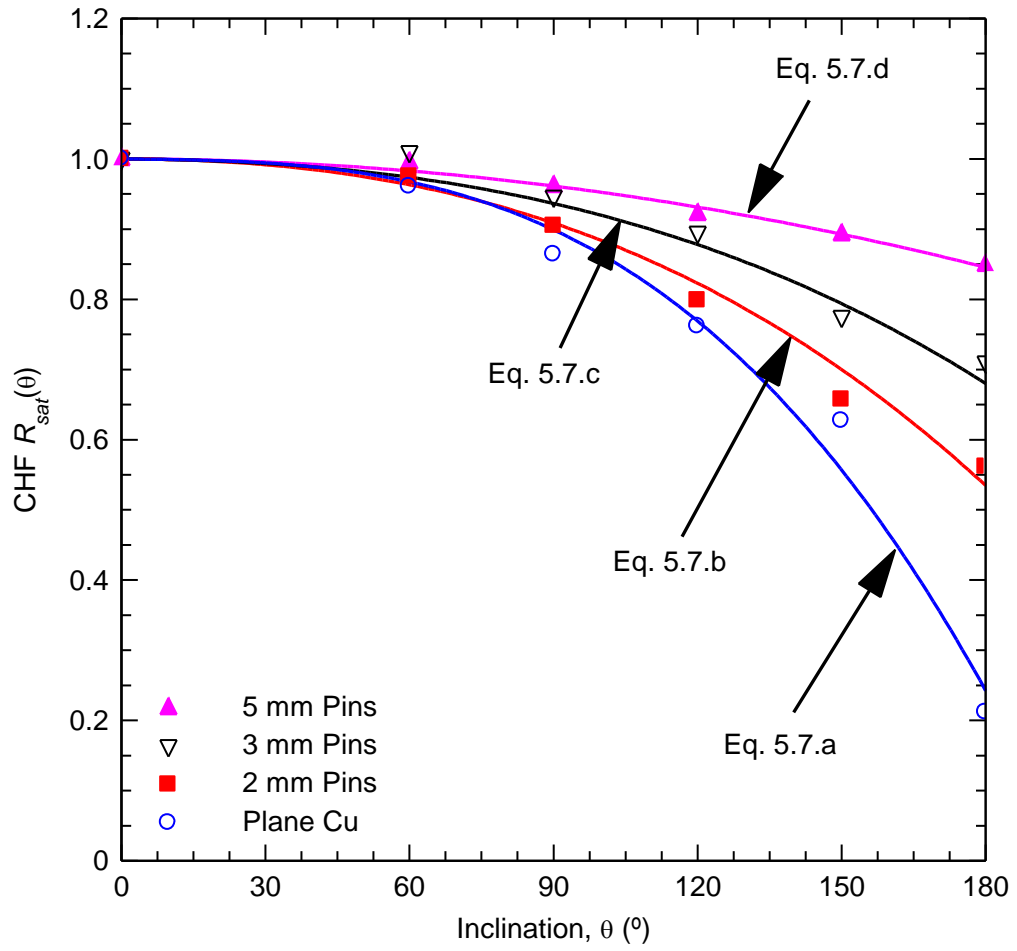


Figure 5.21 Relative decrease in CHF on Cu with different pin heights.

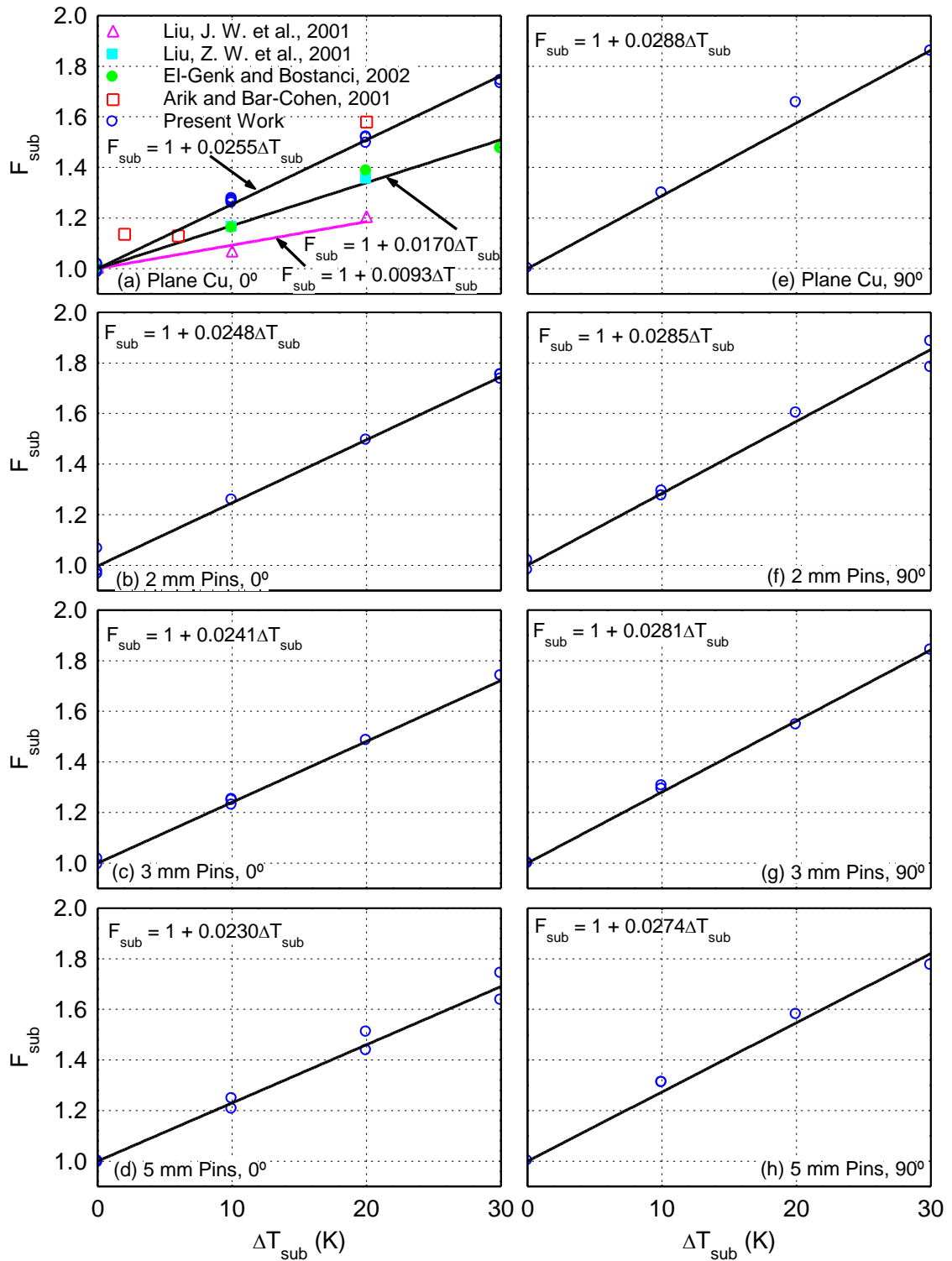


Figure 5.22 Effect of subcooling of CHF on plane surface and Cu surfaces with corner pins.

data of El-Genk and Bostanci (2003b) is in good agreement with that of Z. Lui et al. (2001) giving a subcooled boiling CHF coefficient,  $C_{sub}(\square 0^\circ) = 0.017 \text{ K}^{-1}$ . This value is much lower than that obtained from the present data for plane copper and higher than that deduced from the linear fit of the CHF data reported by J. Liu et al. (2001), which gives  $C_{sub}(\square 0^\circ) = 0.0093 \text{ K}^{-1}$  (Figure 5.22a).

For subcooled boiling of HFE-7100 on plane Cu in the upward-facing orientation, the ratio of the CHF value to that at saturation,  $F_{sub}$ , determined from the linear fit of the data in Figure 5.22a can be given as:

$$F_{sub} = 1 + 0.0255 \Delta T_{sub}. \quad (5.10)$$

For subcooled boiling of HFE-7100 on the present Cu surfaces with square corner pins in the upward-facing orientation ( $\theta = 0^\circ$ ) the value of the CHF subcooling coefficient,  $F_{sub}$ , is slightly lower than for plane Cu and decreases very little with increased pin height (Figures 5.22b – 5.22d). The values of  $C_{sub}(\square 0^\circ)$  vary from 0.023 for the surface with 5 mm tall pins (Figure 5.22d) to 0.0248 for the surface with 2 mm tall pins (Figure 5.22b). Since this variation represents less than 8% difference, for subcooled boiling of HFE-7100 on upward facing copper surfaces with square corner pins this expression may be used:

$$F_{sub} \cong 1 + 0.0240 \Delta T_{sub}. \quad (5.11)$$

The CHF subcooling coefficient,  $C_{sub}(\theta)$  in equation (5.9) increases as the inclination angle of the surface increases. For the vertical orientation, the subcooling coefficient  $C_{sub}(90^\circ)$  is 0.0288 for plane copper surfaces (Figure 5.22e), and decreases to 0.0274 for the copper surfaces with 5 mm tall corner pins (Figure 5.22h). The coefficient  $C_{sub}(\theta)$  can be expressed in terms of that for the upward-facing orientation,  $C_{sub}(\square 0^\circ) = 0.024$  for the Cu surfaces with corner pins, and the inclination angle,  $\theta$ , as:

$$C_{sub}(\theta) = 0.024 + [9.37 \times 10^{-7} \theta^2 - 6.21 \times 10^{-9} \theta^3 + 1.21 \times 10^{-11} \theta^4]. \quad (5.12)$$

This expression is with  $\pm 4\%$  of the present CHF data for subcooled boiling of HFE-7100 on Cu surfaces with square corner pins up to 5 mm in height (Figure 5.23). Figure 5.24 shows that  $C_{sub}(\theta)$  decreases almost linearly by 5 – 10% as the height of the corner pins or the ratio of the wetted surface area,  $AR$ , increases. It also increases as the surface inclination increases. For the plane surface,  $C_{sub}(0^\circ)$  increases by 20% as  $\theta$  moves from  $0^\circ$  to  $180^\circ$ . Similar increases are observed for the surfaces with 2 mm pins (20%), 3 mm pins (23%), and 5 mm pins (23%).

Based on the above analysis, the following expression is proposed for predicting subcooled boiling CHF for HFE-7100 on plane copper and copper surfaces with corner pins in terms of that for saturation boiling (Equation 5.5), liquid subcooling,  $\Delta T_{sub}$ , and the surface orientation,  $\theta$ , as:

$$CHF_{sub}(\theta, AR, \Delta T_{sub}) = CHF_{sat}(\theta, AR)(1 + C_{sub}(\theta)\Delta T_{sub}). \quad (5.13)$$

In this equation,  $CHF_{sat}(\theta, AR)$  is given by equation. (5.5) and  $C_{sub}(\theta)$  is given by equation (5.11). This correlation is in good agreement with the present CHF data for saturation and subcooled boiling of HFE-7100 on plane copper and copper surfaces with corner pins at different orientations, from  $\theta = 0^\circ$  to  $180^\circ$  (downward-facing) and for saturation boiling of FC-72 on macro-structured surfaces in the upward facing orientation (Rainey and You, 2000; Yu and Lu, 2007). It is within  $\pm 10\%$  of the entire data set of a total of 104 CHF values (Figure 5.25).

## **5.5 Photographs of Boiling on Cu with Corner Pins**

As indicated earlier the temperature excursion at boiling incipience, usually associated with using highly wetting liquids like FC-72 and HFE-7100, is reduced or absent on copper surfaces with corner pins. On the surfaces with corner pins, boiling usually starts at the root of the pins. Figure 5.26 presents a sequence of video frames showing bubble nucleation at the base of one of the corner pins. The video is taken during a test for saturation boiling of HFE-7100 on copper with 3 mm corner pins in the vertical orientation ( $\theta = 90^\circ$ ). About a second after the first bubbles appeared, a stream of



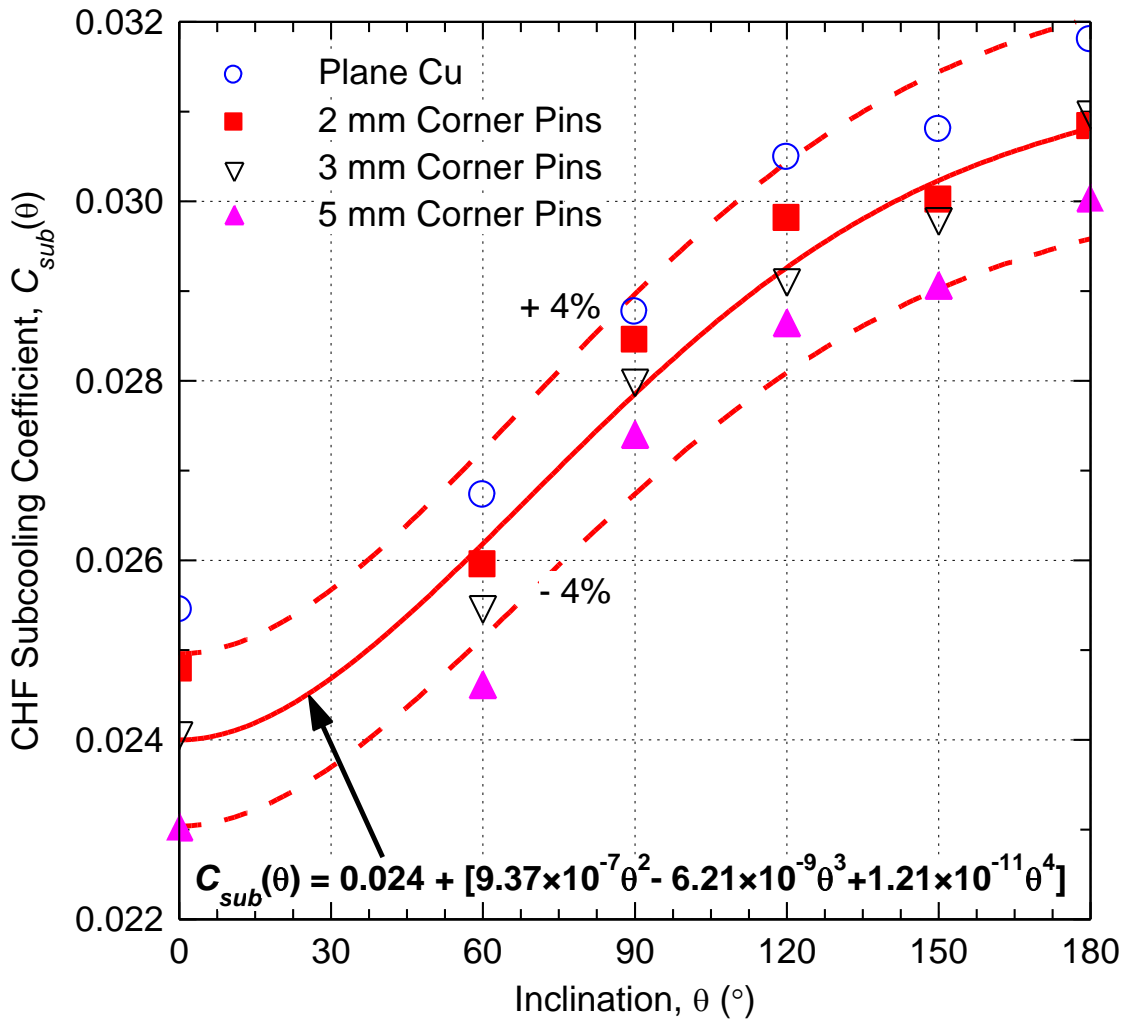


Figure 5.23 Subcooling coefficients for all surfaces and orientations

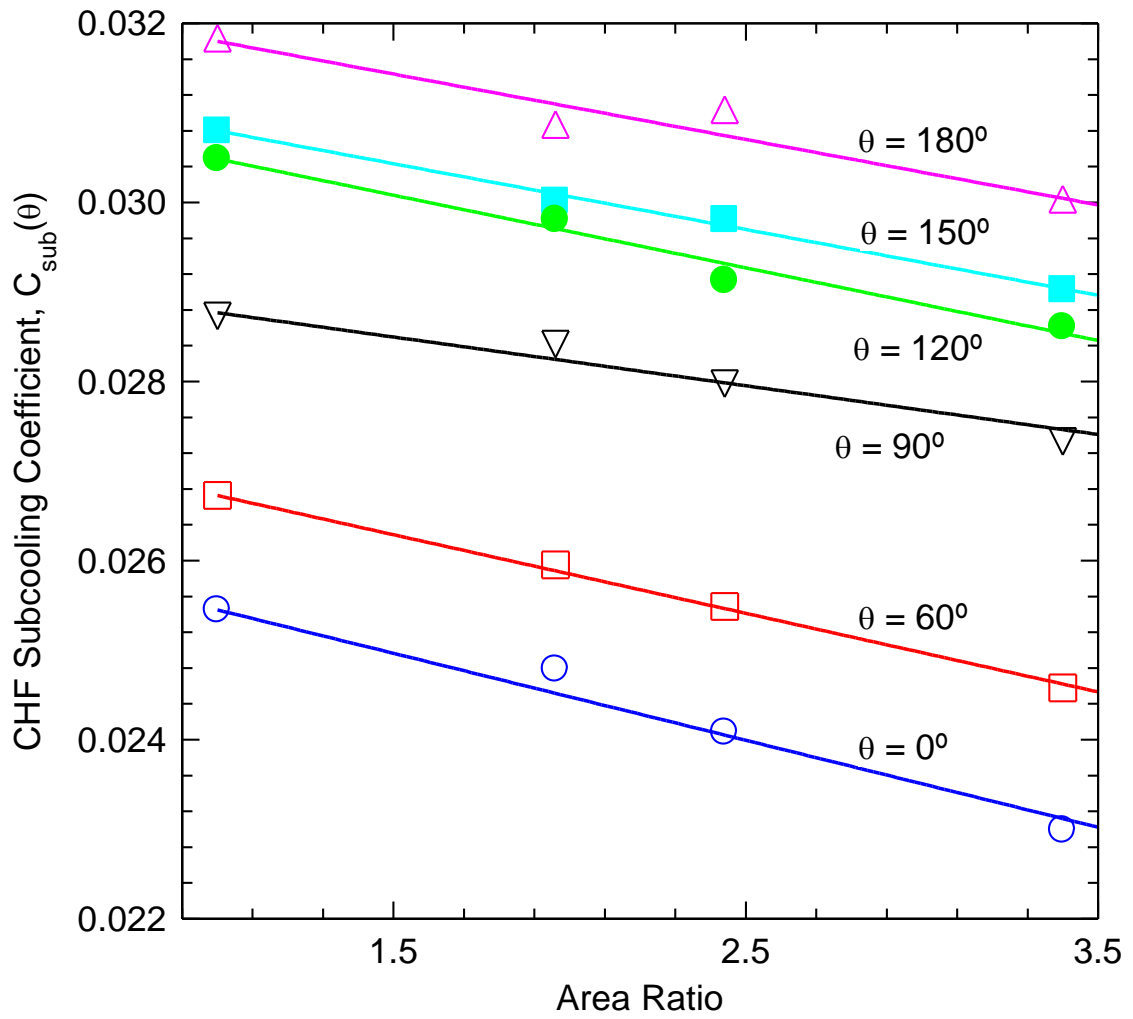


Figure 5.24 Effect of area ratio on the subcooling coefficient at different orientations.

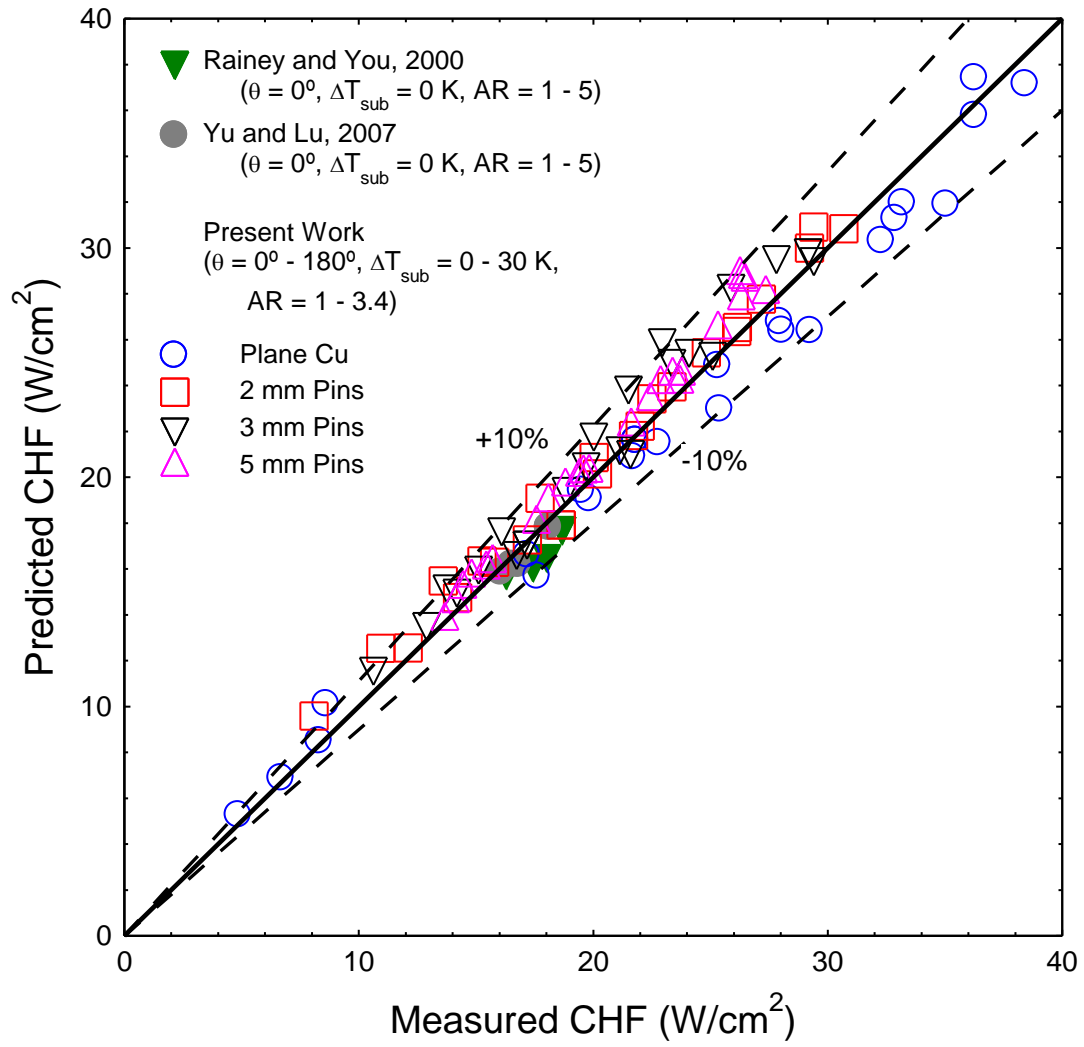
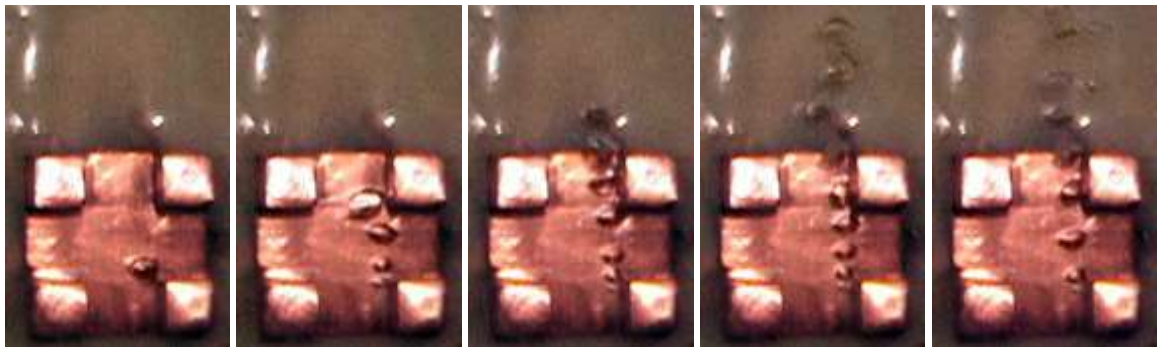
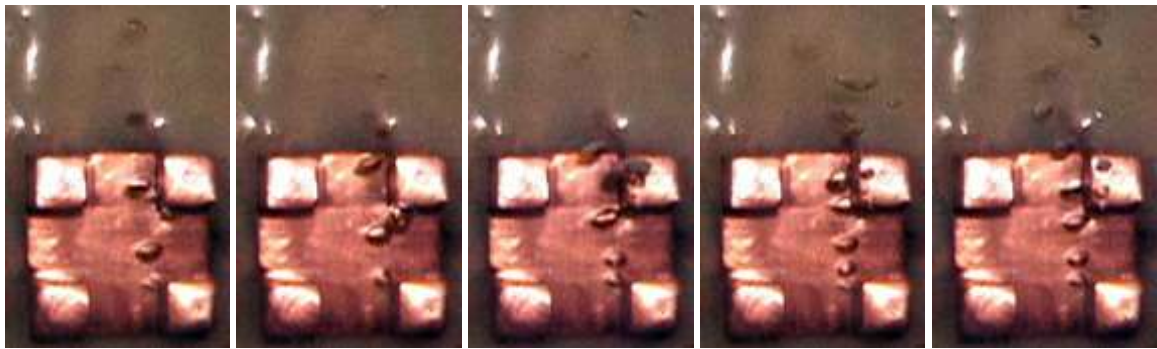


Figure 5.25 Measured and predicted CHF for plane and extended surfaces.



**t = 0 ms      t = 33 ms      t = 37 ms      t = 100 ms      t = 133 ms**

**(a) Initial bubble nucleation at pin base of bottom right-hand-side pin**



**t = 1167 ms      t = 1200 ms      t = 1233 ms      t = 1267 ms      t = 1300 ms**

**(b) Induced bubble nucleation at pin base of top right-hand-side pin**

**Figure 5.26 Boiling incipience from base of a corner pin**

bubbles activated at other sites on another pin located above the first nucleation site (Figure 5.26b). Wei, Guo, and Honda (2005) made similar observations in their study of saturation and subcooled boiling of FC-72 on silicon micro-pins, in which they stated that bubble nucleation usually takes place at the base of the pins.

The enhancements in the power removed from the copper surface with corner pins are mostly due to the increase in the total wetted surface area by the liquid. These enhancements increase linearly with the height of the pins. However, the increase in the thermal power removed is less than the increase in the total surface area. Since the pins effectively function as fins, increasing the pin height also lowers the fin efficiency and results in a smaller increase in the total thermal power removed by nucleate boiling. Furthermore, nucleate boiling on the vertical sides of the pins is less effective than on the flat portion of the surface, reducing the rate of increase in the removed thermal power by nucleate boiling as the height of the pins increases. Conversely, the departed and growing bubbles enhance mixing and the rate of heat removal from the surface.

Figure 5.27 presents a saturation boiling curve on the surface with 3 mm tall corner pins in the vertical orientation ( $90^\circ$ ). The embedded photographs show side and front views of the boiling surface at different nucleate boiling heat fluxes. At low heat flux, the bubbles forming on the lower portions of the surface enhance mixing on the upper portions as they rise in the boundary layer next to the pins' surface. In addition, the extended pins interfere with the free upward movement of the vapor bubbles, causing more turbulence and mixing near the surface. Similar effects are captured at the other orientations of the copper surfaces with corner pins. Figure 5.28a – d show saturation boiling on copper surfaces with 5 mm corner pins at  $60^\circ$  (Figure 5.28a),  $90^\circ$  (Figure 5.28b),  $120^\circ$  (Figure 5.28c), and  $150^\circ$  (Figure 5.28d). The removed thermal power for each photograph is near 45 W. The induced turbulent mixing near the copper surface reduces the thermal boundary layer and improves the convective heat transfer once the bubbles leave the surface.

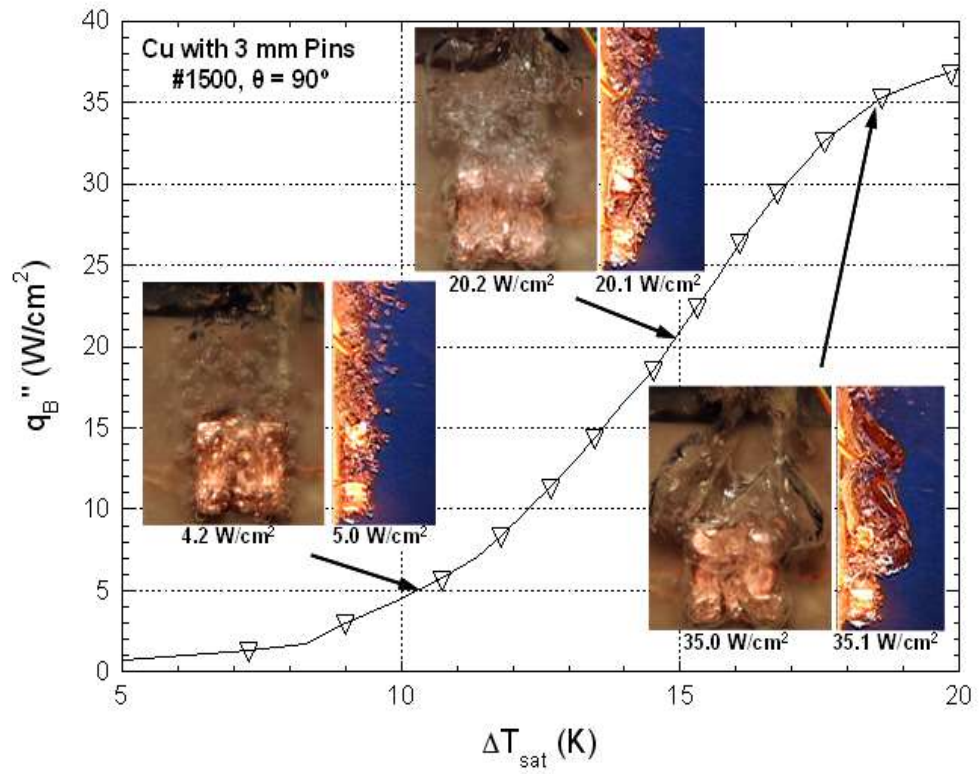


Figure 5.27 HFE-7100 saturation boiling curve for Cu with 3 mm corner pins at  $\theta = 90^\circ$ .



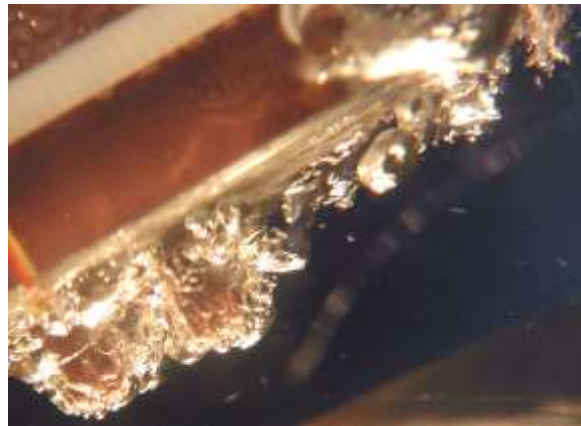
(a) 60°, 45.1 W/cm<sup>2</sup>



(b) 90°, 45.2 W/cm<sup>2</sup>



(c) 120°, 44.9 W/cm<sup>2</sup>



(d) 150°, 45.1 W/cm<sup>2</sup>

**Figure 5.28** Photographs of saturation boiling of HFE-7100 on 5 mm Cu corner pins at different inclination angles.

As nucleate boiling progresses through the region of fully developed nucleate boiling (II), large slugs of vapor form above and near the heated surfaces. Figures 5.29 and 5.30 present collections of photographs of subcooled boiling of HFE-7100 on plane copper and copper surfaces with square corner pins in the upward-facing ( $\theta = 0^\circ$ ) and the vertical ( $\theta = 90^\circ$ ) orientations. Figure 5.31 presents photographs of saturation and subcooled boiling on these surfaces in the downward-facing orientation ( $\theta = 180^\circ$ ). Figure 5.29a for the plane surface shows that the coalescence of departing vapor bubbles results in the formation of a large cluster of vapor slugs near and above the plane copper surface. This photograph is in the bubble coalescence region of the boiling curve (III), while those in Figures 5.29a are for the pinned surfaces. Figures 5.29b and 5.29c in the fully developed nucleate boiling region (II) show a great deal of boiling taking place on the sides of the corner pins. The shorter the pins, the more the coalescence of the departing bubbles. Such coalescence disappears as the liquid subcooling increases because of the condensation of the departed bubbles (Figure 5.29b and 5.29c); however, nucleate boiling still occurs both on the sides of the pins as well as on the plane part of the surface.

In the upward-facing orientation (Figure 5.29), the mixing caused by departing bubbles occurs in the bulk of the liquid above the heated surface. In the vertical orientation, however, departing bubbles from the lower most parts of the heated surface cause significant mixing in the boundary layer as they slide upward along the surface (Figure 5.30). Such mixing also causes some of the growing bubbles to detach earlier from the heated surface. The most mixing occurs in saturation boiling because of the large population and size of the departing bubbles from the heated surface (Figures 5.30a). In addition to the smaller size of the bubbles in the vicinity of the heated surface, increasing the liquid subcooling decreases nucleate boiling at the leading edge of the heated surface, and hence the induced mixing in the boundary layer along the heated surface (Figures 5.30b and 5.30c).

In the downward orientation (Figure 5.31), the generated vapor accumulates forming a large slug that is separated from the heated surface by a very thin liquid film through which the heat is transferred to the liquid-vapor interface. After the amplitude of the

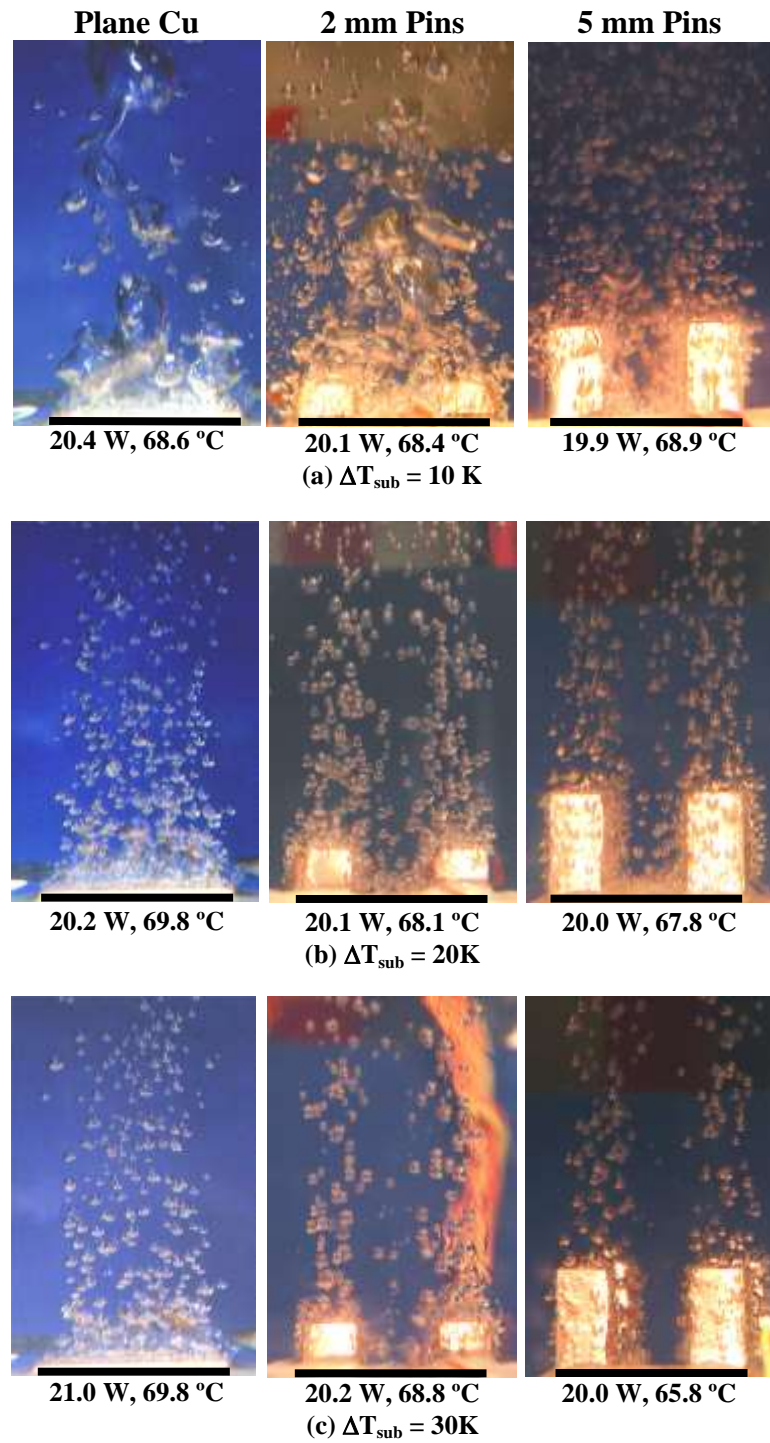


**Figure 5.29 Photographs of subcooled boiling in the upward facing orientation.**

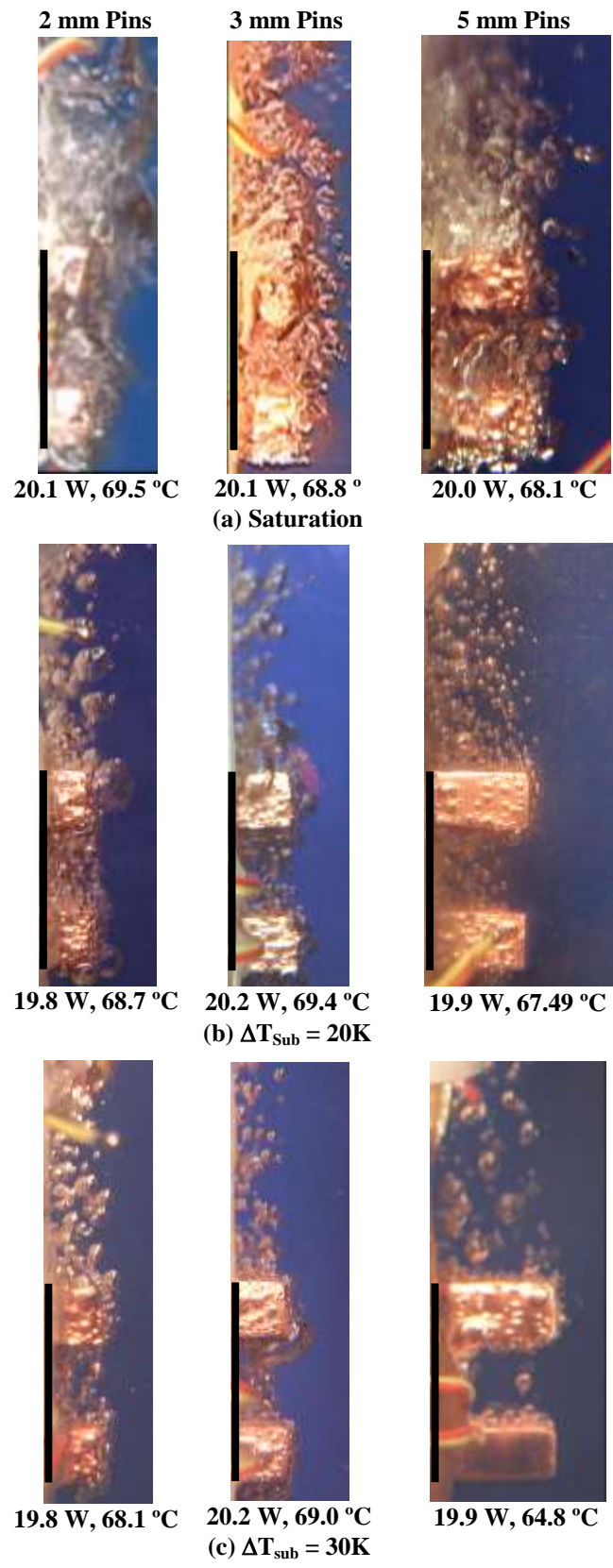
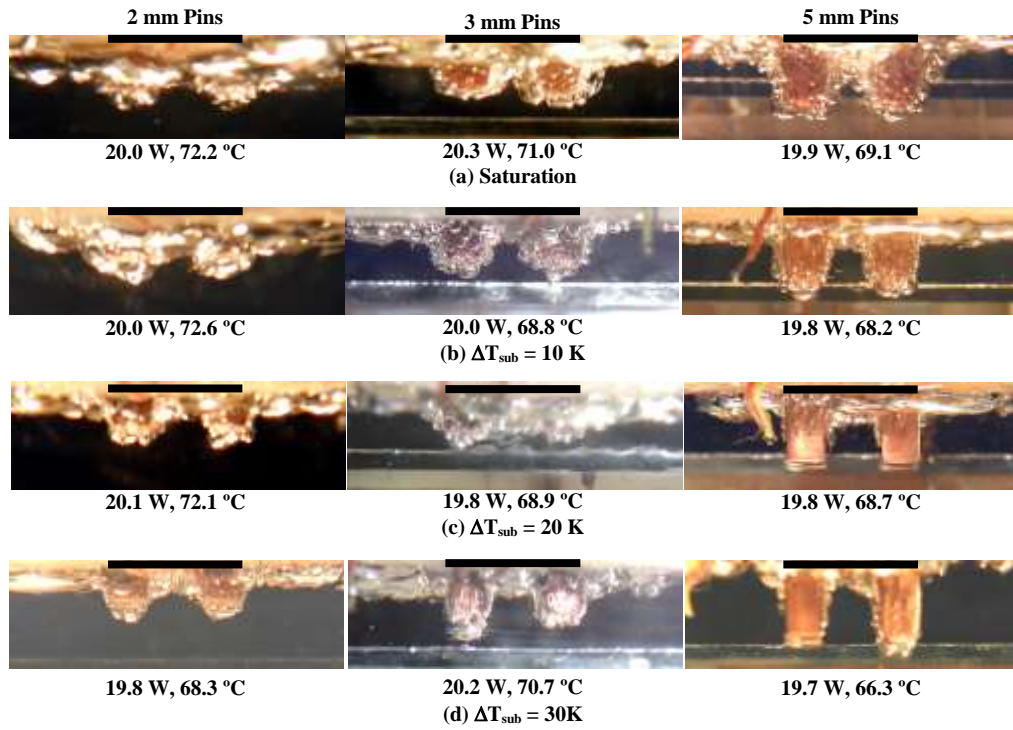


Figure 5.30 Photographs of saturation and subcooled boiling in the vertical orientation.





**Figure 5.31 Photographs of saturation and subcooled boiling in the downward facing orientation.**

vapor mass at the surface peaks, the accumulated vapor slides laterally across the surface and is eventually released to the liquid pool from the edge of the test section. Such lateral movement and release of the vapor slugs forming on the heated surface is accomplished in a pulsating and cyclical fashion. The vapor slug at the surface swells and builds up sufficient pressure against the liquid, which then forces it to slide laterally and to deflate (Figure 5.31).

Based on visual observations, the release of the vapor clusters from the surface occurs at a frequency that decreases slightly as the inclination increases (Figure 5.32a). In the downward facing orientation, the swelling and deflating of the vapor dome also occurs in subcooled boiling at certain frequencies (Figure 5.32b). During saturation boiling, the formation of these clusters increases the resistance of the departing vapor by increasing the back pressure on bubbles trying to rise from the surface. Figure 5.33 shows images captured during saturation boiling of HFE-7100 on plane copper ( $\theta = 0^\circ$ ) at  $20 \text{ W/cm}^2$  showing large vapor clusters forming above the surface. The time between frames is 33 milliseconds. The horizontal lines in the photographs represent increments of 5 mm above the heated surface. Figure 5.33a shows a large mass of vapor above the heated surface. Just above this mass there is a cluster of bubbles being carried away by the wake of the previous vapor mass. As the size of the vapor cluster grows, the cluster rises, and the returning liquid pinches the mass from the bubbles forming on the surface (Figure 5.33b). As the slug of vapor rises, the returning liquid presses down on the bubbles (Figure 5.33c) creating the next slug and the cycle repeats.

## **5.6 Summary**

This chapter presented work that investigated saturation and subcooled boiling of HFE-7100 on copper surfaces with 3 x 3 mm corner pins that are 2, 3 and 5 mm tall. The surface orientation in the experiments varied from  $0^\circ$  to  $180^\circ$  (downward-facing) and the liquid subcooling was 0 K, 10 K, 20 K, and 30K. The obtained boiling curves, natural convection and the nucleate boiling heat transfer coefficients and CHF are compared with those for plane Cu of the same footprint (10 x 10 mm).

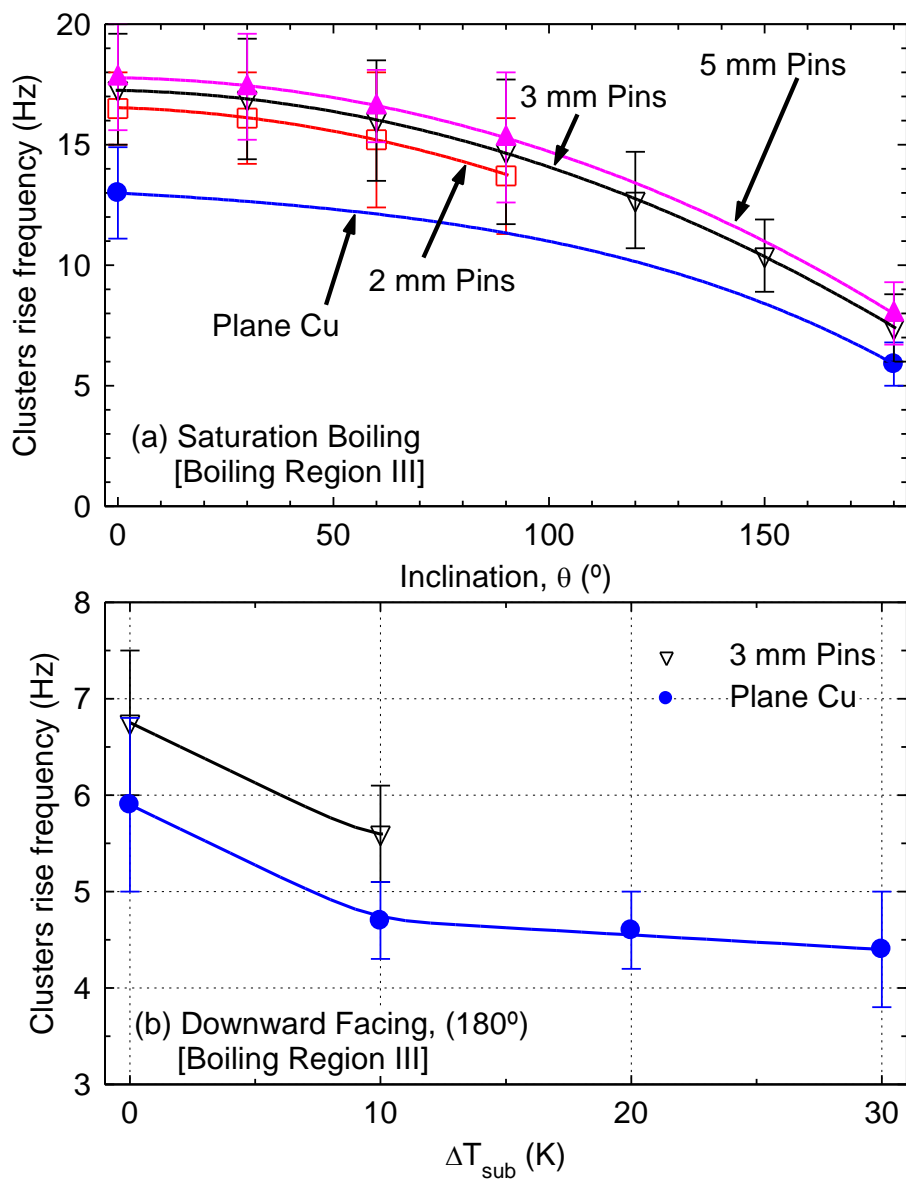
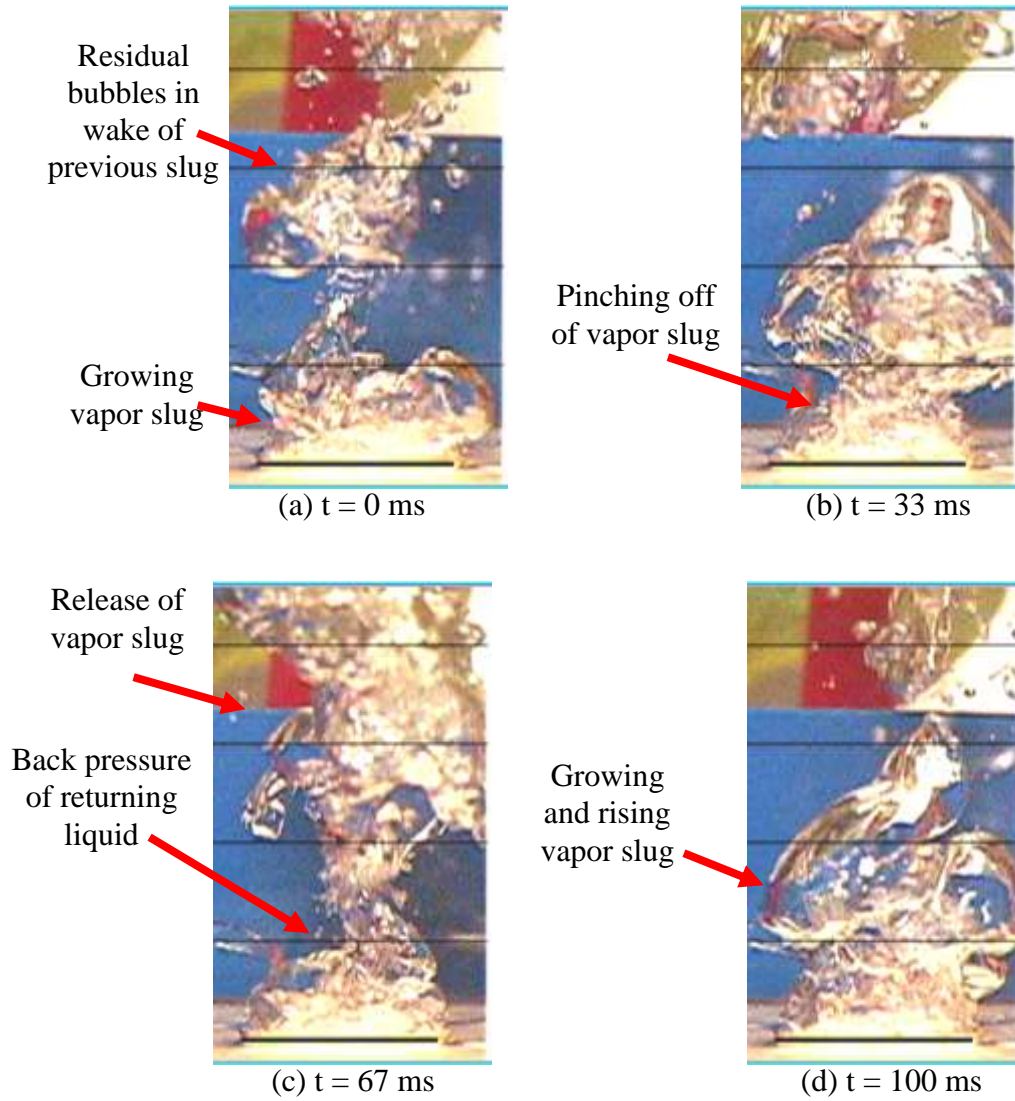


Figure 5.32 Rise frequency of vapor clusters near CHF.



**Figure 5.33 Formation and departure of vapor clusters near boiling surface.**

Results showed significant increases in the total thermal power removed by nucleate boiling, compared to plane copper, at the same liquid subcooling and surface inclination. However, the nucleate boiling surface heat flux and CHF decreased as the height of the corner pins (or the area ratio) increased. These decreases are caused by the fin effect of the corner pins and the increased resistance to the release of growing bubbles on the interior sides of the corner pins with increased pin height. The thermal power removed at CHF from the surface with 5 mm tall corner pins in the upward-facing orientation ( $\theta = 0^\circ$ ) with 30 K subcooled liquid is 93 W, decreasing only to 86 W at  $180^\circ$ . The decrease in CHF with increased orientation of the Cu surfaces with corner pins is much smaller than measured on plane Cu. The values of CHF on both plane Cu and Cu surfaces with corner pins increased linearly with increased liquid subcooling. However, the rate of increase in CHF with increased liquid subcooling on the surfaces with corner pins is lower than that on plane Cu and decreases slightly ( $< 8\%$ ) as the height of the corner pins increases.

A correlation for natural convection heat transfer on the surfaces with corner pins is developed based on the present data and compared to that for plane surfaces of the same footprint. This correlation, which is within  $\pm 12\%$  of the data, showed a 67.5% increase in the heat removal rate by natural convection compared to plane surfaces. A CHF correlation is also developed for both saturation and subcooled boiling on plane Cu and the present surfaces with corner pins. In addition to the surface structure, the CHF correlation accounts for the effect of surface orientation and liquid subcooling; it is within  $\pm 10\%$  of the present data and consistent with reported data by other investigators for CHF of FC-72 on surfaces with pins and other macro-structures.

## 6 Summary and Conclusions

Pool boiling experiments using the dielectric liquids HFE-7100 and FC-72 are conducted, which systematically investigated natural convection, nucleate boiling heat transfer, boiling resistance, and Critical Heat Flux (CHF) on porous graphite and copper. These experiments are conducted on plane surfaces and surfaces with 3 x 3 mm corner pins 2, 3, and 5 mm tall, with a uniformly heated footprint of 10 x 10 mm. The porous graphite increases the nucleation site density, while 3 x 3 mm corner pins increase the area wetted by the boiling liquid by 1.96, 2.44, and 3.4 times. All experiments are carried out using degassed saturated and subcooled liquids (10 K – 30 K subcooled) at inclination angles of the surface from 0° (upward facing) to 180° (downward facing). Results are directly applicable to immersion cooling of high power computer chips by nucleate boiling. With the objective of demonstrating that more than 90 W of thermal power dissipated by 10 x 10 mm chips could be removed while keeping the chip junction temperature  $\leq 85$  °C, the HFE-7100 and FC-72 liquids are chosen for their favorable saturation temperatures (61 °C and 56 °C at 0.1 MPa). These dielectric liquids are also, chemically compatible with common manufacturing materials used in electronic devices and environmentally friendly, with have zero ozone depletion potential.

Thermal analysis using ANSYS showed that the heat losses from the bottom, sides, and top of the assembled test section are less than 3%. These losses are accounted for in the processing of the data. The estimated uncertainties are  $\pm 0.7$  K for temperature measurements and  $\pm 2\%$  for steady state power measurements, and  $\sim 3\%$  in the thermal power removed at CHF and up to 6 K in the surface superheat at CHF.

Prior to boiling incipience, natural convection is the dominant mode of heat transfer for removing the thermal power from a heated surface. Once boiling ensues, three distinct nucleate boiling regimes identified are: the discrete bubble region (region I) at low surface superheat, the fully developed nucleate boiling region (region II) at intermediate surface superheat, and lateral bubble coalescence region (region III) at high surface superheat. In the region of discrete bubbles not all of the potential active nucleation sites are active and there is little bubble coalescence. In the fully developed

nucleate boiling region (region II), the nucleate boiling heat transfer rate is the highest and the slope of the boiling curve is largest. The nucleate boiling heat transfer coefficient increases to a peak at or near the end of the fully developed nucleate boiling region. Lateral coalescence of departing bubbles intensifies as region transitions to the subsequent region of lateral coalescence. In this region, the lateral coalescence of growing bubbles hinders the boiling heat transfer from the surface causing a large increase in the surface superheat as the input power increases. This effect causes the slope of the boiling curve to gradually decrease, eventually reaching CHF.

Immersion cooling of electronics dissipating only a few watts of thermal power in standby mode is likely to be by natural convection. Thus, the developed natural convection correlations for dielectric liquids on plane copper, plane porous graphite, and copper with corner pins would be useful to electronics cooling in stand-by mode. The thermal power removed by natural convection from plane porous graphite is 12% more than that from copper at the same superheat. For the copper surfaces with corner pins, 67% more power is removed by natural convection than from plane copper. These correlations fit the data (~1500 points) for plane surfaces to within  $\pm 7\%$  and the correlation for porous graphite fits the data (> 500 points) to within  $\pm 10\%$ . For natural convection on copper with corner pins, the developed correlation fits the data (> 500 points) to within  $\pm 12\%$ .

At boiling incipience, there is no temperature overshoot on porous graphite, while on plane copper, the temperature overshoot is as much as 35 K. For copper surfaces with corner pins, the temperature overshoot is eliminated or markedly reduced to a few degrees. On plane copper, porous graphite, and copper with corner pins, the nucleate boiling heat transfer coefficient for FC-72 is higher than that for HFE-7100 at low surface superheats. This trend is true in saturation and subcooled boiling at all surface orientations. At a surface superheat of 5.5 K in saturation boiling of FC-72 on porous graphite, the nucleate boiling heat transfer coefficient is 2.8 times larger than for HFE-7100. On plane copper at 11.0 K superheat, the nucleate boiling heat transfer coefficient is 2.4 times larger for FC-72 than HFE-7100. However, as the heat flux increases, the boiling curve for FC-72 transitions to region III (lateral coalescence of bubbles) at lower

heat fluxes than HFE-7100. As a result, the boiling curves for HFE-7100 and FC-72 cross over and at high surface superheats HFE-7100 has better nucleate boiling heat transfer coefficients. Based on these results, FC-72 is the preferred liquid for electronics cooling applications.

Increasing liquid increases the nucleate boiling heat transfer coefficient in the discrete bubble region and extends the region of fully developed nucleate boiling. In subcooled boiling of FC-72 on porous graphite, the thermal power removed at the peak heat transfer coefficient (occurring at the transition from boiling region II to boiling region III) increases from 22.0 W in saturation boiling to 33.6 W, 45.0W, and 53.9 W for 10 K, 20 K, and 30 K subcooled liquid, respectively.

Surface inclination also affects the nucleate boiling heat transfer coefficient. At low surface superheats, increasing surface inclination increases the nucleate boiling heat transfer coefficient. At high superheats, the trend is reversed and the boiling heat transfer coefficients decrease as the surface inclination increases.

The nucleate boiling heat transfer rates from plane porous graphite and the copper with corner pins are much larger than on plane copper. At 11.0 K superheat in saturation boiling of FC-72, the heat flux on porous graphite is  $27.1 \text{ W/cm}^2$  and on copper  $6.3 \text{ W/cm}^2$  (330% increase). Corresponding values for HFE-7100 are  $29.0 \text{ W/cm}^2$  on porous graphite and  $3.1 \text{ W/cm}^2$  on copper (835% increase). For nucleate boiling of HFE-7100 on copper surfaces with corner pins, the thermal power removed at 11.0 K superheat is 6.6 W, an increase of 255% over that removed from the plane copper. The thermal power removed at the peak nucleate boiling heat transfer coefficient is lower than that at CHF. At the peak heat transfer coefficient for saturation boiling of HFE-7100 on plane copper, the thermal power removed is 21.7 W, 5% lower than at CHF (22.7 W). On the copper surface with 5 mm tall corner pins, the difference is about 6%, and the peak nucleate boiling heat transfer coefficient occurs at 50.2 W and CHF at 53.3 W. For saturation boiling of HFE-7100 on plane porous graphite, the peak nucleate boiling heat transfer coefficient occurs at a thermal power of 28.2 W, 13% lower than at CHF value (31.8 W). For saturation boiling of FC-72 on porous graphite, the thermal power at the

peak heat transfer coefficient is at 22.0 W, 20% lower than at CHF (27.3 W). Because the nucleate boiling heat transfer coefficients decrease as CHF is approached, the electronics cooled by nucleate boiling should be at the peak heat transfer coefficient.

As with the nucleate boiling heat transfer coefficient, the value of CHF is affected by the surface material and structure, inclination, and the properties and subcooling of the liquid. The thermal power removed at CHF is higher for HFE-7100 than for FC-72. CHF values for plane porous graphite and copper with corner pins are higher than those on plane copper for both liquids. In addition, increasing the liquid subcooling increases CHF linearly, while increasing the surface inclination decreases CHF. However, the rate of increase in CHF with increased liquid subcooling depends on the liquid properties and the surface structure and orientation. CHF decreases slowly as the surface inclination increases from upward facing ( $0^\circ$ ) to vertical ( $90^\circ$ ), then decreases more rapidly as the inclination angle approaches downward facing ( $180^\circ$ ). As the surface inclination increases, the decrease in CHF with increase surface inclination is less on both porous graphite and copper with corner pins than on plane copper. For plane copper, CHF decreases slowly up to  $\theta = 90^\circ$ , then much more rapidly till it is about 20% of the upward facing value at  $\theta = 180^\circ$ . The relative value of CHF in the downward facing position on plane porous graphite is 54% of that at  $\theta = 0^\circ$ . The CHF values at  $\theta = 180^\circ$  for copper with 2 mm, 3 mm, and 5 mm high corner pins are 53%, 68%, and 85%, respectively, of the CHF values at  $\theta = 0^\circ$ .

The saturation CHF of HFE-7100 on porous graphite ( $31.8 \text{ W/cm}^2$ ) is 40% higher than on plane copper ( $22.7 \text{ W/cm}^2$ ), and for FC-72 saturation CHF on plane porous graphite ( $27.3 \text{ W/cm}^2$ ) is 60% higher than on plane copper ( $17.0 \text{ W/cm}^2$ ). The increase in the thermal power removed at CHF increases on copper with corner pins as pin height increases. On Cu with 5 mm corner pins, the thermal power removed at CHF (53.3 W) is 130% higher than for plane copper (22.7 W).

On plane surfaces, CHF increases by 1.8% per degree subcooling (K or  $^\circ\text{C}$ ) of FC-72, and 2.4% per degree of HFE-7100. For plane porous graphite, the increase in CHF with liquid subcooling is larger than for plane surfaces, 3.6%/K for HFE-7100 and 4.2%/K for

FC-72. For the copper surfaces with corner pins, CHF for HFE-7100 increases with liquid subcooling at the rate of 2.4%/K, which is nearly independent of pin height.

The developed correlation for CHF take to into account, for the first time, the combined effects of surface structure, wetted surface area, surface inclination, and liquid subcooling. Results show that these parameters are not independent of one another. The present CHF data for both FC-72 and HFE-7100 and that of other investigators (~250 points) fit the developed correlation to within  $\pm 10\%$ . The CHF correlation is useful for determining an upper limit of operating for electronic devices that are being cooled by nucleate boiling in dielectric liquids.

## 7 References

3M, Technical Data Sheets, 2001

3M, Tables of Saturation Properties of HFE-7100 and FC-72, 2003.

Agilent Technologies, *User's Guide, Agilent Technologies E3633A and 3634A DC Power Supplies*, Edition 2, 2000.

Al-Hajri, E., M. Ohadi, S. V. Dessiatoun, J. Qi,. "Thermal Performance of Micro-Structured Evaporation Surfaces—Application to Cooling of High Flux Microelectronics", *IMECE 2005, Proc. ASME International Mechanical Engineering Congress and Exposition*, 799-805, 2005.

Arbelaez, F., S. Sett, R. Mahajan, "An Experimental Study on Pool Boiling of Saturated FC-72 in Highly Porous Aluminum Foams," *Proceedings of 34<sup>th</sup> National Heat Transfer Conference*, vol. 1, 759 –767, 2000.

Anderson, T. M., I. Mudawar, "Microelectronic Cooling by Enhanced Pool Boiling of a Dielectric Fluorocarbon Liquid," *ASME J. Heat Transfer*, vol. 111, 752-759, 1989.

Arik, M., A. Bar-Cohen, "Ebullient Cooling of Integrated Circuits by Novec Fluids," *Proc. Pacific Rim Intersociety, Electronics Packaging Conference*, Kauai, Hawaii, 18-23 July 2001.

Arik, M., A. Bar-Cohen, S. M. You, "Enhancement of Pool Boiling Critical Heat Flux in Dielectric Liquids by Microporous Coatings," *Inter. J. Heat & Mass Transfer*, vol. 50, No. 5-6, 997-1009, 2007.

Baldwin, C., S. Bhavnani, R. Jaeger, "Towards Optimizing Enhanced Surfaces for Passive Immersion Cooled Heat Sinks," *Proceedings Intersociety Conf. on Thermal and Thermotechnical Phenomena in Electronic Systems*, 399-407, 1998.

Beduz, C., R. G. Scurlock, A. J. Sousa, "Angular Dependence on Boiling Heat Transfer Mechanisms in Liquid Nitrogen," *Advances in Cryogenic Engineering*, (R. Fast, Ed.) Plenum Press, NY, vol. 33, 363-370, 1988.

Bejan, A., *Heat Transfer*, New York, Wiley and Sons, 1993.

Carey, V. P., *Liquid-Vapor Phase Change Phenomena: An Introduction to the Thermophysics of Vaporization and Condensation Processes in Heat Transfer Equipment*, Hemisphere Publishing Corporation, 1992.

Chang, J. Y., S. M. You, "Heater Orientation Effects on Pool Boiling of Microporous Enhanced Surfaces in Saturated FC-72," *ASME J. Heat Transfer*, vol. 118, 937-943, 1996.

Chang, J. Y., S. M. You, "Boiling Heat Transfer Phenomena from Micro-porous and Porous Surfaces in Saturated FC-72," *Inter. J. Heat & Mass Transfer*, vol. 40, 4437-4447, 1997a.

Chang J. Y., S. M. You, "Enhanced Boiling Heat Transfer from Micro-porous Surfaces: Effects of a Coating Composition and Method," *Inter. J. Heat & Mass Transfer*, vol. 40, 4449-4460, 1997b.

Chang, J. Y., "Enhanced Boiling Heat Transfer from Micro-Porous Surfaces," *Ph.D. Dissertation, University of Texas at Arlington, Arlington, TX*, 1997.

Chang, J., S. You, A. Haji-Sheikh, "Film Boiling Incipience at the Departure From Natural Convection on Flat, Smooth Surfaces," *J. Heat Transfer*, vol. 120, 402-409, 1998.

Chang, S. H., W.-P. Baek, "Understanding, Predicting, and Enhancing Critical Heat Flux," *Proc. 10<sup>th</sup> International Meeting on Nuclear Reactor Thermal Hydraulics (NURETH-10)*, Seoul, South Korea, Oct. 5-9, 2003.

Chen, X. Y. , K. C. Toh, T. N. Wong, J. C. Chai, D. Pinjala, O. K. Navas, H. Z. Ganesh, V. Kripesh, "Direct Liquid Cooling of a Stacked MCM," *Proc. 9<sup>th</sup> Intersociety Conference on Thermal Phenomena*, vol. 1, 199-206, 2004.

Danielson, R. D., L. Tousignant, A. Bar-Cohen, "Saturated Pool Boiling Characteristics of Commercially Available Perfluorinated Inert Liquids," *Proc. ASME/ISME Thermal Engineering Joint Conference 3*, 419-430, 1987.

Diao, Y.-H., Y.-H. Zhao, Q.-L. Wang "Photographic Study of Bubble Dynamics for Pool Boiling of Refrigerant R11," *Heat and Mass Transfer*, vol. 43, 935-947, 2007.

El-Genk, M. S., H. Bostanci, "Saturation Boiling of HFE-7100 from a Copper Surface, Simulating a Microelectronic Chip," *Inter. J. Heat & Mass Transfer*, vol. 46, 1841-1854, 2003a.

El-Genk, M. S., H. Bostanci, "Combined Effects of Subcooling and Surface Orientation on Pool Boiling of HFE-7100 from a Simulated Electronic Chip," *Experimental Heat Transfer*, vol. 16, 281-301, 2003b.

El-Genk, M. S., Z. Guo, "Transient Boiling From Inclined and Downward-facing Surfaces in a Saturated Pool," *Inter. J. Refrigeration*, vol. 16, 414-422, 1993.

El-Genk, M. S., J. L. Parker, "Pool Boiling in Saturated and Subcooled HFE-7100 Dielectric Fluid From a Porous Graphite Surface," *Proc. 9<sup>th</sup> Intersociety Conference on Thermal Phenomena*, vol. 1, pp. 655-662, 2004a.

El-Genk, M. S., J. L. Parker, "Pool Boiling in Saturated and Subcooled FC-72 Dielectric Fluid From a Porous Graphite Surface," *Proc. ASME International Mechanical Engineering Congress (IMECE-2004)*, Paper No. IMECE2004-59905, 2004b.

El-Genk, M. S., J. L. Parker, "Enhanced Boiling of HFE-7100 Dielectric Liquid on a Porous Graphite Surface," *Energy Conversion and Management*, vol. 46, 2455-2481, 2005.

El-Genk, M. S., J. L. Parker, "Nucleate boiling of FC-72 and HFE-7100 on Porous Graphite at Different Orientations and Liquid Subcooling," *Energy Conversion and Management*, vol. 49, 733-750, 2008.

El-Genk, M. S. H. H. Saber, and J. L. Parker, "Thermal Analysis of Composite Copper/Porous Graphite Spreaders for Immersion Cooling Applications," *Proc. Conference on Integration and Packaging of MEMS, NEMS, and Electronics (InterPack'05)*, July 17-22, 2005, San Francisco, CA, IPACK2005-73226, pp. 305-314, 2005.

El-Genk, M. S., H. H. Saber, "Composite Spreader for Submersion Cooling of a Computer Chip with Non-Uniform Heat Dissipation," *Thermomechanical Phenomena in Electronic Systems—Proc. Intersociety Conf. (ITHERM 2006)*, 591-598, 2006.

El-Genk, M. S. H. H. Saber, J. L. Parker, "Efficient Spreaders for Cooling High-Power Computer Chips," *Applied Thermal Engineering*, vol. 27, 1072-1088, 2007.

Ferjančič K., I. Golobič, "Surface Effects on Pool Boiling CHF," *Experimental and Thermal Fluid Science*, vol. 25, 565-571, 2002.

Ferjančič, K., D. Rajšelj, I. Golobič, "Enhanced Pool Boiling CHF in FC-72 from a Modulated Porous Layer Coating", *J. Enhanced Heat Transfer*, vol. 13, no. 2, 175-184, 2006.

Geisler, K. J. L., A. Bar-Cohen, "Surface Effects on Confinement-Driven Pool Boiling Enhancement in Vertical Parallel-Plate Channels," *Proc. ASME Summer Heat Transfer Conference, HT2005*, vol. 2, 195-205, 2005.

Ghiu, C.-D. Y. K. Joshi, "Boiling Performance on Single-Layered Enhanced Structures", *ASME J. Heat Transfer*, vol. 127, no. 7, 675-683, 2005.

Griffith, P., "The Correlation of Nucleate Boiling Burnout Data," ASME Paper No. 57-HT-21, 1957.

Guo, Z., M. S. El-Genk, "Liquid Microlayer Evaporation During Nucleate Boiling on the Surface of a Flat composite Wall," *Inter. J. Heat & Mass Transfer*, vol. 37, no. 11, 1641-1655, 1994.

Haramura, Y. Y, Katto, "A New Hydrodynamic Model of Critical Heat Flux, Applicable Widely to both Pool and Forced Convection Boiling on Submerged Bodies in Saturated Liquids," *Inter. J. Heat & Mass Transfer*, vol. 26, no. 3, 389-399, 1983.

Honda, H., H. Takamastu, J. J. Wei, "Enhanced Boiling of FC-72 on Silicon Chips With Micro-Pin-Fins and Submicron Scale Roughness," *ASME J. Heat Transfer*, vol. 124, 383-390, 2002.

Honda, H., J. J. Wei, "Advances in Enhanced Boiling Heat Transfer From Electronic Components," *JSME International Journal, Series B: Fluids and Thermal Engineering*, vol. 46, 479-490, 2003.

Howard, A. H., I. Mudawar, "Orientation Effects on Pool Boiling Critical Heat Flux (CHF) and Modeling of CHF for Near-Vertical Surfaces," *Inter. J. Heat & Mass Transfer*, vol. 42, 1665-1688, 1999.

Howard, A. H., "Effects of Orientation and Downward-Facing Convex Curvature on Pool Boiling Critical Heat Flux," *Ph.D. Dissertation, Purdue University, West Lafayette, IN*, 1999,

Hsu, Y. Y., "On the Size Range of Active Nucleation Cavities on a Heating Surface," *ASME J. of Heat Transfer*, vol. 84, 207-216, 1962.

ITRS, International Technology Roadmap for Semiconductors, 2007.

Ivey, H., "Relationships Between Bubble Frequency, Departure Diameter, and Rise Velocity in Nuclear Boiling," *Int. J. Heat & Mass Transfer*, vol. 10, 1023-1040, 1967.

Ivey, H. J., D. J. Morris, "Critical Heat Flux of Saturation and subcooled Pool Boiling in Water at Atmospheric Pressure," *Proc. 3<sup>rd</sup> International Heat Transfer Conference*, vol. 3, 129-139, 1966.

Jung, J.-Y. H.-Y. Kwak, "Effect of Surface Condition on Boiling Heat Transfer from Silicon Chip with Submicron-Scale Roughness", *Inter. J. Heat & Mass Transfer*, vol. 49, no. 23-24, 4543-4551, 2006.

Khan, N., K. C. Toh, D. Pinjala, "Boiling Heat Transfer Enhancement Using Micro-Machined Porous Channels for Electronics Cooling," *Heat Transfer Engineering*, vol. 29, no. 4, 366-374, 2008.

Kim, J. H., K. N. Rainey, S. M. You, J. Y. Pak, "Mechanism of Nucleate Boiling Heat Transfer Enhancement from Microporous Surfaces in Saturated FC-72," *ASME Journal of Heat Transfer*, vol. 124, 500-506, 2002.

Kim, J. H., M. R. Kashinath, S. M. Kwark, S. M. You, "Optimization of Microporous Structures in Enhanced Pool Boiling Heat Transfer of Saturated R-123, FC-72, and Water," *Proc. ASME-JSME Thermal Engineering Summer Heat Transfer Conference*, July 8-12, 2007, Vancouver, BC, Canada, HT2007-32339, 2007.

Kim, J. H., "Enhancement of Pool Boiling Heat Transfer using Thermally-Conductive Microporous Coating Techniques," *Ph.D. Dissertation*, University of Texas at Arlington, Arlington, TX, 2006.

Kline, S. J., F. A. McClintock "Describing Uncertainties in Single-Sample Experiments," *ASME Mechanical Engineering*, vol., 75, 3 – 8, 1952.

Knickerbocker, J. U., et al., "An Advanced Multichip Module (MCM) for High-Performance UNIX Servers," *IBM J. Res. and Dev.*, vol. 46 (6), 779 – 804, 2002.

Kurihara, H. M., J. E. Meyers, "The Effects of Superheat and Surface Roughness on Boiling Coefficients," *A. I. Ch. E. Journal*, vol. 6, 83-91, 1960.

Kutateladze, S. S., "Heat Transfer in Condensation and Boiling," AEC-tr-3770, 1952.

Kubo, H., H. Takamatsu, H. Honda, "Effects of Size and Number Density of Micro-Reentrant Cavities on Boiling Heat Transfer from a Silicon Chip Immersed in Degassed and Gas Dissolved FC-72," *J. Enhanced Heat Transfer*, vol. 6, nos. 2-4, 151-160, 1999.

Launay, S., A. G. Fedorov, Y. Joshi, A. Cao, P. M. Ajayan, "Hybrid Micro-Nano Structured Thermal Interfaces for Pool Boiling Heat Transfer Enhancement," *Microelectronics Journal*, vol. 37, no. 11, 1158-1164, 2006.

Lin, S.-C., K. Banerjee, "Cool Chips: Opportunities and Implications for Power and Thermal Management," *IEEE Transactions on Electron Devices*, vol. 55, no. 1, 245-255, 2008.

Liu, Z. W., W. W. Lin, D. J. Lee, X. F. Peng, "Pool Boiling of FC-72 and HFE-7100," *ASME J. Heat Transfer*, vol. 123, 399-400, 2001.

Liu J. W., D. J. Lee, A. Su, "Boiling of Methanol and HFE-7100 on Heated Surface Covered with a Layer of Mesh," *Int. J. Heat & Mass Transfer*, vol. 44, 241-246, 2001.

Marto P., V. Lepere, "Pool Boiling Heat Transfer from Enhanced Surfaces to Dielectric Fluids," *ASME J. of Heat Transfer*, vol. 104, 292-303, 1982.

Mathews, W. S., C. F. Lee, J. E. Peters, "Experimental Investigations of Spray/Wall Impingement," *Atomization and Sprays*, vol. 13 (2,3), 223 – 242, 2003.

Maydanik, Y., S. Vershinin, M. Korukov, J. Ochterbeck, "Miniature Loop heat Pipes – A Promising Means for Cooling Electronics," *Proceedings 9<sup>th</sup> Intersociety Conf. on Thermal Phenomena*, vol. 2, 60-66, 2004.

McNiel, A. "Pool Boiling Critical Heat Flux in a Highly Wetting Liquid," *Masters Thesis*, University of Minnesota, Minneapolis, MN., 1992.

Mikic, B., W. Rohsenow, "A New Correlation of Pool-Boiling Data Including the Effect of Heating Surface Characteristics," *ASME J. Heat Transfer*, vol. 91, 245-250 1969.

Misale, M., G. Guglielmini, M. Frogheri, A. E. Bergles, "FC-72 Pool Boiling from Finned Surfaces Placed in a Narrow Channel: Preliminary Results," *Heat and Mass Transfer*, vol. 34, no. 6, pp. 449-452, 1999.

Mudawar, I, A. H. Howard, C. O. Gersey, "An Analytical Model for Near Saturated Pool Boiling Critical Heat Flux on Vertical Surfaces," *Inter. J. Heat & Mass Transfer*, vol. 40, 2327-2339, 1997.

Nakayama, W., T. Daikoku, H. Kuwahara, T. Nakajima, "Dynamic Model of Enhanced Boiling Heat Transfer on Porous Surfaces Part I: Experimental Investigation," *ASME J. Heat Transfer*, vol. 102, no. 3, 445-450, 1980.

Nimkar, N. K., S. H. Bhavnani, R. C. and Jaeger, "Benchmark Heat Transfer Data for Microstructured Surfaces for Immersion-Cooled Microelectronics," *IEEE Trans. On Components and Packaging Tech.*, vol. 29, no. 1, 89-97, 2006.

Nishikawa, K., Y. Fujita, S. Uchida, H. Ohta, "Effect of Surface Configuration on Nucleate Boiling Heat Transfer," *Inter. J. Heat & Mass Transfer*, vol. 27, 1559-1571, 1984.

O'Connor, J. P., "Enhancement of Pool Boiling Heat Transfer in Highly Wetting Dielectric Liquids," *Ph.D. Dissertation, University of Texas at Arlington, TX*, 1994.

O'Connor, J. P., S. M. You, "A Painting Technique to Enhance Pool Boiling Heat Transfer in Saturated FC-72," *ASME J. Heat Transfer*, vol. 117, 387-393, 1995.

O'Connor, J., S. You, J. Chang, "Gas-Saturated Pool Boiling Heat Transfer From Smooth and Microporous Surfaces in FC-72," *ASME J. Heat Transfer*, vol. 118, 662-667, 1996.

Oktay, S., "Departure from Natural Convection (DNC) in Low-Temperature Boiling Heat Transfer Encountered in Cooling Micro-Electronic LSI Devices," *Proc. Seventh*

*International Heat Transfer Conference*, vol. 4, 113-118, Munich, Fed. Rep. Germany, Sep. 6 - 10, 1982.

Omega, *Temperature Handbook and Encyclopedia*, vol. MMV, 5<sup>th</sup> Ed. 2004.

Parker, J. L., M. S. El-Genk, "Enhanced Saturation and Subcooled Boiling of FC-72 Dielectric Liquid," *Inter. J. Heat and Mass Transfer*, vol. 48, 3736-3752, 2005.

Parker, J. L., M. S. El-Genk, "Effect of Surface Orientation on Nucleate Boiling of FC-72 on Porous Graphite," *ASME Journal of Heat Transfer*, vol. 128, 1159-1175, 2006.

Parker, J. L., M. S. El-Genk, "Subcooled Boiling of Dielectric Liquids on Porous Graphite at Different Orientations," *Proc. International Heat Transfer Conference*, BOI-36, 2006.

Parker, J. L., M. S. El-Genk, "Enhanced Saturation Boiling of HFE-7100 Dielectric Liquid on Extended Copper Surfaces," *Proc, ASME, JSME Summer Heat Transfer conference*, July 8-12, 2007, Vancouver, British Columbia, Canada, HT2007-32496, 2007.

Parker, J. L. M. S. El-Genk, "Subcooled Boiling of HFE-7100 Dielectric Liquid on Copper Surfaces with Corner Pins," *Proc. 5<sup>th</sup> European Thermal-Sciences Conferences*, May 18-22, 2008, Eindhoven, the Netherlands, 2008.

Peterson, G., *An Introduction to Heat Pipes: Modeling, Testing, and Applications*, New York, Wiley and Sons, 1994.

Pirola, I. L., W. Rohsenow, S. S. Doerffer, "Nucleate Pool-Boiling Heat Transfer. I: Review of Parametric Effects of Boiling Surface," *Inter. J. Heat and Mass Transfer*, vol. 47, 5033-5044, 2004.

Priarone, A., "Effect of Surface Orientation on Nucleate Boiling and Critical Heat Flux of Dielectric Fluids," *International Journal of Thermal Sciences*, vol. 44, 822-831, 2005.

Poco Graphite, Properties and Characteristics Data Sheets for Poco HTC, 2004.

Qui, D., V. K. Dhir, "Experimental Study of Flow Pattern and Heat Transfer Associated with a Bubble Sliding on Downward Facing Inclined Surfaces," *Experimental Thermal and Fluid Science*, vol. 26, 605-616, 2002.

Rainey, K. N., S. M. You, "Pool Boiling Heat Transfer from Plain and Microporous, Square Pin-Finned Surfaces in Saturated FC-72," *ASME J. Heat Transfer*, vol.122, pp. 509-516, 2000.

Rainey, K. N., S. M. You, "Effects of Heater Size and Orientation on Pool Boiling Heat Transfer from Microporous Coated Surfaces," *Inter. J. Heat & Mass Transfer*, vol. 44, 2589-2599, 2001.

Rainey, K. N., S. M. You, S. Lee, "Effect of Pressure, Subcooling, and Dissolved Gas on Pool Boiling from Microporous Surfaces in FC-72," *ASME J. Heat Transfer*, vol. 125, 75-83, 2003.

Ramaswamy, C., Y. Joshi, W. Nakayama, W. Johnson, "Thermal Performance of a Compact Two-Phase Thermosyphon: Response to Evaporator Confinement and Transient Loads," *Enhanced Heat Transfer*, vol. 6, 279-288, 1999.

Ramaswamy, C., Y. Joshi, W. Nakayama, W. Johnson, "Combined Effects of Sub-Cooling and Operating Pressure on the Performance of a Two-Chamber Thermosyphon," *IEEE Transactions on Component and Packaging Technology*, vol. 23, 61-69, 2000.

Ramaswamy, C., Y. Joshi, W. Nakayama, W. Johnson, "High-speed Visualization of Boiling from an Enhanced Structure," *Int. J. Heat & Mass Transfer*, vol. 45, 4761-4771, 2002.

Ramaswamy, C., Y. Joshi, W. Nakayama, W. Johnson, "Effects of Varying Geometrical Parameters on Boiling From Microfabricated Enhanced Structures," *ASME J. Heat Transfer*, vol. 125, 103-109, 2003.

Ramilison, J., P. Sadasivan, J. Lienhard, "Surface Factors Influencing Burnout on Flat Heaters," *ASME J. Heat Transfer*, vol. 114, no. 1, 287-290 1992.

Ravigururajan, R. S., M.K. Drost, "Single-Phase Flow Terminal Performance Characteristics of a Parallel Microchannel Heat Exchanger," *Enhanced Heat Transfer*, vol. 6, 383-393, 1999.

Reed, S. J., "Elimination of Boiling Incipience Temperature Drop and Enhancement of Boiling Heat Transfer in Highly Wetting Fluids Through Low Contact Force Attachments," *M. S. Thesis, Purdue University*, West Laffeyette, IN, 1996.

Reed, S. J., I. Mudawar, "Elimination of Boiling Incipience Temperature Drop in Highly Wetting Fluids using Spherical Contact With a Flat Surface," *Inter. J. Heat & Mass Transfer*, vol. 42, 2439-2454, 1997.

Refai-Ahmed, G., "Thermal Challenges in the Present and Next Generation of PC Processors," *Conference on Integration and Packaging of MEMS, NEMS, and Electronics (InterPack'07)*, Vancouver, BC, Canada, IPACK2007-3506, 1029-1032, 2007.

Rini, D. P, R. H. Chen, L. C. Chow, "Bubble Behavior and Heat Transfer Mechanism in FC-72 Pool Boiling," *Experimental Heat Transfer*, vol. 14, 27-44, 2001.

Rohsenow, W. M., "A Method of Correlating Heat-Transfer Data for Surface Boiling of Liquids," *Transactions of the ASME*, vol. 74, 969-976, 1952.

Simmons, R. E., "Direct Liquid Immersion Cooling for High Power Density Microelectronics," *Electronics Cooling*, vol. 2, no. 2, 1996.

Ujereh, S., T. Fisher, I. Mudawar, "Effects of Carbon Nanotube Arrays on Nucleate Pool Boiling, *Int. J. Heat and Mass Transfer*,: vol. 50, no. 19-20, 4023-4038, 2007.

Vemuri, S., K. J. Kim, "Pool Boiling of Saturated FC-72 on Nano-Porous Surface," *Inter. Comm. Heat & Mass Transfer*, vol. 32, 27-31, 2005.

Vishnev, I. P., I. A. Filatov, Ya. G. Vinokur, V. V. Gorokhov, G. G. Svalov, "Study of Heat Transfer in Boiling of Helium on Surfaces with Various Orientations," *Heat Transfer-Soviet Research*, vol. 8, 104-108, 1976.

Wallington, T. J., et al., "Atmospheric Chemistry of HFE-7100 (C<sub>4</sub>F<sub>9</sub>OCH<sub>3</sub>): Reaction with OH Radicals, UV Spectra and Kinetic Data for C<sub>4</sub>F<sub>9</sub>OCH<sub>2</sub>, and C<sub>4</sub>F<sub>9</sub>OCH<sub>2</sub>O<sub>2</sub> Radicals, and the Atmospheric fate of C<sub>4</sub>F<sub>9</sub>OCH<sub>2</sub> Radicals," *Journal of Physical Chemistry A*, vol. 101, no. 44, 8264-8274, 1997.

Watwe, A., A. Bar-Cohen, A. McNeil, "Combined Pressure and Subcooling Effects on Pool Boiling from a PPGA Chip Package," *J. of Electronic Packaging*, vol. 119, 95-105, 1997.

Wei, J. J., H. Honda, "Effects of Fin Geometry on Boiling Heat Transfer from Silicon Chips with Micro-Pin-Fins Immersed in FC-72," *Inter. J. Heat and Mass Transfer*, vol. 46, 4059-4070, 2003.

Wei, J. J., L. J. Guo, H. Honda, "Experimental Study of Boiling Phenomena and Heat Transfer Performances of FC-72 Over Micro-pin-finned Silicon Chips," *Heat Mass Transfer*, vol. 41, 744-755, 2005.

Xu, G., B. Guenin, M. Vogel, "Extension of Air Cooling for High Power Processors," *Proceedings 9<sup>th</sup> Intersociety Conf. on Thermal Phenomena*, vol. 1, 186-193, 2004.

You, S. M., T. W. Simon, A. Bar-Cohen, Y. S. Hong "Effects of Dissolved Gas Content on Pool Boiling of a Highly Wetting Fluid," *ASME J. Heat Transfer*, vol. 117, 687 - 692, 1995.

Yu, C. K., D. C. Lu, T. C. Cheng, "Pool Boiling Heat Transfer on Artificial Micro-Cavity Surfaces in Dielectric Fluid FC-72," *J. Micromechanics and Microengineering*, vol. 16, no. 10, 2092-2099, 2006.

Yu, C. K., D. C. Lu, "Pool Boiling Heat Transfer on Horizontal Rectangular Fin Array in Saturated FC-72," *Inter. J. Heat and Mass Transfer*, vol. 50, no. 17-18, 3624-3637, 2007.

Zuber, N., "Hydrodynamic Aspects of Boiling Heat Transfer," *Ph.D. Dissertation, University of California, Los Angeles, CA, 1959.*

Zuber, N., "Nucleate Boiling. The Region of Isolated Bubbles and the Similarity with Natural Convection," *Inter. J. Heat and Mass Transfer*, vol. 6, pp. 53-76, 1963.

Zuber, N., M. Tribus, and J. W. Westwater, "The Hydrodynamic Crisis in Pool Boiling of Saturated and Subcooled Liquids," *Inter. J. Heat and Mass Transfer*, vol. 4, pp. 230-236, 1961.

## Appendix A. Details of Thermal Analysis

The thermal analyses completed on the tests sections were performed using the ANSYS software, a commercial finite element numerical analysis package. The analysis estimates the heat losses from the test sections by balancing the generated energy in the heater and that removed from the heated surface by nucleate boiling and the exposed sides of the thermal insulation by natural convection. Figure A.1 shows a schematic diagram of the test section. The heat conduction equations were solved in three dimensions throughout the test section:

$$q = \int_{x=0}^{L_{Tef} + Th_{Lex}} \int_{y=0}^{L_{Tef} + Th_{Lex}} \int_{z=0}^{Th_{Lex} + Th_{Tef} + Th_{epo}} \left[ \frac{\partial}{\partial x} \left( k_x \frac{\partial T}{\partial x} \right) + \frac{\partial}{\partial y} \left( k_y \frac{\partial T}{\partial y} \right) + \frac{\partial}{\partial z} \left( k_z \frac{\partial T}{\partial z} \right) \right] dx dy dz \quad , \quad (A.1)$$

subject to the following boundary conditions:

$$k_x \frac{dT}{dx} = 0 \quad (x = 0, y, z) \quad (A.2)$$

$$k_y \frac{dT}{dy} = 0 \quad (x, y=0, z) \quad (A.3)$$

$$k_{epo} \frac{dT}{dz} = h_{NC}(T) [T(x, y) - T_b] \quad , \quad (x > L_{htr}, y > L_{htr}, z = Th_{Lex} + Th_{Tef} + Th_{epo}) \quad (A.4)$$

$$k_{Lex} \frac{dT}{dx} = 1.23 h_{NC}(T) [T(y, z) - T_b] \quad , \quad (x = L_{Tef} + Th_{Lex}, y, z) \quad (A.5)$$

$$k_{Lex} \frac{dT}{dz} = 1.23 h_{NC}(T) [T(x, z) - T_b] \quad , \quad (x, y = L_{Tef} + Th_{Lex}, z) \quad (A.6)$$

$$k_{Lex} \frac{dT}{dz} = 0.5 h_{NC}(T) [T(x, y) - T_b], \quad (x, y, z = 0) \quad (\text{A.7})$$

$$k_{Cu} \frac{dT}{dz} = h_{NB}(T) [T_w(x, y) - T_b], \quad (\text{A.8})$$

$$(x \leq L_{htr}, y \leq L_{htr}, z = Th_{Lex} + Th_{Tef} - Th_{cav} + Th_{htr} + Th_{OB} + Th_{Cu})$$

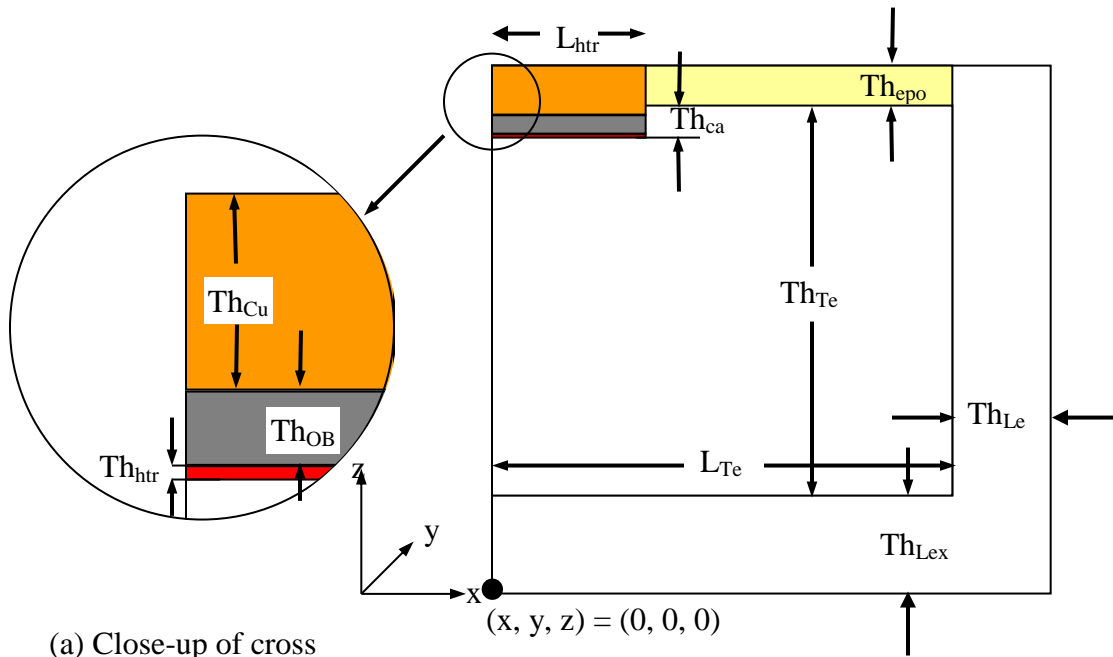
Continuity of both temperature and heat flux is assumed between the interface of the different materials, e.g.

$$k_{Lex} \frac{dT}{dz} = k_{Tef} \frac{dT}{dz} \quad (\text{A.9})$$

$$T_{Lex} = T_{Tef} \quad (\text{A.10})$$

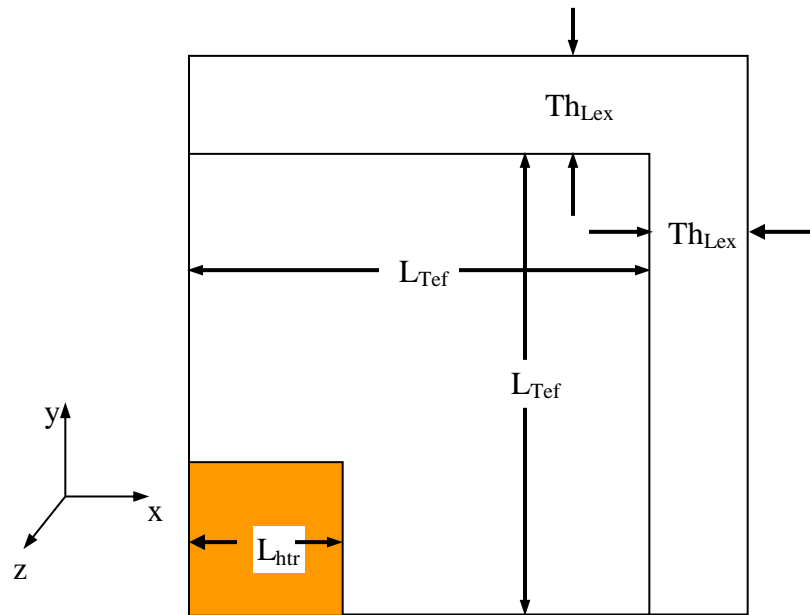
All other interfaces are treated similarly (interfaces between heater and Teflon, heater and Omegabond, Omegabond and copper or porous graphite, Teflon and copper or porous graphite, epoxy filler and copper or porous graphite, epoxy filler and Teflon) (Figure A.1).

The temperature depended boiling heat transfer coefficients were determined from the boiling curves. Figure A.2a shows  $h_{NB}$  for saturation boiling of FC-72 on copper and porous graphite. The temperature depended natural convection heat transfer coefficient,  $h_{NC}$  shown in Figure A.2b, was determined from data obtained in saturation and subcooled experiments using HFE-7100 and FC-72 on smooth, plane surfaces in the upward facing orientation (Section 4.3). For the vertical and downward facing exposed sides of the test section,  $h_{NC}$  was multiplied by 1.23 and 0.5, respectively (Bejan, 1993).



(a) Close-up of cross section of heater and heated surface.

(b) Cross-sectional view of test section.



(c) Plane view of test section.

**Figure A.0.1** Layout of test section for thermal analysis.

## Appendix B: Experimental Uncertainty

An uncertainty analysis of the experimental measurements was conducted to find the range believed to contain the true value of the heat flux, superheat, and the heat transfer coefficient for the pool boiling experiments. There are two basic kinds of uncertainties, systematic and random uncertainties. Systematic uncertainties come from the instrument bias or errors in the experimental techniques. Random uncertainties come from the unpredictable variations in the measurements. In an uncertainty analysis, the uncertainty of the individual measurements must be propagated to determine the overall uncertainty. Estimated uncertainties in the experimental data can be propagated for  $n$  independent parameters  $w_1, w_2, \dots, w_n$ , following the method described by Kline and McClintock (1952) using the function:

$$\Delta G = \left[ \sum_i^n \left( \frac{\partial G(w_i)}{w_i} \Delta w_i \right)^2 \right]^{1/2} \quad (\text{B.1})$$

where  $F$  is a function of the  $n$  variables:

$$G = G(w_1, w_2, \dots, w_n) \quad (\text{B.2})$$

and its uncertainty is represented by  $\Delta G$ . The uncertainties in the present experiments estimated for the parameters of interest—heat flux, surface superheat, and nucleate boiling heat transfer coefficient.

Systematic uncertainties or measurement biases are estimated from the instrument uncertainties are provided by the manufacturers of the power supply, the temperature data acquisition card, and the thermocouples. The stated voltage and current uncertainties are  $0.05\% \pm 5$  mV and  $0.15\% \pm 5$  mA, respectively (Agilent, 2000). These are combined with the random uncertainties in the measurements of voltage and current, estimated by the standard deviation of the 30 measurements obtained during a reading at steady state. The overall uncertainty of the measurement  $M$  of voltage or current is calculated by

$$\Delta M = \left[ \Delta M_{systematic}^2 + \Delta M_{random}^2 \right]^{1/2} \quad (B.3)$$

where  $M$  is either the voltage  $V$  or current  $I$ . In general, the uncertainties in current are  $< 1\%$  and the uncertainties in the voltage are  $\ll 1\%$ . The largest contributor to the uncertainty in the power dissipated is the heat losses from the test section (Chapter 3), which are estimated to be less than 3%.

A similar analysis is done for the temperature measurements. The stated uncertainties for the thermocouples are  $\pm 0.7$  K (Omega, 2004) and the estimated systematic errors for the data acquisition card is  $\pm 0.6$  K. The standard deviation of the thirty measurements used to determine steady state is on the order of 0.07 K. Combining these uncertainties results in an overall uncertainty of the temperature measurement of 0.9 K.

The power removed by the boiling surface is equal to the product of the current through and the voltage drop across the heating element, less the estimated losses:

$$P = IV - P_{loss} \quad (B.4)$$

Applying Equation B.1 to Equation B.4 yields an estimate for the uncertainty in the power measurement of

$$\Delta P = P \left[ \left( \frac{\Delta V}{V} \right)^2 + \left( \frac{\Delta I}{I} \right)^2 + (\Delta P_{loss})^2 \right]^{1/2} . \quad (B.5)$$

The heat flux is calculated by the quotient of the power removed and the area through which it is removed:

$$q'' = P/A \quad (B.6)$$

and thus

$$\Delta q'' = q'' \left[ \left( \frac{\Delta P}{P} \right)^2 + \left( \frac{\Delta A}{A} \right)^2 \right]^{1/2} \quad (\text{B.7})$$

Heat transfer coefficients are calculated from the heat flux divided by the temperature difference between the wall and the bulk liquid:

$$h = \frac{q''}{T_w - T_b} \quad (\text{B.8})$$

The associated uncertainty, using Equation A.1, is

$$\Delta h = h \left\{ \left( \frac{\Delta q''}{q''} \right)^2 + \left[ \frac{\Delta T_w^2 + \Delta T_b^2}{(T_w - T_b)^2} \right] \right\}^{1/2} \quad (\text{B.9})$$

Table B.1 lists the estimated uncertainties of the various parameters at different heat fluxes for 30 K subcooled boiling of HFE-7100 on a plane Cu surface. These values are representative of the values for other configurations. Figure B.1 shows the boiling curve for saturated HFE-7100 boiling on a plane copper surface ( $\theta = 0^\circ$ ) with error bars for heat flux (Figure B.1a) and for superheat (Figure B.1b). As seen in the figure and in the table, the larger uncertainty is associated with the temperature measurements.

**Table B.1 Selected values and associated uncertainties for test measurements.**

Parameter	~10 W/cm <sup>2</sup>	~20 W/cm <sup>2</sup>	~30 W/cm <sup>2</sup>
Current, $I$ (A)	0.848±0.007 (0.8%)	1.186±0.007 (0.6%)	1.445±0.007 (0.5%)
Voltage, $V$ (V)	12.307±0.012 (0.1%)	17.223±0.014 (0.08%)	21.060±0.016 (0.08%)
Area, $A$ (cm <sup>2</sup> )	1.00±0.02 (2%)	1.00±0.02 (2%)	1.00±0.02 (2%)
Superheat, $\Delta T_{sat}$ (K)	11.5±1.0 (7%)	15.5±1.0 (6%)	18.8±1.0 (5%)
Heat Flux, $q''$ (W/cm <sup>2</sup> )	10.3±0.3 (3%)	20.2±0.6 (3%)	30.1±0.9 (3%)
Heat Transfer Coefficient, $h_B$ (W/cm <sup>2</sup> K)	0.90±0.1 (11%)	1.30±0.11 (9%)	1.60±0.3 (7%)



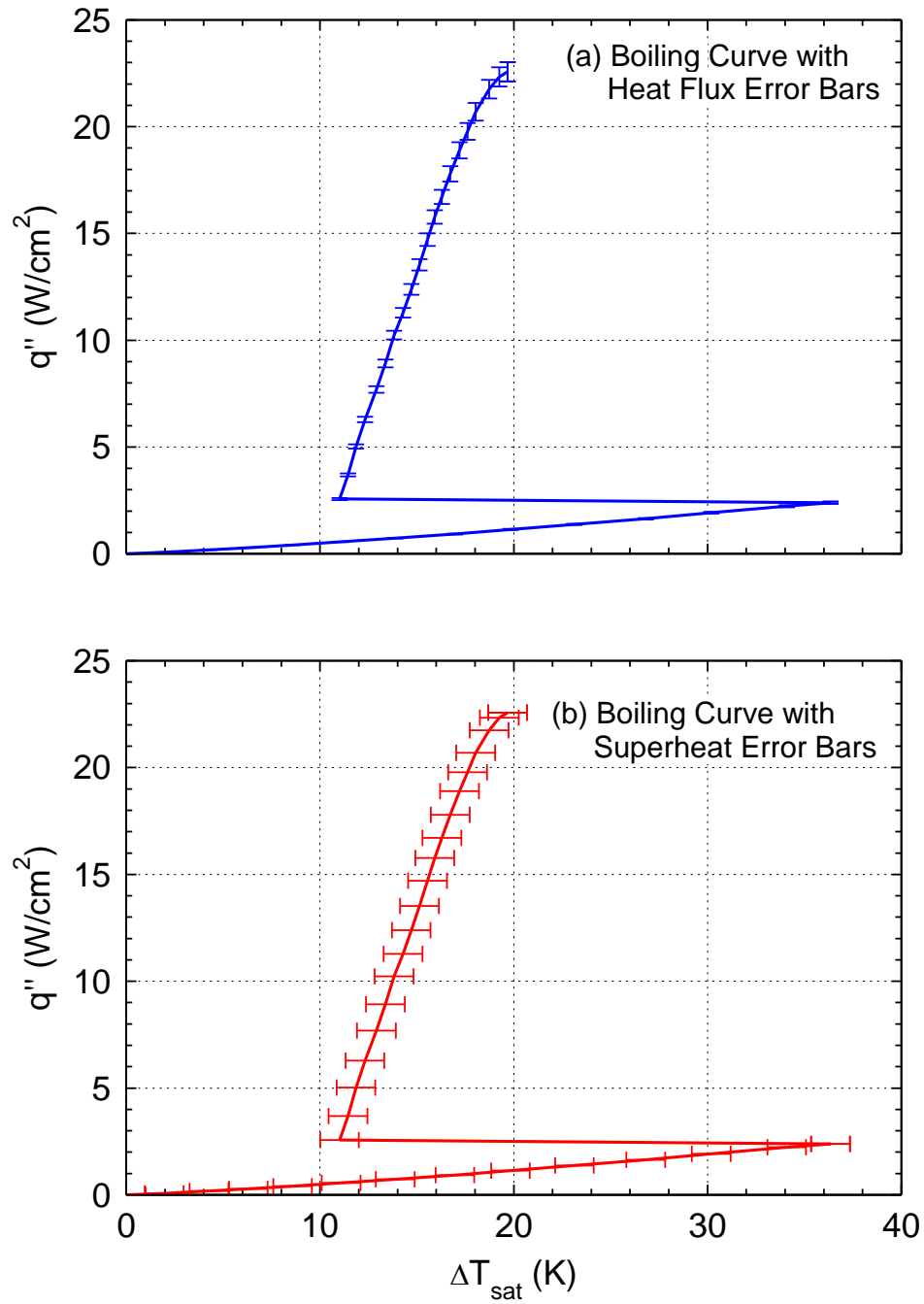


Figure B.0.1 Saturation boiling of HFE-7100 on plane copper with associated uncertainties.

## Appendix C: List of Publications Related to Work

M. S. El-Genk and J. L. Parker, "Nucleate Boiling of FC-72 and HFE-7100 on Porous Graphite at Different Orientations and Liquid Subcooling," *Energy Conversion and Management*, Vol. 49, pp. 733-750, 2008

J. L. Parker and M. S. El-Genk, "Subcooled Boiling of HFE-7100 Dielectric Liquid on Copper Surface with Corner Pins," *Proc. 5th European Thermal-Sciences Conference*, 18-22 May, 2008, Eindhoven, the Netherlands.

M. S. El-Genk and H. H. Saber, "Composite Spreader for Cooling Computer Chip with Non-Uniform Heat Dissipation", *IEEE Transactions on Components and Packaging Technologies*, Vol. 31, No. 1, pp. 167-172, 2008.

J. L. Parker and M. S. El-Genk, "Enhanced Saturation Boiling of HFE-7100 Dielectric Liquid on Extended Copper Surfaces," *Proc. ASME-JSME Thermal Engineering Summer Heat Transfer Conference July 8-12, 2007, Vancouver, British Columbia, Canada*, HT2007-32469.

M. S. El-Genk, H. H. Saber, and J. L. Parker, "Efficient Spreaders for Cooling High-Power Computer Chips," *Applied Thermal Engineering*, Vol. 27, pp. 1072-1088, 2007.

J. L. Parker and M. S. El-Genk, "Effect of Surface Orientation on Nucleate Boiling of FC-72 on Porous Graphite," *ASME Journal of Heat Transfer*, Vol. 128, pp. 1159-1175, 2006.

J. L. Parker and M. S. El-Genk, "Subcooled Boiling of Dielectric Liquids on Porous Graphite at Different Orientations," *Proc. International Heat Transfer Conference, BOI-36*, 2006.

M. S. El-Genk and H. H. Saber, "Composite Spreader for Submersion Cooling of a Computer Chip with Non-Uniform Heat Dissipation," *Thermomechanical Phenomena in Electronic Systems—Proc. Intersociety Conf. (ITHERM 2006)*, 591-598, 2006.

J. L. Parker and M. S. El-Genk, "Effect of Inclination on Pool Boiling of FC-72 Dielectric Liquid on Porous Graphite," *Proc. ASME Summer Heat Transfer conference, July 17-22, 2005, San Francisco, CA*, HT2005-72289, pp. 527-535, 2005.

M. S. El-Genk, H. H. Saber, and J. L. Parker, "Thermal Analysis of Composite Copper/Porous Graphite Spreaders for Immersion Cooling Applications," *Proc. Conference on Integration and Packaging of MEMS, NEMS, and Electronics (InterPack'05)*, July 17-22, 2005, San Francisco, CA, IPACK2005-73226, pp. 305-314, 2005.

J. L. Parker and M. S. El-Genk, "Enhanced Saturation and Subcooled Boiling of FC-72 Dielectric Liquid," *International Journal of Heat and Mass Transfer*, Vol. 48, pp. 3736-3752, 2005.

M. S. El-Genk and J. L. Parker, "Enhanced Boiling of HFE-7100 Dielectric Liquid on Porous Graphite," *Energy Conversion and Management*, Vol. 46, pp. 2455-2481, 2005.

M. S. El-Genk and J. L. Parker, "Pool Boiling in Saturated and Subcooled FC-72 Dielectric Fluid from a Porous Graphite Surface," *American Society of Mechanical Engineers, Heat Transfer Division, (Publication) HTD*, Vol. 375, pp. 203-210, 2004.

M. S. El-Genk and J. L. Parker, "Pool Boiling in Saturated and Subcooled HFE-7100 Dielectric Fluid from a Porous Graphite Surface," *Proc Intersociety Conference on Thermal Phenomena*, Vol. 1, pp. 655-662, 2004